Generation of gases and low-molecular-weight organic acids in Opalinus Clay at elevated temperatures

Dissertation zur Erlangung des Doktorgrades der

Naturwissenschaften

– Dr. rer. nat. –

Am Fachbereich Geowissenschaften

der Universität Bremen

vorgelegt von

Oliver Helten

Bremen

November 2023

"Lauda in illo quod nec eripi potest nec dari, quod proprium hominis est."

– Seneca: Epistulae Morales – Epistula 41

Content

Abstract

Internationally, claystone formations are und   vestigation as host rocks for high-level heat-emitting nuclear waste (HLW). Claystones have beneficial properties as natural barrier for HLW, including: low permeability, high retention capability for radionuclides, and self-sealing of fractures by swelling. A drawback of claystones as host rock is their temperature sensitivity. Temperatures at the surface of HLW containers in claystone formations are expected to be in the range of 90–150 °C. Elevated temperatures in the vicinity of HLW containers might cause clay mineral transformation reactions reducing the radionuclide retention potential of the host rock. Other consequences are changes of the composition of the pore water and the promotion of organic matter decomposition. The latter results in the generation of gases and water-soluble organic compounds. Both initiate further geochemical reactions affecting the mineralogical inventory of a claystone and the composition of the pore water. Thus, an increase in temperature due to HLW disposal in a claystone formation has the potential to affect a vast and interconnected organic and inorganic geochemical reaction network. In response to the numerous geological and technical challenges in nuclear waste management, so-called features, events, and processes (FEPs) catalogues were introduced. FEPs are specifically compiled for a host rock type and aim to provide guidelines for the safety assessment of a repository facility. For safety reasons, the deep geological storage of HLW is designed for a period of several hundred thousand to one million years. Thus, the long-term safety and performance of a repository relies on predictions. In order to make predictions as robust as possible empirical, quantitative data is indispensable.

In this thesis, the thermal transformation of organic matter in a host rock for HLW disposal, the Opalinus Clay (OPA; Mont Terri, St. Ursanne, Switzerland), was investigated in hydrous pyrolysis experiments at temperatures from 80–200 °C – and beyond. For this, ground OPA was mixed with HPLC-grade water in Dickson-type flexible gold-titanium reaction cells ('gold bags'). Isobaric conditions of 20 MPa were maintained over the course of the experiments. The experimental setup allowed to gradually withdraw aqueous samples. Geochemical reactions were monitored over periods of several weeks. Samples were transferred into headspace vials, allowing for analyses of the gas phase, followed by measurements of water-soluble compounds in the aqueous fluid. An additional set of experiments investigated the interaction between water-soluble organic compounds and OPA mineral phases in suspension at room temperature (~20 °C) and atmospheric pressure.

The hydrous pyrolysis experiments demonstrated the release/generation of gaseous CO_2 and C_1–C_4 hydrocarbons. $CO_{2(g)}$ was the dominant gas released/generated. Gas yields increased with increasing temperature. Molecular hydrogen ($H_{2(g)}$) was only generated in two experiments at >300 °C – well beyond the storage conditions of HLW. No hydrogen sulfide ($H_2S_{(g)}$) or carbon monoxide ($CO_{(g)}$) were detected in any of the samples. $CO_{2(g)}$ originated predominantly from the dissolution of carbonate mineral phases in the OPA sample material and, to a lesser extent, from the thermal transformation of OPA organic matter. An isotope mass balance indicated that up to 26 % of the inorganic carbon and up to 6 % of the organic carbon in OPA were transformed to CO_2 – either present as dissolved inorganic carbon (DIC) in the aqueous fluid or, after exsolution, as $CO_{2(g)}$. New kinetic data on gas generation in OPA completes the data set.

Analyses of the aqueous fluid samples showed the generation of low-molecular-weight organic acids (LMWOA), predominantly acetate, followed by oxalate and formate. The yields of the acids increased with increasing temperature, with the exception of significantly lower quantities of oxalate and formate at temperatures $\geq 160\ °C$. The application of kinetic data on thermal LMWOA decomposition (e.g., decarboxylation) from the literature demonstrated that simultaneous generation and decomposition reactions of LMWOA have rarely been taken into account by other studies. Thus, LMWOA generation from organic matter might have been underestimated in other studies. This also affects the prediction of gas generation (e.g., $CO_{2(g)}$ + $CH_{4(g)}$) by decarboxylation. The thermal stability of acetate might cause its accumulation in pore water, which might serve as a (temporary) feedstock for microbial life.

The interaction of the mono- and dicarboxylic LMWOA acetate and oxalate with OPA mineral phases in a suspension at room temperature ($\sim 20\ °C$) suggested that acetate has no/a negligible affinity towards OPA mineral phases, while the concentration of oxalate decreased within minutes after the acid was added to the suspension. The formation of insoluble Ca-oxalate complexes, e.g., $[Ca(C_2O_4)\cdot H_2O]$ with dissolved Ca^{2+} from carbonate mineral dissolution explained the relatively constant concentration of oxalate in this experiment and might have also affected the concentration of oxalate in the hydrous pyrolysis experiments.

Gas generation increases the overall pressure in a repository and initiates pore water displacement, potentially also promoting radionuclide migration. LMWOA affect mineral dissolution reactions and occupy sorption sites of clay minerals, thereby reducing the retention capability of the natural claystone barrier and/or geo-engineered barriers based on clay minerals. These processes pose a risk for the integrity of a HLW repository in claystone formations. This thesis provided new quantitative data on the generation of gases – including new kinetic data – and LMWOA at elevated temperatures relevant for the deep geological disposal of HLW in claystone formations. It is concluded that the quantities of generated gases and LMWOA, when confronted with geochemical reactions decomposing and/or immobilizing some of them, are unlikely to affect the integrity and long-term safety of a HLW repository in the Opalinus Clay.

Zusammenfassung

International werden Tongesteinformationen auf ihre Eignung als Endlager-Wirtsgestein für hochradioaktive, wärmeentwickelnde Abfälle (HLW) untersucht. Vorteilhafte Eigenschaften von Tongestein sind: eine geringe Permeabilität, ein hohes Rückhaltevermögen von Radionukliden und die Fähigkeit der Rissverschließung durch das Aufquellen bestimmter Tonminerale. Nachteilig wird die Temperaturempfindlichkeit von Tongestein bewertet. Derzeit werden Temperaturen an der Oberfläche von Endlagerbehältern von 90–150 °C diskutiert. Erhöhte Temperaturen im direkten Umfeld der Endlagerbehälter verursachen Umwandlungen von Tonmineralen und verringern so die natürliche Barrierewirkung des Gesteins gegenüber Radionukliden. Andere geochemische Reaktionen verändern die Zusammensetzung des Porenwassers und beschleunigen die Umwandlung organischen Materials. Letztere resultiert in der Bildung von Gasen und wasserlöslichen organischen Verbindungen. Beide Komponenten verstärken den Effekt auf die Porenwasserzusammensetzung und Mineralumwandlungen. Damit hat ein Temperaturanstieg im Endlager Einfluss auf das organische und anorganische geochemische Reaktionsnetzwerk. Im Bereich der Endlagerung dienen sogenannte feature, events, processes (FEP; Komponenten, Ereignisse, Prozesse) Kataloge als Basis sicherheitsgerichteter Untersuchungen. FEP-Kataloge sind wirtsgesteinsspezifisch und unterstützen die Bewertung der Sicherheit des Endlagersystems. Um eine sichere Aufbewahrung der HLW zu erreichen, wurden Einlagerungszeiträume von bis zu einer Millionen Jahre festgeschrieben. Die Langzeitsicherheit eines Endlagers wird unter diesen Bedingungen vor allem durch Modelle geprüft werden müssen. Um diese Modelle so belastbar wie möglich zu machen braucht es empirische und quantitative Daten.

In dieser Dissertation wurde die thermische Umwandlung organischen Materials in einem Endlagerwirtsgestein, dem Opalinuston (OPA; Mont Terri, St. Ursanne, Schweiz), mittels wässriger Pyrolysen bei Temperaturen von 80–200 °C – und darüber hinaus – untersucht. Gemahlener OPA wurde mit hochreinem Wasser in flexiblen Gold-Titan Reaktionszellen nach Dickson (Goldbeuteln) vermischt und bei konstantem Druck (20 MPa) aufgeheizt. Der experimentelle Aufbau erlaubte eine regelmäßige Probenahme wässrigen Fluids. Damit wurden geochemische Reaktionen über Zeiträume mehrerer Wochen nachverfolgt. Die Proben wurden in Headspace-Vials gegeben, was das Beproben der Gas- und der Flüssigphase ermöglichte. In einer weiteren Experimentreihe wurden Wechselwirkungen zwischen wasserlöslichen organischen Verbindungen und den OPA-Mineralphasen bei Raumtemperatur (~20 °C) und Atmosphärendruck untersucht.

In den wässrigen Pyrolysen wurde die Bildung von Kohlenstoffdioxid ($CO_{2(g)}$) und kurzkettiger (C_1–C_4) Kohlenwasserstoffe nachgewiesen. $CO_{2(g)}$ war am stärksten vertreten. Die Gasbildung nahm mit steigender Temperatur zu. Wasserstoff ($H_{2(g)}$) wurde in nur zwei Experimenten bei über 300 °C nachgewiesen. Schwefelwasserstoff ($H_2S_{(g)}$) und Kohlenstoffmonoxid ($CO_{(g)}$) wurden nicht nachgewiesen. $CO_{2(g)}$ stammt vorwiegend aus Lösungsreaktionen Karbonat haltiger Mineralphasen und, zu einem geringeren Anteil, aus der thermischen Umwandlung organischen Materials. Eine Isotopenmassenbilanz hat gezeigt, dass bis zu 26 % des anorganischen und bis zu 6 % des organischen Kohlenstoffs des OPA zu CO_2 umgewandelt wurden – entweder als in Wasser gelöstes $CO_{2(aq)}$ oder, nach der Auslösung aus

einer wässrigen Probe, als $CO_{2(g)}$. Neue kinetische Daten erweitern und unterstützen die Aussagekraft des Datensatzes.

In den wässrigen Proben wurden kurzkettige organische Säuren (LMWOA) nachgewiesen. Die häufigste Verbindung war Acetat, gefolgt von Oxalat und Format. Die Bildung der Säuren nahm mit steigender Temperatur zu, wobei Oxalat und Format bei ≥160 °C in deutlich geringeren Mengen gebildet wurden. Unter Zuhilfenahme kinetischer Daten aus der Literatur zur thermischen Zersetzung (Decarboxylierung) der Säuren wurde aufgezeigt, dass die Gleichzeitigkeit der Bildung und Zersetzung der Säuren in anderen wissenschaftlichen Arbeiten kaum Beachtung gefunden hat. Dies weist auf eine flächendeckende Unterschätzung der Bildung von LMWOA aus organischem Material in vielen Arbeiten hin. Davon betroffen könnte auch die Vorhersage von Gasbildung ($CO_{2(g)}$ und $CH_{4(g)}$) aus Decarboxylierungsreaktionen sein. Die hohe thermische Stabilität von Acetat könnte eine deutliche Konzentrationserhöhung im Porenwasser zur Folge haben. Dieses Acetat könnte eine (temporäre) Kohlenstoffquelle für Mikroorganismen darstellen.

Eine Experimentreihe mit Acetat und Oxalat und Mineralphasen des OPA in einer Suspension bei Raumtemperatur (~20 °C) zeigt, dass zwischen Acetat und den Mineralen keine/vernachlässigbare Wechselwirkungen vorliegen. Die Konzentration von Oxalat nahm hingegen innerhalb weniger Minuten nach dessen Zugabe signifikant ab. Die Bildung schwer wasserlöslicher Ca-Oxalat Komplexverbindungen, z. B. $[Ca(C_2O_4) \cdot H_2O]$, mit gelösten Ca^{2+}-Ionen aus der Lösung Karbonat haltiger Mineralphasen erklärt die gemessenen Konzentrationen Oxalats in dieser Experimentreihe und möglicherweise auch in den wässrigen Pyrolysen.

Gasbildung führt zur Erhöhung des Ducks im Endlagersystem und bewirkt die Verdrängung von Porenwasser, was die Migration von Radionukliden einschließen kann. Kurzkettige organische Säuren bewirken Minerallösungsprozesse, besetzen Sorptionsplätze und verringern damit das Rückhaltevermögen der natürlichen und geotechnischen Tongestein-/Tonmineralbarrieren. Diese Prozesse stellen Sicherheitsrisiken für Endlager in Tongesteinformationen dar. Diese Dissertation hat neue quantitative Daten zur Gasbildung – inklusive neuer kinetischer Daten – und der Bildung kurzkettiger organischer Säuren unter Endlager-nahen Temperaturbedingungen, wie sie in Tongesteinformationen erwartet werden, hervorgebracht. Es wird geschlussfolgert, dass die negativen Auswirkungen der gebildeten Mengen an Gasen und kurzkettigen organischen Säuren wahrscheinlich keinen negativen Einfluss auf die Integrität eines Endlagersystems im Opalinuston haben werden. Eher werden sie durch andere geochemische Reaktionen, die zur Immobilisierung und/oder der Zersetzung dieser Verbindungen führen, aufgewogen. Die Gefährdung eines Endlagersystems für HLW im Opalinuston und dessen Langzeitsicherheit durch die in dieser Dissertation beschriebenen Verbindungen wird daher als unwahrscheinlich angesehen.

Schlüsselwörter: Acetat | Format | Hochradioaktive wärmeerzeugende Abfälle | Isotopenmassenbilanz | Kinetik | Kohlenstoffdioxid | Kohlenwasserstoff Gase | Komplexbildung | Molekularer Wasserstoff | Oxalat | Sorption | Tongestein | Wässrige Pyrolyse | Wirtsgestein

Acknowledgements

Mr. Schneemann and the workshop team, and my superiors and colleagues Martin Blumenberg and Kerstin Beckmann. There are many more to name and I hope they excuse me for interrupting the list here.

At the University of Bremen and the MARUM, many wonderful people supported me in many ways in the past five years. Among these people are: Florence Schubotz, Heidi Taubner, Jenny Wendt, Susanne Alfken, Qing Zeng Zhu, Yvonne von Klenze, Marcus Elvert, Xavi Prieto, Igor Obreht, Lars Wörmer, Julius Lipp, Verena Heuer, Christian Hansen and others. Thank you for all the good times we had and ones to come.

I am convinced that one group of people contributed immensely to the finalization of this thesis and maybe even without being aware of how much their support means to me – my family and my friends. Although it is common to differentiate between the two, my family and my closest friends are simply one big family to me. My parents have supported me throughout my life. I have wet eyes writing this: Mama und Papa, danke für alles! Thank you, Cari, for being there and for knowing that I can always count on you. Gerd, Gabi, Phil, you are wonderful people and I am happy to have you in my life. Recently Liah joined us and I hope I can do my share to make the world a better place for Liah with my work as a scientist. My grandparents always used to have a smile on their face, thinking of me going into academics and doing a PhD. They passed away and cannot see this work finished. Nevertheless, I am truly grateful for all of their support over countless years. Jannis, Stefan Lars, Freddy, Ruben, Vanessa, Marius, Yannik, Eibee, Hannah, the Schluffis, the climbing gang and many more wonderful people, I thank you from the depth of my heart for all the precious moments with you and the endless support you gave me and still give to me.

By the end of this paragraph the author went through a substantial amount of handkerchiefs and hopes that the following chapters will take the reader through interesting, exciting, and stimulating realms of geochemical research.

List of abbreviations

BGE	Federal Company for Nuclear Waste Disposal
BGR	Federal Institute for Geosciences and Natural Resources
CCS	Carbon capture and storage
DAD	Diiodic array detection
DIC	Dissolved inorganic carbon
DOM	Dissolved organic matter
EA	Elemental analyzer
EDZ	Excavation damage zone
FEP	Features, events, processes
FID	Flame ionization detection
GB	Gold bag
GC-c-irmMS	Gas chromatography coupled to isotope ratio mass spectrometry
GICU	Gas inlet control unit
HLW	High-level heat-emitting nuclear waste
HPLC	High performance liquid chromatography
IC	Inorganic carbon
IMB	Isotope mass balance
IRMS	Isotope ratio mass spectrometry
LMWOA	Low-molecular-weight organic acids
Ma	Million years
MS	Mass spectrometry
NAGRA	Swiss National Cooperative for the Disposal of Radioactive Waste
OM	Organic matter
OPA	Opalinus Clay
PDB	Pee Dee Belemnite standard
PTFE	Polytetrafluorethylene
RGA	Refinery gas analyzer

RPM	Revolutions per minute
StandAG	Site Selection Act
TCD	Thermal conductivity detection
THMC	Thermo-hydro-mechanical-chemical
TIC	Total inorganic carbon
TOC	Total organic carbon
TS	Total sulfur
URL	Underground rock laboratory
UV-VIS	Ultraviolet-visible spectroscopy
VPDB	Vienna Pee Dee Belemnite standard

Chapter I

1. General Introduction

1.1. The importance of geochemical research in nuclear waste disposal

Internationally, a consensus exists for the long-term storage of high-level heat-emitting nuclear waste (HLW) in deep geological formations e.g., in claystones. Safety criteria for a repository are addressed in feature, events and process (FEP) catalogues. Among safety-relevant components are gases such as H_2, CO_2, and C_1-C_4 hydrocarbons. Gas generation promotes a rise in pressure in a repository. $CO_{2(aq)}$ and also low-molecular-weight organic acids (LMWOA) are involved in mineral dissolution, which might reduce the integrity of natural and geo-engineered barriers. Moreover, thermal decarboxylation reactions of LMWOA are a potential additional source of gases. If gases and/or low-molecular-weight organic acids were generated in vast quantities by temperature-driven geochemical processes in claystone formations, the long-term safety of a repository, i.e. the retention of radionuclides from the high-level nuclear waste inventory by natural and geo-engineered barriers could be at risk. The retention properties of clay minerals are affected e.g., by the amount of dissolved ions in pore water, including organic compounds. Those can occupy sorption sites on mineral surfaces, reducing the retention capacity of the natural barrier. Thus, the interaction between organic compounds and a claystone is an additional factor to consider in the safety assessment for a HLW repository.

1.2. Host rocks for high-level, heat-emitting nuclear waste disposal

Ewing et al. (2016) stated that the absence of operating HLW repositories is the 'Achilles Heel' of the international use of nuclear power. In 2017, the Site Selection Act (StandAG, 2017), which regulates the search for a deep geological repository for HLW in Germany took effect. The law states that the site selection process for a HLW repository must be science-based in order to locate the best possible geological formation to host HLW for one million years (StandAG, 2017). In Germany, three rock types, crystalline rock (magmatic rocks and higher-metamorphic rocks), rock salt, and claystone are currently under consideration as host rocks for a repository facility.

The identification of host rock formations suitable for the disposal of HLW is based on geoscientific exclusion criteria including: large-scale vertical movements with an average uplift rate of >1 mm per year over the course of one million years; the presence of active fault zones; potential damage of the host rock formation by past or present mining activity; seismic activity; volcanic activity; and groundwater ages (StandAG, 2017; Lommerzheim et al., 2019; Kneuker et al., 2020). In addition to the exclusion criteria, potential host rocks have to fulfill a number of minimum requirements including a permeability below 10^{-10} m/s, a vertical extent of ≥100 m, its confinement providing rock zone must be located >300 m below the surface (mbs), the horizontal extent of the host rock formation has to be large enough for the underground repository facilities, and the natural barrier properties of the rock must not fail during construction, operation, and after repository closure. While the above-stated criteria are indispensable in the site selection process, the exclusion of geological formations is based on more detailed characteristics of the potential host rock. One example is the retention potential for radionuclides released from the HLW inventory by physico-chemical adsorption on mineral surfaces provided by the host rock. In this context, hydrogeological properties of a host rock are of importance, because radionuclides are also present as dissolved ions in pore water and might migrate away from the repository. Other parameters are, e.g., the temperature sensitivity of a host rock and the impact of gas generation on (geo-) mechanical properties of a host rock formation. Currently, approximately 27,000 m^3 of German HLW need to be relocated into a deep geological repository in Germany. The schedule of the site selection process aims to identify the best possible location for a HLW repository in Germany between the 2040's and the 2060's (BGE, 2022a; 2022b).

1.3. Claystone formations in the context of HLW disposal

Clay is a clastic sediment with a grain-size <2 µm, which is further characterized by its mineral composition. A large set of different terms is used to refer to a clay-rich rock e.g.: mudstone, shale, claystone, siltstone, pelite, pelitic rock, or argillaceous rock (Hoth et al., 2007). In addition to the mineralogical inventory, organic matter (OM) content, water content, and the consolidation state based on the diagenetic history of the material are used to characterize clays (Alpin et al., 1999). In this thesis, the term 'claystone' will be used to refer to consolidated sedimentary material predominantly composed of clay minerals (e.g., illite, smectite/montmorillonite, kaolinite, chlorite) and other mineral components (e.g., quartz, feldspar, calcite, dolomite, gypsum, etc.). Accordingly, claystones can contain contributions of sandstone and/or limestone (carbonates).

Globally, claystone formations demonstrated their effectiveness as cap rock for natural oil and gas reservoirs (Grunau, 1987; Bjørlykke, 2015), as aquitards (Rübel et al., 2002), and they are under investigation in the context of carbon capture and storage (CCS; Song and Zhang, 2013; Makhnenko et al., 2017), which translates to their general suitability as host rock for HLW (e.g., Dohrmann et al., 2013). Claystone formations represent the preferred/chosen host rock for HLW e.g., in Switzerland, France, Belgium (Delage et al., 2010), and are under consideration as host rocks in Germany, Japan, and Canada (Hoth et al., 2007; Hendry et al., 2015; StandAG, 2017). Generally, claystone formations are not attractive for mining operations aiming to extract resources (Grambow, 2016; Lommerzheim et al., 2019), which makes them promising candidate host rocks for the final disposal and long-term storage HLW. Containers for HLW will likely fail within 10,000 years after their emplacement in a repository (Landolt et al., 2009; Bossart et al., 2017; King, 2017). Therefore, demonstrating the long-term safety properties of a host rock e.g., by models is an important factor for the public acceptance of a HLW repository site (Gaucher et al., 2010).

In the context of HLW disposal, two main characteristics of claystones are especially important: a low permeability for water and gases and a high retention potential for radionuclides by adsorption on clay mineral surfaces (Van Loon et al., 2005; Delage et al., 2010; Hendry et al., 2015). According to Grambow (2016), OM can alter the sorption properties of a claystone by the occupation of sorption sites on the clay mineral surfaces, which in turn might affect radionuclide migration. The amount of OM present in claystones varies greatly. While some contain between 0.1 wt.% and 5 wt.% OM (e.g., Opalinus Clay, Callovo-Oxfordian claystone, Boom Clay; Claret et al., 2004; Elie and Mazurek, 2008; Durce et al., 2015), source rocks for oil and gas often have an OM content of >10 wt.% (Barth et al., 1989; Littke et al., 1991; Knauss et al., 1997).

Depending on the mineral inventory of a claystone, it has self-sealing properties, resulting from swelling of clay minerals (smectite) in the presence of water (Grambow, 2016). At temperatures of ≥70 °C smectite loses interlayer water, which causes it to transform to illite (Inoue and Udata, 1983; Pytte and Reynolds, 1989; Inoue et al., 1992; Zheng et al., 2015; Heuer et al., 2020). This transformation can, therefore, occur in clay and claystone that has not been exposed to elevated temperatures during burial and diagenesis. In consequence, the rock mechanical and hydrogeological properties of a claystone formation and its effectiveness as natural barrier might change by heat emission from HLW containers. Information on past temperature conditions in rock formations can be found e.g., in the OM composition by the analysis of the

vitrinite reflectance and the biomarker inventory (Mazurek et al., 2006; Elie and Mazurek, 2008).

1.4. Claystone formations in Germany

Hoth et al. (2007) compiled a comprehensive study identifying clay formations suitable for a detailed investigation as potential host rocks for HLW in Germany. The basis of the study by Hoth et al. (2007) were numerous data sets from deep boreholes drilled in the context of oil, gas, and other resource exploration programs.

Close to the geological basement in Germany hardly any claystones are present, because pressure and temperature conditions are in the range of low grade metamorphism resulting in predominantly schist as clay-based rock type (Hoth et al., 2007). The intense compaction results in foliation and the development of preferential flow paths along the foliation planes. The brittle, metamorphosed material often contains fractures that increase the permeability of the rock. Geologically young clay deposits from the Quaternary found in northern Germany and the Alpine foreland are mostly unconsolidated, occur in very shallow depth and, therefore, do not fulfill the requirement of a low permeability ($<10^{-10}$ m/s) and a minimum depth of >300 mbs (StandAG, 2017). The state of consolidation of clays and claystones is an important parameter in the site selection process. While geologically younger clay deposits e.g., from the Tertiary are still rather plastic, older clay formations e.g., from the Mesozoic are considered to be sufficiently consolidated to host a HLW repository (Hoth et al., 2007). Nevertheless, ongoing research in the Boom Clay formation in Belgium demonstrates the feasibility of the construction of galleries and the operation of an underground research facility in semi-consolidated (plastic) claystone (e.g., Neerdael and Boyazis, 1997).
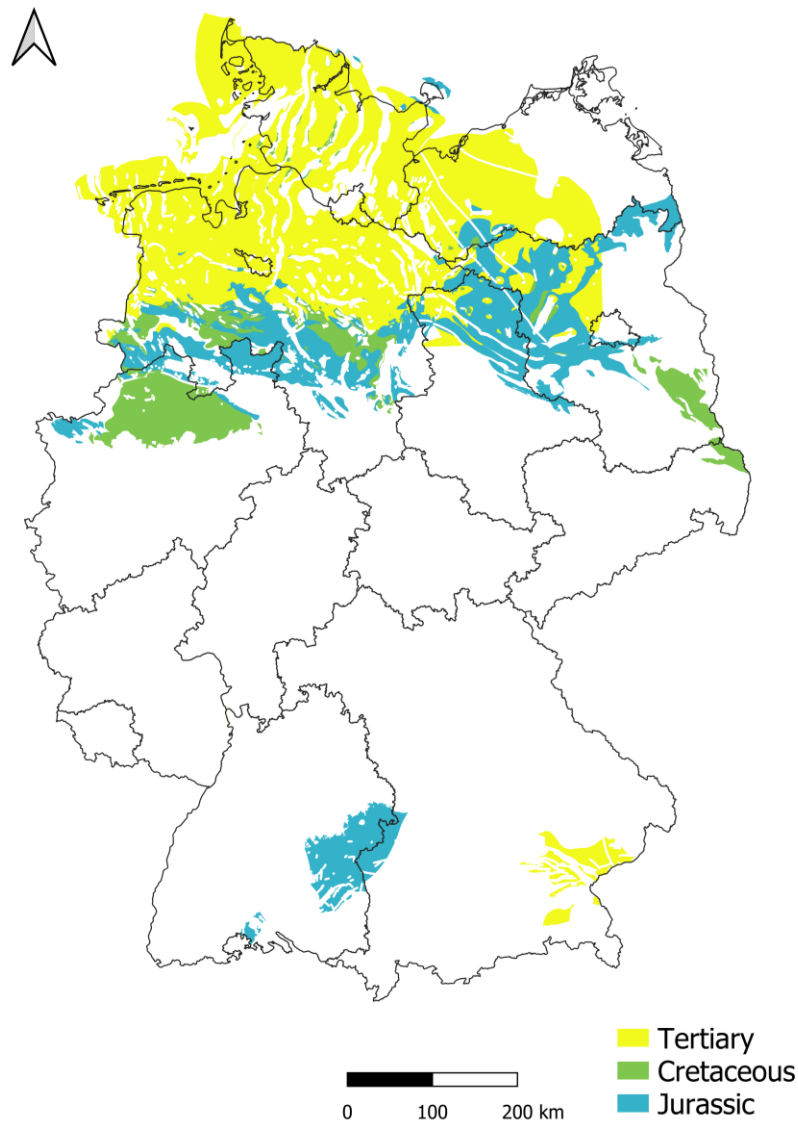
Figure 1.1: Claystone formations under consideration for the disposal of high-level, heat-generating nuclear waste (HLW) in Germany. Shape files were provided by the Federal Company for Nuclear Waste Disposal (BGE).

Two major geological structures in Germany promoted the accumulation and burial of large amounts of sedimentary material, the North German Basin and the Northern Alpine Molasse Basin (Hoth et al., 2007; Fälber et al., 2022). The basin evolution in those two areas resulted in favorable depth conditions and vertical extent for a HLW repository in claystone formations from the Cretaceous and the Jurassic (Hoth et al., 2007). A global rise in sea-level around the Triassic-Jurassic transition turned the area of the North German Basin into a marine-dominated depositional environment, favoring the accumulation of several hundred-meter-thick clay formations, locally interrupted by sandy horizons (Scheck and Beyer, 1999; Hoth et al., 2007). In the Northern Alpine Molasse Basin, the Opalinus Clay was deposited in a shallow

epicontinental sea (Hoth et al., 2007). Due to the exclusion criteria stated in the German Site Selection Act, relevant areas for the Opalinus Clay as a potential host rock for HLW can be found predominantly in Baden-Würtemberg (Hoth et al., 2007; Bossart and Thury, 2008; Zwaan et al., 2022). In the proximity of the Alps, the Opalinus Clay formation dips gently southwards to depths of several thousand meters. In Baden-Würtemberg, close to Ulm, the Opalinus Clay has its highest vertical extent of approximately 150 m (Hoth et al., 2007).

Hoth et al., (2007) summarized claystone formations with sufficient depth and vertical extent as follows: Jurassic claystones are present in Lower Saxony, Saxony-Anhalt, Mecklenburg-Vorpommern, Bavaria, and Baden-Würtemberg; Lower-Cretaceous claystones in Lower-Saxony, Saxony-Anhalt, Mecklenburg-Vorpommern, and Brandenburg. Upper-Cretaceous claystones are locally present in southern Germany; Tertiary claystones are common in Schleswig-Holstein, Mecklenburg-Vorpommern, Brandenburg, Lower-Saxony, and in the Northern Alpine Molasse Basin. The Tertiary claystones, however, are mostly unconsolidated and were not exposed to high temperatures during diagenesis. Thus, no or little mineral transformations took place (Hoth et al., 2007). In summary, the geological situation in Germany demonstrates a large inventory of potential host rocks in claystone formations that are currently under investigation as part of the German site selection process (BGE, 2020; Fälber et al., 2022).

2. The Opalinus Clay – Swiss host rock for nuclear waste

2.1. The Mont Terri Underground Rock Laboratory

In September 2022, the Swiss National Cooperative for the Disposal of Radioactive Waste (NAGRA) recommended Nördlich Lägern in northern Switzerland as site for a HLW repository in the Opalinus Clay. A thorough scientific investigation of rock-specific properties of the Opalinus Clay in Switzerland started in the Mont Terri Underground Rock Laboratory (URL; St. Ursanne, Switzerland) in 1996 (Nussbaum et al., 2011). Since then, an international consortium of federal organizations and research institutions performed numerous in situ and lab-based experiments and obtained sample material e.g., drill cores for a detailed characterization of the evolution of the Opalinus Clay at Mont Terri (Wersin et al., 2022). Multidisciplinary studies conducted over more than two decades provide a rich geoscientific data base for the Opalinus Clay. Numerous studies indicate the transferability of individual parameters, methods, process understanding, and models that are specific to the Opalinus Clay (Bossart et al., 2017). Although an excellent data base for the Opalinus Clay exists for Mont

Terri, this does not guarantee that the data are applicable to other locations where the Opalinus Clay is present. Properties of a rock can vary on every scale, from nanometers to kilometers. In addition to the research performed at the Mont Terri URL, several deep boreholes were drilled in northern Switzerland to provide complementary information on the evolution of the Opalinus Clay. The Mont Terri URL is a mere research facility and no nuclear waste will ever be stored there (Nussbaum et al., 2011).
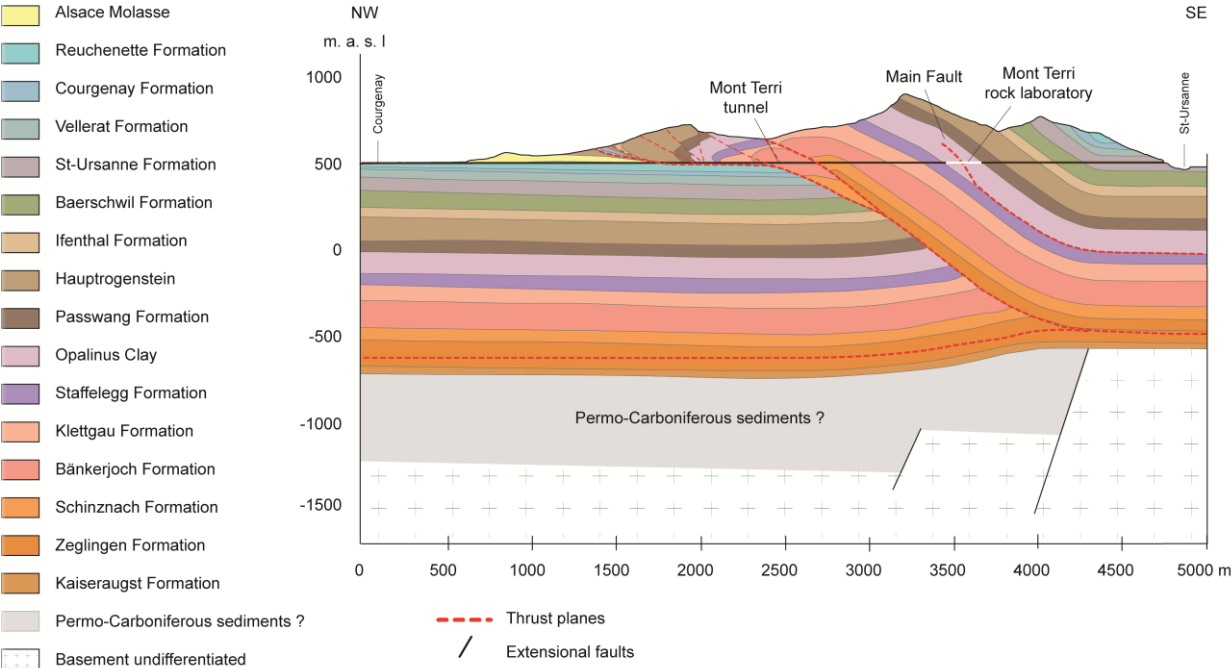
Figure 1.2: Geological cross-section of the Mont Terri anticline and location of the Mont Terri Underground Rock Laboratory (URL) in the Opalinus Clay formation. This figure was kindly provided by Dr. David Jaeggi (Project Manager of the Mont Terri Project).

Figure 1.3: Overview of the Mont Terri Underground Rock Laboratory (URL) with indications of different facies within the Opalinus Clay and in situ experiments. The names of the galleries refer to the different stages of construction (1996–2018) and finalization in the URL. The figure was kindly provided by Dr. David Jaeggi (Project Manager of the Mont Terri Project).

2.2. Geological history of the Opalinus Clay in Switzerland

The basin evolution and accumulation of sediments in the Swiss Molasse Basin was initiated by extensional tectonics, which was deduced from observations made at the Mesozoic margins of the alpine Tethys (Wildi et al., 1989). Schegg et al. (1999) proposed a multi-step process for the evolution of the basin, starting with the Variscan Orogeny and the formation of Permo-Carboniferous grabens in an active transpressive strike-slip regime in the Paleozoic (Mazurek et al., 2006). Subsidence during the Lower Jurassic (Lauper et al., 2018) triggered by extensional tectonics and several stages of rifting, then coincided with the continuous deposition of shallow-marine sediments in an epicontinental sea (Mazurek et al., 2006; Mazurek et al., 2011; Lauper et al., 2018). Basin closure and the erosion of 600–700 m of Cretaceous and late Jurassic deposits occurred prior to the development of the North Alpine Foreland Basin during the end of the Cretaceous (Schegg et al., 1999; Mazurek et al., 2006). In the Miocene to Pliocene, Mesozoic and Cenozoic sediments experienced detachment due to crustal shortening

(Mazurek et al., 2006), deformation, and uplift as a result of the collision of the European and Adriatic plates (Mazurek et al., 2006). The Swiss Molasse Basin represents a continental and shallow-marine component of the North Alpine Foreland Basin, which is regarded as a cold foreland basin with very low coalification gradients and a low level of thermal maturity (Schegg et al., 1999). Underlying the Molasse Basin, Mesozoic carbonates, shales, and clastic rocks rest on the Hercynian basement (Schegg et al., 1999). The western part of the Swiss Molasse Basin experienced strong deformation in the Miocene, approximately 12 Ma ago, stopping the subsidence of the basin and initiating the erosion of parts of the Mont Terri anticline ~10.5 Ma ago (Schegg et al., 1999; Mazurek et al., 2011). In the northwestern part of the Swiss Molasse Basin, the Folded Jura is a mountain belt where thrusting and folding of Mesozoic strata occurred in the late stages of Alpine deformation (late Miocene-Pliocene, ~10–3 Ma; Mazurek et al., 2006). The inclination of strata in the Mont Terri anticline is between 30° and 50°, dipping towards SSE (Hostettler et al., 2017).

Mazurek et al. (2006) investigated the basin evolution of the Swiss Molasse Basin on samples from the Mont Terri URL and the Benken borehole (northern Switzerland) with a multi-proxy approach consisting of vitrinite reflectance data, apatite fisson tracks, and the ratios of temperature sensitive biomarkers e.g., sterane and hopane. These authors concluded that maximum temperatures for the Opalinus Clay at Mont Terri were around 85 °C during the Cretaceous. The findings from the Benken borehole, i.e. low maturity levels (Mazurek et al., 2006), agree well with data obtained from Mont Terri sample material.

At Mont Terri, the Opalinus Clay was deposited 180–174 Ma ago, which corresponds to the Late Toarcian to Lower Aalenian (Early to Mid-Jurassic). The depositional age was derived from findings of ammonites, palynomorphs, ostracodes, foraminifers and geophysical logging data (Bossart and Thury, 2008; Nussbaum et al., 2011; Hostettler et al., 2017). According to Houben et al. (2013), minerals, fossils, and organic matter are homogeneously distributed among the clay matrix. The Opalinus Clay is a moderately over-consolidated claystone (Senger et al., 2013) and has a thickness of approximately 130 m with a present overburden at Mont Terri of 230–320 m (Hostettler et al., 2017). Three major facies have been identified: a shaly, a sandy, and a carbonate-rich facies (Bossart and Thury, 2008; Hostettler et al., 2017). In addition, five sub-units were differentiated on the basis of variations in the mineralogical composition and the grain size distribution (Hostettler et al., 2017; Lauper et al., 2018). Hostettler et al. (2017) gave the following description of these units: (I) a shaly facies consisting of mica-bearing calcareous claystones with lenses or mm-thick layers of quartz in the silt fraction, (II) a thin carbonate-rich sandy facies, characterized by quartz-bearing calcareous biodetritic layers

of up to 10 cm thickness, (III) a sandy facies with calcareous silty claystones, which is overlain by (IV) a dark grey mica-bearing and slightly silty claystone of to the shaly facies. Finally, (V) the uppermost unit of the Opalinus Clay at Mont Terri consists of a sandy facies, a light grey silty claystone with laminated silt lenses, and lenses of bioclastic material. Small heterogeneities in and below the centimeter scale (Wenk et al., 2008) indicate that substantial parts of the Opalinus Clay are of terrigenous origin (Elie and Mazurek, 2008). Elie and Mazurek (2008) suggested that some of the sediments in the Opalinus Clay might have been deposited between 10–30 m below sea level within the range where storm waves cause mixing of water masses. For more detailed information on the depositional environment the reader is referred to Lauper et al. (2018). On a regional scale, the Opalinus Clay shows a remarkable homogeneity and a uniform thickness over a distance of several tens of kilometers (Senger et al., 2013). The Opalinus Clay is overlain and underlain by limestone units containing karstic features, one being the Lower Dogger, the other a Liassic marl (Bossart and Thury, 2008). During the Oligocene, tectonic activity in the Rhine Graben caused fracturing of rocks in a N–S direction (Mazurek et al., 2011; Nussbaum et al., 2011). Older tectonic features with a ENE-orientation date back to the Variscan Orogeny (>350 Ma; Nussbaum et al., 2011). The most prominent tectonic feature at Mont Terri is the 1–3-m wide 'main fault', which consists of numerous fault planes indicating overthrusting (Bossart and Thury, 2008; Nussbaum et al., 2011).

2.3. Thermo-hydro-mechanical (THM) processes

In northern Switzerland, the HLW repository will be located at a depth of approximately 900 mbs in the Opalinus Clay (Morosoli et al., 2023). The layout of the disposal system foresees the HLW to be stored in steel containers, emplaced within horizontal tunnels, where bentonite will be used as backfilling material around and in between the containers (Johnson et al., 2002; Bossart et al., 2017). Due to the radioactive decay of the waste inventory, heat will be emitted from the containers and will be transmitted into the host rock formation. The maximum temperature at the container surface is expected to be around 150 °C (Johnson et al., 2002), slowly decreasing over time (Johnson et al., 2002; Bossart et al., 2017). According to Johnson et al. (2002), temperatures in the host rock formation and in the engineered bentonite barrier are expected to remain below 90 °C. However, this is within the temperature range where illitization (reduction of the swelling capacity of clay minerals) takes place (Inoue and Udata, 1983; Pytte and Reynolds, 1989; Inoue et al., 1992; Heuer et al., 2020). The process of illitization also depends on the concentration of potassium (K^+) in pore water (Cuadros, 2006; Zheng et al., 2015). The effect of temperature on the geochemical, geomechanical, and hydrogeological properties of the Opalinus Clay has been investigated in in situ experiments

(Jockwer et al., 2007; Kull et al., 2007) and lab-based experiments (Jockwer et al., 2006; Sauer et al., 2020). The temperature in the Opalinus Clay formation at Mont Terri is 13–18 °C (Pearson et al., 2003; Jockwer et al., 2007; Kull et al., 2007; Wersin et al., 2008). Kull et al. (2007) reported results from an in situ heating experiment where a heater was gradually set to 100 °C, which was equal to a heat output of 1950 W, and maintained for eight months. In this context, pore water pressure, gas migration, and the deformation of the surrounding Opalinus Clay were monitored. At a distance of ~1.5 m from the heater pore water pressure increased from 0.7 to 4 MPa (Kull et al., 2007). The temperature increase to 100 °C did not cause any damage to the rock closest to the heater, which is in agreement with observations made by other studies (Kull et al., 2007; Jobmann and Meleshyn, 2015; Zhang et al., 2017).

The extent of the thermal impact on thermo-hydro-mechanical properties of a claystone is controlled by its saturation state (Zhang et al., 2017). A claystone is weakened by increasing temperature in its saturated and undrained state because of increasing pore pressure and a subsequent decrease in effective confining stress and a reduction of cohesion and friction resistance of the bound pore water between solid particles (Zhang et al., 2017). In drained conditions, an increase in temperature initiates pore water displacement enhancing the consolidation of a claystone, increasing the inner friction resistance between minerals against shearing, strengthening the rock (Zhang et al., 2017). The mechanical stability of the Opalinus Clay for seismic activity was assessed by Orellana et al. (2018). Although various tectonic fault systems were identified in the Opalinus Clay e.g., the main fault, shear experiments demonstrated the seismic safety of the Opalinus Clay to host a HLW repository (Orellana et al., 2018).

2.4. Mineralogy and microstructure of the Opalinus Clay

There are distinct differences in the mineralogy of the Opalinus Clay, depending on the respective facies (shaly, sandy, carbonate-rich). Bossart and Thury (2008) compiled a comprehensive summary of mineralogical and physical parameters of the Opalinus Clay at Mont Terri. The Opalinus Clay contains approximately 30–80 % clay minerals and the best estimate of the overall mineralogical composition given in [% total dry weight] is: 23 % illite (15–30 %), 11 % illite/smectite mixed layers (5–20 %), 22 % kaolinite (15–37 %), 10 % chlorite (3–18 %), 14 % quartz (10–32 %), 2 % feldspar (0–6 %), 13 % calcite (4–22 %), and up to 5 % other minerals such as dolomite, siderite, pyrite, gypsum (Bossart and Thury, 2008). The bulk density of saturated Opalinus Clay is ~2.45 g/cm^3, the average water content is 6.6 wt.%, and the average total physical porosity is ~18 Vol.% (Bossart and Thury, 2008).

The orientation of rock-forming minerals is an important parameter in the determination of rock-specific properties affecting transport processes of fluids through a claystone formation. Due to the very small grain size of clay minerals, their orientation has been difficult to quantify (Wenk et al., 2008). Wenk et al. (2008) reported that the clay minerals in the Opalinus Clay show moderate to strong preferred orientation, while quartz is randomly orientated, and the calcite texture is variable. The orientation pattern of clay minerals in samples from Mont Terri is consistent with the complex geological processes of sedimentation, compaction, and tectonic deformation (Wenk et al., 2008). The microstructure of claystones is influenced largely by the amount and type of clay minerals present (Wigger and Van Loon, 2017). From their deposition to their compaction and deformation during diagenesis, clay-rich rocks undergo different stages alternating the properties of the rock. In the process, unconsolidated clay minerals stacked like a house-of cards with a high porosity become gradually oriented, preferentially perpendicular to the direction of the stress field (Bennett et al., 1981; Van Loon et al., 2004a). As a result, clay minerals become aligned and porosity diminishes by compaction due to overburden. Pores in the shaly facies in the Opalinus Clay are divided into micro- and macro-/mesopores in the range of 1–100 nm (Marschall et al., 2005; Philipp et al., 2017; Wigger and Van Loon, 2017), with a predominance of pore radii in the range between 10 and 50 nm and a mean pore length within the bedding plane of around 10 µm (Keller et al., 2011). Marschall et al. (2005) reported that 10–30 % of the pores in the Opalinus Clay have a pore radius of >25 nm. Philipp et al. (2017) observed that most pores are located within the clay matrix, whereas quartz, calcite, and feldspar contain only few isolated intragranular pores. N_2-adsorption experiments suggested a total physical porosity of the shaly facies in the Opalinus Clay of up to 24 vol.% (Keller et al., 2011; Houben et al., 2013) with approximately 10 vol.% in the <10 nm range (Keller et al., 2011). These findings indicated that the fine-grained clay matrix might consist of a considerable pore network with small pore radii. The 3D-structure of the pore space in Opalinus Clay was investigated by Keller et al. (2011). These authors visualized the spatial distribution of pore space, including pore path orientation, tortuosity, and length. Pore paths in Opalinus Clay exhibit relatively straight, elongated orientation (low tortuosity) within the bedding plane (Keller et al., 2011; Houben et al., 2013; Philipp et al., 2017). The spatial distribution of pores and their interconnectivity is a crucial parameter for transport processes in low-permeability rocks such as the Opalinus Clay (Van Loon et al., 2004a; Senger et al., 2013). The orientation of pores parallel and perpendicular to the bedding plane results in an anisotropy in the Opalinus Clay (Keller et al., 2011), meaning that (diffusive) transport processes are faster parallel to the bedding plane and slower perpendicular to it (Van Loon et al., 2004a). A comprehensive

understanding of anisotropic transport processes requires detailed information of the 3D-structure of pore space. Keller et al. (2011) observed that most pores in samples from the Opalinus Clay formation at Mont Terri appeared as non-connected objects. Due to a limitation in resolution (~10 nm), Keller et al. (2011) assumed that many pores might be interconnected by pathways smaller than 10 nm, which was confirmed by Houben et al. (2013). Due to the very small pore sizes, the Opalinus Clay has a very low permeability of 10^{-20} to 10^{-23} m^2 (Marschall et al. 2005; Villar et al. 2015; Philipp et al. 2017).

2.5. Pore water geochemistry

The investigation of geochemical parameters of Opalinus Clay pore water includes measurements of the E_h, pH, and salinity (Fernández et al., 2007). These are important e.g., for the solubility of radionuclides. Concentrations of dissolved ions and pore water-related parameters from different studies were compiled in Table 1.1. Different techniques used in the geochemical characterization of Opalinus Clay pore water (in situ measurements, sampling from boreholes, squeezing, and pore water displacement; Fernández et al., 2014; Mazurek et al., 2015; Mäder and Waber, 2017) demonstrated a good reproducibility. A recent study by Mazurek et al. (2023) investigated the pore water composition at Mont Terri, starting at weathered near-surface conditions, going deeper into the undisturbed Opalinus Clay. These authors confirmed a good (inter-)regional agreement between pore water data obtained from samples at ~40 m depth with other settings in the Opalinus Clay and contributed detailed information on the redox conditions and iron-bearing mineral phases in the Opalinus Clay (Mazurek et al., 2023).

Table 1.1: Concentrations of dissolved ions and pore water-related parameters in the Opalinus Clay at Mont Terri (St. Ursanne, Switzerland).

Parameter/ component	Thury and Bossart (1999)	Thury and Bossart (1999)	Fernández et al. (2007)	Mäder and Waber (2017)
Source	Borehole	Squeezing	Borehole	Displacement
EC [mS/cm]	-	-	26.2	-
pH	7.7	7.5	7.6	7.5
Eh [mV]	-	-	-24.2	-
Alkalinity (HCO_3^-) [mg/l]	203	77	280	-
Cl^- [mg/l]	10,800	9,970	11,800	9,000
Br^- [mg/l]	35	30	22	29
SO_4^{2-} [mg/l]	1,570	1,620	1,600	1,415
Na^+ [mg/l]	5,870	5,320	6,000	5,410
K^+ [mg/l]	76	30	80	67
Ca^{2+} [mg/l]	853	789	806	580
Mg^{2+} [mg/l]	420	502	395	361
Fe^{2+} [mg/l]	-	-	1.3	-
Sr^{3+} [mg/l]	35	47	37	35
Al^{3+} [mg/l]	<0.3	<0.3	<0.1	-
SiO_2 [mg/l]	-	-	8.3	-

2.6. Migration and transport of fluids and dissolved ions

Diffusion was identified as the main transport process in Opalinus Clay and is in the order of 10^{-14} to 10^{-10} m/s for the undisturbed rock (Rübel et al., 2002; Van Loon et al., 2003; Van Loon et al., 2005; Wersin et al., 2008; Mazurek et al., 2011; Jacops et al., 2017; Yuan and Fischer, 2022; Gonçalvès et al., 2023). The rate of diffusion depends on (I) the diffusion accessible porosity, (II) the pore geometry, and (III) a retardation factor, which depends on the chemical properties of the diffusing species as well as the surface characteristics of the pores (Keller et al., 2011). Natural tracers such as the noble gases $^4He_{(g)}$ and $^{40}Ar_{(g)}$ are present in clay formations for millions of years (Rübel et al., 2002; Mazurek et al., 2011), demonstrating that the migration of fluids in the Opalinus Clay is extremely slow. $^4He_{(g)}$ and $^{40}Ar_{(g)}$ are produced in situ by natural radiogenic processes and their distribution in the Opalinus Clay was validated by models (Rübel et al., 2002; Seltzer et al., 2021). Diffusion in clay-rich rocks is also affected by anion exclusion effects caused by negatively charged clay mineral surfaces (e.g., illite and illite/smectite mixed layers) repelling anionic compounds (Van Loon et al., 2003; Wersin et al., 2008; Wigger and Van Loon, 2017). Kaolinite and chlorite are almost uncharged clay minerals and, therefore, do not particularly affect the anion accessible porosity (Wigger and Van Loon, 2017). Thus, in addition to the pore size, also the surface charge within the pores significantly affects ion migration and limits the anion-accessible pore space. The surface charge depends

on the type of clay mineral and the pH of the pore water (Schoonheydt and Johnston, 2006). Chen et al. (2018a) observed only low retention of anionic organic compounds e.g., of the low-molecular-weight organic acid (LMWOA) anions propionate and butyrate, in through-diffusion experiments with Opalinus Clay. These authors concluded that a combination of anion exclusion by mineral phases and putative microbial activity might explain the migration pattern of LMWOA in Opalinus Clay.

2.7. Gas generation and gas migration in Opalinus Clay

Gas generation is part of the risk assessment for a HLW repository (Johnson et al., 2004) and is included in feature, events, and processes (FEP) catalogues (Lommerzheim et al., 2019), which provide a basis for safety cases for HLW repositories. Once gas pressure builds-up in a sealed repository it changes the properties of the engineered barriers, the host rock e.g., by the initiation of pore water displacement mobilizing radionuclides (Johnson et al., 2004; Senger et al., 2013). Research on gas generation in a HLW repository concentrated predominantly on the amount of molecular hydrogen ($H_{2(g)}$) that will be produced by the anaerobic oxidation of iron and reduction of water of steel components (waste containers, construction materials) in a repository (Johnson et al., 2004; Papafotiou and Senger, 2014; Diomidis et al., 2016; Jacops et al., 2017). The equation for the chemical reaction yielding H_2 is:

$$3Fe + 4H_2O \rightarrow Fe_3O_4 + 4H_{2(g)}$$
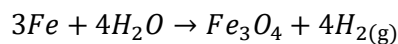
Diomidis et al. (2016) performed model-based calculations on gas generation in a repository in Opalinus Clay and found that by the end of the time frame for the safety assessment (10^6 years) only small amounts of CO_2 or CH_4 will be produced. Johnson et al. (2004) performed calculations of gas generation and compared those to the maximum diffusive loss into the surrounding rock. Their results demonstrated that diffusion alone cannot prevent gas pressure build-up in a repository. A model investigating the impact of the anaerobic corrosion of steel and subsequent generation of $H_{2(g)}$ in a HLW repository suggested that within 2000 years, gas pressures of 2–5 MPa will be reached (Papafotiou and Senger, 2014). Papafotiou and Senger (2014) concluded that the integrity of a repository in Opalinus Clay can be ensured at those pressures, because the gas pressure does not overcome the lithostatic pressure of the rock formation.

The natural inventory of gases in the Opalinus Clay consists of $CO_{2(g)}$, C_1–C_6 alkanes, nitrogen ($N_{2(g)}$), and noble gases (Pearson et al., 2003; Jockwer et al., 2007; Lerouge et al., 2015; Vinsot et al., 2017). As one potential origin of hydrocarbon gases and $N_{2(g)}$ in the Opalinus Clay at Mont Terri, deeper, organic-rich formations such as the Posidonia shale were suggested (Vinsot et al., 2017; Nakata and Tomioka, 2019). In situ gas generation in the Opalinus Clay was investigated by Jockwer et al. (2007), who conducted a heating experiment (100 °C for 18 months) in a borehole surrounded by additional monitoring boreholes. Carbon dioxide ($CO_{2(g)}$) was the predominant gas in the boreholes. An elevated concentration of bicarbonate (HCO_3^-) in pore water indicated carbonate mineral dissolution (Jockwer et al., 2007). In addition, hydrogen sulphide ($H_2S_{(g)}$) and C_1–C_4 hydrocarbon gases were detected.

In consolidated and water saturated claystones, gas migration is essentially related to the gas pressure in the claystone formation, the location of gas generation within the rock, the pore water pressure, and the confining rock stress (Johnson et al., 2004; Marschall et al., 2005; Senger et al., 2013). The swelling ability of the Opalinus Clay causes fractures to heal over time. Thus, fluid transport in the Opalinus Clay is restricted predominantly to the pore spaces in the rock (Senger et al., 2013). This also involves diffusion of gases dissolved in pore water. If a free gas phase forms, gas can displace pore water and flow through the pores. The term 'flow' might be misleading, since gas flow rates also depend on the pore structure and gas transport is expected to occur along the most conductive pathway, i.e. interconnected pores of >25 nm (Johnson et al., 2004; Marschall et al., 2005). For claystones, gas entry pressures for pores in the range of 0.4–18 MPa were measured for the gas to migrate through the rock (Harrington and Horseman, 1999; Marschall et al., 2005; Villar et al. 2015). Within the Opalinus Clay formation high capillary pressures in the range of 10 to 25 MPa prevail (Senger et al., 2013; Vinsot et al., 2017). Marschall et al. (2005) concluded that it is unlikely that the integrity of the Opalinus Clay as a host rock for HLW can be compromised by gas pressure build-up during the post-closure phase in a repository.

2.8. Migration of radionuclides in claystone

The migration of radionuclides in any host rock formation is probably the most important process that needs to be considered in a repository for HLW. The ability of the host rock to retain radionuclides is influenced by sorption, diffusion, and the characteristics of the pore water (Joseph et al., 2011). Sedimentary organic matter can reduce the mobility of radionuclides by providing additional binding sites to the solid phase, whereas dissolved organic compounds can enhance the transport of radionuclides as organo-radionuclide complexes (Santschi et al.,

2002; Courdouan et al., 2007; Cumberland et al., 2016; Dziadkowiec and Royne, 2020). One group of mobile organic carriers are humic acids, which are subject to mineral-organic interactions themselves (Davis, 1982; Hummel et al., 1999; Lippold and Lippmann-Pipke, 2009; Joseph et al., 2011; Bryan et al., 2012). The aqueous fluid pH was identified as an influencing parameter on the sorption and complexation behavior of (humic) organic compounds on mineral surfaces and with radionuclides (Arnarson and Keil, 2000; Lippold and Lippmann-Pipke, 2009). A change in pH affects metal adsorption in the presence of humic acid, as an increasing number of binding sites on mineral surfaces become available by deprotonation of surface hydroxyl groups (Lippold and Lippmann-Pipke, 2009; Joseph et al., 2011). Glaus et al. (2001) pointed out that only a low percentage of the Opalinus Clay dissolved organic matter (DOM) consists of humic acids. Based on UV-VIS spectra, these authors assumed that most of the organic matter is composed of low-molecular-weight compounds and/or macromolecules with only few ligand sites (Glaus et al., 2001). A representative of low-molecular-weight organic compounds are carboxylic acids. Wood (1993) assumed that trivalent rare earth elements can act as a model compound for radionuclides, simulating the interaction between low-molecular-weight organic acids (LMWOA) with a varying number of carboxylic groups. The results showed that monocarboxylic acids (e.g., acetic acid/acetate) expressed no or only weak interaction with the model compounds, suggesting that they are not involved in the mobilization/retardation of radionuclides (Davis, 1982; Wood, 1993; Kautenburger et al., 2019). Di- and polycarboxylic acids exhibited stronger interaction with the model compounds, indicating that they might also affect radionuclide mobility (Wood, 1993). The interaction of LMWOA with radionuclides is, in turn, affected by competing cations such as Ca^{2+} and Mg^{2+} (Wood, 1993). The effect of competing ions on radionuclide behavior in an aqueous solution was also observed for the sorption of radionuclides on mineral surfaces. Joseph et al. (2011) saw that Uranium (U(VI)) sorption on Opalinus Clay was low and not influenced by the presence of humic acid at a pH of 7.6. These authors attributed their observations to the formation of calcium-uranium complexes ($Ca_2UO_2(CO_3)_{3(aq)}$; see also Henning et al., 2020; Henning and Kühn, 2021). Joseph et al. (2011) emphasized that the speciation of radionuclides and (humic) acids is affected by the presence of dissolved ions such as Ca^{2+}, which is a prominent complex-forming compound (see also Surdam et al., 1984; Wood, 1993).

In the context of radionuclide migration, models based on experimental data and in situ measurements are indispensable for the long-term (10^6 Ma) performance assessment of a HLW repository. A model-based study by Henning and Kühn (2021) found that the migration of uranium in the shaly facies of the Opalinus Clay with a clay mineral content >50 wt.% would result in migration path lengths of 10–19 m over 10^6 Ma. Similar values were reported for the carbonate-rich facies, while migration path lengths of up to 35 m might be possible within the sandy facies (Henning and Kühn, 2021). Chen et al. (2022) investigated the diffusion of radionuclides in a model of the sandy facies of the Opalinus Clay. The observation period of only 2,000 years in the model cannot be transferred to the long-term safety aspect for HLW storage over the course of one million years. Nevertheless, Chen et al. (2022) observed increased distances covered by the diffusion of $Na^+_{(aq)}$ ions along inclined bedding planes (30° and 50°) compared to a horizontal orientation of the bedding plane.

2.9. Characterization of Opalinus Clay organic matter

Elie and Mazurek (2008) conducted experiments to characterize the geochemical properties of sedimentary organic matter in Opalinus Clay from northern Switzerland. According to these authors, the Opalinus Clay contains low amounts of organic matter of 0.1–1 wt.% with a low thermal maturity (T_{max} <435 °C; see also Pearson et al., 2003; Leu and Gautschi, 2012), which is typical for type III kerogens (Elie and Mazurek, 2008). Pyrolysis of sample material as well as GC–MS analyses of saturated hydrocarbons and C_{29}-sterane and C_{32}-hopane isomerization ratios led Elie and Mazurek (2008) to conclude that the Opalinus Clay contains mostly terrigenous organic matter deposited under oxidizing conditions. Due to the low organic matter content and low thermal maturity in Opalinus Clay, it is not considered as a source rock for oil and gas generation, which would be an exclusion criterion for a potential HLW repository site (mining activity for present or future resources; Leu and Gautschi, 2012).

Although most of the organic matter in claystones is associated with mineral phases, some of the organic matter is dissolved in the pore water. In the Opalinus Clay, dissolved organic matter (DOM) content ranges from 3 to 250 mg/L with a low humic and fulvic acid fraction (Glaus et al., 2001; Stroes-Gascoyne et al., 2007). Courdouan et al. (2007) performed anoxic aqueous extractions of Opalinus Clay to determine the amount and composition of the DOM. About 0.4 % of the total organic carbon was extractable and consisted predominantly of hydrophilic low-molecular-weight organic compounds (Courdouan et al., 2007). The LMWOA formate, acetate, and lactate were present in all extracts and in the pore water, accounting for nearly 40 % of the DOM (Courdouan et al., 2007).

In the context of organic matter characterization and source identification for minerals and organic molecules, stable carbon isotope values provide process-related information on carbon cycling in natural processes (Freeman et al., 1990; Clark and Fritz, 1997; Whiticar, 1999; Schubotz et al., 2011; Hoefs, 2015). The stable carbon isotope composition is generally reported as the ratio of $^{13}C/^{12}C$ in a sample compared to the ratio of $^{13}C/^{12}C$ in a standard of known composition. The so-called delta-notation ($\delta^{13}C$) expresses the isotopic composition of a sample in per mil [‰]. The equation is:

$$\delta^{13}C \ [‰] = \left(\frac{\left(\frac{^{13}C}{^{12}C} \right)_{sample}}{\left(\frac{^{13}C}{^{12}C} \right)_{standard}} - 1 \right) \times 1000$$

The Opalinus Clay contains different carbon-bearing compounds. Carbonate minerals such as calcite ($CaCO_3$) are ubiquitous in the claystone formation and their $\delta^{13}C$ values are between -2.0‰ and -0.2‰ (e.g., Pearson et al., 2003). When carbonate minerals dissolve in an aqueous fluid, they are present as dissolved CO_2-species ($CO_{2(aq)}$, $HCO_3^-{}_{(aq)}$, and $CO_3^{2-}{}_{(aq)}$) and their speciation distribution is pH-dependent. The dissolved CO_2-species are termed dissolved inorganic carbon (DIC). The stable carbon isotope composition of DIC is a mixed value based on the percentage of each species contributing to the overall signal at a given pH. The $\delta^{13}C_{DIC}$ in the in situ pore water in Opalinus Clay is between -16‰ to -9‰ (Pearson et al., 2003; Wersin et al., 2011). The stable carbon isotope composition of gaseous $CO_{2(g)}$ ($\delta^{13}C_{CO2}$) in the Opalinus Clay at Mont Terri of -15‰ to -10‰ limits the possible origins of $CO_{2(g)}$ to an equilibrium between dissolved CO_2 species (e.g., HCO_3^-) and carbonate minerals (Gaucher et al., 2010; Lerouge et al., 2015). The stable carbon isotope composition of hydrocarbon gases of -49‰ to -30‰ in Opalinus Clay points towards a thermogenic origin of these compounds (Pearson et al., 2003; Lerouge et al., 2015; Vinsot et al., 2017; Nakata and Tomioka, 2019). Lerouge et al. (2015) suggested that hydrocarbon gases represent a limited amount of dissolved gases that were initially generated in the rock formation during diagenesis. The organic matter in Opalinus Clay has a $\delta^{13}C$ in the range of -28‰ to -26‰ (Pearson et al., 2003).

2.10. Microbial activity in the Opalinus Clay

In the context of HLW disposal in claystone formations, microbial activity might affect the repository performance e.g., by the production of chelating agents, metal corrosion, mineral dissolution, changes in pH and E_h by metabolic activity, influencing radionuclide sorption and solubility and hence migration (Stroes-Gascoyne et al., 2007; Mitzscherling et al., 2023). Moreover, microorganisms are known to produce $CO_{2(g)}$ and $CH_{4(g)}$ (Whiticar, 1999; Martini et al., 2003) that could contribute to a pressure build-up in the post-closure phase of a repository. Mauclaire et al. (2007) investigated whether an active in situ microbial community is present in the Opalinus Clay at Mont Terri. These authors conducted incubation experiments and performed biomarker (phospholipid fatty acids) extractions. Based on their results, Mauclaire et al. (2007) concluded that mainly sulfate-reducing bacteria are present in the Opalinus Clay, which was confirmed by Stroes-Gascoyne et al. (2007) and Poulain et al. (2008). However, cell counts after several months were low (1 to 18×10^3 cells/ml media). Due to space and water shortage, Opalinus Clay is probably only inhabited by a small microbial community of mostly dormant microorganisms (Stroes-Gascoyne et al., 2007). The number of cells per gram dry weight based on biomarker data were estimated to be 5×10^6 cells per gram of dry claystone (Mauclaire et al., 2007; Poulain et al., 2008). Stroes-Gascoyne et al. (2007) suggested that the amount of nutrients to support growth of indigenous and non-indigenous microorganisms is sufficient to support a microbial community for two months. The microorganisms found in the Opalinus Clay (180–174 Ma) are similar to those encountered in modern analogues of recently deposited near-shore marine sediments where early diagenetic processes (e.g., sulfate-, iron-, and manganese reduction, fermentation, and methanogenesis) take place (Mauclaire et al., 2007). Libert et al. (2011) pointed out that molecular hydrogen (H_2) represents one of the most energetic substrates for microorganisms in deep subsurface environments, where extreme conditions (absence of oxygen, high temperature, high pressure, low organic matter content) prevail and only highly adapted microbes survive. There are striking similarities between the conditions in the deep biosphere (e.g., Inagaki et al., 2015; Heuer et al., 2020) and those expected in a HLW repository, suggesting that microbial life might be possible under repository conditions where high concentrations of H_2 are expected (Libert et al., 2011; Colwell and D'Hondt, 2013). In in situ tracer experiments with $H_{2(g)}$ in a borehole (Mont Terri URL), the disappearance of $H_{2(g)}$ was observed at rates from 2×10^{-4} to 3×10^{-4} mol/day/m^2, which was approximately 20-times more than the calculated rate for dissolution and diffusion of $H_{2(g)}$ (Vinsot et al., 2014). Based on the composition of water from the borehole, Vinsot et al. (2014) concluded that microbial activity involving hydrogen oxidation, sulphate reduction, and Fe(III)

reduction might be responsible for the observed rapid decrease in $H_{2(g)}$. The presence of an active hydrogenotrophic microbial community in Opalinus Clay was confirmed by Bagnoud et al. (2016a, 2016b).

2.11. (Bio-) Geochemical processes in a claystone host rock

The previous paragraphs frame a portrait of the Opalinus Clay, consisting of numerous and complex processes and parameters that are strongly interconnected. A visualization of some of these processes occurring in the water-saturated Opalinus Clay can be seen in Figure 1.4.
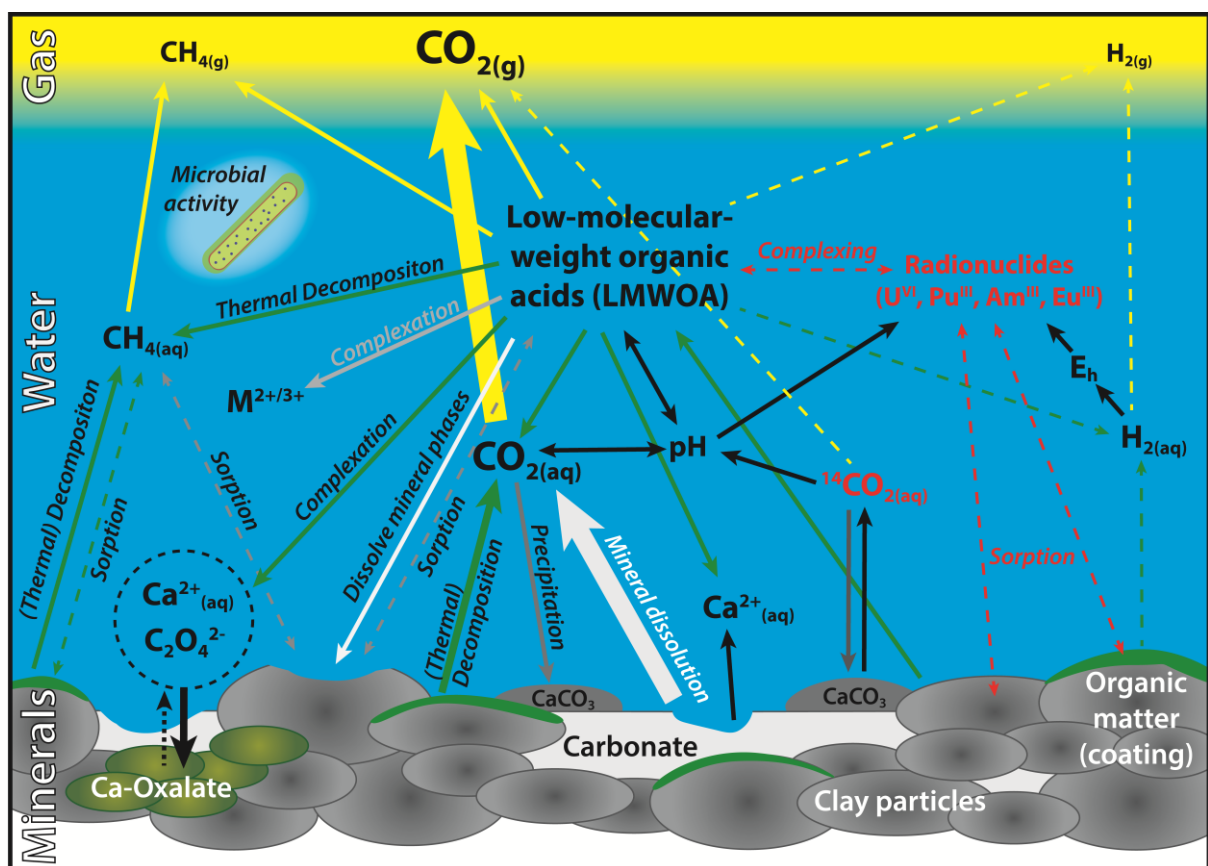
Figure 1.4: Schematic overview of processes in the organic matter–minerals–water system in a claystone (based on an illustration by Christian Ostertag-Henning, BGR). The stratified representation of separate phases is a strong simplification of processes that actually take place in the pore spaces of claystones.

3. Thermal transformation of organic matter

3.1. The classical model vs. geocatalysis

In classical geological models, the generation of oil and gas results from the breaking of C–C carbon bonds in complex, higher-molecular-weight organic matter at elevated temperatures during basin evolution (Tissot and Welte, 1978; Hunt, 1996). In this process, the chemical reactions yielding oil and gas are kinetically-controlled processes that are irreversible and depend on parameters including time, temperature, and the composition of the organic matter (Seewald, 2003). The generation of oil occurs between 50 and 150 °C (Tissot and Welte, 1978; Hunt, 1984; Surdam et al., 1984; Quigley and Mackenzie, 1988; Seewald, 2003), whereas thermogenic gas generation takes place between 150 and 220 °C (Hunt, 1984; Quigley and Mackenzie, 1988). An illustration of the classical geological model and complementary perspectives are presented in Figure 1.5.

Galimov (1988) questioned the classical geological view on the transformation of complex, immature, terrestrial organic matter to methane, stressing that there was a discrepancy between the classical model assuming burial depths of ≥4 km and relatively shallow natural gas reservoirs (1.5–3 km) where temperatures must have been well below those in the models. Although the thermal decomposition of constituents of petroleum bears the potential for gas generation, Mango and Hightower (1997) found that lab-based experiments aiming to simulate this process failed to reproduce high contributions of methane in the gas mix. In addition to the classical geological model, the impact of 'geocatalytic' materials (Ma et al., 2018) yielding high amounts of methane was considered. Examples for this are reactions of oil-constituents and kerogen with transition metals such as Ni, Cr, Fe, or Co (Mango, 1992, 1996; Mango and Hightower, 1997). Clay minerals were also considered to have geocatalytic properties. Fripiat and Cruz-Cumplido (1974) described clay minerals as a salt of a weak acid surrounded by an electrostatic field, potentially initiating the transformation of organic molecules in the presence of water. Recent studies on geocatalytic properties of clay minerals investigated the transformation of organic matter by pyrolysis experiments. Bu et al. (2017) conducted pyrolysis experiments in gold capsules (350 °C) with organic molecules ($\geq C_{18}$) in the presence of montmorillonite. Bu et al. (2017) demonstrated that montmorillonite acts as a weak acid, which promotes the transformation of organic molecules, also enhancing yields of hydrocarbon gases.

Ma et al. (2018) showed that the presence of geocatalytic materials such as smectite, iron, and pyrite resulted in higher gas yields in heating experiments with kerogen isolates. Rahman et al. (2018) found that the closer organic matter and clay minerals were spatially associated with

each other, the lower were activation energies derived from pyrolysis experiments, supporting the effectiveness of clay minerals as geocatalytic materials. The implications of the data were a reduction of temperatures for organic matter transformation during diagenesis by approximately 20 °C (Rahman et al., 2018). Ma et al. (2021) conducted heating experiments with immature to early mature claystone sample material at comparatively low temperatures between 80 °C and 120 °C for up to 38 months. These authors suggested that the amounts of $CO_{2(g)}$ and methane generated in the experiments were closely related to the geocatalytic properties of the sample material (Ma et al., 2021). The studies cited above highlight the role of clay minerals in organic matter transformation processes at elevated temperatures. All three components, organic matter, clay minerals, and elevated temperatures are included in scenarios for the disposal of high-level, heat-emitting nuclear waste (HLW) and are complemented by liquid water as an additional and important factor in chemical reactions. Thus, it is essential to investigate chemical reaction processes in the system organic matter–clay minerals–water at elevated temperatures with sample material from potential host rock formations.

3.2. Experimental studies at elevated temperatures

The concurrence of low-molecular-weight organic acids (LMWOA) in oil-field waters with petroleum source rock formations set off a great interest in these acids as potential indicators for oil reservoirs (Carothers and Kharaka, 1978; Barth, 1987; Means and Hubbard, 1987; MacGowan and Surdam, 1988; Seewald and Seyfried, 1991; Borgund and Barth, 1993; Kharaka et al., 1993b). In this context, heating experiments (dry and hydrous pyrolysis) became a powerful tool to investigate the transformation of organic matter as well as the generation potential of source rocks for organic compounds, including LMWOA, hydrocarbon gases, and $CO_{2(g)}$ (Lewan et al., 1979; Kharaka et al., 1983; Kawamura et al., 1986; Eglinton et al., 1987; Kawamura and Kaplan, 1987; Lundegard and Senftle, 1987; Barth et al., 1988; Barth et al., 1989; Kharaka et al., 1993a; Andresen et al., 1994; Borgund and Barth, 1994; Knauss et al., 1997; Lewan, 1997; Seewald et al., 1998; Seewald, 2001a; Lewan et al., 2014; Song et al., 2021).
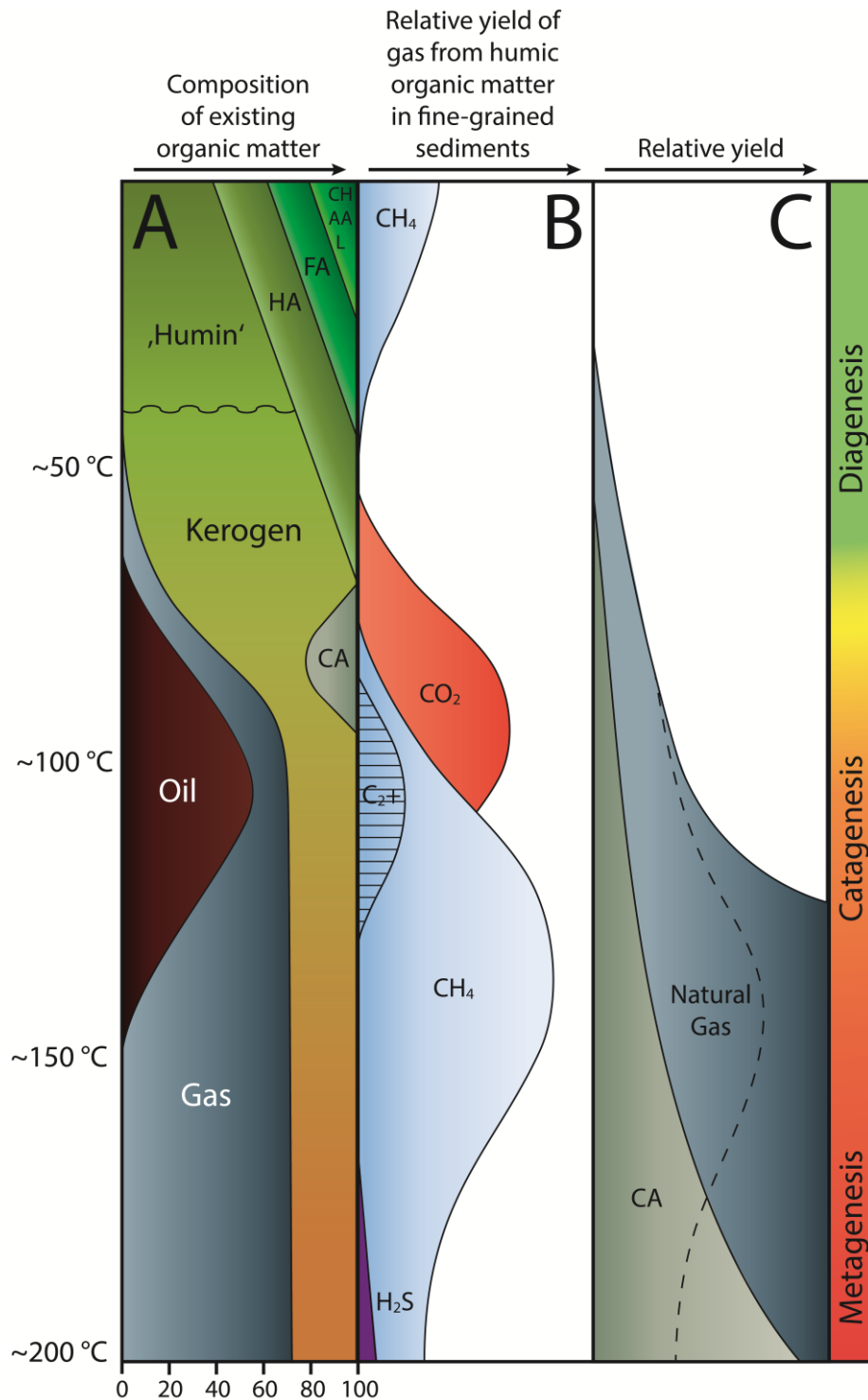
Figure 1.5: Schematic visualization of the transformation of organic matter during basin evolution/burial of sediments. The temperatures on the y-axis are approximate values referring to potential subsurface conditions. (A) Classical geological model (modified after Tissot and Welte, 1978 and Surdam et al., 1984). AA = amino acids; CA = carboxylic acids; CH = carbohydrates; FA = fulvic acids; HA = humic acids; L = lipids. (B) Relative yields of gas generation from humic organic matter (modified after Hunt, 1979). (C) Relative yields of natural gases and low-molecular-weight organic acids (CA = carboxylic acids), emphasizing the impact of water and minerals, extending the generation potential for natural gases and CA beyond the range indicated by the classical model (modified after Seewald, 2003).

24

Moreover, the effect of LMWOA on mineral dissolution and secondary porosity in source rocks was investigated on the basis of pyrolysis experiments (Lundegrad et al., 1984; Surdam et al., 1984; Bevan and Savage, 1989; Lundegrad and Land, 1989; MacGowan and Surdam, 1990; Barth and Bjørlykke,1993; Small, 1994). The use of hydrous pyrolysis experiments was also extended to processes encountered in hydrothermal environments such as in the Guaymas Basin (Thornton and Seyfried, 1987; Seewald et al., 1990) and at vent systems (McCollom and Seewald, 2001a, 2006, 2007; Seewald et al., 2006). The advantage of lab-based pyrolysis experiments at high temperatures is the acceleration of geochemical reactions, which usually take thousands to millions of years, to durations of hours, days, weeks, or months.

For dry and hydrous pyrolysis experiments, a large set of different reaction vessels is available, including glass tubes (Crossey, 1991; Ong et al., 2013; Wei et al., 2018), stainless steel vessels (Kharaka et al., 1983; Lewan, 1983; Stalker et al., 1994; McCollom et al., 1999; Lewan et al., 2014), titanium vessels (Palmer and Drummond, 1986; Truche et al., 2009; Wu et al., 2016; Li et al., 2017; Li et al., 2018), gold capsules (Landais and Monthioux, 1988; Freund et al., 1993; Ko et al., 2016; Bu et al., 2017; Yang et al., 2018; Wei et al., 2019), and flexible gold-titanium reaction cells (gold bags; Seyfried et al., 1987; Small, 1994; Seewald, 1996; McCollom and Seewald, 2003a, 2003b; McCollom et al., 2010, 2020; Hawkes et al., 2016; Song et al., 2021; Helten et al., 2022). The vessel materials can affect the chemical reactions within them significantly e.g., by catalysis (e.g., Kharaka et al., 1983). Titanium oxide (TiO_2) and gold are, to a large extent, chemically inert and, therefore, well-suited for pyrolysis experiments (Seyfried et al., 1987). Heating and hydrous pyrolysis experiments were also used to obtain kinetic parameters for organic matter transformation reactions including gas generation and the generation/decomposition of LMWOA (Palmer and Drummond, 1986; Barth et al., 1989; Crossey, 1991; Barth and Nielsen, 1993; Bell et al., 1994; Knauss et al., 1997; McCollom and Seewald, 2003a, 2003b; Li et al., 2017; Li et al., 2018) and to investigate mineral dissolution and precipitation (Dickson et al., 1963; Knauss et al., 1985, 1987; Sauer et al., 2020). An overview of different heating experiments is provided in Table 1.2.

In the context of HLW disposal it is worthwhile to mention that there is a number of experimental studies that also looked into the transformation of organic matter by irradiation (Lewan and Buchardt, 1989; Lewan et al., 1991; Ostertag-Henning, 2019; Naumenko-Dèzes et al. (2022); Wang et al., 2022a). This process also contributes to gas generation in a HLW repository.
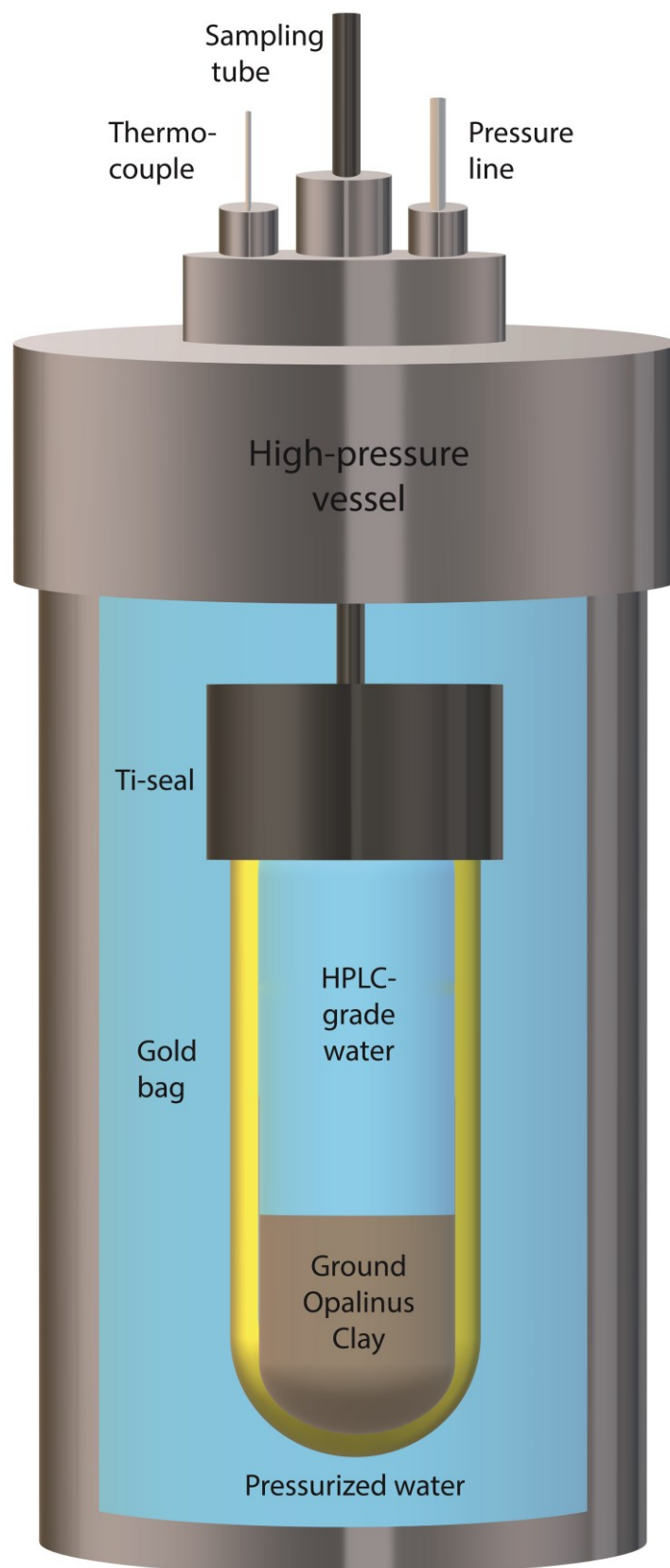
Figure 1.6: Schematic visualization of the experimental setup for hydrous pyrolysis experiments with ground Opalinus Clay in a flexible gold-titanium reaction cell (gold bag) placed in a high-pressure vessel. For the experiments, the vessel is also equipped with a heating sleeve.

Table 1.2: Overview of heating experiments with source rocks, oils, kerogen isolates, coals, and low-molecular-weight organic acid (LMWOA) solutions. Data is presented chronologically. This compilation is not aiming for completeness.

General aim	Vessel Material	Headspace	Temperature [°C]	Pressure [MPa]	Time [h]	Sample material / compound	Total organic carbon (TOC) [wt.%]	Other compounds	Literature
Thermal decomposition of LMWOA	Stainless steel	He	200–300	1.5, 8.5	≤4393	Acetic acid			Kharaka et al. (1983)
Generation of LMWOA	Pyrex glass tubes		200–300		≤1000	Green River Shale Kerogen, Monterey Shale Kerogen		Montmorillonite, Illite, Calcite, H_2O	Kawamura et al. (1986)
Thermal decomposition of LMWOA	Gold, stainless steel, titanium, titanium alloy, fused quartz tubes, pyrex tubes	Some with Ar	300–440		≤2653.5	Acetic acid, sodium acetate			Palmer and Drummond (1986)
Generation of LMWOA and gases	Stainless steel	Air	250–360	11.5–30	72	Kimmeridge Clay (Dorset), HRZ (Alaskan North Slope)	6–54		Cooles et al. (1987)
Generation of LMWOA	Stainless steel	N_2	250–330	VP*	≤720	Kimmeridge Kerogen		Limonite	Eglinton et al. (1987)
Generation of LMWOA	Pyrex glass tubes	N_2	200–400	VP*	≤1000	Green River Shale Kerogen, Monterey Shale Kerogen		Montmorillonite, Illite, Calcite, H_2O	Kawamura and Kaplan (1987)
Generation of LMWOA and gases	Stainless steel	He	250–350	4–16.3	≤360	Non-marine carbonaceous shale	4–8		Lundegard and Senftle (1987)

27

General aim	Vessel Material	Headspace	Temperature [°C]	Pressure [MPa]	Time [h]	Sample material / compound	Total organic carbon (TOC) [wt.%]	Other compounds	Literature
Generation of LMWOA	Stainless steel	N₂, He, H₂O	200–350	VP*	72	Kimmeridge Oil Shale (Dorset), Coaly Shale(Norwegian Continental Shelf), Coal (Norwegian Continental Shelf), Kimmeridge Clay (Norwegian Continental Shelf)	5–40		Barth et al. (1988)
Thermal decomposition of LMWOA	Borosilicate glass	N₂	160–200	1–2.8	24–96	Oxalic acid	13	pH buffer, salts	Crossey et al. (1991)
Generation of LMWOA	Stainless steel	N₂, He, H₂O	200–350	VP*	72	Kimmeridge Oil Shale (Dorset)			Barth et al. (1989)
Generation of LMWOA and gases	Stainless steel	N₂, H₂O	280–350	VP*	72	Kimmeridge Clay (Dorset), Kimmeridge Clay (North Sea), Heather (North Sea), Coaly Shale(Norwegian Continental Shelf), Coal (Norwegian Continental Shelf), Brent Coal (Norwegian Continental Shelf), Brown Coal (Western Germany)	5–70		Barth and Bjørlykke (1993)
Generation of LMWOA	Gold-plated vessel + tubing	Ar	200–300	2–11	≤20240	Lower-oxygen oil Kirkuk field (Iraq), High-oxygen Obispo Shale oil Midway Sunset field San Joaquin Valley (California, U.S.),			Kharaka et al. (1993)
Generation of LMWOA and gases	Stainless steel	N₂, H₂O	150–365	VP*	≤456	Brown Coal (Germany), Coal (Ness Formation North Sea), Kimmeridge Clay	51–61		Andresen et al. (1994)

General aim	Vessel Material	Headspace	Temperature [°C]	Pressure [MPa]	Time [h]	Sample material / compound	Total organic carbon (TOC) [wt.%]	Other compounds	Literature
Thermal decomposition of LMWOA	Gold-titanium reaction cell, Titanium, Quartz glass	Some with Ar	335–355	≤40	≤5637.5	Acetic acid; sodium acetate		Quartz, fused quartz, calcite, natural pyrite, titanium oxide and gold, pyrex glass, Ca-montmorillonite, Fe-bearing montmorillonite, hematite, synthetic pyrite, magnetite	Bell et al. (1994)
Generation of LMWOA	Stainless steel	N_2, He, H_2O	260–350	VP*	72	Petroleum/oil		Quartz, Carbonate (Denmark), Carbonate (Rhodes)	Borgund and Barth (1994)
Generation of LMWOA and gases; thermal decomposition of LMWOA	Gold-titanium reaction cell	None	270–330	30–60	≤3024	New Albany and Phosphoria Shales	11–17		Knauss et al. (1997)
Thermal decomposition of LMWOA	Hastelloy C-276	He	320–500	18–30.7	≤0.2	Formic acid			Yu and Savage (1998)
Generation of LMWOA	Stainless steel, Hastelloy-C	He	200–365	VP*	72	Green River Mahogany Shale, Green River Black Shale, New Albany Shale, Ghareb (Israel), Ghareb (Jordan), Wilcox Coal	6–58		Dias et al. (2002)
Thermal decomposition of LMWOA	Gold-titanium reaction cell		175–260	35	≤2951	Formic acid, formate		NiFe-powder, ground olivine, hematite, magnetite	McCollom and Seewald (2003a)
Thermal decomposition of LMWOA	Gold-titanium reaction cell		325	35	≤3811	Acetic acid, sodium acetate, valeric acid		Hematite + magnetite + pyrite, pyrite + pyrrhotite + magnetite, hematite + magnetite	McCollom and Seewald (2003b)

General aim	Vessel Material	Headspace	Temperature [°C]	Pressure [MPa]	Time [h]	Sample material / compound	Total organic carbon (TOC) [wt.%]	Other compounds	Literature
Thermal decomposition of LMWOA	Fused silica capsules		250	VP*	<72	Formic acid, acetic acid			Ong et al. (2013)
Mineral-water interaction	Gold–titanium reaction cell	None	200–300	15	≤4400	Opalinus Clay, Wyoming bentonite	~1	Synthetic pore water, Fe_3O_4, Fe^0, different types of steel, Cu-foil	Sauer et al. (2020)
Generation of gases	Pyrex glass tubes	None	80–120		<28.000	New Albany Shale, Second White Specks Formation, Springfield Coal	4–69	Na_2SO_3 (oxygen scavenger)	Ma et al. (2021)

*VP = vapor pressure (water vapor + initial headspace gas + generated gases at the experimental temperature)

Hydrous pyrolysis experiments with source rocks or kerogen demonstrated that chemical reaction processes in the system organic matter–minerals–water at elevated temperatures with sample material from clay-rich rocks yield low-molecular-weight organic compounds such as hydrocarbon gases and LMWOA. Wei et al. (2018) demonstrated that gas generation from organic matter takes place at temperatures as low as 60 °C and Helten et al. (2022) found that LMWOA were already produced at 80 °C. Both temperatures are well within the range of temperatures that are expected in a HLW repository (up to 160 °C at the container surface and up to 90 °C in the host rock formation; Johnson et al., 2002; Delage et al., 2010). Most studies cited above performed hydrous pyrolysis at temperatures of 200–350 °C (Table 1.2), which is significantly higher than the temperature conditions expected in a HLW repository. Moreover, many of these studies used sample material with a high organic matter content. Therefore, a lack of quantitative data exists for organic matter transformation at temperatures that are to be expected in a HLW repository (<<200 °C).

Chapter II

1. Scope and outline

1.1. Thesis objectives

Time, temperature, the availability of water, the presence of different mineral phases, and the type and amount of organic matter affect the generation of oil, hydrocarbon and non-hydrocarbon gases, and low-molecular-weight organic acids. There are distinct similarities between the natural transformation of organic matter in geological processes and in the human-made deep geological disposal of high-level, heat-emitting nuclear waste (HLW) in claystone formations. Both environments encompass the above mentioned 'ingredients' needed for organic matter transformation to take place. In the Opalinus Clay, most studies focused on thermo-hydro-mechanical (THM) changes. There is, however, also a chemical component to the changes in a host rock formation, which is included in the term thermo-hydro-mechanical-chemical (THMC) processes. However, the chemical component addressed predominantly mineralogical aspects and the composition of the pore water in the Opalinus Clay. Only very few studies have been undertaken to establish a link between the temperature conditions that are expected after the emplacement of HLW in Opalinus Clay and relevant temperature conditions for the transformation of organic matter. The previous chapter showed that experimental studies investigating the transformation of organic matter in a divers set of source rocks high in organic carbon (OC) content chose short experimental times and high temperatures (>>200 °C). As a result, there is a significant lack of lower temperature quantitative data for OC-lean clay-rich rocks such as the Opalinus Clay, the chosen host rock for HLW in Switzerland and a candidate host rock for HLW in Germany.

In the broader context of nuclear waste disposal, Diomidis et al. (2016) pointed out that:

'In order to estimate the impact of organic materials on gas generation, it is necessary to assess their stability and the degradation mechanisms that may occur under repository-relevant conditions. However, only limited relevant empirical data regarding the stability and degradation mechanisms of organic compounds is currently available from experiments, since the majority of the organics degrade very slowly and because experimental conditions are often not comparable with those expected in the repository.'

It is known and accepted that gas generation is a safety-relevant parameter for the post-closure phase in a HLW repository. Our knowledge on gas generation from organic matter in the Opalinus Clay – a representative claystone for HLW disposal projects – is, however, still very limited and the underlying chemical reactions and processes have not been identified and contextualized.

The aim of this thesis was to provide quantitative data on organic matter transformation reactions in the system organic matter–minerals–water in the Opalinus Clay at elevated temperatures relevant to the deep geological disposal of HLW. Data on the stable carbon isotope composition of reactants and kinetic parameters were utilized to establish a link between reaction products and the mineralogical inventory and the organic matter composition in the Opalinus Clay. Hydrous pyrolysis experiments were conducted in flexible gold-titanium reaction cells (gold bags) at temperatures ranging from 80–200 °C, simulating temperature conditions in the post-closure phase of a HLW repository – and beyond.

Chapter III addresses the thermal transformation of Opalinus Clay organic matter and the dissolution of carbonate minerals as sources for hydrocarbon and non-hydrocarbon gases. The generation of gases from organic matter at elevated temperatures as well as the dissolution of carbonate minerals releasing $CO_{2(g)}$ are well-known processes in the natural environment. Having said that, the overlap between natural processes at elevated temperatures e.g., in sedimentary basins, and heat-emission from HLW has been overlooked. The release/generation of CO_2 by carbonate mineral dissolution at elevated temperatures has been underestimated as a source of (gaseous) CO_2 in the Opalinus Clay. Stable carbon isotope data ($\delta^{13}C$) was used to establish a link to the sources of the

generated hydrocarbon and non-hydrocarbon gases. Kinetic parameters, i.e. activation energies and frequency factors) complement the data set.

Research questions addressed in Chapter III were:

- *What is the molar amount of hydrocarbon and non-hydrocarbon gases released/generated by hydrous pyrolysis of Opalinus Clay?*
- *What are the sources of hydrocarbon and non-hydrocarbon gases in the hydrous pyrolysis of Opalinus Clay?*
- *Is the generation of hydrocarbon and non-hydrocarbon gases in the Opalinus Clay controlled by temperature-controlled reaction kinetics?*
- *What might be consequences arising for the integrity of a HLW repository facility in Opalinus Clay from the gas generation experiments?*

Chapter IV explores the thermal transformation of Opalinus Clay organic matter to low-molecular-weight organic acids (LMWOA). LMWOA are associated with mineral dissolution reactions and metal ion complexation. LMWOA represent a large portion of the dissolved organic matter (DOM) in Opalinus Clay pore water and are produced by thermal decomposition of organic matter and microbial respiration. LMWOA and their corresponding acid anions express compound-specific thermal stabilities, affecting the impact a LMWOA might have on mineral dissolution processes in the Opalinus Clay. Moreover, the thermal decarboxylation of LMWOA is known to produce gases such as $CH_{4(g)}$ and $CO_{2(g)}$. Kinetic parameters from the literature were employed to assess the gas generation potential of the predominant LMWOA in Opalinus Clay. At elevated temperatures, the generation and decomposition of LMWOA proceed simultaneously. The comparison of reaction rates demonstrated that the decomposition of some LMWOA exceeds their generation rates, thus, limiting the impact of individual LMWOA e.g., on mineral dissolution.

Research questions addressed in Chapter IV were:

- *What is the quantity of low-molecular-weight organic acids generated by hydrous pyrolysis of Opalinus Clay?*
- *To which extent is the net-generation of the low-molecular-weight organic acids affected by simultaneous thermal decarboxylation reactions?*
- *What is the quantity of $CO_{2(g)}$ and hydrocarbon gases generated by simultaneous decarboxylation reactions of low-molecular-weight organic acids during hydrous pyrolysis of Opalinus Clay?*
- *What might be consequences arising for the integrity of a HLW repository facility in Opalinus Clay from LMWOA-initiated processes including mineral dissolution reactions at elevated temperatures?*

Chapter V investigates the interaction between the low-molecular-weight organic acids (LMWOA) acetate and oxalate with Opalinus Clay mineral phases in a suspension. Organic compounds are known to occupy sorption sites on clay mineral surfaces. LMWOA are a major constituent of dissolved organic matter (DOM) in Opalinus Clay pore water. Therefore, the behavior of acetate and oxalate in a suspension containing Opalinus Clay materials was assessed quantitatively. The experiments were designed following an extensive upstream testing phase. The final approach included an equilibration step between ground Opalinus Clay and water, followed by the addition of acetate and oxalate spike solutions, and short sampling intervals to exclude bias by microbial activity. The experiments were conducted in an overhead shaker at room temperature (~20 °C). Research question addressed in Chapter V was:

- *What is the quantity of acetate and oxalate retained by Opalinus Clay mineral phases in a suspension at room temperature?*
- *What might be consequences arising for the integrity of a HLW repository facility (e.g., radionuclide mobility) in Opalinus Clay?*

1.2. Contributions to publications

1.2.1　As first author

Chapter III: Generation and decomposition of low-molecular-weight organic acids in hydrous pyrolysis experiments with Opalinus Clay rock

Oliver Helten, Christian Ostertag-Henning, Wolfgang Bach, Kai-Uwe Hinrichs

Published in *Organic Geochemistry (172) 104481*

C.O.-H. and O.H. designed the research; O.H. conducted the lab work; BGR technical staff performed the sample measurements; O.H. and C.O.-H. performed the data analysis; W.B. contributed to the research with additional data; O.H. wrote the manuscript with contributions from all co-authors.

Chapter IV: Thermally induced release and generation of gaseous $CO_{2(g)}$ and C_1–C_4 hydrocarbons in Opalinus Clay from Mont Terri (Switzerland)

Oliver Helten, Christian Ostertag-Henning, Wolfgang Bach, Kai-Uwe Hinrichs

In preparation for *Applied Geochemistry*

C.O.-H. and O.H. designed the research; O.H. conducted the lab work; W.B. performed the thermodynamic calculations; BGR technical staff performed the sample measurements; O.H. and C.O.-H. performed the data analysis; O.H. wrote the manuscript with contributions from all co-authors.

Chapter V: Interactions between mono- and dicarboxylic low-molecular-weight organic acids and Opalinus Clay mineral phases in suspension

Oliver Helten, Christian Ostertag-Henning

In preparation for *t.b.d.*

O.H. and C.O.-H. designed the research; O.H. conducted the lab work; BGR technical staff performed the sample measurements; O.H. performed the data analysis; O.H. wrote the manuscript with contributions from C.O.-H.

1.2.2 As co-author

Using Flexible Gold-Titanium Reaction Cells to Simulate Pressure-Dependent Microbial Activity in the Context of Subsurface Biomining

Christian Ostertag-Henning, Ruiyong Zhang, Oliver Helten, Thomas Weger, Axel Schippers

Published in *Journal of Visualized Experiments (152), e60140*

R.Z., A.S., and C.O.-H. designed the original research, C.O.-H., R.Z., O.H., T.W., and A.S. designed the filming of lab work with substantial contributions of Niels Wölki (BGR); O.H. and C.O.-H. wrote the script for the video; O.H. spoke the commentary; Niels Wölki (BGR) and O.H. conducted the editing of the video; C.O.-H. wrote the manuscript with contributions from all co-authors.

1.2.3 Milestone reports (R+D Nuclear Waste Disposal) for the Federal Institute for Geosciences and Natural Resources (BGR), Hannover

Gasbildung aus verschiedenen Wirtsgesteinen – Zwischenbericht MS09
Oliver Helten and Christian Ostertag-Henning (Report B3.5/B50112-18/2019-0003/001; 2019)

Bildung polarer wasserlöslicher organischer Verbindungen – kurzkettiger organischer Säuren – in Wirtsgesteinen unter Temperatureinfluss
Oliver Helten (Report B3.5/B50112-18/2020-0002/001; 2020)

Beschreibung eines standardisierbaren experimentell-analytischen Verfahrens zur Untersuchung der Gasbildung in Wirtsgesteinen - Zwischenbericht MS11
Oliver Helten and Christian Ostertag-Henning (Report B3/B50112-18/2022-0002/001; 2022)

Chapter III

Generation and decomposition of low-molecular-weight organic acids in hydrous pyrolysis experiments with Opalinus Clay rock

Oliver Helten[a,b]*, Christian Ostertag-Henning[a], Wolfgang Bach[b,c], Kai-Uwe Hinrichs[b,c]

[a]Federal Institute for Geosciences and Natural Resources (BGR), 30655 Hannover, Germany

[b]Faculty of Geosciences, University of Bremen, 28334 Bremen, Germany

[c]Center for Marine Environmental Sciences (MARUM), University of Bremen, 28334 Bremen, Germany

*Corresponding author. E-mail address: helteno@uni-bremen.de

Abstract

Increasing temperature in claystone formations accelerates geochemical reactions between organic matter, water and mineral phases, promoting the generation and decomposition of organic compounds such as low-molecular-weight organic acids (LMWOA). LMWOA presence in claystone formations can enhance mineral dissolution, stimulate gas generation through thermal decomposition reactions, affect metal-ion complexation, alter sorption processes, and provide feedstock for microbial life. Hydrous pyrolysis experiments (80–200 °C and 20 MPa) using Dickson-type flexible gold-titanium reaction cells were conducted to investigate the thermal generation and decomposition of LMWOA in organic matter poor (0.64 wt.%) Opalinus Clay. Maximum concentrations of dominant species were 44 µmol/kg clay formate (120 °C), 310 µmol/kg clay acetate (200 °C), and 74 µmol/kg clay oxalate (120 °C). Calculated half-live ranges of the dominant compounds were between 8.88×10^{10} and 2.81×10^{-3} years for the experimental conditions. Comparison of observed and calculated reaction rates suggest that the thermal generation and decomposition of LMWOA proceed simultaneously. Therefore, the observed generation rates in these – and other previously published – experiments are minimum estimates that need to be corrected for parallel decomposition reactions. The new quantitative reaction rate data presented here facilitates modelling of production/decomposition and local pore water concentrations of LMWOA by the extrapolation of kinetic data to temperatures encountered for example in natural heating during subsidence or by thermal intrusions.

1. Introduction

Low-molecular-weight organic acids (LMWOA) with one to five carbon atoms (Hatton, 1982; Fisher, 1987) are ubiquitous compounds in the natural environment. These acids contain at least one carboxyl group (R-COOH, where R represents the molecule's alkyl group; Dias et al., 2002). LMWOA are common constituents of aqueous fluids in many geological settings including oil-producing formations (Carothers and Kharaka, 1978; Hanor and Workman, 1986; Seewald, 2001b; Orem et al., 2014; Engle et al., 2020; Varonka et al., 2020), hypersaline brines (Kawamura and Nissenbaum, 1992), lacustrine environments (Miller et al., 1979; Heuer et al., 2009; Conrad et al., 2014, 2020), marine environments (Sansone and Martens, 1982; Shaw et al., 1984; Ijiri et al., 2012; Zhuang et al., 2019a, 2019c), and hydrothermal systems (Martens, 1990; Lang et al., 2010; McDermott et al., 2015; Zhuang et al., 2019b). LMWOA are energy substrates for microbial communities, even at elevated temperatures (Horsfield et al., 2006; Takai et al., 2008; Heuer et al., 2020) and are important compounds in the deep biosphere (Wellsbury et al., 1997; Vieth et al., 2008; Heuer et al., 2020).

LMWOA account for up to 80% of the dissolved organic carbon in aqueous fluids such as formation waters (≤98 °C; Kharaka et al., 1985), with acetic acid and acetate as the predominant compounds (Carothers and Kharaka, 1978; Barth, 1991; Heuer et al., 2009, 2020; Glombitza et al., 2019). At standard conditions and a pH-value of >5, LMWOA in aqueous solutions are mainly present as their dissociated acid anions (Means and Hubbard, 1987). Concentrations of LMWOA in aqueous fluids depend on both, thermal and biological generation and decomposition as well as the miscibility of aqueous fluids (Means and Hubbard, 1987). Concentrations of LMWOA in temperate terrestrial and marine environments (≤25 °C) usually are in the order of several micromoles per liter (Albert and Martens, 1997; Courdouan et al., 2007; Mäder and Waber, 2017; Glombitza et al., 2019), but can also reach millimolar levels at elevated temperatures (≥80 °C and >500 m below the (seafloor's) surface; Carothers and Kharaka, 1978; Heuer et al., 2020).

LMWOA are relevant for geochemical processes including mineral dissolution (Lundegard et al., 1984; Surdam et al., 1984; Bennet and Siegel, 1987; Bevan and Savage, 1989; Welch and Ullman, 1993, Ulrich and Bower, 2008; Strąpoć et al., 2011; Li et al., 2021a), metal ion complexation (Harrison and Thyne, 1992), water-mineral interaction

(i.e., sorption processes; Davis, 1982; Kubicki et al., 1999; Rasamimanana et al., 2017), and the generation of natural gas (Carothers and Kharaka, 1978; Kharaka et al., 1983). LMWOA can originate from the thermal decomposition of high-molecular organic matter such as kerogen during diagenesis (Tissot and Welte, 1978; Surdam et al., 1984; Lewan and Fisher, 1994).

The rate of the thermal decomposition of LMWOA increases with increasing temperature (Palmer and Drummond, 1986; Crossey, 1991; Bell et al., 1994; McCollom and Seewald, 2003a). A common thermal decomposition pathway of LMWOA is decarboxylation, here exemplified for acetate in an aqueous solution:

$$CH_3COO^-_{(aq)} + H^+_{(aq)} \xrightarrow{T[°C]} CH_{4(aq)} + CO_{2(aq)}$$
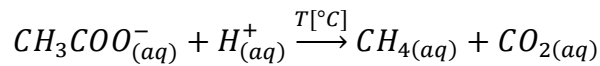
The thermal decarboxylation rate changes due to the LMWOA speciation (different thermal stabilities; Palmer and Drummond, 1986), the pH of an aqueous solution (Crossey, 1991), the material of the reaction vessel (Kharaka et al., 1983), the presence of a free gas phase (Yu and Savage, 1998; McCollom and Seewald, 2003b), the addition of mineral phases (Bell et al., 1994; Seewald, 1996; McCollom and Seewald, 2003a, 2003b), and as a function of temperature. Other means of LMWOA decomposition can be deformylation and oxidation e.g., in the presence of Fe(III)-bearing minerals such as hematite (Bell et al., 1994; Seewald, 1996; McCollom and Seewald, 2003b).

Numerous authors conducted hydrous pyrolysis experiments to investigate the generation of LMWOA from natural samples like oil shales, crude oil, or kerogen isolates (Surdam et al., 1984; Kawamura and Kaplan, 1987; Barth et al., 1988; Kharaka et al., 1993; Dias et al., 2002). Some studies used grains from one mineral or as mixtures including quartz, carbonates, iron oxides, and sulfur-containing minerals. Their aim was to investigate the impact of minerals on LMWOA generation from organic matter (Kawamura et al., 1986; Eglinton et al., 1987; Barth and Riis, 1992), or to assess the catalytic effect of minerals on the decomposition of selected LMWOA (Bell et al., 1994; McCollom and Seewald, 2003a, 2003b).

In the past, most experimental research focused on LMWOA generation or decomposition above 200 °C (Kharaka et al., 1983; Kawamura et al., 1986; Palmer and Drummond, 1986; Cooles et al., 1987; Eglinton et al., 1987; Kawamura and Kaplan, 1987; Lundegard

and Senftle, 1987; Barth et al., 1988; Crossey, 1991; Barth and Bjorlykke, 1993; Kharaka et al., 1993; Bell et al., 1994; Borgund and Barth, 1994; Knauss et al., 1997; Yu and Savage, 1998; Seewald, 2001b; Dias et al., 2002; McCollom and Seewald, 2003a, 2003b). Very few studies at lower temperatures (diagenetic conditions) have been published (Surdam et al., 1984) and most studies have been conducted on organic-rich rock material (2–12 wt.% total organic carbon; Barth et al., 1989; Li et al., 2018). Deeper subsurface LMWOA studies have focused on molecular composition and abundance, gas generation potential, or influence on mineral dissolution (e.g., secondary porosity) in organic carbon rich basins. This is due to the geochemical impacts of LMWOA on fluid-mineral properties, storage and flow in low porosity shale-dominated stratigraphic units that are important to commercial petroleum activity (e.g., Orem et al., 2014; Zhu et al., 2015; Yuan et al., 2019; Li et al., 2021b).

The analysis of concentrations of LMWOA in pore water over time provides important insights in underlying geochemical processes, but it often lacks a critical temporal dimension as present day concentrations established over long periods (hundreds to millions of years) in the complex interplay between water, mineral phases, and organic matter.

The aim of the present study is to investigate the effect of temperature (80–200 °C) on the generation of LMWOA in the presence of water and natural mineral phases in a Jurassic claystone, the Opalinus Clay (Mont Terri, St. Ursanne, Switzerland). The Opalinus Clay is a candidate host rock for heat-generating, high-level radioactive waste. Insights on the generation potential for LMWOA from Opalinus Clay have implications for the interpretation of concentrations of LMWOA in pore water in the natural environment. LMWOA presence might accelerate mineral dissolution, enhance gas generation by thermal decomposition, affect metal-ion complexation, alter sorption processes, and provide feedstock for microbial life. Moreover, quantification of reaction products from organic matter transformation at 80–200 °C in the presence of water and minerals will result in a deeper understanding of how concentrations of LMWOA in natural environments evolve.

2. Materials and methods

2.1 Sample material

An Opalinus Clay drill core from the borehole BHE-F1 (section 2.02 to 2.22 m) in the Swiss underground rock laboratory (URL) at Mont Terri (St. Ursanne, Switzerland) was crushed with a jaw crusher, freeze-dried and ground with an automatic agate mortar and pestle at ambient conditions. The latter was thoroughly cleaned with distilled water and dichloromethane (DCM) to remove potential organic contaminants. In order to maintain its original organic matter composition, no sterilization treatment was performed for the sample material. During the grinding process if mortar and pestle became warm to the touch, the grinding process was suspended until the material cooled down to room temperature to preserve labile organic matter. All ground sample material from the core section was mixed and stored under an inert atmosphere of argon gas.

2.2 Experimental

2.2.1 Flexible gold-titanium reaction cell

The experiments were conducted in a custom-made, Dickson-type flexible gold-titanium reaction cell (further referred to as 'gold bag'; Dickson et al., 1963; Seyfried Jr et al., 1987; Ostertag-Henning et al., 2019). The gold bag's total volume was approximately 0.12 L. Prior to use, the gold bag was cleaned with 50 °C hydrochloric acid (HCl, 10 % technical grade) for three hours, thoroughly rinsed with distilled water, and submerged in nitric acid (HNO_3, 67 %) for ten minutes. Again, the gold bag was rinsed with distilled water, dried at 105 °C, and then placed in a muffle furnace at 500 °C for approx. 20 hours. Afterwards, it was temperature-treated with a torch until the entire gold surface had experienced red heat. The heat-treatment makes the gold softer and, therefore, less prone to failure during the gold bag's installation and the experiments. Titanium parts of the reaction cell were cleaned in a similar way (heated at 400 °C, no torch treatment). Heat treatment of titanium forms a colored titanium oxide (TiO_2) layer, which increases the chemical inertness of the material.

2.2.2 Hydrous pyrolysis experiments

In the hydrous pyrolysis experiments, 50 g of ground Opalinus Clay were used. A volume of ~90 ml of N_2-flushed HPLC grade water was added into the gold bag, resulting in a solid-liquid mass ratio of approximately 1:1.8. The gold bag with the attached titanium tubing and valve was installed into a high-pressure vessel (Parr Instruments Company, 4650 series). Prior to the experiments, the remaining gaseous headspace in the gold bag was removed and leak tests were performed at 1 bar excess N_2 pressure. The software SpecView was used to log the temperature profile over the course of the experiments. A TELEDYNE ISCO syringe pump, model 100DM, kept the experiment at isobaric conditions of 20 MPa. This pressure was chosen because it presents an analog for a water depth of 2000 m or a lithostatic pressure approximately 800 m below the earth surface, assuming an average rock density of 2500 kg/m³. The latter depth is relevant in the context of heat-emitting, high-level nuclear waste disposal in deep geological formations. The pressure was logged by the pump's software. Experiments were conducted at temperatures of 80, 120, 160 and 200 °C. These temperatures are representative of diagenetic to catagenetic conditions in source rock formations (see Carothers and Kharaka, 1978; Tissot and Welte, 1978). Moreover, these temperatures are also relevant in the above-mentioned nuclear waste disposal context, where the host rock might heat up to 150 °C (Delage et al., 2010; Lommerzheim et al., 2019). During the experiments, temperatures were stable within ±1 °C; the pressure was constant within ±0.5 MPa. Experimental parameters are summarized in Table 3.1.

Table 3.1: Experimental parameters of the hydrous pyrolysis experiments with ground Opalinus Clay (OPA). The subscript 'set' indicates the input values, the subscript 'log' gives the recorded values averaged over the duration of the respective experiment.

Mass OPA [g]	HPLC-H_2O [l]	Time [h]	T_{set} [°C]	T_{log} [°C]	p_{set} [MPa]	p_{log} [MPa]
50.0	0.090	719	80	80.6	20.0	19.7
50.0	0.089	906	120	119.2	20.0	19.6
50.0	0.091	672	120	120.2	20.0	19.6
50.0	0.084	504	160	160.1	20.0	19.6
50.0	0.081	504	200	199.9	20.0	19.7

2.2.3 Sampling of aqueous fluid from the gold bag

Samples were taken with a gastight glass syringe, which was attached to a Luer-lock adapter on the titanium sampling valve connected to the gold bag via a titanium tube. Prior to use, the syringe was rinsed three times with HPLC-gradient water. Two subsamples were taken from the experiments at each time point. First, a flush volume of 1 ml was removed (combined dead volume of the titanium tube and the sampling valve). This sample was used to measure the pH of the aqueous fluid directly after sampling at room temperature. Then, 2 ml were withdrawn from the gold bag and transferred into a N_2-flushed headspace vial sealed with a PTFE-lined aluminum cap. The mass of the vial was gravimetrically determined before and after sample addition to obtain a sample's exact mass (accuracy was 0.001 g). Samples were stored at −20 °C until HPLC-analysis.

2.3 HPLC-DAD analysis

LMWOA were analyzed following a slightly modified version of the protocol by Albert and Martens (1997). In brief, LMWOA in a 1-ml aqueous sample were derivatized to form colored 2-nitrophenylhydrazide derivatives, which were separated on a HPLC-column and subsequently detected by the absorption of visible light at 550 nm with a diode array detector (DAD). Samples were measured with a HP 1100 HPLC equipped with a Phenomenex C18 4×3.0 mm trap-column, an Agilent Eclipse XDB-C8 4.6×12.5 mm pre-column, and an Agilent Eclipse XDB-C8 4.6×250 mm separating column. A sequence always contained a water sample for the conditioning of the trap, two blanks, four calibration standards (10, 30, 100, 300 µmol/l) prepared daily from stock solutions, and the samples. Comparison of eleven calibrations showed compound and concentration specific standard deviations between 0.19% and 1.42%, which include potential errors introduced during sample derivatization. Molar amounts of the LMWOA in control blanks from the gold bag experiments (HPLC-gradient water transferred into N_2-flushed headspace vials) were generally below the limit of quantification or even the limit of detection. For all compounds, the limit of detection was 1 µmol/l and the limit of quantification was 5 µmol/l.

2.4 Quantification of CO_2 in headspace gas

A sample volume of 1 ml gas was taken from a headspace vial with a gastight syringe and was manually injected into a modified Fast Refinery Gas Analyzer (FAST-RGA) system. A gas injection control unit (GICU) distributed the gas sample to different channels in a HP 7890 gas chromatograph. The channel for the quantification of CO_2 consisted of a 250-µl sample loop with a splitless injector. The gas sample was divided into three subsamples, which were then transported by a He carrier gas flow. They were subsequently separated on a 1-m and a 2-m packed Q Plot column as well as a 1-m MS5A molecular sieve column (all isotherm at 70 °C). CO_2 was quantified, using a thermal conductivity detector. The limit of quantification was 150 nmol.

2.5 Stable carbon isotopes

2.5.1   Gaseous CO_2

Based on the concentration of CO_2 in the gas sample, a gas volume was injected by hand into an Agilent 6890 gas chromatograph and separated on a 25-m Poraplot Q column. The GC was coupled to a Thermo Scientific MAT253 isotope mass spectrometer, which was used to determine the isotope ratio in CO_2. Results are reported in the delta notation in per mil against the international Vienna Pee Dee Belemnite standard [‰ vs. VPDB].

2.5.2   Solid inorganic carbon (carbonate)

Based on the carbonate content of the Opalinus Clay, ~0.7 mg ground sample material was given into a glass tube and sealed with a septum-lined cap. The tube was placed in an autosampler at 72 °C and was He-flushed. Concentrated phosphoric acid was added to the sample material. The material was homogenized, placed in the autosampler and was allowed to equilibrate for several hours. Measurements were performed with a Thermo Fisher Scientific Gasbench II coupled with a Thermo Fisher Scientific ConFlo-IV to a Thermo Fisher Scientific Delta V Advantage isotope ratio mass spectrometer (IRMS). Results are presented as the mean value from triplicates and reported in the delta notation in per mil against the international Vienna Pee Dee Belemnite standard [‰ vs. VPDB].

2.5.3   Bulk organic matter

Prior to analysis, sample material was treated with dilute HCl at 80 °C to remove inorganic carbonate carbon constituents. A Thermo Fisher Scientific Flash EA 1112

elemental analyzer was used to oxidize the sample material at 1020 °C. Chromatographic separation was achieved in a Thermo Fisher Scientific ConFlo IV open-split-system equipped with a Porapak column (isotherm at 55 °C). The isotope ratio was determined with a Thermo Fisher Scientific Delta V Advantage mass spectrometer (IRMS). Results are presented as the mean value from triplicates and reported in the delta notation in per mil against the international Vienna Pee Dee Belemnite standard [‰ vs. VPDB].

2.6 Calculation of the cumulative molar amount of LMWOA formed

In this study, the LMWOA generation is reported as the cumulative amount of substance in [μmol] that was produced in the gold bag aqueous fluid. The cumulative amount of the LMWOA was calculated by adding up the concentrations detected after each sampling event. Volumes removed and liquid remaining in the gold bag were quantified at each sampling event.

2.7 Thermodynamic computations

Equilibrium constants for organic acid pyrolysis reactions were calculated for 25 °C and 1 bar as well as for 80, 120, 160 and 200 °C and 200 bar using SUPCRT92 (Johnson et al., 1992). Those were used to compute the pH dependency of organic acid speciation (Fig. 3.3).

Additional thermodynamic calculations were conducted with Geochemist's Workbench (Bethke, 1996) to determine if the steady state observed was close to equilibrium state. We created an isobaric (25 MPa) database with 147 aqueous species, 195 minerals, and 9 gases, using SUPCRT92 and the OBIGT database to calculate the equilibrium constants. In these computations, rock (composition of the rock is given in *Section 3.1*) was added incrementally to water until the system was completely rock-buffered and subsequent addition of rock to the model system did not cause further changes in aqueous fluid composition. All minerals were allowed to react with the aqueous solution instantaneously. An arbitrary reaction kinetic was introduced by adding rock to the system in small increments. We closely evaluated the composition and speciation of the fluid for (a) the full extent of water-rock reaction (all rock equilibrated, i.e., W/R=1.8) and (b) for highly incomplete extents of water-rock reactions (W/R=50). The actual extents of water-rock reaction are between these two extremes.

3. Results

3.1 Geochemical characterization of the sample material

The Opalinus Clay sample material contained 0.64 wt% organic carbon, 4.10 wt% inorganic carbon, and 1.0 wt% sulfur. Duplicates suggested a homogenous distribution of organic carbon in the sample material and the standard deviation of the analytical method was 0.01% (n=20). Elemental analysis (EA IRMS) gave a stable carbon isotopic composition for decarbonated sample material of −26.2‰. Kerogen characterization by Rock-Eval pyrolysis gave the following results: $S_1 = 0.01$ mg/g, $S_2 = 0.59$ mg/g, $S_3 = 0.26$ mg/g, and $T_{max} = 433$ °C. The corresponding oxygen index (OI) and hydrogen index (HI) were 38 mg CO_2/g TOC and 95 mg HC/g TOC, respectively. The mineralogy of the sample material was determined by X-ray diffraction analysis and gave a composition of 26 wt% illite/smectite, 21 wt% calcite, 19 wt% kaolinite, 11 wt% muscovite, 10 wt% quartz, 4 wt% chlorite, 4 wt% feldspar, and 5 wt% other minerals (gypsum, dolomite, pyrite, anatase).

3.2 pH of aqueous samples

The evolution of pH values measured at room temperature in fluids retrieved over the course of each of the five experiments is shown in Fig. 3.1 A. At 80 and 120 °C, the aqueous fluids showed an increasing pH over the initial 24 to 48 hours, after which the pH slowly decreased and leveled out to near-constant values between 6 and 6.5 (analytical reproducibility was better than 0.1 pH units). The pH in aqueous fluid samples from the 160 and 200 °C experiments rapidly dropped by one pH unit to 5.9 and 5.7 within 48 hours and remained constant within 0.1 pH units. In the five experiments conducted, a lowering of these steady-state pH values late in the experiments from 6.4 (at 80 °C) to 5.7 (at 200 °C) was observed.
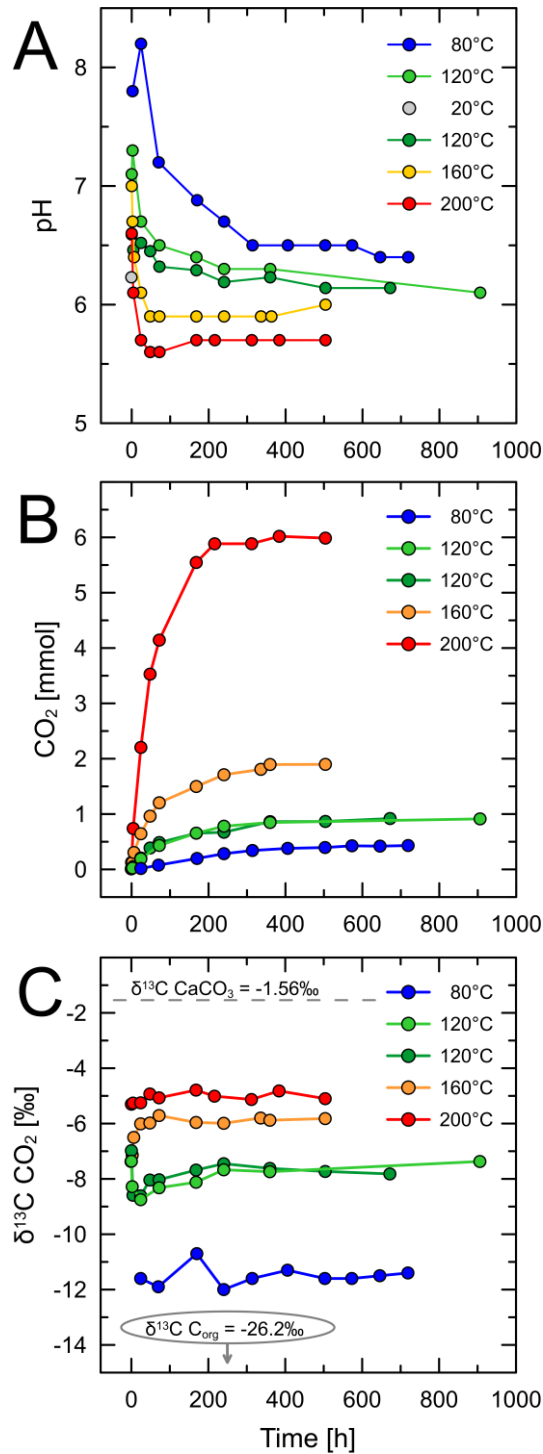
Figure 3.1: (A) Measured pH values (room temperature) of gold bag aqueous fluid samples from hydrous pyrolysis experiments with Opalinus Clay at 80, 120, 160, and 200 °C (20 MPa). Grey circle = pH prior to heating of one experiment, measured after approximately 68 hours at 20 °C and 20 MPa. (B) Cumulative amount of substance of CO_2 in the gold bag reported in [mmol]. (C) Stable carbon isotope data of CO_2 reported in per mil against the Vienna Pee Dee Belemnite standard. Indicated by the dashed grey line is the stable carbon isotope value, which was determined for carbonate minerals in Opalinus Clay.

3.3 CO_2 generation and $\delta^{13}C$ data

The starting stable carbon isotope composition of inorganic carbon constituents in Opalinus Clay was −1.56‰, the organic matter had a $\delta^{13}C$ value of −26.2‰. With increasing temperature, an increasing amount of dissolved $CO_{2(aq)}$ was observed in the gold bag experiments (Fig. 3.1 B). This coincided with the decrease of the pH of the aqueous fluid (Fig. 3.1 A). At 200 °C, the pH and the CO_2 data both showed distinct changes from 72 to 168 hours. The curves notably flattened and stabilized around a pH of 5.7 and an amount of substance of approx. 6 mmol, respectively. Stable carbon isotope data of CO_2 showed that lower $\delta^{13}C$ values of CO_2 coincided with lower experimental temperatures (Fig. 3.1 C). At 80 °C, $\delta^{13}C$ values were nearly constant at −11.5‰. At 120 and 160 °C, however, two opposing trends were visible in the first 72 hours. At 120 °C, CO_2 first became depleted in ^{13}C within 48 hours, before $\delta^{13}C$ increased to −8‰. By contrast, at 160 °C, $\delta^{13}C$ of CO_2 slowly increased from −6.3‰ to −5.9‰. At 200 °C, $\delta^{13}C$ values were almost constant at –5‰.

3.4 LMWOA generation

The quantities of formate, acetate and oxalate, reported in [µmol], generated in time in five hydrous pyrolysis experiments at four temperatures (80, 120, 160, and 200 °C), are shown in Fig. 3.2 A–C. The most abundant component was acetate, followed by oxalate and formate. The highest cumulative amount of substance produced in the experiments was 15.5 µmol (acetate at 200 °C). The generation proceeded rapidly in the first 100 hours. The three compounds showed distinctly different generation patterns. Rapid generation of formate took place within the first 6 to 48 hours, and then decreased soon after in the experiment (Fig. 3.2 A). At 160 °C as well as 200 °C, the amount of substance dropped rapidly between 48 and 96 hours and then remained nearly constant between 72 and up to 400 hours. There was no significant decrease in the cumulative amount of formate at 80 °C. For the interpretation of formate data, several data points between 400 and 700 hours in the range of 6–13 µmol/l were used. Acetate generation proceeded almost continuously at all temperatures with yields increasing with increasing temperature (Fig. 3.2 B). The amount of oxalate increased only slightly in the 80 °C experiment over time. At 120 °C, the generation of oxalate resulted in up to five times higher molar amounts compared to the 80 °C experiment (Fig. 3.2 C). At 160 °C, the

51

amount of oxalate also increased with time, but did not reach the same level of the 120 °C experiment, although the values began to scatter after 200 hours. After less than 24 hours in the 200 °C experiment, the concentration of oxalate was below the limit of quantification (<5 µmol/l; Fig. 3.2 C). After approximately 200 hours, it was below the limit of detection (<1 µmol/l).

At 120 °C, a duplicate experiment was performed for better sample coverage at this temperature and to assess the reproducibility of LMWOA generation in a gold bag experiment using the same sample material and procedures. However, analysis of the total organic carbon (TOC) content of sample material after the second experiment at 120 °C gave 0.97 wt.% compared to 0.66 wt.% after the first. This correlates with an observed offset between the acetic acid data from the two 120 °C experiments of 1.7 µmol at 168 hours, which represents about 40% of the cumulative molar amount of acetic acid indicated by the light green curve (Fig. 3.2 B). The discrepancies in the quantities of the other two acids between the two 120°C experiments are of similar magnitude. The temporal changes in the generated molar amounts of all three organic acids are similar between the two experiments. The TOC values in the other solid sample material recovered after the other experiments were 0.92 wt.% (80 °C), 0.65 wt.% (160 °C), and 0.66 wt.% (200 °C).
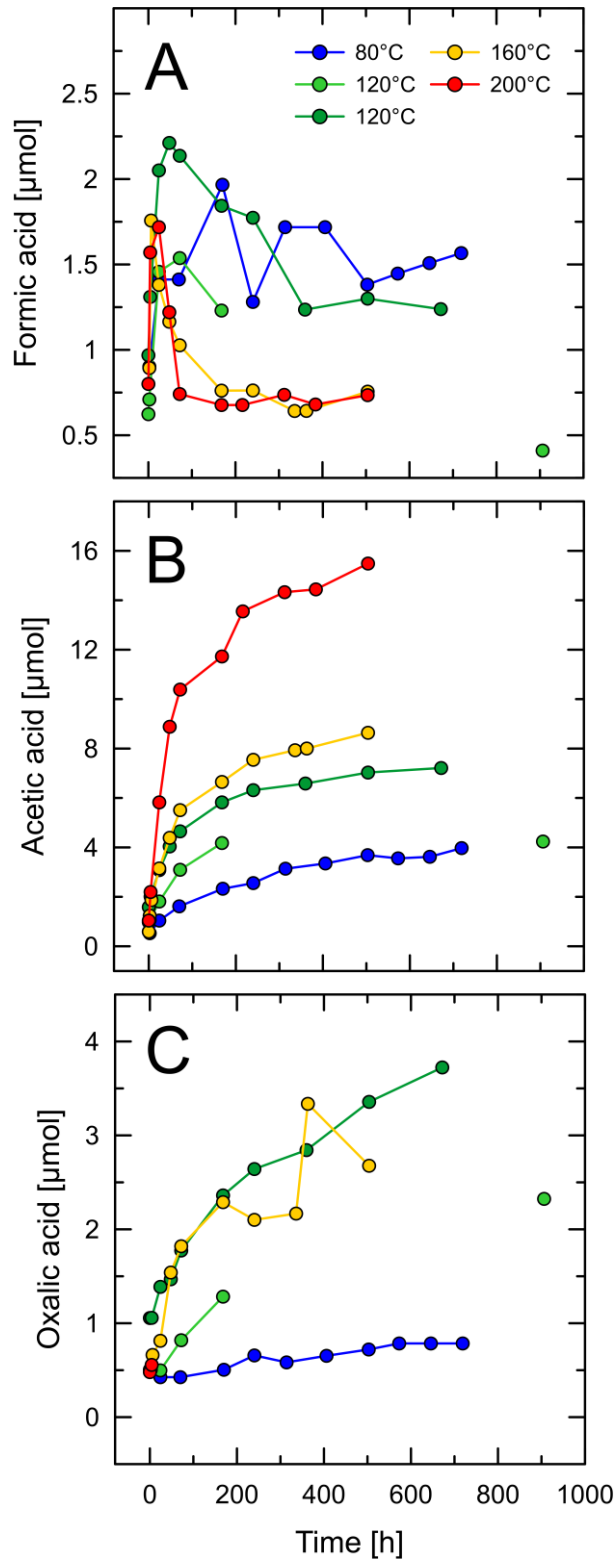
Figure 3.2: Cumulative molar amounts [µmol] of low-molecular-weight organic acids (LMWOA) in gold bag aqueous fluid samples generated in hydrous pyrolysis experiments with Opalinus Clay at 80, 120, 160, and 200 °C (20 MPa). (A) Formate; (B) acetate; (C) oxalate. The dark green lines for 120 °C represent the repetition of the first 120 °C experiment (light green lines).

4. Discussion

4.1 Temperature-dependence of LMWOA speciation

Under thermal stress, the acid form of a LMWOA decomposes at a different rate than its corresponding dissociated acid anion (Kharaka et al., 1983; Palmer and Drummond, 1986; Bell et al., 1994). Crossey (1991) pointed out that the acid dissociation constant K_a is temperature dependent, demonstrating for bicarbonate, formic-, acetic-, and oxalic acid, that K_a has considerably different values at 200 °C compared to those determined at 25 °C (see also Seewald and Seyfried Jr, 1991; Reijenga et al., 2013). Fig. 3.3 shows the speciation diagram for formic acid, acetic acid, and oxalic acid at reference state.
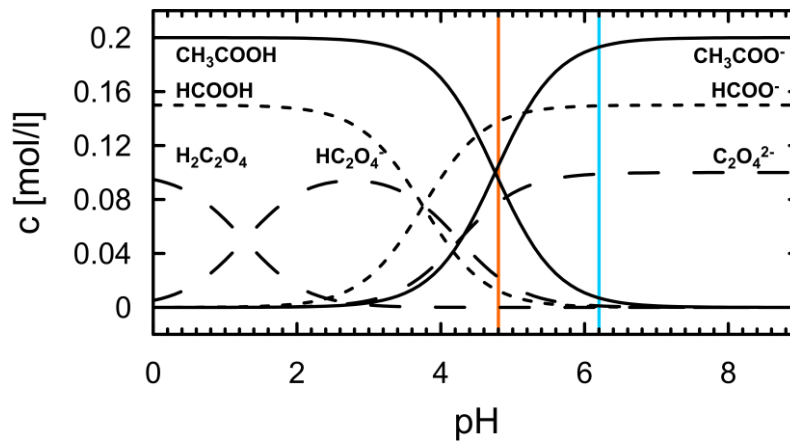
Figure 3.3: Calculated pH-dependent speciation of the low-molecular-weight organic acids (LMWOA) formic- (HCOOH), acetic- (CH$_3$COOH), and oxalic acid (H$_2$C$_2$O$_4$) in pure water at 25 °C and 0.1 MPa. Orange line = reference pH of 4.8 for orientation; blue line = measured gold bag aqueous fluid pH after approximately 68 hours at 20 °C and 20 MPa.

Thermodynamic calculations, using the software SUPCRT92 (Johnson et al., 1992), were employed to determine the acid dissociation constants of formic-, acetic-, and oxalic acid in water at 80, 120, 160, and 200 °C for 20 MPa. The speciation of the three acids was then calculated for the pH range from 0 to 9 and is shown in Fig. 3.5. While the measured pH values (Fig. 3.1 A) in the aqueous samples do not reflect the in situ pH in the gold bag, calculated in situ pH of aqueous fluid samples from heating experiments (≥200 °C) may be higher by up to 0.7 pH units (Seewald et al., 1990). The difference between measured and in situ pH are more pronounced with increasing temperature by up to 1.2 pH units (e.g., Knauss et al., 1997; see also Table 3.2).

A comparison of measured and predicted pH values for the experimental conditions (Table 3.2) suggests that pH values of the aqueous fluid from the experiments should have been higher than the measured pH values. One explanation for this discrepancy might be the exclusion of a contribution of dissolved organic compounds to the aqueous fluid pH in the simulation. Nevertheless, the predicted pH values and the corresponding in situ pH show an offset of 0.6 pH units at lower temperatures. The decrease in pH with increasing temperature in the experiments correlates with the increase in dissolved CO_2 (DIC; Table 3.2), the increase in the generation of e.g., acetate/acetic acid (Fig. 3.2 B), and was likely affected by water-rock reactions at the respective temperatures.

Table 3.2: Comparison of measured (subscript m), predicted (subscript p) molalities of dissolved CO_2, and aqueous fluid pH in gold bag experiments, including an in situ prediction, at experimental temperatures. Predictions reported here refer to a liquid-to-solid ratio of 1.8. Predicted CO_2 values are presented as dissolved inorganic carbon ($DIC_{(p)}$), including different dissolved CO_2 species in the aqueous fluid. Experimental data refer to measurements on samples taken after 360 to 406 h, depending on respective sampling intervals.

T [°C]	$CO_{2(m)}$ [mmolal]	$DIC_{(p)}$ [mmolal]	$pH_{(m)}$	$pH_{(p)}$	$pH_{(in\ situ)}$
80	5.0	4.2	6.5	8.1	7.5
120	9.8	26.8	6.2	7.5	6.9
160	26.8	37.1	5.9	7.1	7.1
200	85.8	75.6	5.7	6.8	6.8

Therefore, it was assumed that the in situ pH in the hydrous pyrolysis experiments was lower by up to 0.7 pH units, compared to the measured pH after ~400 hours (grey lines in Fig. 3.5). After 400 hours, pH and CO_2 values stabilized, indicating steady state between the fluid and the solids in a gold bag (Fig. 3.1 B and C). Thermodynamic reaction path calculations (cf. *Section 2.7*) indicate that the fluids were fully rock-buffered after about half of the rock mass had reacted. A comparison of total CO_2 contents and pH determined for the aqueous fluids retrieved from the gold bags with those computed for the rock-buffered equilibrium state indicates a reasonable similarity between observation and prediction (Table 3.2). This indicates that conditions in the gold bag were close to equilibrium towards the end of the experimental runtime. When the model only included carbonate as a solid phase, it achieved a poor match with the measured data. This result suggests that the observed relationship between the pH in the gold bag experiments and

the dissolved CO_2 released from carbonate minerals was due to a complex interplay of silicates, carbonate, and fluids. Since the amount of CO_2 generated in the experiments was higher than predicted from silicate-carbonate-water reactions in some cases, it is possible that CO_2 resulting from organic matter transformation and LMWOA generation/decomposition also affected dissolved species of CO_2 (DIC) and pH in the aqueous fluid. However, the fact that $\delta^{13}C$ values of CO_2 do not become systematically enriched in ^{12}C as CO_2 accumulated in a gold bag (Fig. 3.1) suggests either that the contribution of organic matter breakdown to the DIC pool in the system was small, or that the contribution of organic matter derived CO_2 is masked by rapid mineral dissolution-(re-)precipitation reactions of carbonates. A small contribution of organic matter derived CO_2 is also derived from the cross plot of the cumulative amount of CO_2 and its carbon isotopic composition at 24 hours compared to that after 504 hours (Fig. 3.4). Instead, the observed changes towards more positive $\delta^{13}C$ values at 120 °C and 160 °C indicate an increased release of CO_2 from carbonate minerals.
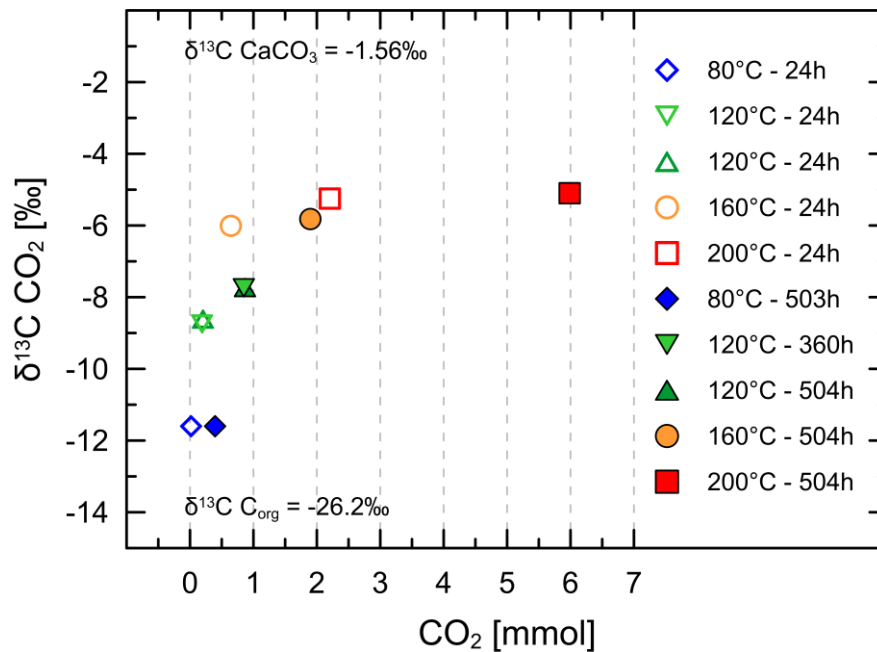
Figure 3.4: Cross plot of the cumulative amount of CO_2 in gold bag experiments with Opalinus Clay given in [mmol] and the carbon isotopic composition ($\delta^{13}C$) of the CO_2 given in [‰] after 24 hours (open symbols) and 504 hours (filled symbols). The experimental temperatures were 80, 120, 160, and 200 °C. The experiments were conducted under isobaric conditions of 20 MPa. For one 120 °C experiment (light green symbols), no data was available at 504 hours. A data point at 360 hours was chosen instead.

The resulting speciation of the three acids, here given as percent of the protonated species, was as following for formic, acetic, and oxalic acid: at 80 °C 3%, 25% and <1%; at 120 °C 7%, 44% and <1%; at 160 °C 4%, 30% and <1%; at 200 °C 27%, 80% and <1% (Fig. 3.5). Therefore, at 200 °C the predominant LMWOA species in the aqueous gold bag fluid were formate, acetic acid, and oxalate, respectively. Hereafter, only the dominant species will be addressed in the discussion of the decomposition kinetics. Although a significant percentage of formic acid and acetate were present in the aqueous fluid, the rate constants for the thermal decomposition of the two compounds differ only by one to two orders of magnitude (Palmer and Drummond, 1986; McCollom and Seewald, 2003a). Therefore, the following discussion likely slightly underestimates the impact of formic acid/formate and acetic acid/acetate decomposition.

4.2 Thermal decomposition of LMWOA

4.2.1 Reaction rate constants

In order to assess the generation of LMWOA in combination with their simultaneous thermal decomposition, reaction rate constants k for the thermal decomposition of the dominant species formate, acetic acid, and oxalate were calculated from literature data (Table 3.3). Reaction rate constants were determined for this study's experimental temperatures, using the Arrhenius equation:

$$k\left[1/s\right] = A \times exp - \left(\frac{E_a}{RT}\right)$$

where A is the frequency factor in [1/s], E_a is the activation energy in [J/mol], R is the universal gas constant in [J/mol K], and T is the absolute temperature in [K]. The kinetic parameters were chosen based on the speciation of each compound, as discussed in Section 4.1. The kinetic parameters from Table 3.3 were originally determined in aqueous solutions with a LMWOA or its corresponding acid anion. The experiments were conducted without mineral phases, except for the study by Bell et al. (1994), and in reaction vessels made from different materials (e.g., gold bag, titanium, or borosilicate glass). Therefore, the kinetic parameters are only the best estimate available for the thermal decomposition processes of LMWOA in this study's hydrous pyrolysis experiments and might underestimate the reaction rate of the LMWOA in the presence of Opalinus Clay minerals. Calculated reaction rate constants are reported in Table 3.4.
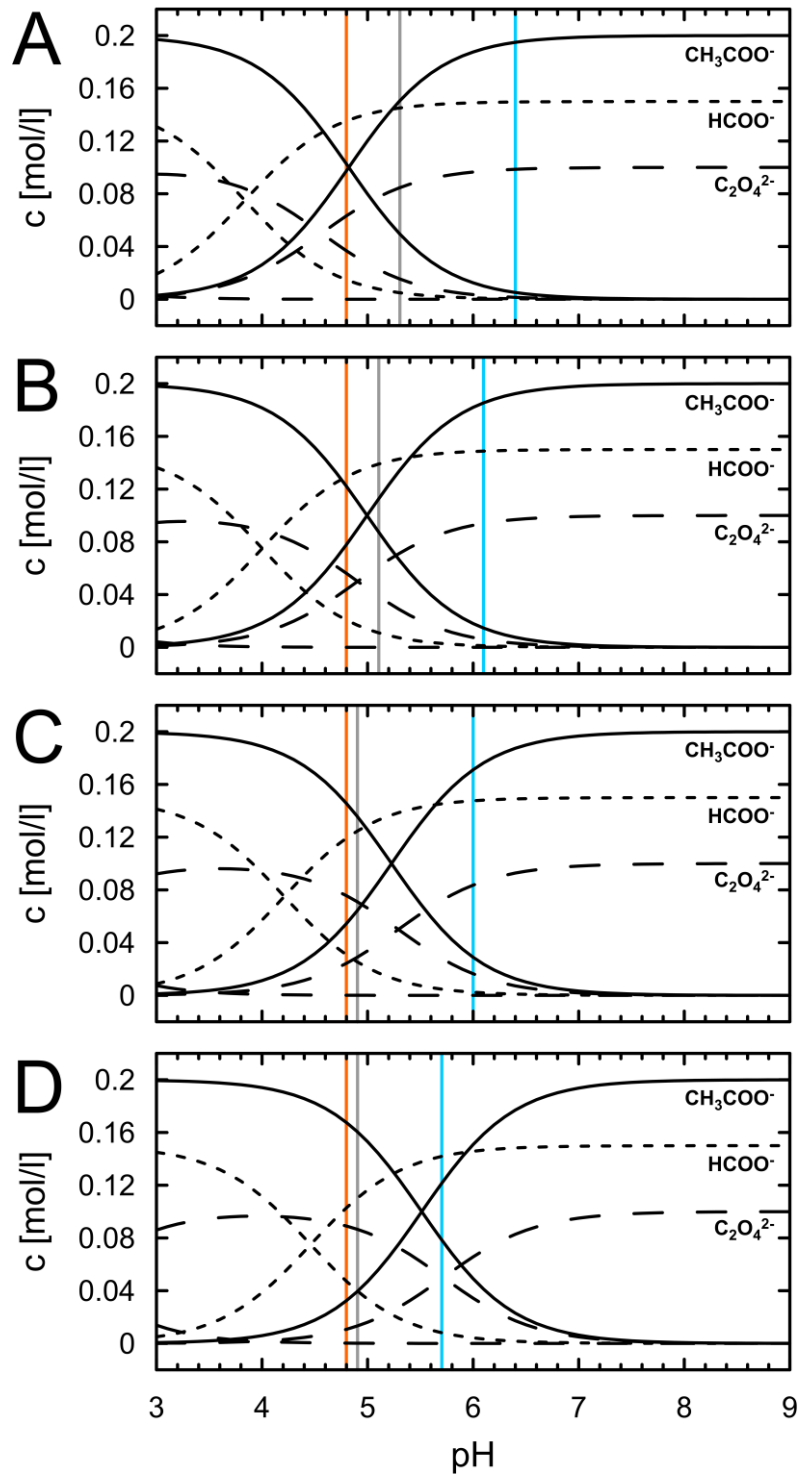
Figure 3.5: Calculated pH-dependent speciation of the low-molecular-weight organic acids (LMWOA) formic-, acetic-, and oxalic acid in pure water at (A) 80 °C, (B) 120 °C, (C) 160 °C, and (D) 200 °C. Shown on the right are the respective acid anions $HCOO^-$, CH_3COO^-, and $C_2O_4^{2-}$. All curves relate to a pressure of 20 MPa. Orange line = reference pH of 4.8 for orientation; blue line = measured gold bag aqueous fluid pH after approximately 400 hours; grey line = inferred gold bag aqueous fluid pH based on results from heating experiments by Seewald et al. (1990).

Table 3.3: Kinetic parameters for the thermal decomposition of formate, acetic acid, and oxalate in an aqueous solution. Given are the frequency factor A and the activation energy E_a. Values for acetic acid and oxalate were calculated based on experimental data from the reported literature below.

Thermal decomposition reaction and vessel type	A [1/s]	E_a [J/mol]	Reference
Formate in Au-TiO$_2$	5200	94600	McCollom & Seewald (2003a)
Acetic acid in TiO$_2$	22527	144145	Palmer & Drummond (1986)
Acetic acid in TiO$_2$	3627043	170064	Bell et al. (1994)
Acetic acid in TiO$_2$ + montmorillonite	0.0000528	32922	Bell et al. (1994)
Oxalate in borosilicate glass vials	3.82	51400	Crossey (1991)

4.2.2 Half-lives ($t_{1/2}$)

The time in years by which half of the molar amount of each of the three LMWOA would have decomposed at the elevated temperatures was calculated using the equation below. The resulting half-lives are reported in Table 3.4.

$$t_{1/2}\ [y] = \left(\frac{\ln 2}{k}\right) \times 31{,}536{,}000$$

The results in Table 3.4 indicate that half-lives for acetic acid range from thousands to several millions of years under the experimental conditions, depending on mineral assemblages. In the presence of montmorillonite, the half-lives of acetic acid are drastically reduced to only a few years. Formate is characterized by a pronounced decrease of the duration of its half-lives from hundreds of years at 80 °C to less than a year for 200 °C. The half-lives of oxalate decrease with increasing temperature from approximately three months to about one day. As a result, the thermal decomposition of acetic acid in an aqueous solution proceeds over geological timescales. At elevated temperatures above 100 °C, formate and oxalate are removed from an aqueous solution by thermal decomposition within a few years or less.

Table 3.4: Reaction rate constants k in [1/s] and calculated half-lives ($t_{1/2}$) in years [y] of acetic acid (Palmer and Drummond, 1986; Bell et al., 1994), acetic acid in the presence of montmorillonite (Bell et al., 1994), formate (McCollom and Seewald, 2003a), and oxalate (Crossey, 1991) for the temperatures 80, 120, 160, and 200 °C.

T [°C]	Formate		Acetic acid[1]		Acetic acid[2]		Acetic acid + montmorillonite		Oxalate	
	k [1/s]	$t_{1/2}$ [y]	k [1/s]	$t_{1/2}$ [y]	k [1/s]	$t_{1/2}$ [y]	k [1/s]	$t_{1/2}$ [y]	k [1/s]	$t_{1/2}$ [y]
80	5.29×10^{-11}	426	1.07×10^{-17}	2.10×10^9	2.54×10^{-19}	8.88×10^{10}	7.14×10^{-10}	31.6	9.44×10^{-8}	0.24
120	1.40×10^{-9}	16.1	1.59×10^{-15}	1.42×10^7	9.20×10^{-17}	2.45×10^8	2.23×10^{-9}	10.1	5.61×10^{-7}	0.04
160	2.03×10^{-8}	1.11	9.32×10^{-14}	2.42×10^5	1.12×10^{-14}	2.01×10^6	5.66×10^{-9}	4.0	2.40×10^{-6}	0.01
200	1.87×10^{-7}	0.12	2.75×10^{-12}	8.20×10^3	6.08×10^{-13}	3.70×10^4	1.23×10^{-8}	1.8	8.02×10^{-6}	0.003

[1]Palmer and Drummond (1986); [2]Bell et al. (1994)

4.2.3 Simultaneous LMWOA generation and decomposition – net and gross reaction rates

The activation energy for the generation of acetic acid from Opalinus Clay was calculated as 21.0 kJ/mol, which is close to 22.9 kJ/mol determined for acetic acid generation from the Kimmeridge oil shale by Barth et al. (1989). The activation energy for the generation of oxalate was calculated as 23.0 kJ/mol. All three activation energies mentioned were derived from experimental data obtained after 70 or 72 hours. This time was chosen in order to allow comparison of our data with that of other experimental studies, which determined kinetic parameters after 72 hours (e.g., Barth et al., 1989). Due to the rapid decrease in formate concentration early in the experiments, no reliable activation energy could be calculated for the generation of formate in our study. With respect to the molecular pattern in the generation profile (Fig. 3.6 A–C), Kharaka et al. (1993) observed very similar changes in concentrations of formate, acetate, and oxalate during hydrous pyrolysis of crude oils at 200 to 300 °C. These authors reported a rapid initial generation of formate and oxalate, followed by a sudden drop in concentrations of both compounds. Kharaka et al. (1993) attributed this to rates of thermal decomposition exceeding those of the compounds' generation. By contrast, acetate was generated continuously (Kharaka et al., 1993).

At 120 °C, generation rates of the LMWOA in this study were as high as ~80 nmol/h (1.6 µmol/h kg clay) for formate, ~100 nmol/h (2 µmol/h kg clay) for acetic acid, and ~15 nmol/h (0.3 µmol/h kg clay) for oxalate (Fig. 3.6 A–C). The decomposition rates for all three compounds were calculated using kinetic parameters determined for 120 °C and for the cumulative molar amounts of each LMWOA generated between two time points of sampling. The decomposition rates are in the order of -10^{-3} nmol/h for formate, -10^{-6} nmol/h for acetic acid, -10^{-2} nmol/h for acetic acid in the presence of montmorillonite, and up to -6 nmol/h for oxalate.
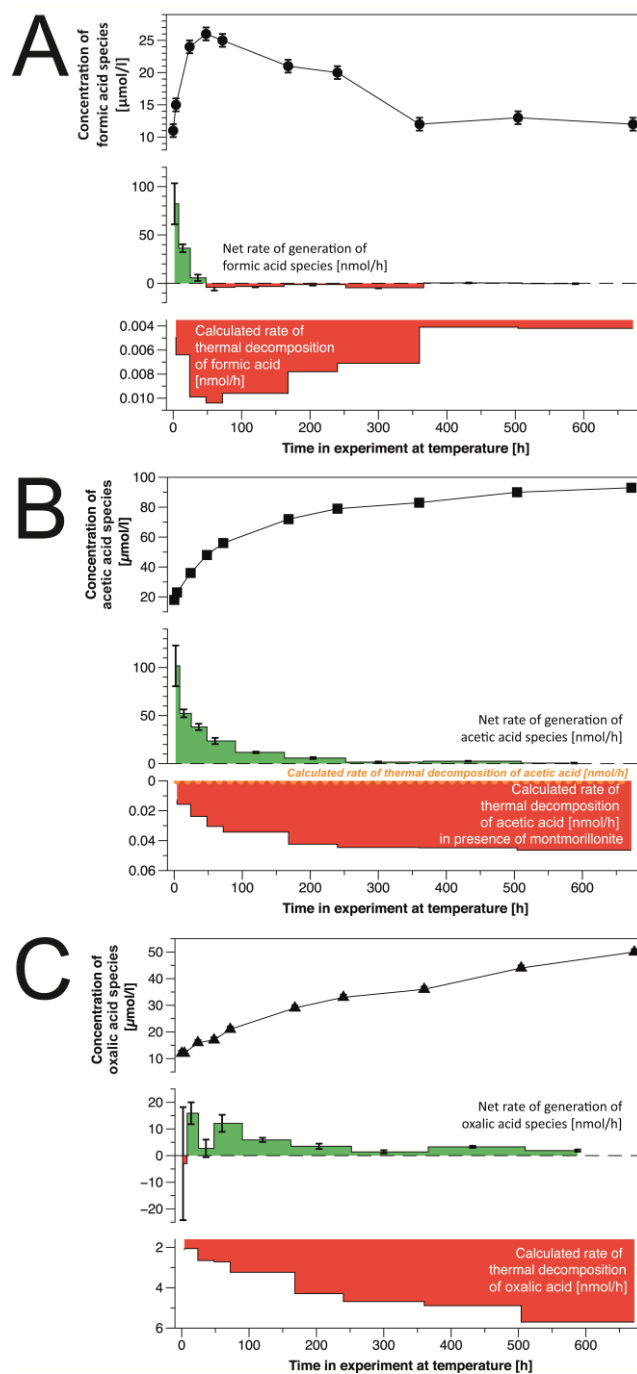
Figure 3.6: Concentrations of the species of formic acid (A), acetic acid (B), and oxalic acid (C) in aqueous subsamples from hydrous pyrolysis experiments at 120 °C, given in [μmol/l]. For the intervals between data points, mid-point step plots representing the derived net generation rates (green) of the three LMWOA and their respective calculated thermal decomposition rates (red) complement the data. The decomposition rates are based on published kinetic data. The rates are reported in [nmol/h]. For acetic acid species, two different decomposition rates are depicted – one by the dashed yellow line for an aqueous acetic acid solution, another in the red area for an aqueous acetic acid solution in the presence of the clay mineral montmorillonite. Error bars assume an analytical reproducibility of ±1 μmol/l and are often smaller than the symbol size used in the figure.

In a short initial interval, net generation rates of formate at 120 °C exceeded calculated rates of thermal decomposition by four orders of magnitude (Fig. 3.6 A). When the generation of formate from Opalinus Clay organic matter slowed down or ceased, the net rate of generation became negative. Based on the presence of formate in samples throughout the hydrous pyrolysis experiments, formate generation probably occurred. In this context, the calculated rate of thermal decomposition of formate after McCollom and Seewald (2003a) illustrates two points. First, while the net rate of generation does not show any indication of thermal decomposition of formate in the beginning of the experiment, the kinetic data emphasizes that a small portion of the formate must have decomposed simultaneously. Consequently, the gross rate comprises the rate of the thermal decomposition at a given temperature and in a specific time interval, added to the observed rate of the generation in the same time interval. Therefore, the concentration is a snapshot of competing reaction rates. Secondly, the negative net rate of generation in this study is three to four orders of magnitude higher than the one calculated using the kinetic data of McCollom and Seewald (2003a). This might be due to different experimental approaches. This study used ground natural claystone composed of several minerals and complex organic matter mixed with water. McCollom and Seewald (2003a), on the other hand, used aqueous solutions of formate in the presence of different sets of catalytically active minerals (hematite, magnetite, serpentinized olivine, NiFe-alloy). The presence of clay minerals (e.g., smectite) in the present study might have accelerated the thermal decomposition of formate, contributing to the generation of different CO_2 species (Muraleedharan et al., 2021). In order to investigate the speciation behavior and reaction mechanisms of formic acid and water in the presence of Na-montmorillonite, Muraleedharan et al. (2021) performed experiments and IR-measurements at 200 °C and 0.1 MPa. These authors demonstrated that – amongst others – formic acid decomposed via a water-assisted surface catalytic pathway to CO, which led to the indirect formation of CO_2. The clay interlayer, notably the edges and facets, facilitated the transformation of formic acid to CO, CO_2 and other aqueous CO_2 species. As a result, Na-carbonate precipitation from carbonic acid conversion (kinetically favored over formate; 121 kJ/mol vs. 419 kJ/mol) was observed in the clay interlayer (Muraleedharan et al., 2021). This might have an impact on porosity in natural environments where pronounced formic acid/formate generation from organic matter occurs (e.g., Zhu et al. 2015). Porosity changes are relevant in the Opalinus Clay since it was chosen as the host rock for heat-generating, high-level nuclear waste (Delage et al., 2010) in Switzerland.

In the case of acetate, the net rate of generation clearly demonstrates that the generation of acetic acid in the experiments significantly exceeds its thermal decomposition by at least four

orders of magnitude (Fig. 3.6 B). This is consistent with the increasing concentration over the course of the experiments (Fig. 3.6 B). Even though the net rate of generation significantly decreases over time, the rate of thermal decomposition never surpasses it. The rate data underline that a concentration profile may show no sign of a simultaneous thermal decomposition process over several hundred hours, while kinetic data emphasize its presence. In addition, the two calculated rates of thermal decomposition of acetate in the absence (Fig. 3.6, orange dashed line) and in the presence of the clay mineral montmorillonite (Fig. 3.6, red step plot) demonstrate the impact of some mineral phases, i.e., the acceleration of the thermal decomposition of acetate.

In contrast to the several orders of magnitude difference between the rates of net generation and the rates of thermal decomposition for formate and acetate, there is only about one order of magnitude difference in the two rates for oxalate (Fig. 3.6 C). After a short interval of slightly elevated rates of net generation (experimental data), the calculated rate of the thermal decomposition of oxalate (kinetic data) approximately equals its net rate of generation. This finding suggests that twice the amount of oxalate was generated under the experimental conditions, which is not evident from the concentration data. If this finding was applied to a natural subsurface environment (~120 °C), a doubling in the concentration of oxalate in pore water likely has direct implications for the interpretation of mineral dissolution and the assessment of secondary porosity (Surdam et al., 1984).

The combination of experimental LMWOA generation data at different temperatures with the supporting kinetic thermal decomposition data from the literature clearly is strong evidence that experimental LMWOA generation – in this and other experimental studies – needs to be corrected for the quantity of the thermal decomposition of individual LMWOA. This is needed to obtain reliable quantitative information on the gross generation of LMWOA.

4.3 Implications for geological settings

4.3.1 Concentrations of LMWOA in pore water

The highest amount of LMWOA of 15.5 µmol was observed at 200 °C after 504 hours. This quantity corresponds to 315 µmol/l, which is higher than concentrations of LMWOA in pore water in most natural environments including natural claystone formations (Thury and Bossart, 1999; Courdouan et al., 2007; Mäder and Waber, 2017), marine sediments (Heuer et al., 2009; Glombitza et al., 2019), or hydrothermal systems (Martens, 1990; Lang et al., 2010; Zhuang et al., 2019b). Hence, physical parameters such as the bulk density, porosity, and water content need to be considered when LMWOA generation under elevated temperature conditions are studied in a theoretical natural setting. The solid-liquid ratio in the experiments is significantly higher than in claystone formations or (semi-) consolidated marine sediments. To provide a comparison between experimental results and a natural environment, we assume the LMWOA generated in the hydrous pyrolysis experiments were released within a body of claystone or marine sediment of known porosity and water content. The resulting concentrations of formate, acetate, and oxalate were calculated in pore water of a sedimentary body with known physical parameters. Two geological settings were chosen: (1) the Opalinus Clay formation (Mont Terri, Switzerland; Bossart and Thury, 2008) and (2) a Nankai Trough sediment consisting of semi consolidated mudstone (Heuer et al., 2017). The selected physical parameters and the results are presented in Table 3.5. The following relationship gave the expected concentration of a compound in pore water:

$$c_{(LMWOA)} \ [\mu mol/l] = (n/(m_s/\rho_s) \times \Phi)/1000$$

where *n* is the amount of substance of a LMWOA from the gold bag experiments in [µmol] in 1 kg of claystone, m_S is the mass of the rock/sediment in [kg] (assumed to be 1 kg), ρ_S is the bulk density of the rock/sediment in [kg/m³], and Φ is the porosity (dimensionless). It was assumed that the resulting pore volume was completely filled with water and it was not account for variations in salinity or temperature.

The calculations suggest that the generation of LMWOA at elevated temperatures and in the presence of minerals and water saturation can result in concentrations of LMWOA in pore water from 60 µmol/l to 5.4 mmol/l – depending on the respective compound (Table 3.5). It is likely that higher concentrations of LMWOA in pore water could result from the exposure of organic carbon-rich clay and claystone to elevated temperatures (e.g., Barth et al., 1989).

Table 3.5: Calculated pore water concentrations of formate, acetate, and oxalate in two environmental settings after Bossart and Thury (2008) and Heuer et al. (2017). Results refer to 1 kg of sediment, the pore space of which was assumed to be water saturated. The molar amount of each compound that was used for this calculation was the maximum molar amount determined in aqueous fluid samples from hydrous pyrolysis experiments at the respective temperature.

Parameter/Compound	Opalinus Clay (Mont Terri, Switzerland)	Nankai Trough (IODP Exp. 370 Site C0023A)*
Bulk density [g/cm³]	2.45	2.01
Porosity	0.14	0.415
Pore water [l]	0.057	0.206
Formate (80 °C) [µmol/l]	690	190
Formate (200 °C) [µmol/l]	600	170
Acetate (80 °C) [µmol/l]	1390	390
Acetate (200 °C) [µmol/l]	5420	1500
Oxalate (120 °C) [µmol/l]	1300	360

*Sample 370-C0023A-26R-5, 101.0; 508.73 m below seafloor; https://doi.org/10.14379/iodp.proc.370.103.2017

The calculations, together with the net and gross generation rate information presented in S*ection 4.2.3*, demonstrate that millimolar concentrations of LMWOA in pore water might accumulate on short timescales (~14 d) after a claystone was exposed to elevated temperatures. Therefore, the additional information gained by using reaction rate data could aid the interpretation of vertical pore water profiles of individual LMWOA. If one considers microbial activity as an additional and simultaneous process enhancing or reducing the concentration of LMWOA in pore water, differences between biological processes (i.e., an active deep biosphere) and thermochemical reactions might be separable from each other and be used as individual constituents to a net generation and decomposition estimation.

Mauclaire et al. (2007) and Stroes-Gasconye et al. (2007) identified an active indigenous microbial community in the Opalinus Clay. Cell counts from incubation experiments gave up to 2×10^3 cells per mL media. Pearson et al. (2003) found that the stable hydrogen and carbon isotopic composition of methane in boreholes at the Mont Terri URL were affected by acetate fermentation. Acetate oxidation gave rates of approximately 2 nmol/l×s in batch incubations using marine sediments conducted over 13 days in the dark at 6 °C (Vandieken et al., 2012). At this rate, acetate in the Opalinus Clay pore water (Table 3.5, $c_{(acetate)}$ at 80 °C) would be consumed within eight days, assuming no further generation of acetate from organic matter transformation takes place. The transfer of acetate oxidation rates from their experiments to the Opalinus Clay environment is an estimation indicating that an active microbial community might affect the concentration of LMWOA in pore water drastically. As in situ temperatures in

the Opalinus Clay at Mont Terri are ~15 °C, microbial activity might proceed under cryophilic to mesophilic temperature conditions (e.g., 5–35 °C).

4.3.2 Gas generation and mineral dissolution (secondary porosity)

Methane and CO_2 can originate from the thermal decarboxylation of e.g., acetic acid (Carothers and Kharaka, 1978). The rate constant for the thermal decomposition of acetic acid in the presence of montmorillonite ($k = 1.30 \times 10^{-9}$/s at 100 °C; Bell et al., 1994) was employed to estimate gas generation under diagenetic to catagenetic conditions. The application of the decomposition rate to a fixed amount of 145 µmol/kg clay acetic acid ($\approx$120 µmol/l, gold bag experiment at 120 °C) produced by the heating of Opalinus Clay organic matter suggests that 0.7 nmol CO_2 and CH_4 per kg Opalinus Clay per hour [nmol/kg h] might be generated, respectively. This translates to approximately 610 µmol CO_2 and CH_4 per kg Opalinus Clay in one hundred years. According to CO_2 concentration data (Fig. 3.1 B), this amount is still significantly below the amount of CO_2 observed at the quasi-steady state in the hydrous pyrolysis experiments after >600 hours. The above-mentioned amount of CO_2 from the thermal decomposition of acetic acid might be an overestimation, as Bell et al. (1994) added pure montmorillonite to their experiments. In contrast, in the natural Opalinus Clay system montmorillonite accounts only for about a quarter of the total mineral assemblage (see *section 3.1*). In addition, this calculation considered only acetic acid as a potential source of natural gas, while a multitude of other organic molecules are likely subjected to thermal decomposition and subsequent gas generation, too. McCollom and Seewald (2003b) observed the oxidation of acetic acid and acetate in the presence of iron minerals such as hematite. These authors concluded that the oxidation of acetic acid and acetate can have a larger impact than decarboxylation of the compounds, resulting in high CO_2 yields instead of the release of equal amounts of CO_2 and CH_4. Jockwer et al. (2007) performed an in situ heating experiment in the Opalinus Clay formation in Switzerland (Mont Terri). They monitored gas generation in experiments over the duration of 18 months. Eventually, the concentration of CO_2 in gas samples stabilized within a range of 2 vol% to 3.6 vol%. At the same time, CH_4 accounted for up to 0.3 vol% of the gases.

At the end of the hydrous pyrolysis experiment of the current study, the amount of CO_2 and CH_4 generated at 120 °C and after 672 h was 18 mmol/kg clay and 1 µmol/kg clay, respectively. Therefore, CO_2 generated from the thermal decomposition of LMWOA is less significant than from other possible sources such as dissolved organic matter and carbonate mineral dissolution during the heating of Opalinus Clay. CH_4 might be generated in significant proportions via

LMWOA decomposition, compared to its generation from other organic compounds during heating experiments.

Oxalate increases metal-ion solubility (Surdam et al., 1984; MacGowan and Surdam, 1988; Harrison and Thyne, 1992) and, hence, might enhance the porosity in a geological formation (Surdam et al., 1984). At 100 °C and in the presence of 10 mmol oxalate, Surdam et al. (1984) observed mineral dissolution within two weeks. The calculated half-lives of oxalate for ≤160 °C in combination with the generation data (Fig. 3.2 C) indicate that oxalate is likely stable in a geological setting for several weeks or more. Consequently, oxalate may have the potential to affect the porosity in geological formations (e.g., Li et al., 2018). On the other hand, Bevan and Savage (1989) suggested that K-feldspar dissolution was higher at 95 °C than at 70 °C and at a neutral pH. Under those experimental conditions, the K-feldspar dissolution was not the predominant result of aluminum complexation by LMWOA (Bevan and Savage, 1989).

The results of the present study suggest that at elevated temperatures, monocarboxylic LMWOA are more stable than dicarboxylic LMWOA (acetic acid >> formate ~ oxalate). This observation is in line with the kinetic reaction rate constants for the individual compounds (Palmer and Drummond, 1986; Crossey, 1991; McCollom and Seewald, 2003a). In addition, Kharaka et al. (1993) observed very similar molecular LMWOA generation patterns in hydrous pyrolysis experiments with crude oils. Kharaka et al. (1993) pointed out that the thermal decomposition rate of formate and oxalate surpassed their respective generation rates after a short initial maximum concentration early in their experiments. Meanwhile, the concentration of acetate showed a constant increase over the course of the experiments.

5. Conclusion

In hydrous pyrolysis experiments, the organic matter poor Opalinus Clay (TOC 0.64 wt.%) produced significant amounts of low-molecular-weight organic acids under elevated temperature and pressure conditions mimicking diagenesis and catagenesis (80–200 °C, 20 MPa). The effect of temperature was investigated using Dickson-type flexible gold-titanium reaction cells. The approach yielded amounts of LMWOA up to 15.5 μmol per kilogram clay and compound at the investigated temperatures.

Calculated reaction rates from experiments and literature data indicate that thermal LMWOA generation and decomposition proceed simultaneously in the temperature range of 80 to 200 °C. Net rates of LMWOA generation in hydrous pyrolysis experiments are minimum estimates and can be improved using compound specific thermal decomposition reaction rate constants.

Our study suggests that under certain conditions, thermal LMWOA generation results in millimolar concentrations in claystone formations, higher than known measured concentrations. Referring to earlier studies investigating the characteristics of LMWOA, these compounds have the potential to accelerate mineral dissolution, enhance gas generation, affect metal-ion complexation, alter sorption processes, and provide feedstock for microbial life in the Opalinus Clay. Calculated half-lives for the thermal decomposition of selected LMWOA ($\leq$200 °C) down to 2.81×10^{-3} years support the relevance for such a (bio-) geochemical impact of the LMWOA.

The new quantitative data will facilitate the modelling of production/decomposition and local pore water concentrations of LMWOA during for example natural heating during subsidence, or a nearby thermal intrusion.

Finally, our study highlights the need of further research focusing on the thermal decomposition of LMWOA in aqueous solutions in the presence of natural mineral assemblages containing sedimentary organic matter. New kinetic data for the thermal decomposition of specific LMWOA in the presence of claystone would enable LMWOA quantification in mineral phases–organic matter–water interactions.

Supplementary Material

Raw data for this chapter can be found here:

https://ars.els-cdn.com/content/image/1-s2.0-S0146638022001152-mmc1.xlsx

(last accessed: 21.11.2023)

Chapter IV

Thermally induced release and generation of gaseous $CO_{2(g)}$ and C_1–C_4 hydrocarbons in Opalinus Clay from Mont Terri (Switzerland)

Oliver Helten[a,b]*, Wolfgang Bach[b,c], Kai-Uwe Hinrichs[b,c], Christian Ostertag-Henning[a]

[a]Federal Institute for Geosciences and Natural Resources (BGR), 30655 Hannover, Germany

[b]Faculty of Geosciences, University of Bremen, 28334 Bremen, Germany

[c]Center for Marine Environmental Sciences (MARUM), University of Bremen, 28334 Bremen, Germany

*Corresponding author. E-mail address: helteno@uni-bremen.de

Abstract

Claystone formations are candidate host rocks for high-level heat-emitting nuclear waste (HLW). Temperatures from 90–150 °C at the container surface are discussed internationally as potential emplacement and storage conditions. The thermal energy emitted from waste containers will be transported into the host rock formation, accelerating chemical reactions including the release of sorbed and dissolved gases and the generation of new gases. This study investigated gas release and generation in Opalinus Clay from Mont Terri (Switzerland) at elevated temperature and pressure conditions relevant for HLW storage and beyond. Hydrous pyrolysis experiments were conducted in Dickson-type flexible gold-titanium reaction cells and gold capsules in the temperature range of 80–345 °C and at 20 MPa. $CO_{2(g)}$ was the predominant product, followed by C_1–C_4 hydrocarbons, which decrease in abundance with increasing carbon atom number. Neither CO nor H_2S was detected. H_2 was generated only in high temperature experiments at 315 °C and 345 °C, respectively. A combination of $CO_{2(g)}$ quantification, stable carbon isotopic composition data, thermodynamic calculations and aqueous fluid composition (dissolved ions, pH) demonstrated that $\geq$80 % of the measured $CO_{2(g)}$ originated from carbonate mineral dissolution. The model calculations also suggest that the fraction of $CO_{2(aq)}$ in DIC increases from ~50 % at 80 °C to nearly 100 % at higher temperatures. Thermal transformation of organic matter represented an additional source for $CO_{2(g)}$ and was the predominant process yielding the C_1–C_4 hydrocarbons. Our findings stress the importance of quantitative geochemical data for the safety assessment of potential host rocks for HLW storage. We demonstrated that two sources are involved in gas release and generation at temperatures relevant for HLW storage, e.g., in the Opalinus Clay – organic matter and carbonate minerals. Our data will contribute to numerical modelling studies and the refinement of feature, events, and processes (FEP) catalogues.

1. Introduction

Gas generation during the post-closure phase of a repository for high-level heat-emitting nuclear waste (HLW) is a scenario in features, events, and processes (FEP) catalogues (Lommerzheim et al. 2019), which develop safety concepts for future repository system evolution. Gas generation is an integral safety criterion for the long-term operation of a repository due to the possibility of e.g., gas pressure induced pore water displacement (Kim et al. 2011) and subsequent mobilization of radionuclides. Gas release might occur in areas of a repository where fracturing of the rock from the construction of drifts results in a pressure gradient between the surrounding rock formation and the drift, allowing gases to migrate or to exsolve from pore water. The part of the rock affected by construction-related fracturing is called the excavation damage zone (EDZ; Bossart et al. 2017) with an extension of up to 3 m into the surrounding rock (value reported for Opalinus Clay; Rübel et al. 2002). Internationally, different host rock types and storage concepts for HLW are under consideration, also claystone formations. In the vicinity of waste containers, temperature conditions are expected to reach 90–150 °C (Delage et al. 2010; Greenberg et al. 2013; Grambow 2016; Lommerzheim et al. 2019; Tourchi et al. 2021). Elevated temperatures will prevail for several hundred to thousands of years (Johnson et al. 2002; Delage et al. 2010; Bossart et al. 2017) before heat emission from the radioactive decay ceases. Therefore, safety concepts for a repository include engineered barriers around waste containers. One is a compacted mixture of sand and bentonite, which offers good heat-conduction into the host rock formation (Delage et al. 2010). The natural barrier properties of claystone formations were not negatively affected by thermal stress applied to the rock in laboratory experiments or during in situ testing in underground research laboratories (URL; Kull et al. 2007; Savoye et al. 2011; Zhang et al. 2017). Nevertheless, increasing temperature in a host rock formation will accelerate chemical reactions such as organic matter transformation, mineral dissolution and precipitation, and sorption processes for dissolved ions, water-soluble organic compounds and gases (e.g., Hendry et al. 2015).

Jobmann and Meleshyn (2015) implied that organic matter transformation in a clay host rock might be negligible at temperatures between 100–150 °C over a period of 10,000 years. The possibility of gas release through carbonate mineral dissolution at elevated temperatures in the presence of pore water was not addressed (see Jobmann and Meleshyn 2015). In contrast, numerous experimental studies demonstrated that organic matter transformation at elevated temperatures generates substantial amounts of $CO_{2(g)}$ and hydrocarbons (e.g., Andresen et al. 1995; Ma et al. 2021). Moreover, high temperatures caused a significant increase in thermal

maturity of organic matter as indicated by changes in biomarker composition (Elie and Mazurek 2008). Wei et al. (2018) showed that gas generation from shales and coals in laboratory experiments occurred at temperatures as low as 60 °C.

Gas release/generation was investigated in in situ studies as well as in laboratory experiments using sample material from the Opalinus Clay formation, the host rock for the geological disposal of HLW in Switzerland. An in situ heating (HE-) experiment in the Mont Terri URL (Switzerland) demonstrated that gas release/generation occurred when a heater (100 °C) was placed in the rock formation over a period of several months (Jockwer et al. 2007). A significant increase in the amount of $CO_{2(g)}$ and C_1–C_4 hydrocarbons in monitoring boreholes around the heater was observed. The molecular abundance pattern of the gases was $CO_{2(g)} \gg CH_4 > \sum C_2$–$C_4$ (Jockwer et al. 2007).

In a full-scale emplacement in situ experiment in the Mont Terri URL, three heaters (140 °C) were placed in a repository-like drift in the Opalinus Clay. The experiment initiated gas generation and the long-term heating led to increased gas partial pressures by a few millibar over the course of several months (Tomonaga et al. 2019). Tomonaga et al. (2019) concluded that Opalinus Clay pore water might be a source for gases including $CO_{2(g)}$ and CH_4. While Tomonaga et al. (2019) did not include information on pore water chemistry, Henning et al. (2020) stressed the importance of pore water chemistry data as the concentrations of dissolved ions and the aqueous fluid pH directly affect the speciation of radionuclides such as uranium. Moreover, the speciation of dissolved $CO_{2(aq)}$, HCO_3^-, and CO_3^{2-} (dissolved inorganic carbon; DIC) are equally affected by solution pH and dissolved ions (Tripati et al. 2015). DIC comprises the dissolved carbon-species stated above, but also related contact ion pairs such as $CaHCO_3^+{}_{(aq)}$, $MgHCO_3^+{}_{(aq)}$, and $MgCO_{3(aq)}$.

Jockwer et al. (2006) conducted heating experiments with Opalinus Clay drill cores in the laboratory. The cores were heated in stainless steel vessels at 95 °C for up to 100 days in the absence of water. $CO_{2(g)}$ was the most abundant gas. The experiments demonstrated that the concentration of $CO_{2(g)}$ was constant after 10 days, but changes in the concentration of the C_1–C_4 hydrocarbons were observed afterwards (Jockwer et al. 2006).

Sauer et al. (2020) performed hydrous pyrolysis experiments (200–300 °C) with Opalinus Clay and Wyoming bentonite in Dickson-type flexible gold-titanium reaction cells. During sampling of aqueous fluid samples, these authors often observed a gas phase in the gastight syringe containing the aqueous sample. Due to the absent smell of H_2S and the sample material used,

Sauer et al. (2020) assumed that the gas phase might be dominated $CO_{2(g)}$. However, no analyses of the gas composition were performed.

In order to assess chemical reaction mechanisms of the thermal transformation of organic matter, several studies performed heating experiments at different temperatures to calculate kinetic parameters for gas generation reactions yielding $CO_{2(g)}$ and C_1–C_4 hydrocarbons (Barth et al. 1989; Knauss et al. 1997). Barth et al. (1989) calculated activation energies between 70 and 90 kJ/mol for C_1–C_4 hydrocarbons generated from Kimmeridge oil shale. The activation energy for $CO_{2(g)}$ generation was 43 kJ/mol (Barth et al. 1989). Seewald et al. (1998) compiled an activation energy distribution for the generation of $CO_{2(g)}$ and C_1–C_4 hydrocarbons from three different shales, in which inorganic carbon was removed prior to the experiments. Seewald et al. (1998) demonstrated that the generation of $CO_{2(g)}$ from organic matter proceeded in an activation energy range from 40–60 kJ/mol. For the majority of C_1–C_4 hydrocarbons, Seewald et al. (1998) reported activation energies of ≥ 60 kJ/mol. Burnham et al. (1992) determined activation energies of 44–48 kJ/mol for the generation of $CO_{2(g)}$. For experimental data obtained at a pressure of 30 MPa, Knauss et al. (1997) calculated activation energies for the generation of C_1–C_4 hydrocarbons between 52 kJ/mol and 65 kJ/mol.

Although several studies investigated gas release/generation from Opalinus Clay, little attention had been payed to underlying geochemical processes and the sources of the gases. Therefore, we performed five hydrous pyrolysis experiments using Dickson-type flexible gold-titanium reaction cells (further referred to as 'gold bags'; Dickson et al. 1963; Seyfried Jr. et al. 1987; Ostertag-Henning et al. 2019) and nine hydrous pyrolysis experiments in gold capsules in order to quantify the amount of gases generated from Opalinus Clay (Mont Terri URL, Switzerland). The chosen temperature range was 80–345 °C and the pressure was 20 MPa. To our knowledge only Sauer et al. (2020) performed hydrous pyrolysis experiments with Opalinus Clay in gold bags in an overlapping temperature range (200–300 °C). However, their focus was on potential mineralogical changes through the interaction of Opalinus Clay with Wyoming bentonite at high temperatures caused by modelled container surface temperatures up to 299 °C (see Greenberg et al. 2013). In the present study, we also calculated kinetic parameters for formation reactions of $CO_{2(g)}$ and C_1–C_4 hydrocarbons. We identified the contributions of the inorganic carbon pool (carbonate minerals and DIC) and of the bulk organic matter to the overall $CO_{2(g)}$ released/generated by using the stable carbon isotopic information ($\delta^{13}C$) of $CO_{2(g)}$. The origin of $CO_{2(g)}$ and C_1–C_4 hydrocarbons is of importance for FEP catalogues and long-term HLW repository safety concepts. Moreover, quantitative data is used in numerical models simulating the post-closure phase in a repository for HLW.

2. Materials and methods

2.1. Sample material

A drill core was obtained from borehole BHE-F1 in the Opalinus Clay formation at Mont Terri URL (St. Ursanne, Switzerland). Immediately after drilling, the material was stored in an evacuated aluminum-lined bag, which was placed in a sealed core liner at room temperature and nitrogen overpressure to prevent oxygen from entering the liner. The sample material for this study came from the core section of 2.02–2.22 m. The material was crushed with a jaw crusher at room temperature and further homogenized by grinding with an automatized mortar and pestle at ambient conditions. In order to prevent alteration of the organic matter in the sample material by thermal stress, special attention ensured that the grinding did not substantially heat the sample material. The grinding process was stopped when the equipment became hand-warm. The ground sample material was stored in glass bottles at room temperature in a nitrogen atmosphere. Mineralogical and geochemical information on the sample material are presented in Table 4.1.

Table 4.1: Geochemical parameters and mineralogical composition (quantitative XRD analysis) of Opalinus Clay sample material from the BHE-F1 borehole in the Mont Terri underground rock laboratory (URL; Switzerland) after Helten et al. (2022). TOC = total organic carbon; TIC = total inorganic carbon; TS = total sulfur.

TOC	TIC	TS	Illite/ smectite	Calcite	Kaolinite	Muscovite	Quartz	Chlorite	Feldspar	Other
[wt%]	[wt%]	[wt%]	[wt%]	[wt%]	[wt%]	[wt%]	[wt%]	[wt%]	[wt%]	[wt%]
0.64	4.11	1.02	26	21	19	11	10	4	4	5

2.2. Hydrous pyrolysis experiments

2.2.1 Flexible gold-titanium reaction cells (gold bags)

One set of hydrous pyrolysis experiments was performed in Parr Instrument Company high-pressure vessels (type 4650) connected to a Teledyne ISCO syringe pump. The pump maintained isobaric conditions of 20 MPa throughout the experiments. The pressure conditions equal those encountered approximately 800 m below the surface, which is a potential depth for a HLW repository facility (Lommerzheim et al. 2019). Five hydrous pyrolysis experiments were conducted at 80, 120, 120, 160, and 200 °C, respectively. This temperature range covers the presumed temperature conditions close to waste containers in a repository environment and exceeds this range in order to calculate kinetic parameters. Temperature and pressure were logged for each experiment. Gold bags (V ~0.12 l) were loaded with 50 g ground Opalinus Clay

and 80–90 ml N$_2$-purged HPLC-grade water – taking into account the expansion of the water at elevated temperatures and at 20 MPa. Detailed experimental parameters can be obtained from Helten et al. (2022).

A thorough protocol describing the design and assembly of the reaction cell can be found in Ostertag-Henning et al. (2019). Prior to the start of an experiment, two leak tests were performed to assure the tightness of the reaction cell. Then, the gas headspace in the gold bag was removed. The duration of the experiments was 504–906 hours, with intermittent sampling of the gold bags. Aqueous fluid samples were withdrawn from the gold bags through a titanium valve with a gastight syringe equipped with a Luer-lock adapter. Since the aqueous fluid in the titanium tube and in the sampling valve was probably not well mixed with the fluid in a gold bag between sampling events, a flush volume of 1 ml was removed. The flush volume was used for pH measurements (Mettler Toledo Seven Excellence, analytical precision = 0.01 pH units). The fast diffusion rate of protons should ensure a representative sample. The sampling volume was 2 ml. Aqueous samples were transferred into N$_2$-purged 21.5-ml headspace vials sealed with PTFE-lined aluminum caps with a butyl septum. The exact sample mass was determined gravimetrically.

2.2.2 Gold capsules

Gold tube was cut into 6-cm long pieces. The tube pieces were cleaned with acetone and, after evaporation of all solvent, were placed in a muffle furnace at 700 °C for 10 minutes. The gold tubes were taken from the hot furnace and were tipped over into a large beaker filled with distilled water to quench the gold. The gold tubes were dried at 105 °C. Flat pliers were used to manually compress one end of a gold tube. A straight edge was created by cutting the edge with a pair of scissors. Then, the straight edge was spot-welded. Gold capsules were loaded with 0.25 g ground Opalinus Clay and 0.45 ml N$_2$-purged HPLC-grade water – the same water-rock ratio used for the gold bag experiments. A custom-made setup was used to evacuate the half-sealed and loaded gold tubes. Some water might have evaporated in the process. They were flushed twice with N$_2$ to remove traces of remaining air, and a final pressure of 0.2 MPa N$_2$ (absolute) was established. Then, the other end of the gold capsule was sealed. Prior to an experiment, a leak test was performed at 105 °C for 30 minutes with all gold capsules to be used in experiments at temperatures above 120 °C. If the mass of a capsule was constant within ≤0.00005 g it was considered tight.

Parr Instrument Company high-pressure reactors (type 4740) were used for the hydrous pyrolysis experiments with gold capsules. The capsules were placed in a sample holder, which was submerged in the water-filled reactor body. Prior to heating, a safety and a leak check were performed. A Teledyne ISCO syringe pump was used to maintain isobaric conditions of 20 MPa. A heating sleeve maintained isothermal conditions after a short heating phase. The temperature and the pressure were logged over the course of the experiments. After an experiment, the gold capsules were cleaned with water, methanol (MeOH), and dichloromethane (DCM). After drying, each capsule was transferred into a 21.5-ml headspace vial, which was sealed with a PTFE-lined butyl septum and an aluminum cap. The headspace vials were flushed with N_2 for 15 minutes to remove air. Approximately 15 minutes prior to analysis, a gold capsule was pierced several times through the septum with a sharp tungsten electrode and the vial was shaken carefully to allow the gases from the gold capsule to migrate into the headspace.

2.3. Quantification of gases

A 1-ml gas sample was transferred into an evacuated gas injection unit (V = 6.8 ml; p = 6 hPa) of a modified refinery gas analyzer (RGA). For each sample, the gas inlet pressure was recorded to calculate the molar amount of substance [nmol] of each gas in the sample. $CO_{2(g)}$ was separated on a 1-m and a 2-m packed Plot Q column as well as on a 1-m mole sieve (MS5A) column after splitless injection from a 250-µl sample loop. Compound separation was achieved under isothermal conditions of 70 °C. $CO_{2(g)}$ was detected with a thermal conductivity detector (TCD). Pre-separation of hydrocarbons was performed on a 1.4-m HP polysiloxane-polymer column after split (1:1 or 1:30)/splittless injection from a 1-ml sample loop in a helium carrier gas flow. Afterwards, the separation of hydrocarbons was achieved on a 50-m HP Al_2O_3 Plot column. The temperature program consisted of an isothermal phase at 50 °C for three minutes, followed by a heating phase with 20 °C/min to a final temperature of 130 °C, which was held for five minutes. Signal acquisition took place using a flame ionization detector (FID). The limit of quantification for $CO_{2(g)}$ with the TCD was 150 nmol, the limit of quantification at the FID was 0.7 nmol for methane, 0.3 nmol for ethane, 0.2 nmol for propane, and 0.1 nmol for *n*-butane, respectively. The relative standard deviation for compounds quantified with the FID was less than ±1.5 %rel, and for compounds quantified using the TCD less than ±2.5 %rel.

2.4. Stable carbon isotopic composition ($\delta^{13}C_{CO2}$)

Depending on the molar amount of $CO_{2(g)}$ in a sample, an adequate volume of from a sample was injected into a GC-c-irmMS system. An Agilent 6890 gas chromatograph equipped with a 25-m Poraplot Q column coupled to a Thermofisher MAT253 isotope ratio mass spectrometer was used. The stable carbon isotopic composition of the $CO_{2(g)}$ is reported in the delta notation ($\delta^{13}C$) in per mil calculated against the international Pee Dee Belemnite (PDB) standard ($R_{PDB} = 0.0112372$).

2.5. Thermodynamic model calculations

For the gold bag experiments, the molar amount of dissolved $CO_{2(aq)}$ in the aqueous fluid was first approximated by the quantification of the molar amount of $CO_{2(g)}$ exsolving from the aqueous fluid sample aliquot in a gastight headspace vial (Fig. 4.1).
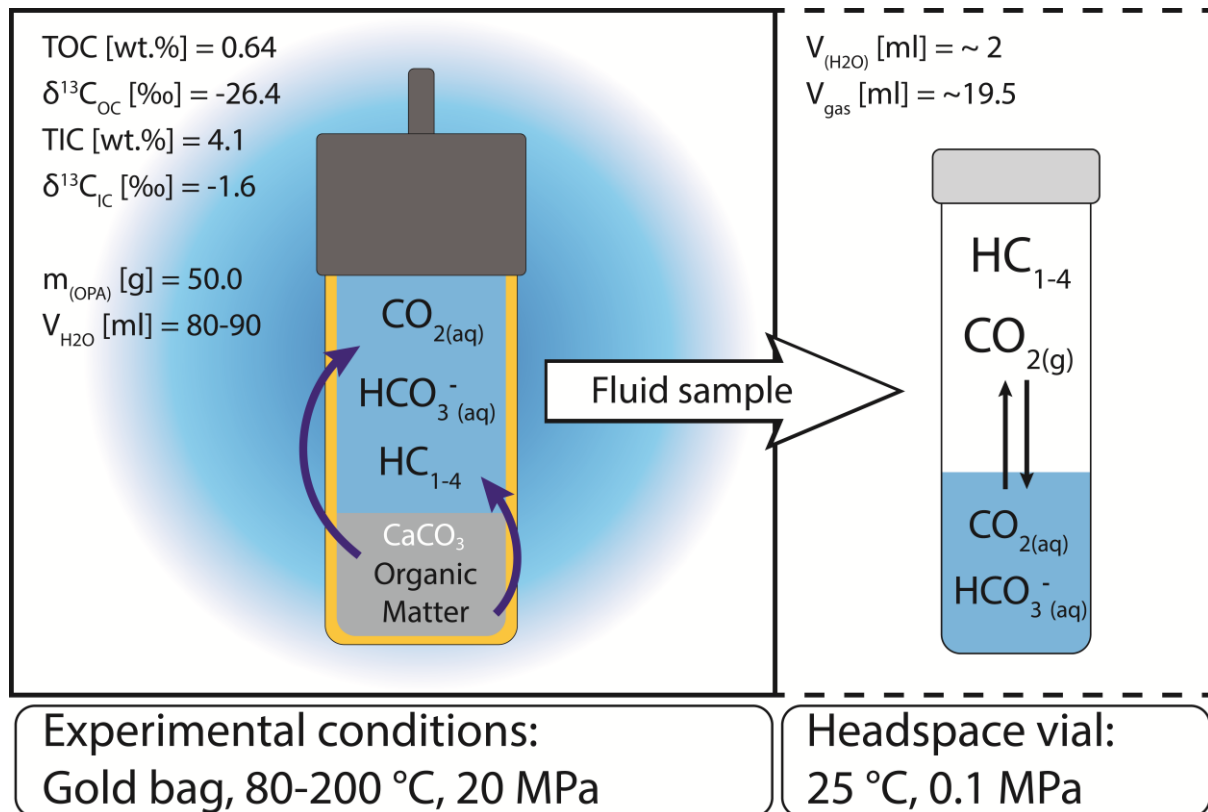
Figure 4.1: Illustration of the experimental setup and conditions. Shown are the gold bag and the headspace vial containing an aqueous sample from the gold bag. In addition, some of the carbon-bearing components in the Opalinus Clay and in the aqueous fluid are indicated. HC_{1-4} = hydrocarbons methane, ethane, propane, and *n*-butane. Information on $CO_{2(g)}$ and on the aqueous fluid composition (dissolved ions) were used in thermodynamic model calculations to determine the concentration of dissolved inorganic carbon (DIC) and the partial pressure of $CO_{2(g)}$ (pCO_2) under experimental in situ conditions.

At pH values below 6 the amount of $CO_{2(g)}$ represents the bulk of the inorganic carbon present in a fluid sample at in situ pT-conditions. However, at pH values higher than 6, i.e. for most of the samples taken during the gold bag experiments (Fig. 4.4 B), the amount of inorganic carbon that remains dissolved in the aqueous fluid in the headspace vial is not negligible. To include the amount of dissolved CO_2-species in the calculation of the in situ partial pressure of $CO_{2(g)}$ (pCO_2) and to correct for the temperature difference (20 °C vs. ≥80 °C), a three-step modelling approach using Geochemist's Workbench (GWB) 2021 (Bethke 1996) was employed:

(1) In a first approximation the exsolved molar amount of $CO_{2(g)}$ in a headspace vial was converted into a pCO_2 in the headspace vial using the known amount of gas volume in the vial. (2) For this pCO_2 at room temperature (20 °C), which was the temperature in the headspace vial during exsolution of $CO_{2(g)}$, an equilibrium concentration of dissolved CO_2-species in an aqueous phase with the measured concentrations of cations (Na^+ 512 mg/l, Ca^{2+} 130 mg/l, Mg^{2+} 56.3 mg/l, K^+ 80.7 mg/l) and anions (Cl^- 211 mg/l, SO_4^{2-} 1154 mg/l) in the sample was calculated with pH as variable and charge balance option. Mineral precipitation was suppressed in the calculations, but the fluid saturation state for minerals was monitored. The system parameters after the equilibrium calculation were taken as new starting conditions and the molar amount of $CO_{2(g)}$ present in the headspace was back-dissolved into the aqueous fluid. (3) Again, the entire system was taken as new starting composition and the temperature was raised stepwise to the terminal experimental conditions of 80 and 120 °C. The resulting DIC concentrations and pCO_2 are presented in Table 4.3 in *Section 4.1*. For 120 °C, the calculations were carried out accordingly using the chemical composition data of the fluid at 120 °C (Na^+ 564 mg/l, Ca^{2+} 151 mg/l, Mg^{2+} 67.3 mg/l, K^+ 68.8 mg/l, Cl^- 205 mg/l, SO_4^{2-} 1234 mg/l).

GWB was also used to compute equilibrium compositions of rock and aqueous solution as a function of temperature. The rock composition was taken from the mineralogical analyses of Opalinus Clay reported in Table 4.1. To match the water-to-rock ratios in the experiments, 555 g of rock were added to 1 kg of water in the reaction path model. All thermodynamic calculations were performed using a tailor-made SUPCRT92 thermodynamic database (Johnson et al. 1991) for a pressure of 25 MPa.

3. Results

3.1. CO$_{2(g)}$ in gold bag experiments

The amount of CO$_{2(g)}$ is reported for 1-ml gas samples taken from headspace vials (V = 21.5 ml), which contained an aqueous fluid sample of approximately 2 ml. The data on CO$_{2(g)}$ presented here is the result of the exsolution of CO$_{2(g)}$ from the aqueous fluid sample. At 80 °C the amount of substance of CO$_{2(g)}$ was ~10 μmol and ~180 μmol at 200 °C (Fig. 4.2). The stable carbon isotopic composition of CO$_{2(g)}$ shows an enrichment of ^{13}C with increasing temperature. Between 80 °C and 200 °C, an increase of 6.3‰ was observed. The difference in the δ^{13}C-values between the experiments was largest between 80 °C and 120 °C (approx. 4‰). In contrast, the difference in the δ^{13}C-values between the experiments at 160 °C and 200 °C was 0.7‰.
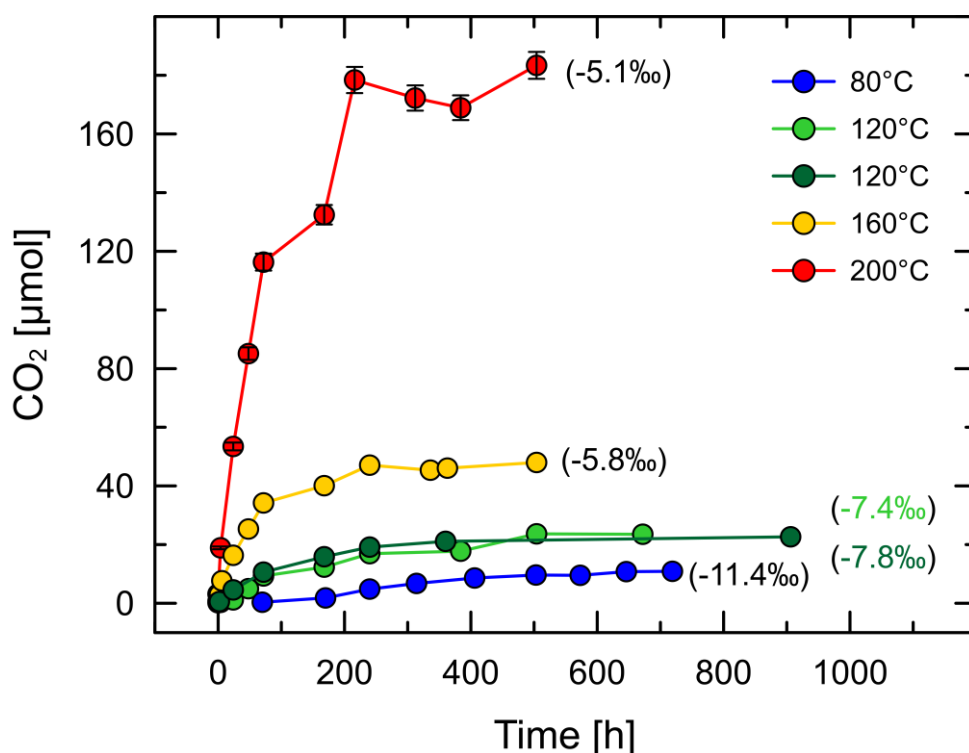
Figure. 4.2: Amount of substance of CO$_{2(g)}$ [μmol] exsolved from ~2-ml aqueous fluid samples in headspace vials (V = 21.5 ml). The headspace vial was purged with N$_2$ prior to sample addition. The gold bag experiments were conducted under isobaric conditions (20 MPa) and at 80, 120, 160 and 200 °C, respectively. A second experiment was conducted at 120 °C to validate the experimental approach. Each data point represents a single measurement. The relative standard deviation was less than ±2.5 %rel. For data ≤160 °C, error bars are smaller than the symbol size. Samples were measured at room temperature. The stable carbon isotopic composition of CO$_{2(g)}$ in the last sample in each experiment is shown in parentheses next to the plotted data. Isotopic information is presented in the δ-notation as δ^{13}C$_{CO2(g)}$ reported in [‰ vs. PDB].

3.2. C_1–C_4 hydrocarbons in gold bag experiments

The amount of C_1–C_4 hydrocarbons is reported for 1-ml gas samples taken from headspace vials ($V = 21.5$ ml), which contained an aqueous fluid sample of approximately 2 ml. The data on C_1–C_4 hydrocarbons presented here is the result of the exsolution of the gases from aqueous fluid samples. The amount of substance of C_1–C_4 hydrocarbons [nmol] increased with increasing temperature (Fig. 4.3). The molecular pattern in the order of the highest abundance was $CH_4 > C_2H_6 \sim C_3H_8 > n\text{-}C_4H_{10}$ for all samples. The highest yield was ~38 nmol for CH_4 at 200 °C and after 504 hours. The amounts of the other three gases were 3–5 nmol (200 °C, 504 h). At temperatures ≤160 °C only CH_4 and C_2H_6 showed a continuous increase, while the amount of C_3H_8 and $n\text{-}C_4H_{10}$ were relatively constant with increasing time. In contrast, at 200 °C the amount of substance of all gases showed a continuous increase.
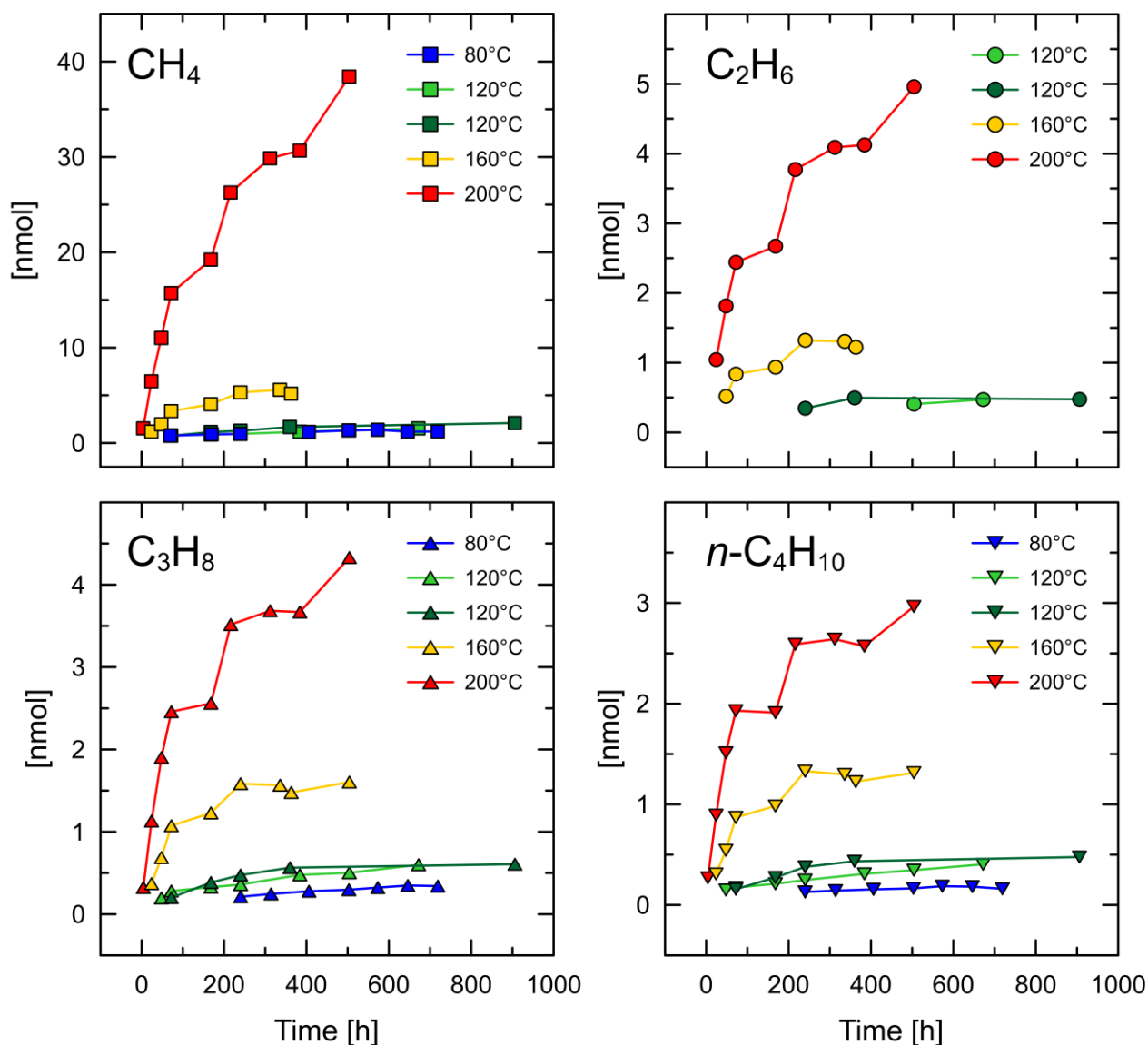
Figure 4.3: Amounts of C_1–C_4 hydrocarbons [nmol] in a headspace vial (V = 21.5 ml) with approximately 2 ml aqueous sample fluid from gold bag hydrous pyrolysis experiments, using 50 g of ground Opalinus Clay with a rock-water ratio between 1:1.8 and 1:1.6. Experimental temperatures were 80, 120, 160, and 200 °C, respectively. Isobaric pressure conditions of 20 MPa were maintained throughout the experiments. A second experiment was conducted at 120 °C to validate the experimental approach. Each data point represents a single measurement. The relative standard deviation was less than ±1.5 %rel and resulted in error bars smaller than the symbol size.

3.3. $CO_{2(g)}$ and C_1–C_4 hydrocarbons in gold capsules

The amounts of $CO_{2(g)}$ and C_1–C_4 hydrocarbons are reported for 1-ml gas samples taken from headspace vials (V = 21.5 ml), which contained a punctured gold capsule with 0.25 g OPA and 0.45 ml HPLC-water. The data on $CO_{2(g)}$ and C_1–C_4 hydrocarbons presented here are the result of the exsolution of the gases from the aqueous fluid and from a free gas phase present in the gold capsules.

The experimental data obtained from experiments with ground Opalinus Clay in gold capsules after 72 hours resemble observations made in the sections above. The amount of $CO_{2(g)}$ and C_1–C_4 hydrocarbons increased with increasing temperature (Table 4.2). Two duplicate experiments at 200 °C and 315 °C showed a reproducibility better than 10 % for the individual yields. $CO_{2(g)}$ was the most abundant gas. The yields of the hydrocarbons decreased with increasing carbon atom number ($CH_4 > C_2H_6 > C_3H_8 > n\text{-}C_4H_{10}$). At 80 °C and 120 °C, no hydrocarbons were detected. This is in agreement with observations made for ethane (80, 120 °C), propane (80 °C), and n-butane (80 °C) in the hydrous pyrolysis experiments in gold bags (Fig. 4.3).

Table 4.2: Amounts of $CO_{2(g)}$, C_1–C_4 hydrocarbons and H_2 [nmol] in 1-ml gas samples taken from headspace vials (V = 21.5 ml) after hydrous pyrolysis experiments in gold capsules under isobaric conditions (20 MPa) and temperatures between 80 °C and 345 °C. The gold capsules contained 0.25 g ground Opalinus Clay and 0.45 ml N_2-purged HPLC-grade water. Each value represents a single measurement. The relative standard deviation for $CO_{2(g)}$ was less than ±2.5 %rel and less than ±1.5 %rel for the hydrocarbons.

Temperature [°C]	Time [h]	$CO_{2(g)}$ [nmol]	CH_4 [nmol]	C_2H_6 [nmol]	C_3H_8 [nmol]	n-C_4H_{10} [nmol]	H_2 [nmol]
80	72	730	n.d.	n.d.	n.d.	n.d.	n.d.
120	72	3280	n.d.	n.d.	n.d.	n.d.	n.d.
160	72	6610	1.3	0.3	0.3	0.2	n.d.
200	72	27520	3.9	0.6	0.5	0.3	n.d.
200	72	26120	4.3	0.6	0.4	0.3	n.d.
260	72	38890	39.5	5.6	3.6	1.5	n.d.
315	72	88310	407	107	53	21	195
315	72	80740	379	102	51	20	n.d.
345	72	169640	708	214	109	46	473

n.d. = not detected.

84

4. Discussion

$CO_{2(g)}$ was the predominant compound among the released/generated gases from ground Opalinus Clay, followed by C_1–C_4 hydrocarbons. This is in good agreement with results from heating experiments in/with Opalinus Clay (Jockwer et al. 2006, 2007; Tomonaga et al. 2019) or in hydrous pyrolysis experiments with shales (Barth et al. 1989; Knauss et al. 1997; Seewald et al. 1998). Evidently, gas generation is a process to consider in the context of high-level heat-emitting nuclear waste (HLW) disposal in claystone formations – even below 100 °C.

4.1. Dissolved inorganic carbon (DIC)

The measured amounts of $CO_{2(g)}$ in the headspace vials (Fig. 4.2) clearly show that CO_2 is released from Opalinus Clay in the course of interactions with water. The data also shows that the CO_2 contents level after an initial increase, with the plateau height increasing with temperature. For the 80 °C and 120 °C experiments, the amounts of DIC were calculated from the measurement of $CO_{2(g)}$ in the headspace (see *Section 2.5*).

For the experiment at 80 °C, a DIC concentration of 11.4 mmol/kg was calculated, and at 120 °C the calculated DIC concentration was 19.8 mmol/kg (Table 4.3). The calculated pCO_2 for these experiments were 0.68 bar (80 °C) and 1.78 bar (120 °C). These pCO_2 values correspond to $CO_{2(aq)}$ concentrations of 6.1 and 12.2 mmol/kg, respectively (Table 4.3), indicating that >50 % of the DIC was $CO_{2(aq)}$. The pronounced rise in $CO_{2(g)}$ in the gold capsules (Table 4.2) and in the gold bag experiments (Fig. 4.2) with increasing temperature is consistent with the results of model calculations in which Opalinus Clay (Table 4.1) was reacted with water (Fig. 4.4 A). The model calculations also suggest that the fraction of $CO_{2(aq)}$ in DIC increases from ~50 % at 80 °C (Table 4.3) to nearly 100 % at temperatures that are close to or higher than 200 °C. As Henning et al. (2020) pointed out, the geochemical composition of a solution and its pH are highly relevant in the context of HLW disposal and repository safety.

Table 4.3: Measured pH of aqueous fluid samples from hydrous pyrolysis experiments with Opalinus Clay at 80 °C (sample 1908417, 719 h) and 120 °C (sample 2008018, 672 h). The pH was measured in a 1-ml flush volume sample at 20 °C. In situ pH values and the concentrations of DIC, $CO_{2(aq)}$, and pCO$_2$ were calculated with GWB React for in situ conditions in the flexible gold-titanium reaction cells. STP = standard temperature and pressure; 20 °C and 1 bar absolute.

Temperature [°C]	pH (measured at STP)	pH (calculated)	DIC at in situ conditions [mmol/kg fluid]	pCO$_2$ at in situ conditions [bar]	$CO_{2(aq)}$ in situ conditions [mmol/kg fluid]
80	6.4	6.02	11.42	0.676	6.1
120	6.1	6.05	19.80	1.783	12.2
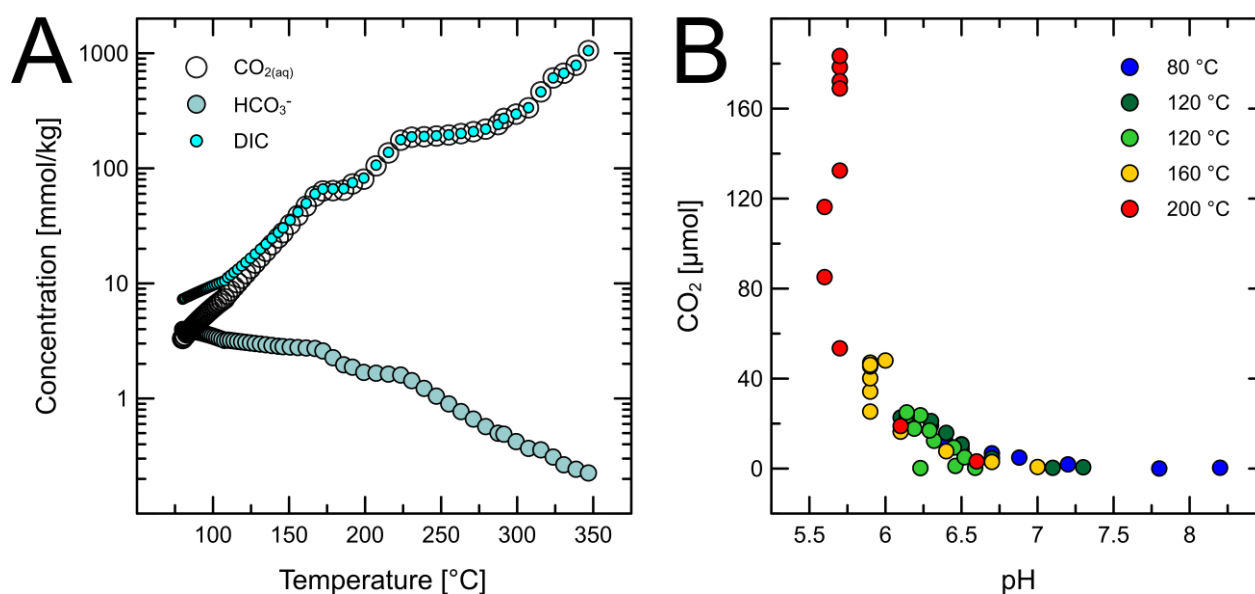
Figure 4.4: (A) Predicted relation between temperature and DIC concentration and speciation during reaction of water and Opalinus Clay (Table 4.1). Note the increase in $CO_{2(aq)}$ by a factor of >300, which matches the measured increase in $CO_{2(g)}$ in the headspace of the gold capsule experiments (Table 2). Also note that the DIC speciation changes from subequal proportions of $CO_{2(aq)}$ and HCO$_3^-$ at 80 °C (Table 4.3) to completely $CO_{2(aq)}$-dominated at higher temperatures. (B) Cross plot of the amount of $CO_{2(g)}$ [µmol] measured in 1-ml gas samples from headspace vials and the solution pH in the respective flush volume (from Helten et al. 2022). It has to be noted that the pH likely shifted to slightly higher values due to the loss of some CO$_2$ by outgassing after samples were transferred into a 2-ml Eppendorf cup.

4.2. Stable carbon isotopic composition and sources of $CO_{2(g)}$

The contributions of inorganic and organic carbon-sourced $CO_{2(aq)}$ to the DIC in the gold bag experiments were assessed through the interpretation of the stable carbon isotopic composition ($\delta^{13}C$) of the measured $CO_{2(g)}$. The discussion of the $\delta^{13}C_{CO2}$ includes a description of the experimental procedure, the consideration of processes such as temperature-dependent isotope fractionation, organic matter transformation at elevated temperatures, and the influence of the solution pH on the speciation of $CO_{2(aq)}$ in water.

The gold bags contained Opalinus Clay minerals, Opalinus Clay organic matter, and HPLC-grade water. No free gas phase was present in a gold bag prior to heating and it was assumed that no free gas phase formed during the experiment. Thus, chemical reactions proceeded between dissolved compounds and solids. Gold bags were kept at isobaric (20 MPa) and isothermal conditions (80, 120, 160, and 200 °C). During sampling, the aqueous fluid removed from a gold bag was depressurized to near-atmospheric pressure, resulting in exsolution of dissolved gases (Becker et al. 2015), including $CO_{2(g)}$. Helten et al. (2022) noted that this caused a shift in pH by up to 1.2 pH units (5.9 vs. 7.1 at 160 °C), which affects the speciation of $CO_{2(aq)}$ in water significantly. A cross-plot of the amount of substance of $CO_{2(g)}$ measured in 1-ml samples from headspace vials and the respective solution pH indicated that the pH is primarily controlled by $CO_{2(aq)}$ and vice versa (Fig. 4.4 B). Based on the $CO_{2(g)}$ data (Fig. 4.2) it was assumed that an equilibrium-like state was attained between carbonate minerals and CO_2-species by the end of an experiment (see also Sauer et al. 2020). Each aqueous fluid sample was a representative aliquot from the gold bag. On this basis, stable carbon isotopic fractionation calculations were employed to interpret $\delta^{13}C_{CO2(g)}$ and to quantify contributions from organic and inorganic carbon sources in an isotope mass balance (IMB). The stable carbon isotopic composition of the organic (TOC) and inorganic carbon (TIC) served as endmembers contributing to a mixed $\delta^{13}C$ signal in $CO_{2(g)}$. The $\delta^{13}C_{TOC}$ in Opalinus Clay sample material was –26.2‰ and the $\delta^{13}C_{TIC}$ was –1.6‰ (Helten et al. 2022). The temperature for the fractionation calculations during room temperature degassing and equilibration in the headspace vials was assumed as 25 °C. An exact IMB cannot be achieved for the experimental data as the influence of contact ion pairs (dissolved ions) in the aqueous fluid complicates a reconstruction of the stable carbon isotope fractionation in the experiments (e.g., Leśniak and Zawidzki 2006). Details on the stable carbon isotopic fractionation calculations and supporting information can be found in the supplementary material of this study.

The results of the IMB demonstrated that $CO_{2(g)}$ originated predominantly (>80 %) from inorganic carbon, i.e. carbonate minerals. Up to 26 % of inorganic carbon and up to 6 % of organic carbon were dissolved or transformed, respectively, at 200 °C (see supplementary material Table S9).

The calculations demonstrated that carbonate mineral dissolution is a significant $CO_{2(g)}$-yielding process, which needs to be accounted for during the post-closure phase of a repository for HLW in water-saturated, carbonate-containing host rocks.

4.3. Sources for C_1–C_4 hydrocarbons

A potential origin for methane could be the Sabatier-reaction, in which carbon monoxide (CO) and/or CO_2 react(s) with hydrogen (H_2) to form methane (CH_4). In the hydrous pyrolysis experiments in gold bags, neither CO nor H_2 were detected. An exception were two experiments in gold capsules at 315 °C and 345 °C. Therefore, at high temperatures the possibility of methane generation from Opalinus Clay via the Sabatier-reaction exists – but this is beyond temperatures discussed in the context of HLW disposal.

The thermal transformation of organic matter represented the main source of the C_1–C_4 hydrocarbons in the hydrous pyrolysis experiments with Opalinus Clay. Hydrocarbon gas generation from source rocks has been demonstrated by several studies (Barth et al. 1989; Knauss et al. 1997; Seewald et al. 1998; Wei et al. 2018). For samples from the Monterey, Smackover, and Eutaw Shale, Seewald et al. (1998) reported a generation behavior similar to the one observed in this study, i.e. increasing yields with increasing temperature and a molecular pattern of $CO_{2(g)} > CH_4 > C_2H_6 > C_3H_8 > n\text{-}C_4H_{10}$ for the hydrous pyrolysis products. The increase of gas yields with increasing temperature and its approximation to a quasi-constant amount of substance (Fig. 4.3) suggests that the extent of the generation of hydrocarbons might be limited by the chemical composition of the kerogen, i.e., the availability of reactive groups. As a result, once isothermal conditions prevail the thermal generation of hydrocarbons might cease as most reactive groups available for thermal transformation will be removed from the kerogen over time. This might limit the impact of hydrocarbons on pressure build-up in a HLW repository.

The amount of gases that were released/generated at elevated temperatures (Fig. 4.2, Fig. 4.3, and Table 4.2) within a few hours to weeks contradict the assumption of Jobmann and Meleshyn (2015) according to which gas generation from organic matter transformation might be negligible in potential host rocks in a period of 10,000 years. Nevertheless, it is acknowledged

that due to the low quantities of hydrocarbons generated from Opalinus Clay at elevated temperatures (Fig. 4.3), the effect of hydrocarbons on a pressure build-up in a HLW repository might be small. But as the hydrocarbons are a possible carbon source for microorganisms, this formation of new hydrocarbons should be considered nevertheless.

4.4. Reaction kinetics

To facilitate an extrapolation of gas release/generation over longer times, reaction rates and kinetic parameters, i.e. activation energies (E_a) and frequency factors (A) were calculated. For this, the data from hydrous pyrolysis experiments in gold bags and in gold capsules obtained after 72 hours was used. The reaction rate constant k was calculated for a given temperature using the Arrhenius equation:

$$k = A \times \exp{-(E_a/RT)}$$

where k is the reaction rate constant in [1/s], A is the frequency factor in [1/s], E_a is the activation energy in [J/mol], R is the universal gas constant defined as 8.314 J/mol K, and T the absolute temperature in [K].

4.4.1 Activation energies E_a and frequency factors A

The data for the calculation of activation energies and frequency factors was selected based on the linearity among the data on a $\log_{10}$-based scale. For $CO_{2(g)}$ this applied to quasi-linear data from 80–200 °C. For the hydrocarbons data from 160 °C to 200 °C have been used, also because of the relevance of this temperature range in the context of HLW disposal in claystone formations. The calculated activation energies and frequency factors are presented in Table 4.4.

Table 4.4: Calculated activation energies (E_a) [kJ/mol] and frequency factors (A) [1/s] for the release/generation of $CO_{2(g)}$ and C_1–C_4 hydrocarbons from ground Opalinus Clay. In order to assess the individual performance of the two experimental systems, i.e. gold bags and gold capsules, the results are presented in separate columns. For $CO_{2(g)}$, gold bag and gold capsule data was used in the temperature range from 80–200 °C and 160–200 °C for hydrocarbons.

	Gold bags					Gold capsules				
	$CO_{2(g)}$	CH_4	C_2H_6	C_3H_8	n-C_4H_{10}	$CO_{2(g)}$	CH_4	C_2H_6	C_3H_8	n-C_4H_{10}
E_a [kJ/mol]	43.7	67.2	47.5	36.8	35.5	40.8	49.5	26.2	25.4	25.1
A [1/s]	7.69×10^{10}	4.06×10^9	4.22×10^6	2.83×10^5	1.60×10^5	4.41×10^{10}	6.61×10^7	2.54×10^4	1.64×10^4	1.09×10^4

Most activation energies calculated from the hydrous pyrolysis data are in line with those from other studies (Barth et al. 1989; Burnham et al. 1992; Knauss et al. 1997; Seewald et al. 1998). In the case of $CO_{2(g)}$, the calculated activation energies are in excellent agreement with values reported in the literature.

Seewald et al. (1998) used fixed frequency factors (pre-exponential factors) for their activation energy distribution model. Their frequency factors were in the order of 10^{13} [1/s] for $CO_{2(g)}$ and 10^{16} [1/s] for C_1–C_4 hydrocarbons, respectively. However, Seewald et al. (1998) pointed out that a decrease of the frequency factor by one log unit results in a lowering of the respective activation energy by 3 kcal/mol (~12.6 kJ/mol). Knauss et al. (1997) determined frequency factors in an unconstrained model and reported a range from 10^{11} to 10^{17} [1/s] for C_1–C_4 hydrocarbons (200–330 °C). Burnham et al. (1992) also used a kinetic model approach in which the frequency factor for the generation of $CO_{2(g)}$ was constrained to 10^{13} [1/s] for temperatures >250 °C. The experimentally derived frequency factors in the present study sharply contrast the constrained model values stated above. For C_1–C_4 hydrocarbons, values in the order of 10^4 to 10^9 [1/s] were calculated from the experimental data (160–200 °C). Frequency factors for $CO_{2(g)}$ were in the order of 10^{10} [1/s] (80–200 °C). The significant differences in frequency factors used in the literature and the experimentally derived values in the present study might be due to the respective focus of the studies. As the discussed temperature range for HLW disposal is <200 °C, other studies were interested in gas yielding processes at temperatures mostly between 200 and 400 °C. Frequency factors for C_1–C_4 hydrocarbons from gold capsule experiments at 260–345 °C are significantly higher with values in the order of 10^{12} to 10^{14} [1/s] and in the same range as constrained values used in model calculations (Burnham et al. 1992; Knauss et al. 1997; Seewald et al. 1998). Only the frequency factor of $CO_{2(g)}$ from gold capsule experiments at 260–345 °C does not change and is still in the order of 10^{10} [1/s]. This might be due to the high carbonate content in the Opalinus Clay (Table 4.1) and the absence of carbonates in kerogen-focused model calculations (Knauss et al. 1997; Seewald et al. 1998).

4.4.2 Reaction mechanism of gas generation

The Arrhenius-graph for $CO_{2(g)}$ (Fig. 4.5) implies that the release/generation of $CO_{2(g)}$ in hydrous pyrolysis experiments in gold bags and gold capsules is to a large extent controlled by a temperature-driven first order kinetic reaction. In contrast, the early $CO_{2(g)}$ data from the hydrous pyrolysis experiments in gold bags presented in Fig. 4.2 display a rapid mobilization of $CO_{2(g)}$ from Opalinus Clay (160 and 200 °C), which was probably followed by an equilibrium-like state between carbonate minerals and $CO_{2(aq)}$ (>200 h). The rapid increase of

$CO_{2(g)}$ was interpreted as dominated by carbonate dissolution, potentially masking the contribution of organic matter derived $CO_{2(g)}$ e.g., the decarboxylation of carboxylic groups linked to kerogen at ≥ 200 °C (see also Fig. SF1 in the supplements; Ashida et al. 2005; Larsen et al. 2005; Helten et al. 2022). As a result, activation energies for the release/generation of $CO_{2(g)}$ have to be interpreted carefully as the $CO_{2(g)}$ signal consists of contributions from carbonate mineral dissolution and organic matter transformation (see *Section 4.2*). Data from the literature suggests, however, that the activation energies calculated in the present study are well within the range of activation energies for the generation of $CO_{2(g)}$ from sample material containing carbonate minerals (Barth et al. 1989) as well as for material that was decalcified prior to experiments (Seewald et al. 1998).
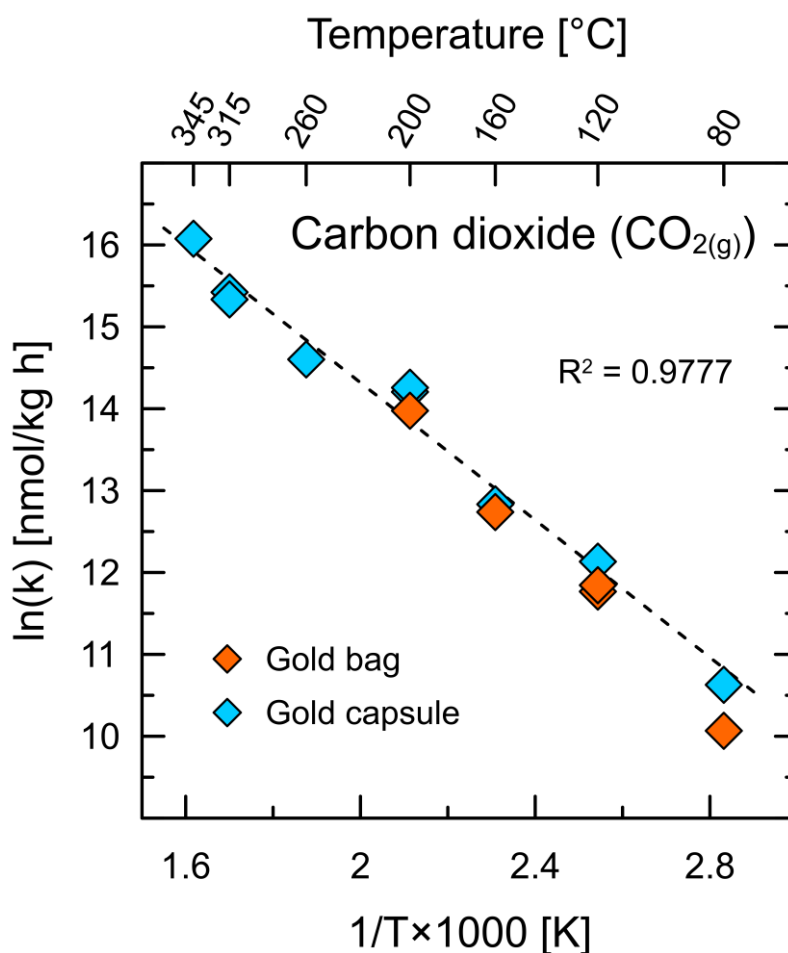
Figure 4.5: Arrhenius-graph showing the reaction rates of $CO_{2(g)}$ reported as ln(k) in [nmol/kg h] over the inverted temperature (1/T×1000) in [K] after 72 hours in hydrous pyrolysis experiments with ground Opalinus Clay. Orange diamonds = gold bags (temperature range 80–200 °C); blue diamonds = gold capsules (temperature range 80–345 °C). Some symbols in the plot overlap because of the good reproducibility of the experiments. The relative standard deviation of ±2.5 % applied to the data resulted in error bars smaller than the symbol size. The unit [nmol/kg h] refers to a mass of ground Opalinus Clay.

The Arrhenius-graphs for C_1–C_4 hydrocarbons (Fig. 4.6 A–D) display an overall good reproducibility among the hydrous pyrolysis data sets. At lower temperatures the gold bags yielded different amounts of gases than to be expected from the linear first order reaction following Arrhenius, which might point to another process at low temperatures, e.g., sorption processes including the retention of hydrocarbons by the clay-rich mud in the gold bag. The graphs indicate that the generation of C_1–C_4 hydrocarbons from Opalinus Clay organic matter is a temperature-driven process.
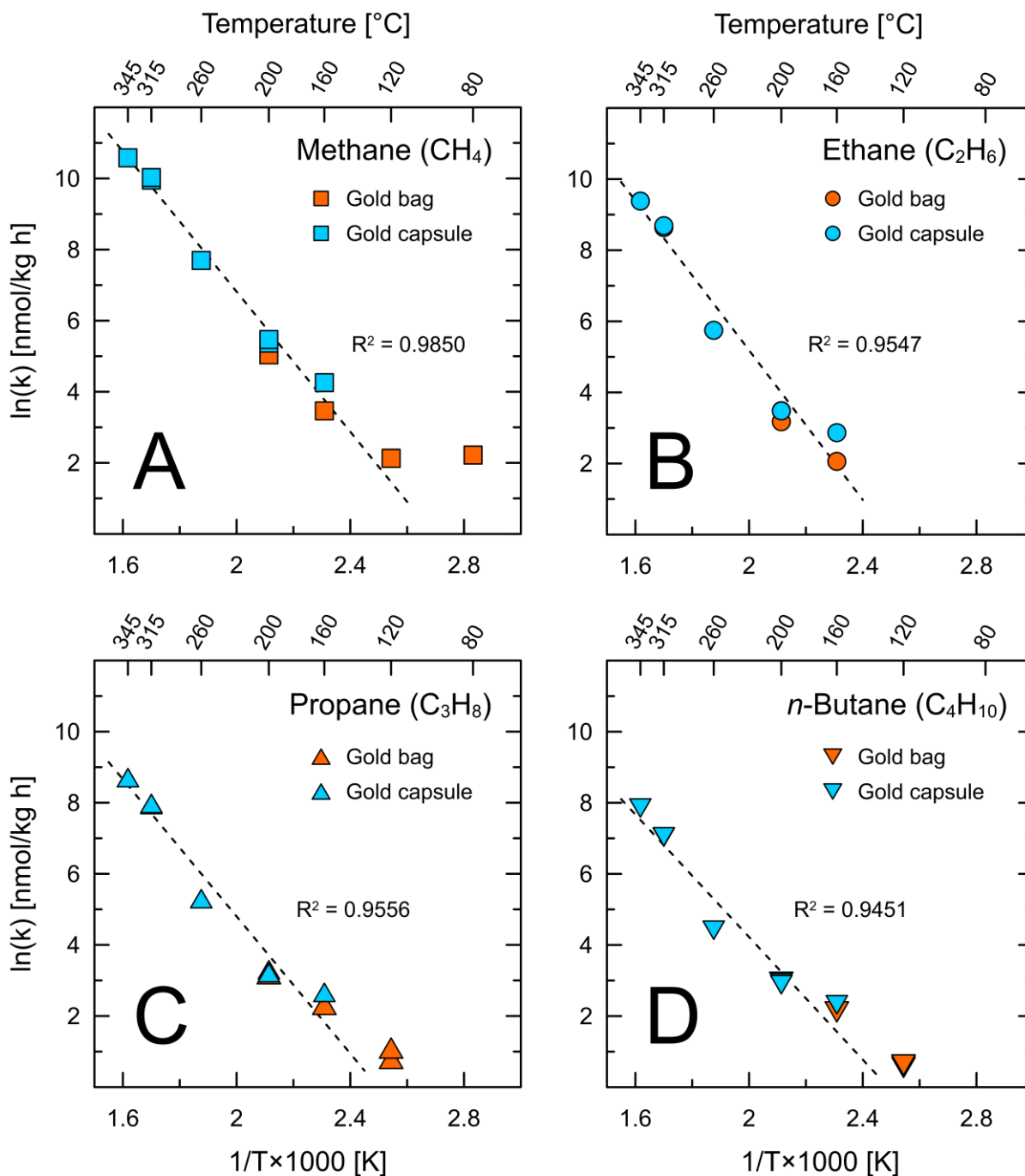
Figure 4.6: Arrhenius-graphs showing the reaction rates of C_1–C_4 hydrocarbons reported as ln(k) in [nmol/kg h] over the inverted temperature (1/T×1000) in [K] after 72 hours in hydrous pyrolysis experiments with ground Opalinus Clay. Orange symbols = gold bags (temperature range 80–200 °C); blue symbols = gold capsules (temperature range 80–345 °C). Some scattering was found in the plots at ≤120 °C, which coincides with data obtained close to the limit of quantification. Some symbols in the plot overlap because of the good reproducibility. The dotted linear regression line refers to gold capsule data only, because it covered the largest temperature range. The relative standard deviation of ±1.5 % applied to the data resulted in error bars smaller than the symbol size. The unit [nmol/kg h] refers to a mass of ground Opalinus Clay.

5. Conclusion

Hydrous pyrolysis experiments in flexible gold-titanium reaction cells (gold bags) and gold capsules containing ground Opalinus Clay (Mont Terri, Switzerland) and HPLC-grade water were conducted at temperatures relevant for the storage of high-level heat-generating nuclear waste (HLW; 90–150 °C) – and up to 345 °C. The release/generation of $CO_{2(g)}$ and C_1–C_4 hydrocarbons was observed over the whole temperature range. The total amount of gases increased with increasing temperature. Molecular hydrogen (H_2) was only detected in two samples at 315 and 345 °C, which exceeds the temperature range discussed for HLW disposal. Neither carbon monoxide (CO) nor hydrogen sulfide (H_2S) were detected. $CO_{2(g)}$ was the predominant gas, followed by $CH_4 > C_2H_6 \sim C_3H_8 > n\text{-}C_4H_{10}$. The evaluation of the stable carbon isotopic composition of $CO_{2(g)}$, reaction rates and kinetic parameters identified temperature-driven organic matter transformation as the major process leading to the generation of C_1–C_4 hydrocarbons in Opalinus Clay. Combined information on the amount of $CO_{2(g)}$, thermodynamic calculation data on the concentration of dissolved inorganic carbon (DIC), and information on the stable carbon isotopic composition of $CO_{2(g)}$ from gold bag samples demonstrated that $\geq 80\,\%$ of the $CO_{2(g)}$ originated from carbonate mineral dissolution. The model calculations also suggest that the fraction of $CO_{2(aq)}$ in DIC increases from $\sim 50\,\%$ at 80 °C to nearly 100 % at higher temperatures. In total, up to 26 % of the inorganic carbon as well as up to 6 % of the organic carbon in the Opalinus Clay were dissolved or transformed, respectively, into $CO_{2(g)}$ at 200 °C. However, no significant quantitative changes of inorganic carbon in the solid sample, i.e. carbonate minerals, were detected on sample material analyzed after the hydrous pyrolysis experiments, which is in line with literature data. Our findings emphasize the importance of the safety criterion 'gas generation' in the feature, events, and processes (FEP) catalogues for a repository for HLW. Our new quantitative data on gas generation in Opalinus Clay and thermodynamic parameters will be used in numerical models for assessing geochemical processes in claystone formations.

Acknowledgements

Supplementary Material

Supplement I

Raw data for gases in gold bag (GB) experiments.

Table S1: Experimental gold bag sample data at 80 °C.

LIMS#	Time [h]	Vol. GB before sampling [ml]	Vol. sample [ml]	pH	CO_2 [nmol]	CH_4 [nmol]	C_2H_6 [nmol]	C_3H_8 [nmol]	n-C_4H_{10} [nmol]
1908407	2	87.054	1.948	7.8	36	0.30	0.00	0.00	0.00
1908408	24	84.106	1.930	8.2	361	0.54	0.00	0.00	0.00
1908409	70	81.176	1.958	7.2	1838	0.77	0.00	0.11	0.08
1908410	170	78.218	1.977	6.9	4853	0.92	0.00	0.16	0.09
1908411	240	75.241	1.890	6.7	6763	0.95	0.17	0.21	0.13
1908412	314	72.251	1.970	6.5	8630		0.21	0.25	0.14
1908413	406	69.281	1.958	6.5	9648	1.16	0.24	0.28	0.16
1908414	503	66.323	1.850	6.5	9515	1.32	0.27	0.30	0.17
1908415	573	63.473	1.920	6.5	10795	1.39	0.28	0.32	0.19
1908416	646	60.553	1.970	6.4	10878	1.20	0.29	0.35	0.18
1908417	719	57.583	1.990	6.4	11382	1.21	0.30	0.34	0.16

Table S2: Experimental gold bag sample data at 120 °C.

LIMS#	Time [h]	Vol. GB before sampling [ml]	Vol. sample [ml]	pH	CO_2 [nmol]	CH_4 [nmol]	C_2H_6 [nmol]	C_3H_8 [nmol]	n-C_4H_{10} [nmol]
1912310	0	89	1.946	7.1	305	0.00	0.00	0.00	0.00
1912311	2	86.054	1.962	7.3	569	0.00	0.00	0.00	0.00
1912312	24	83.092	1.998	6.7	4554	0.53	0.17	0.13	0.11
1912313	72	80.094	1.999	6.5	10599	0.76	0.18	0.20	0.16
1912314	168	77.095	1.94	6.4	15872	1.16	0.26	0.38	0.27
1912315	240	74.255	1.943	6.3	19143	1.29	0.35	0.48	0.38
1912316	360	71.312	1.953	6.3	21114	1.68	0.50	0.56	0.43
1912317	906	68.359	1.93	6.1	22671	2.10	0.48	0.61	0.48

Table S3: Experimental gold bag sample data at 120 °C.

LIMS#	Time [h]	Vol. GB before sampling [ml]	Vol. sample [ml]	pH	CO₂ [nmol]	CH₄ [nmol]	C₂H₆ [nmol]	C₃H₈ [nmol]	n-C₄H₁₀ [nmol]
2008009	0	88.005	1.995	6.59	318	0.0	0.0	0.0	0.0
2008010	4	84.998	2.007	6.46	1162	0.0	0.0	0.0	0.0
2008011	24	82.088	2.01	6.52	4989	0.7	0.0	0.0	0.0
2008012	48	79.162	2.026	6.45	9323	0.7	0.0	0.2	0.1
2008013	72	76.295	1.967	6.32	12326	0.8	0.2	0.3	0.2
2008014	168	73.298	2.041	6.29	16905	0.9	0.2	0.3	0.2
2008015	240	70.273	2.025	6.19	17739	1.0	0.3	0.4	0.2
2008016	384	67.208	2.065	6.23	23677	1.2	0.3	0.5	0.3
2008017	504	64.138	2.07	6.14	23525	1.3	0.4	0.5	0.3
2008018	672	61.09	2.048	6.14	24949	1.5	0.5	0.6	0.4

Table S4: Experimental gold bag sample data at 160 °C.

LIMS#	Time [h]	Vol. GB before sampling [ml]	Vol. sample [ml]	pH	CO₂ [nmol]	CH₄ [nmol]	C₂H₆ [nmol]	C₃H₈ [nmol]	n-C₄H₁₀ [nmol]
2002009	0	84	1.961	7.0	667	0.00	0.00	0.00	0.00
2002010	2	81.139	1.933	6.7	2905	0.00	0.00	0.00	0.00
2002011	6	78.306	2.01	6.4	7672	0.49	0.00	0.12	0.12
2002012	24	75.396	1.968	6.1	16355	1.20	0.29	0.37	0.31
2002013	48	72.428	1.997	5.9	25325	1.97	0.52	0.69	0.54
2002014	72	69.531	2.119	5.9	34196	3.35	0.84	1.07	0.87
2002015	168	66.512	1.953	5.9	40083	4.07	0.94	1.23	0.98
2002016	240	63.659	1.976	5.9	47077	5.31	1.32	1.58	1.33
2002017	336	60.783	1.789	5.9	45366	5.58	1.31	1.57	1.30
2002018	363	58.194	1.719	5.9	46083	5.18	1.22	1.48	1.23
2002814	504	55.575	1.794	6.0	48005	6.11	1.39	1.60	1.31

Table S5: Experimental gold bag sample data at 200 °C.

LIMS#	Time [h]	Vol. GB before sampling [ml]	Vol. sample [ml]	pH	CO₂ [nmol]	CH₄ [nmol]	C₂H₆ [nmol]	C₃H₈ [nmol]	n-C₄H₁₀ [nmol]
2003222	0	80	2.004	6.6	3160	0.00	0.00	0.00	0.00
2003223	4	76.996	1.983	6.1	18902	1.54	0.29	0.32	0.27
2003224	24	74.013	1.822	5.7	53444	6.47	1.04	1.13	0.89
2003225	48	71.191	1.776	5.6	85134	11.02	1.82	1.90	1.51
2003226	72	68.415	2.043	5.6	116303	15.71	2.44	2.46	1.93
2003227	168	65.372	1.695	5.7	132447	19.23	2.67	2.56	1.91
2003228	216	62.877	2.136	5.7	178396	26.27	3.77	3.52	2.59
2003229	312	59.741	2.062	5.7	172253	29.86	4.09	3.68	2.64
2003230	384	56.679	1.967	5.7	168929	30.67	4.12	3.67	2.57
2003263	504	53.712	2.154	5.7	183381	38.42	4.96	4.33	2.97

Table S6: Raw data for aqueous fluid composition in gold bag experiments (selected ions). The sample at 80 °C is LIMS 1908418, the sample at 120 °C is LIMS 2008030.

Temperature [°C]	K^+ [mg/l]	Na^+ [mg/l]	Ca^{2+} [mg/l]	Mg^{2+} [mg/l]	Cl^- [mg/l]	SO_4^{2-} [mg/l]	SiO_2 [mg/l]
80	80.7	512	130	56.3	211	1154	6.6
120	68.8	564	151	67.3	205	1234	23.3

Supplement III

Thermodynamic calculations using Geochemist's Workbench (2021).

Not published yet. Selected data was included in Supplement V.

Supplement IV

Description of the calculations of isotopic fractionation and the isotope mass balance.

Inorganic carbon signatures in $\delta^{13}C_{CO2(g)}$

Stable carbon isotopic fractionation between dissolved CO_2-species is temperature dependent (Myrttinen et al., 2012). As a result, the fractionation between ^{12}C and ^{13}C in the gold bags (80–200 °C) differed from that in the headspace vials (25 °C). Stable carbon isotopic fractionation ($CO_{2(g)}$–$CaCO_{3(s)}$) in the gold bags was approximated, using Equation 1 (Bottinga, 1968). The effect of pressure on CO_2-speciation (Becker et al., 2011) and on isotopic fractionation was not considered in the calculation.

$$1000 \ln(\alpha)_{CO_{2(g)}-CaCO_{3(s)}} = -2.4612 + 7.6663 \times 10^3/T - 2.988 \times 10^6/T^2 \quad (1)$$

Equation 2 by Vogel et al. (1970) was used to calculate the stable carbon isotopic fractionation for ($CO_{2(aq)}$–$CO_{2(g)}$) in a headspace vial.

$$1000 \ln(\alpha)_{CO_{2(aq)}-CO_{2(g)}} = -0.373 \times 10^3/T + 0.19 \quad (2)$$

According to the calculation after Bottinga (1968), the stable carbon isotopic fractionation for ($CO_{2(g)}$–$CaCO_{3(s)}$) in gold bags was -4.7‰ at 80 °C and +0.4‰ at 200 °C. This means the $\delta^{13}C$ of $CO_{2(g)}$ at 80 °C is lower than that of $CaCO_{3(s)}$, but with increasing temperature $CO_{2(g)}$ is enriched in ^{13}C relative to $CaCO_{3(s)}$.

The difference between the calculated $\delta^{13}C_{CO2(g)}$ and the measured $\delta^{13}C_{CO2(g)}$ from headspace vials at the end of the experiments was 1.6‰ (80 °C) and 2.9‰ (200 °C). The measured $\delta^{13}C_{CO2(g)}$ was depleted in ^{13}C compared to the calculated equilibrium carbon isotopic composition of $CO_{2(g)}$–$CaCO_{3(s)}$ after Bottinga (1968). This points to an additional source for dissolved $CO_{2(aq)}$, possibly the ^{13}C-depleted organic matter.

Emrich et al. (1970) formulated an empiric equation for the stable carbon isotopic fractionation between solid carbonate ($CaCO_{3(s)}$) and bicarbonate ($HCO_3^-{}_{(aq)}$) for the temperature range of 20–60 °C. At 25 °C, the fractionation caused $HCO_3^-{}_{(aq)}$ to be depleted in ^{13}C by -1.6‰. With increasing temperature, fractionation did not increase significantly (Emrich et al., 1970). Therefore, it is plausible to assume that $\delta^{13}C$ values of $HCO_3^-{}_{(aq)}$ in the experiments were close to $\delta^{13}C_{CaCO3}$. At 80 °C, the aqueous fluid in the gold bag contained up to 11 mmol/kg fluid DIC, which is in the range of concentrations of DIC in natural pore waters in marine sediments at elevated temperatures in the Guaymas Basin (Burdige et al., 2016). The speciation of $CO_{2(aq)}$ in water at 25 °C and 0.1 MPa was calculated in PHREEQC (Table S7). Sauer et al. (2020) reported pH values between 5 and 6 (at 25 °C) from experiments with Opalinus Clay and Wyoming bentonite. An OPA-only experiment at 300 °C and 15 MPa (water–rock ratio was 8:1) gave a pH value of ~6 after six weeks and recalculated in situ pH values were between 4.7 and 5.0 (Sauer et al., 2020). This is in excellent agreement with calculated in situ pH values for hydrous pyrolysis experiments with OPA reported by Helten et al. (2022). At higher water–rock ratios, Sauer et al. (2020) observed higher pH values, suggesting that the pH values measured in aqueous samples from gold bag experiments in the present study (water–rock ratio ≤1.8:1) are characteristic for the interaction between water and OPA at elevated temperatures and pressure.

Table S7: CO_2-speciation in aqueous samples at ambient conditions (25 °C and 0.1 MPa) calculated in PHREEQC for pH values in aqueous samples obtained at the end of the gold bag (GB) experiments conducted at different temperatures.

	GB 80 °C	GB 120 °C	GB 160 °C	GB 200 °C
pH	6.4	6.1	6.0	5.7
$CO_{2(aq)}$	0.4070	0.5764	0.6361	0.7749
$HCO_3^-{}_{(aq)}$	0.5929	0.4235	0.3638	0.2251
$CO_3^{2-}{}_{(aq)}$	0.0001	<0.0001	<0.0001	<0.0001

The stable carbon isotopic composition of the DIC was calculated in (3) after Myrttinen et al. (2012), using the speciation data (Table S7) and the measured $\delta^{13}C_{CO2(g)}$ data. Due to the negligible presence of $CO_3^{2-}{}_{(aq)}$ at the aqueous fluid pH (Table S7), $CO_3^{2-}{}_{(aq)}$ was not included in the calculation of $\delta^{13}C_{DIC}$.

$$\delta^{13}C_{DIC} = \frac{[CO_{2(aq)}] \times \left(\delta^{13}C_{CO_2} + 10^3 \ln(\alpha)^{13}C_{CO_{2(aq)} - CO_{2(g)}} \right) + [HCO_{3(aq)}^-] \times \left(\delta^{13}C_{CO_2} + 10^3 \ln(\alpha)^{13}C_{HCO_{3(aq)}^- - CO_{2(g)}} \right)}{\left([CO_{2(aq)}] + [HCO_{3(aq)}^-] \right)} \quad (3)$$

The calculated $\delta^{13}C_{DIC}$ at the end of the gold bag experiments was -6.3‰ at 80 °C, -3.4‰ at 120 °C, -2.3‰ at 160 °C, and -2.5‰ at 200 °C. The differences between the measured and the calculated values for $\delta^{13}C_{HCO3-(aq)}$ (Emrich et al., 1970) and $\delta^{13}C_{DIC}$ (Myrttinen et al., 2012) suggest that the CO_2-speciation and a contribution of $CO_{2(aq)}$ from an organic carbon source need to be taken into account to explain the measured $\delta^{13}C_{CO2(g)}$.

Organic carbon signatures in $\delta^{13}C_{CO2(g)}$

There is evidence for release of CO_2 from organic matter in the Opalinus Clay in Rock-Eval data (Fig. SF1 A). The oxygen index (OI) of sample material from before and after the heating experiments was plotted against the experimental temperature. A significant decrease in the oxygen index (OI) with increasing temperature and relative to non-heated sample material indicated that oxygen-containing functional groups such as alcohol- and carboxy-moeities were removed from the organic matter during hydrous pyrolysis of Opalinus Clay. Carboxyl groups are a part of (low-molecular-weight) organic acids, which are a constituent of kerogen (Eglinton et al., 1987; Barth et al., 1988). $CO_{2(g)}$ can be generated from carboxyl groups via thermal decarboxylation. This process is slow at lower temperatures as is the generation of low-molecular-weight organic acids (LMWOA; Palmer and Drummond, 1986; Helten et al., 2022). Helten et al. (2022) found that in total between 6.3 µmol (80 °C) and 16.2 µmol (200 °C) LMWOA (formate, acetate, and oxalate) were generated in gold bag experiments with Opalinus Clay. Considering the thermal decomposition behavior of formate (1.87×10^{-7}/s), acetate (1.07×10^{-13}/s), and oxalate (8.02×10^{-6}/s) at 200 °C (Helten et al., 2022) and over 504 hours, the resulting yield of $CO_{2(g)}$ can be estimated. This calculation depends largely on the simultaneous generation and decomposition of formate and oxalate as their reaction rate constants are six orders of magnitude higher than that of acetate. Moreover, the fast thermal decomposition of formate and oxalate at 200 °C makes the calculation more complicated because concentration data over time does not reflect the actual amounts of these compounds that were generated from Opalinus Clay (Helten et al., 2022). Experimental data by Helten et al. (2022) for temperatures from 80–160 °C indicated that formate and oxalate were generated in at least two times lower

amounts than acetate. According to this, the yield of $CO_{2(g)}$ from hydrous pyrolysis with Opalinus Clay might have been around 16 µmol (200 °C, 504 hours). Thus, the contribution of $CO_{2(g)}$ from the thermal decomposition of LMWOA is presumably lower than the release of $CO_{2(g)}$ from O-bearing functional groups in the Opalinus Clay organic matter (kerogen).
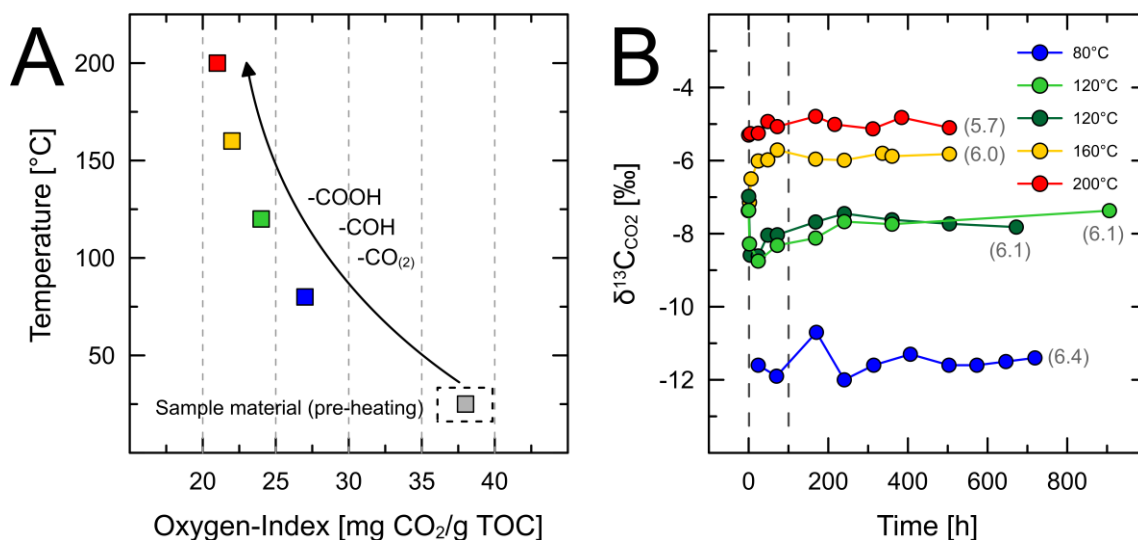

Figure SF1: Source indicators for gas release/generation from Opalinus Clay organic matter and carbonate minerals. (A) Oxygen-Index (OI) in sample material before and after hydrous pyrolysis experiments in gold bags. Values are reported in [mg CO_2/g TOC]. (B) Stable carbon isotopic composition in $CO_{2(g)}$ ($\delta^{13}C_{CO2}$) from experiments in gold bags, modified after Helten et al. (2022). Gold bag aqueous fluid sample pH for the last data point is included in parentheses (grey values). Results are reported in per mil [‰] measured against the PDB standard.

Andresen et al. (1994) reported $\delta^{13}C$ values for $CO_{2(g)}$ from organic matter transformation in hydrous pyrolysis experiments with organic carbon-rich (TOC >51 wt%), decarbonized source rocks. Andresen et al. (1994) observed a relatively small (≤4.3‰) fractionation from $\delta^{13}C_{kerogen}$ to $\delta^{13}C_{CO2(g)}$. Since the dissolution of carbonates did not influence the $\delta^{13}C$ values reported by Andresen et al. (1994), the impact of Opalinus Clay carbonate mineral dissolution on the $\delta^{13}C_{CO2(g)}$ might have been considerable. Nevertheless, the $\delta^{13}C_{CO2(g)}$ data in the dashed interval (Fig. SF1 B) indicates that organic carbon-sourced $CO_{2(g)}$ significantly contributed to the overall $\delta^{13}C_{CO2(g)}$ signal in the early stage of the experiments. For instance, the curves of the 120 °C experiments showed an initial drop followed by an increase of the $\delta^{13}C$ values. This drop might mark a fast generation of $CO_{2(g)}$ from organic matter, which was superimposed later by $CO_{2(g)}$ from inorganic carbon, i.e. the dissolution of carbonate minerals. These processes are the same for experiments at higher temperatures, but due to the rise in temperature the reaction rates increase and the overlap of the processes becomes larger. This can be seen in the experiment at 160 °C where an increase in $\delta^{13}C$ was observed within the first hours of the

experiment. Again, this indicates an early contribution of organic matter-sourced CO_2 followed by the release of CO_2 from inorganic carbon.

Kotarba et al. (2022b) performed hydrous pyrolysis experiments at 330 °C and 355 °C with Miocene shales (type III/II kerogen) and reported that $CO_{2(g)}$ generation was caused predominantly by carbonate dissolution. These authors reported a reduction of the initial amount of various carbonate minerals by 33–77 % with calcite being at the lower end. Moreover, decarboxylation reactions involving humic organic matter added to the measured $CO_{2(g)}$ to a lesser extent (1.8–4.6 %; Kotarba et al., 2022b). Overall, $CO_{2(g)}$ was the main gas generated in the experiments with a contribution of $\geq$94.2 % and $\delta^{13}C_{CO2(g)}$ values were between -3.5‰ and +1.1‰ (Kotarba et al., 2022b). The $\delta^{13}C_{kerogen}$ was between -25.8‰ and -24.8‰ (Kotarba et al., 2022a). The proportion of $CO_{2(g)}$ in the total amount of gases quantified and the $\delta^{13}C_{CO2(g)}$ reported by Kotarba et al. (2022b), on the other hand, agree well with our findings. In the present study, quantitative XRD analyses showed no significant change in the amount of carbonate minerals in sample material before and after the hydrous pyrolysis experiments (data not shown). A similar observation was made by Sauer et al. (2020), who did not see changes in the calcite content in mixed OPA–bentonite sample material after hydrous pyrolysis experiments at 200 °C. However, these authors reported a decrease in calcite content (16 wt.% to 8 wt.%) in OPA sample material analyzed after hydrous pyrolysis experiments at 300 °C.

Wang et al. (2022b) performed hydrous pyrolysis experiments (350 °C) with a set of marine source rocks, investigating the origin of inorganic $CO_{2(g)}$. These authors demonstrated that $CO_{2(g)}$ yields and $\delta^{13}C_{CO2}$ values increased with increasing carbonate mineral content in the sample material. Reported $\delta^{13}C$ values for $CO_{2(g)}$ higher than -8‰ were classified as predominantly inorganic, while a mixed $\delta^{13}C_{CO2}$ inorganic-organic signal was suggested for the range of -16‰ to -8‰ (Wang et al., 2022b). The study by Wang et al. (2022b) and other studies cited above provide convincing evidence for inorganically sourced $CO_{2(g)}$ released predominantly by carbonate mineral dissolution in hydrous pyrolysis experiments with shales. The $\delta^{13}C$ values of $CO_{2(g)}$ are a reliable tool indicating potential sources for CO_2. Unfortunately, the above cited studies did not look deeper into stable carbon isotopic fractionation. In the present study, an isotope mass balance was performed to obtain refined information on the respective contribution of CO_2 from two endmembers: inorganic carbon and organic carbon.

Stable carbon isotope mass balance

In order to calculate the isotope mass balance (IMB) for the contributions of the two sources for DIC, i.e. organic and inorganic carbon the following assumptions were made: There was no free gas phase in the gold bag. The salinity/ion activity in aqueous samples was not accounted for. Dissolution and precipitation of carbonate minerals did occur during the experiment, but by its end an equilibrium had been attained for ($CaCO_{3(s)}$–$CO_{2(aq)}$). No significant change in the original organic/inorganic carbon reservoir ($\delta^{13}C$ and mass) occurred (that has been confirmed by analyses of $\delta^{13}C_{org}$ after the experiment).

Knowing the total amount of substance of organic carbon (OC) and inorganic carbon (IC) in the Opalinus Clay sample material, the stable carbon isotopic composition of both carbon reservoirs, the amount of substance of $CO_{2(g)}$, the amount of substance of DIC and its calculated stable carbon isotopic composition ($\delta^{13}C_{DIC}$), the IMB was calculated for each experiment as:

$$\delta^{13}C_{IMB}[‰] = \frac{(n_{DIC} \times \delta^{13}C_{DIC} + n_{IC} \times \delta^{13}C_{IC} + n_{OC} \times \delta^{13}C_{OC})}{(n_{DIC} + n_{IC} + n_{OC})} \quad (4)$$

where n is the amount of substance of OC, IC, and DIC and where $\delta^{13}C$ is the stable carbon isotopic composition of the respective reservoir, given in [‰ vs. PDB]. The results are presented in Table S8.

Table S8: Parameters and results for the stable carbon isotope mass balance (IMB) for gold bag experiments with 50 g ground Opalinus Clay at 80, 120, 160, and 200 °C. The stable carbon isotopic composition ($\delta^{13}C$) is reported in per mil vs. PDB [‰]. OC = organic carbon; IC = inorganic carbon; DIC = dissolved inorganic carbon.

	Amount of substance [μmol]	$\delta^{13}C$ [‰]
OC	26,640	-26.2
IC	170,680	-1.6
DIC$_{80°C}$	3,110	-6.3
DIC$_{120°C}$	7,980	-3.4
DIC$_{160°C}$	12,840	-2.3
DIC$_{200°C}$	46,700	-2.5

The results in Table S8 demonstrate that the DIC was enriched in ^{13}C with increasing temperature. At the same time, the calculation of $\delta^{13}C_{IMB}$ resulted in rather positive $\delta^{13}C$ values close to the isotopic composition of the IC. Two additional calculations were performed to determine the contribution of organic and inorganic carbon to obtain the calculated $\delta^{13}C_{DIC}$ and, moreover, to quantify how much of the Opalinus Clay organic carbon was oxidized to $CO_{2(g)}$ and what percentage of the inorganic carbon (i.e. carbonate minerals) was dissolved.

Table S9: Contribution [%] of inorganic carbon (IC) and organic carbon (OC) to the calculated $\delta^{13}C_{DIC}$ values and the proportion [%] of IC and OC in Opalinus Clay that need to be dissolved/transformed to obtain the calculated $\delta^{13}C_{DIC}$ values.

	$\delta^{13}C$ [‰]	IC to $\delta^{13}C_{DIC}$ [%]	OC to $\delta^{13}C_{DIC}$ [%]	IC dissolved [%]	OC oxidized [%]
$DIC_{80°C}$	-6.3	81.0	19.0	1.5	2.2
$DIC_{120°C}$	-3.4	92.5	7.5	4.3	2.2
$DIC_{160°C}$	-2.3	97.0	3.0	7.3	1.4
$DIC_{200°C}$	-2.5	96.5	3.5	26.4	6.1

The results in Table S9 demonstrate that $CO_{2(g)}$ originated predominantly (>80 %) from an inorganic carbon source (i.e. carbonate minerals) and that up to 26.4 % of inorganic carbon (200 °C) and up to 6.1 % of organic carbon (200 °C) were dissolved/transformed under the experimental conditions.

Supplement V

Selected thermodynamic calculations performed with Geochemist's Workbench (2021).

Output for 80 °C

Step #100

Temperature = 80 °C   Pressure = 250 bars   pH = 6.021

Ionic strength	0.042693	molal
Activity of water	0.999799	
Solvent mass	0.0019900	kg
Solution mass	0.0019953	kg
Mineral mass	-	kg
Solution density	0.990	g/cm³
Solution viscosity	0.004	poise
Chlorinity	0.005782	molal
Dissolved solids	2669	mg/kg solution
Elect. conductivity	2990.2	µS/cm
Hardness	539.19	mg/kg solution as $CaCO_3$
of which carbonate	261.05	mg/kg solution as $CaCO_3$
of which non-carbonate	278.13	mg/kg solution as $CaCO_3$
Carbonate alkalinity	261.05	mg/kg solution as $CaCO_3$
Water type	Na-SO_4	
Bulk volume	2.02	cm³
Fluid volume	2.02	cm³
Mineral volume	-	cm³
Inert volume	-	cm³
Porosity	100	%
Permeability	98.7	cm²

(No minerals in system.)

Aqueous species	Molality	[mg/kg solution]	Activity coefficient	log (activity)
Na^+	0.02085	478.0	0.8131	-1.7708
SO_4^{2-}	0.009128	874.4	0.4313	-2.4049
$CO_{2(aq)}$	0.006102	267.8	1.0000	-2.2145
Cl^-	0.005752	203.4	0.8032	-2.3354
HCO_3^-	0.005153	313.6	0.8131	-2.3778
Ca^{2+}	0.002165	86.56	0.4687	-2.9936
K^+	0.001918	74.77	0.8032	-2.8124
Mg^{2+}	0.001377	33.39	0.5018	-3.1604
$CaSO_{4(aq)}$	0.000884	120.0	1.0000	-3.0538
$MgSO_{4(aq)}$	0.000802	96.24	1.0000	-3.0960
$NaSO_4^-$	0.000769	91.32	0.8131	-3.2039
$CaHCO_3^+$	9.255×10^{-5}	9.33	0.8131	-4.1235
KSO_4^-	8.758×10^{-5}	11.81	0.8131	-4.1475
$MgHCO_3^+$	6.647×10^{-5}	5.66	0.8131	-4.2673
$NaCl_{(aq)}$	1.985×10^{-5}	1.16	1.0000	-4.7023
$CaCl^+$	6.086×10^{-6}	0.458	0.8131	-5.3056
$MgCl^+$	4.166×10^{-6}	0.248	0.8131	-5.4702
$CaCO_{3(aq)}$	3.455×10^{-6}	0.345	1.0000	-5.4616
HSO_4^-	1.982×10^{-6}	0.192	0.8131	-5.7927
H^+	1.120×10^{-6}	0.00113	0.8508	-6.0211
CO_3^{2-}	1.097×10^{-6}	0.0657	0.4411	-6.3153
$MgCO_{3(aq)}$	6.652×10^{-7}	0.0559	1.0000	-6.1771
OH^-	3.952×10^{-7}	0.00670	0.8083	-6.4956
$MgOH^+$	1.013×10^{-7}	0.00417	0.8131	-7.0843
$KCl_{(aq)}$	7.478×10^{-8}	0.00556	1.0000	-7.1262
$CaOH^+$	1.709×10^{-8}	0.00097	0.8131	-7.8572

(only species $>10^{-8}$ molal listed)

Mineral saturation states (only minerals with log Q/K > -3 listed).

Mineral	log(Q/K)
Dolomite-ord	0.2366s/sat
Dolomite	0.2360s/sat
Calcite	-0.5073
Anhydrite	-0.5226
Magnesite	-0.6067
Aragonite	-0.6419
Dolomite-dis	-0.9731

Gases	Partial pressure [bar]	Fugacity	Fugacity coefficient	log(fugacity)
$CO_{2(g)}$	0.6755	0.6755	1.000*	-0.1704
$H_2O_{(g)}$	0.4583	0.4583	1.000*	-0.3388

(*no data, gas taken to be ideal)

Original basis	Moles [mol]	[mg/kg]
H_2O	0.110	9.97×10^5
Ca^{2+}	6.27×10^{-6}	126
Cl^-	1.15×10^{-5}	204
H^+	1.21×10^{-5}	6.1
HCO_3^-	2.27×10^{-5}	695
K^+	3.99×10^{-6}	78.2
Mg^{2+}	4.48×10^{-6}	54.6
Na^+	4.31×10^{-5}	496
SO_4^{2-}	2.32×10^{-5}	1120

Elemental composition		In fluid	
	Total moles [mol]	[mol]	[mg/kg]
Calcium	6.271×10^{-6}	6.271×10^{-6}	126
Carbon	2.272×10^{-5}	2.272×10^{-5}	137
Chlorine	1.151×10^{-5}	1.151×10^{-5}	204
Hydrogen	0.2209	0.2209	11,160
Magnesium	4.478×10^{-6}	4.478×10^{-6}	54.6
Oxygen	0.1106	0.1106	88,690
Potassium	3.990×10^{-6}	3.990×10^{-6}	78.2
Sodium	4.306×10^{-5}	4.306×10^{-5}	496
Sulfur	2.323×10^{-5}	2.323×10^{-5}	373

Output for 120 °C

Step #100

Temperature = 120 °C   Pressure = 250 bars   pH = 6.046

Ionic strength	0.042697	molal
Activity of water	0.999802	
Solvent mass	0.0019900	kg
Solution mass	0.0019963	kg
Mineral mass	-	kg
Solution density	0.958	g/cm³
Solution viscosity	0.002	poise
Chlorinity	0.005728	molal
Dissolved solids	3148	mg/kg solution
Elect. conductivity	-	µS/cm
Hardness	560.48	mg/kg solution as $CaCO_3$
of which carbonate	368.07	mg/kg solution as $CaCO_3$
of which non-carbonate	192.41	mg/kg solution as $CaCO_3$
Carbonate alkalinity	368.07	mg/kg solution as $CaCO_3$
Water type	Na-SO_4	
Bulk volume	2.08	cm³
Fluid volume	2.08	cm³
Mineral volume	-	cm³
Inert volume	-	cm³
Porosity	100	%
Permeability	98.7	cm²

(No minerals in system.)

Aqueous species	Molality	[mg/kg solution]	Activity coefficient	log (activity)
Na^+	0.02227	510	0.7966	-1.7510
SO_4^{2-}	0.00850	813	0.3972	-2.4718
$CO_{2(aq)}$	0.01218	534	1.0000	-1.9143
Cl^-	0.00568	201	0.7858	-2.3503
HCO_3^-	0.007231	440	0.7966	-2.2396
Ca^{2+}	0.002234	89.3	0.4359	-3.0115
K^+	0.002175	84.8	0.7858	-2.7672
Mg^{2+}	0.000887	21.5	0.4703	-3.3799
$CaSO_{4(aq)}$	0.001338	181	1.0000	-2.8735
$MgSO_{4(aq)}$	0.000756	90.7	1.0000	-3.1216
$NaSO_4^-$	0.001026	122	0.7966	-3.0877
$CaHCO_3^+$	0.000257	25.9	0.7966	-3.6887
KSO_4^-	0.000144	19.4	0.7966	-3.9416
$MgHCO_3^+$	0.000114	9.7	0.7966	-4.0405
$NaCl_{(aq)}$	3.091×10^{-5}	1.8	1.0000	-4.5099
$CaCl^+$	1.246×10^{-5}	0.94	0.7966	-5.0033
$MgCl^+$	4.385×10^{-6}	0.26	0.7966	-5.4567
$CaCO_{3(aq)}$	1.233×10^{-5}	1.2	1.0000	-4.9089
HSO_4^-	6.151×10^{-6}	0.60	0.7966	-5.3098
H^+	1.073×10^{-6}	0.0011	0.8379	-6.0461
CO_3^{2-}	1.624×10^{-6}	0.0972	0.4073	-6.1794
$MgCO_{3(aq)}$	1.138×10^{-6}	0.0957	1.0000	-5.9437
OH^-	1.839×10^{-6}	0.0312	0.7914	-5.8370
$MgOH^+$	6.569×10^{-7}	0.0271	0.7966	-6.2812
$KCl_{(aq)}$	1.971×10^{-7}	0.0147	1.0000	-6.7053
$CaOH^+$	1.532×10^{-7}	0.0087	0.7966	-6.9134
$NaOH_{(aq)}$	1.976×10^{-8}	0.00079	1.0000	-7.7043

(only species $>10^{-8}$ molal listed)

Mineral saturation states (only minerals with log Q/K > -3 listed)

Mineral	log(Q/K)
Dolomite-ord	1.5181s/sat
Dolomite	1.5171s/sat
Calcite	0.1871s/sat
Anhydrite	0.0647s/sat
Magnesite	0.1345s/sat
Aragonite	0.0498s/sat
Dolomite-dis	0.4921s/sat
Huntite	-0.4846

Gases	Partial pressure [bar]	Fugacity	Fugacity coefficient	log(fugacity)
$CO_{2(g)}$	1.783	1.783	1.000*	0.2511
$H_2O_{(g)}$	1.886	1.886	1.000*	0.2756

(*no data, gas taken to be ideal)

Original basis	Moles [mol]	[mg/kg]
H_2O	0.110	9.97×10^5
Ca^{2+}	7.67×10^{-6}	154
Cl^-	1.14×10^{-5}	202
H^+	2.42×10^{-5}	12.2
HCO_3^-	3.94×10^{-5}	1200
K^+	4.61×10^{-6}	90.4
Mg^{2+}	3.51×10^{-6}	42.7
Na^+	4.64×10^{-5}	535
SO_4^{2-}	2.34×10^{-5}	1130

Elemental composition			In fluid
	Total moles [mol]	[mol]	[mg/kg]
Calcium	7.671×10^{-6}	7.671×10^{-6}	154
Carbon	3.940×10^{-5}	3.940×10^{-5}	237
Chlorine	1.140×10^{-5}	1.140×10^{-5}	202
Hydrogen	0.2209	0.2209	11,150
Magnesium	3.508×10^{-6}	3.508×10^{-6}	42.7
Oxygen	0.1107	0.1107	88,680
Potassium	4.614×10^{-6}	4.614×10^{-6}	90.4
Sodium	4.643×10^{-5}	4.643×10^{-5}	535
Sulfur	2.341×10^{-5}	2.341×10^{-5}	376

Chapter V

Interactions between mono- and dicarboxylic low-molecular-weight organic acids and Opalinus Clay mineral phases in suspension

Oliver Helten[a,b]*, Christian Ostertag-Henning[a]

In preparation for *t.b.d.*

[a]Federal Institute for Geosciences and Natural Resources (BGR), 30655 Hannover, Germany

[b]Faculty of Geosciences, University of Bremen, 28334 Bremen, Germany

*Corresponding author. E-mail address: helteno@uni-bremen.de

Abstract

Internationally, claystone formations are candidate host rocks for high-level heat-emitting nuclear waste in deep geological disposal programs. One quality of claystones is the high retention potential of clay minerals towards radionuclides by sorption processes involving the positively charged dissolved metal ions and the negatively charged clay mineral surfaces. However, sorption sites can also be occupied by compounds other than radionuclides. Low-molecular-weight organic acids (LMWOA) are ubiquitous compounds in the natural environment and are generated at elevated temperatures in clay-rich rocks. It had been demonstrated that these acids can adsorb to clay minerals, thereby reducing the retention capacity for radionuclides. This study investigated the interaction of acetate (monocarboxylic acid) and oxalate (dicarboxylic acid) with Opalinus Clay mineral phases in a suspension. A low affinity of acetate towards mineral phases was observed. Concentrations of acetate remained largely unchanged after the addition to an Opalinus Clay suspensions. Although oxalate is known for an increased sorption behavior, in the present study it was immobilized by reactions with Ca^{2+} ions and the formation of highly insoluble Ca-oxalate. Under the geochemical in situ conditions, e.g., pH of the pore water in the Opalinus Clay, Ca-oxalate dissolution is additionally hampered. Consequently, the investigated LMWOA are unlikely to occupy sorption sites of Opalinus Clay mineral phases. Therefore, the retention capacity for radionuclides is probably not negatively affected by the thermal generation of LMWOA from Opalinus Clay organic matter. The results of this study contribute to the understanding and the (quantitative) evaluation of safety-relevant parameters for nuclear waste repository facilities.

1. Introduction

Claystone formations are under investigation as host rocks for high-level heat-emitting nuclear waste (HLW). HLW contains radionuclides that are harmful to the biosphere and must, therefore, be kept save in a repository by natural and engineered barriers. In order to achieve the highest possible safety of a repository, geological formations with low permeability (e.g., 10^{-23} m^2; Villar et al., 2015) and low hydraulic conductivity below 10^{-10} m/s (Bossart and Thury, 2008; Grambow et al., 2016) are essential to fulfill the requirements as suitable storage environment for HLW. These parameters are especially important as the adsorption of organic compounds to clay mineral surfaces and the occupancy of sorption sites can increase the mobility and transport of dissolved ions including radionuclides (Kautenburger et al., 2019; Dziadkowiec and Royne, 2020; Henning et al., 2020). HLW containers will probably fail within 10,000 years after emplacement (Landolt et al., 2009; Bossart et al., 2017; King, 2017). Therefore, a thorough understanding of the behavior of organic compounds towards mineral surfaces is essential to predict radionuclide mobility in future, long-term safety scenarios.

One compound class of organic molecules are low-molecular-weight organic acids (LMWOA). They are ubiquitous compounds in the natural environment (e.g., Orem et al., 2014; Mäder and Waber, 2017; Zhuang et al., 2019; Conrad et al., 2020; Heuer et al., 2020), are involved in metal-ion complexation (MacGowan and Surdam, 1988; Wood, 1993; Giordano and Kharaka, 1994), and mineral dissolution (Surdam et al., 1984; Bevan and Savage, 1989; Blake and Walter,1999; Li et al., 2021). LMWOA are water-soluble and are organic molecules in the range of C$_1$–C$_5$ containing at least one functional carboxyl group (R–COOH). Helten et al. (2022) demonstrated that significant amounts of water-soluble LMWOA were generated in Opalinus Clay, the chosen host rock for HLW disposal in Switzerland and a candidate host rock in Germany, at 80 °C. Temperatures between 90 °C and 150 °C at the waste containers' surfaces are under discussion for HLW storage in claystone formations (Delage et al. 2010; Grambow 2016; Lommerzheim et al. 2019; Tourchi et al. 2021).

Diffusion is the primary transport process for LMWOA dissolved in pore water in claystones (Rübel et al., 2002; Van Loon et al., 2003; Yuan and Fischer, 2022). Anion exclusion effects, molecular size, heterogeneity of the pore structure, pH and pH-dependent clay mineral surface charge influence diffusive processes (Schoonheydt and Johnston, 2006; Dagnelie et al., 2014; Chen et al. 2018a). Percolation experiments with Opalinus Clay core samples demonstrated that LMWOA were mobilized by pore water displacement (Mäder and Waber, 2017). The decay of radioelements in the HLW will cause an increase in temperature in the surrounding host rock,

potentially leading to pore water displacement due to the increase in volume of water at higher temperatures (Johnson et al., 2004; Senger et al., 2013). This might promote the transport of radionuclides dissolved in pore water.

Organic compounds with carboxylic functional groups can form complexes with radionuclides (Santschi et al., 2002; Gadd et al., 2014; Cumberland et al., 2016). For instance, humic compounds offer binding sites with various affinities and strengths for metal ions and radionuclides (Hummel et al., 1999; Bryan et al., 2012). Bryan et al. (2012) described the interactions between (1) organic compounds and metal ions/radionuclides, (2) organic compounds and mineral surfaces, (3) mineral surfaces and metal ions/radionuclides, and (4) ternary complexes where either an organic compound or a metal ion/radionuclide serves as a bridge between the other two. Bryan et al. (2012) pointed out that the impact of the interactions described above immensely depends on the rate of (pore) water flow, i.e. the residence time of water allowing for the interactions to proceed. Wood (1993) conducted an extensive study on LMWOA-rare-earth element interaction, where rare-earth elements were used as analogues for trivalent radionuclides such as Americium (Am^{3+}) and Curium (Cm^{3+}). Wood (1993) used a large set of structurally different LMWOA and concluded that polycarboxylic acids have a large potential to increase the mobility of rare-earth elements and, thus, potentially also of radionuclides. The extent to which LMWOA can form complexes with radionuclides depends, however, on the concentration of the LMWOA and competing complex-forming cations like Ca^{2+} or Al^{3+} in pore water (Wood, 1993).

Fein and Hestrin (1994) reported that the dicarboxylic acid anion oxalate affects the concentration of Al^{3+} by Al-oxalate complexation. These authors suggested that the complexing ability of oxalate might be relevant to temperatures as high as 100 °C (Fein and Hestrin, 1994). However, Fein and Hestrin (1994) reported that the effectiveness of Al-complexation by oxalate was limited in the presence of Ca^{2+}, which causes the formation of highly insoluble Ca-oxalate complexes. Gadd et al. (2014) noted that Ca-oxalate solubility increases at pH <5. Ibis et al. (2020) determined the solubility of Ca-oxalate monohydrate (whewellite, $[Ca(C_2O_4) \cdot H_2O]$; see also Echigo and Kimata, 2010) in ultrapure water experimentally. Ibis et al. (2020) reported a solubility of 105.4 µmol/l at 25 °C and of 133.2 µmol/l at 90 °C. Giordano (1993) reported the solubility of Ca-oxalate at 96 °C to be 100 µmol/kg solution. Lide (2005) gave a value of 0.0061 mg/l or ~40 µmol/l for the solubility of Ca-oxalate at 20 °C. Hofmann and Bernasconi (1998) pointed out that, based on its in situ occurrence, whewellite is thermally stable to up to 68 °C. A common source of oxalate is the (thermal) transformation of organic matter (Hofmann and Bernasconi, 1998; Helten et al., 2022).

The amount of available literature on sorption behavior for specific organic compounds towards different surface materials such as clay minerals (Sansone et al., 1987; Kubicki et al., 1999; Rasamimanana et al., 2017; Dziadkowiec and Royne, 2020), iron oxides (Gu et al., 1994, 1995; Filius et al., 1997; Curti et al., 2021), or organic matter coating (Philippe and Schaumann, 2014) varies significantly. Wang and Lee (1993) found that organic matter content, redox conditions, and particle size influence sorption processes between organic molecules and clay minerals. For acetate, Wang and Lee (1993) found that little to no adsorption to pure clays occurred, but it weakly adsorbed to natural marine sediments, especially those with higher organic matter content. Kubicki et al. (1999) conducted sorption experiments with LMWOA and the clay minerals illite, kaolinite, and montmorillonite. Kubicki et al. (1999) noted that LMWOA sorption involves the deprotonated acid species (acid anion; $R–COO^-$) in many natural environments (pH > 4). Infrared spectra generated after rinsing (desorption) suggested that LMWOA sorption on clay minerals was rather weak (Kubicki et al., 1999). Results by Rasamimanana et al. (2017) demonstrated an increasing irreversibility of adsorption of organic acids to natural Callovo-Oxfordian claystone (Paris basin, France) with increasing number of carboxyl groups. Curti et al. (2021) observed the same for LMWOA and iron (oxyhydr)oxides.

Arnarson and Keil (2000) described different mechanisms for the adsorption of organic compounds to mineral surfaces, including e.g., ligand exchange or cation bridges. Ligand exchange involves the interaction between oxygen-rich functional groups like R–COOH and hydroxyl groups (R–OH) of minerals such as the hydroxylated edges of distinct clay minerals (Arnarson and Keil, 2000; Kang and Xing, 2007; Kaufhold and Dohrmann, 2013; Dziadkowiec and Royne, 2020). A spectroscopic study by Kang and Xing (2007) indicated that outer-sphere complexes at neutral pH with low energy bonds mostly dominated the adsorption of carboxylic acids on clay minerals (see also Kaufhold and Dohrmann, 2013; Dziadkowiec and Royne, 2020). Moreover, Kang and Xing (2007) pointed out that montmorillonite had a higher sorption capacity for dicarboxylic acids than kaolinite and that sorption was highly pH-dependent. Cation bridges, on the other hand, represent electrostatic interactions between a negatively charged mineral surface a cation and e.g., an acid anion (Arnarson and Keil, 2000; Dziadkowiec and Royne, 2020).

In the present study, we investigated the affinity of the mono- and dicacboxylic acids acetate and oxalate towards Opalinus Clay minerals in a suspension. The Opalinus Clay is the chosen host rock for the disposal of HLW in Switzerland and a candidate host rock in the site selection process for a HLW repository in Germany.

2. Materials and methods

2.1. Sample material and sample preparation

Opalinus Clay sample material was obtained from borehole BHE-F1 in the Mont Terri underground rock laboratory (Mont Terri, St. Ursanne, Switzerland). The core material was drilled dry, using N_2 as drilling fluid. A cylindrical core section from 2.02–2.22 m (d = 101 mm) was crushed with a jaw crusher to a grain size of approximately 5 mm. The material was further homogenized with an automated mortar and pestle. No sterilization treatment was performed in order to preserve the sample's natural properties. Sieving was avoided in order to exclude the discrimination of harder minerals, which might have altered the mineralogical composition of the sample. The sample material was stored in glass bottles under inert gas atmosphere (N_2).

Helten et al. (2022) reported the mineralogical composition of the Opalinus Clay sample material based on quantitative XRD analyses to be: 26 wt% illite/smectite, 21 wt% calcite, 19 wt% kaolinite, 11 wt% muscovite, 10 wt% quartz, 4 wt% chlorite, 4 wt% feldspar, and 5 wt% other minerals (gypsum, dolomite, pyrite, anatase).

2.2. Chemicals

HPLC-grade water (Roth) was used for the pre-testing and the experiments. Acetic acid (Fluka, $\geq$99.7 %) and oxalic acid (anhydrous, Sigma-Aldrich, $\geq$99.0 %) were used to prepare spike solutions with five different concentrations (50, 100, 200, 500, and 1000 µmol/l) in 50-ml suspension in glass tubes. In addition, aqueous formic acid solution (Honeywell/Fluka, 50 % in H_2O) and sodium-L-lactate (Aldrich, >99.0 %) were used for pre-experimental testing.

2.3. Experimental

2.3.1. Pre-experimental testing

Three pre-experimental tests were conducted in order to determine suitable experimental conditions for the interaction between the LMWOA and Opalinus Clay minerals. The first test focused on the influence of the solid-liquid ratio (S/L) on the interaction between LMWOA and Opalinus Clay in suspension. The second test payed special attention to the possibility of microbial activity in the LMWOA-Opalinus Clay suspensions and addressed ways to inhibit it. The third test was a slightly modified version of the second test with a smaller sample set, in order to validate the observations made in the second test.

2.3.2. Solid-liquid ratio (S/L)

Experimental investigations of ion-clay mineral interaction often involve distinct ratios of solid and liquid phases (solid-liquid ratio, S/L). Ionic compounds commonly used in this context are conservative tracers (Appelo et al., 2010), radionuclides (Joseph et al., 2011), and/or organic molecules (Chen et al., 2018a,b). The pre-experimental testing in this study was laid out to determine a S/L at which LMWOA interact with Opalinus Clay minerals with an adsorption of ~50 % of the acids (see Joseph et al., 2011). A target concentration of 100 µmol/l was chosen for testing, based on analytical requirements of the HPLC-system.

2.3.3. (Pre-) Equilibration time

Ion-clay mineral interaction often involves a pre-equilibration between either pure or artificial pore water and sample material, e.g., pure clay minerals (Wang and Lee, 1993; Kang and Xing, 2007), mixtures of clay minerals and other minerals such as iron (oxyhydr-)oxides (Curti et al., 2021), or a natural clay-rich sample (Wang and Lee, 1993; Descostes and Tevissen, 2004; Joseph et al., 2011). Pre-equilibration times in the literature vary greatly, especially when organic molecules are involved. This is due to the consumption of LMWOA by microbial activity (see *section 2.3.6*). During pre-experimental testing, the equilibration time between HPLC-grade water and Opalinus Clay as well as the equilibration between LMWOA and Opalinus Clay in suspension was seven days, respectively. The resulting suspension was then used in the tests.

2.3.4. Effect of solution/suspension pH

Most studies investigating ion-clay mineral interaction adjust the pH of the solution/suspension in order to activate or deactivate the surface of clay minerals. Arnarson and Keil (2000) demonstrated that the pH of an aqueous solution had a significant impact on the adsorption behavior of organic matter dissolved in pore water (>1000 Da) towards montmorillonite. At a pH = 4.5 more than 60 % of the dissolved organic matter were adsorbed, whereas only ~35 % were at pH = 8 (Arnarson and Keil, 2000). This was attributed to the increasingly hydrophobic character of protonated acidic functional groups at lower pH. Furthermore, Arnarson and Keil (2000) pointed out that the negative surface charge of montmorillonite decreases with decreasing pH, resulting in less electrostatic repulsion of ions and molecules.
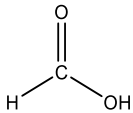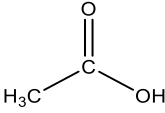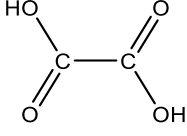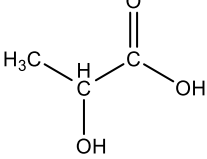
In this study, no pH-adjustment of the solutions/suspensions was attempted because the LMWOA-Opalinus Clay interaction were to take place under pH conditions characteristic for the equilibration between the sample material and water. Thus, at a solution/suspension pH >5,

most if not all LMWOA were present as their deprotonated acid anion (R–COO⁻). The pH of samples from different S/L pre-tests was measured in order to map the experimental conditions that were to be expected for the interaction of LMWOA in an Opalinus Clay suspension.

2.3.5. Selection of low-molecular-weight organic acids

Previous work (Helten et al., 2022) and literature data on LMWOA in Opalinus Clay pore water and experiments with Opalinus Clay (Pearson et al., 2003; Mäder and Waber, 2017; Chen et al., 2018a) were consulted for the selection of LMWOA. Formic acid, acetic acid, oxalic acid, and lactic acid were chosen due to the differences in carbon atom number and functional groups, i.e. hydroxyl-groups (R–OH) and carboxyl-groups (R–COOH).

Table 5.1: Information on low-molecular-organic acids (LMWOA) used in the pre-experimental and in the experimental part of this study.

Chemical compound (acid / corresponding acid anion)	Molecular structure of the acid	Formula	Molecular mass [g/mol]	pK_{S1}	pK_{S2}
Formic acid / formate		CH_2O_2	46.03	3.77	-
Acetic acid / acetate		$C_2H_4O_2$	60.05	4.76	-
Oxalic acid / oxalate		$C_2H_2O_4$	90.04	1.23	4.19
Lactic acid / lactate		$C_3H_6O_3$	90.08	3.86	-

2.3.6. Microbial activity and means of its inhibition

There are numerous physical and chemical methods available to inhibit microbial activity. For a thorough methodical comparison the reader is referred to Otte et al. (2018). Sample treatment with heat (e.g., autoclavation) beyond the temperature conditions under which microorganisms can survive is one way to sterilize sample material. Even though, bacterial endospores might be able to remain unharmed by such procedures (Trevors, 1996). Drawback of this method are the transformation of organic matter and of properties of clay minerals (Jenneman et al., 1986;

Lotrario et al., 1994; Berns et al., 2008).

Irradiation of sample material, on the other hand, damages the cell structure of microorganisms beyond repair, but affects the molecular structure of the organic matter and mineral properties as well (Lotrario et al., 1994; Berns et al., 2008).

The use of chemicals, such as sodium azide (NaN_3) can inhibit microbial activity for several weeks (Hendrix et al., 2019). The effectiveness of NaN_3 has been questioned by some studies (Skipper and Westermann, 1973; Lee et al., 1992) and NaN_3 did not perform well under anoxic conditions (Lee et al., 1992). Moreover, Chen et al. (2018b) pointed out that NaN_3 might interact with organic molecules. Chemical treatment of samples with mercuric chloride ($HgCl_2$) is a standard method in many fields (Lee et al., 1992; Tuominen et al., 1994). Chen et al. (2018a) pointed out that the highly acidic Hg^{2+} ion can adsorb to Opalinus Clay mineral surfaces, blocking sorption sites for other ions and reducing its effectiveness as a microbial inhibitor. Based on the information from the literature, the application of any of the above-mentioned procedures was ruled out for this study as the (potential) negative side-effects of the physical and/or chemical pre-treatment of samples might have biased the experimental results. The effect of microbial activity on the experiments was accounted for by the use of an anoxic glovebox for sample preparation. Pre-tests with samples prepared under ambient, i.e. oxic, conditions and another sample set handled in a N_2-atmosphere were compared for the concentrations of LMWOA after the tests (data not shown). Samples prepared and handled under ambient conditions showed overall lower concentrations of LMWOA than their anoxic counterparts. However, also the anoxic samples showed significantly lower concentrations of LMWOA. It was suggested that, in both cases, microbial activity might have been the reason for the low concentrations measured after the tests. In order to exclude microbial activity altering the results of sorption experiments, the time for the interaction between organic compounds and minerals was often restricted to ≤24 hours (Sansone et al., 1987; von Oepen et al., 1991; Wang and Lee, 1993; Kubicki et al., 1999; van Hees et al., 2003; Kang and Xing, 2007; Saidy et al., 2013; Ramos and Huertas, 2014; Dagnelie et al., 2014; Fralova et al., 2021). This was adapted to the layout of this study and resulted in a very short interval for the interaction between LMWOA and Opalinus Clay, expecting that early sampling might outpace microbial activity while still providing meaningful results.

2.3.7. Reaction vessel material

There exists no general consensus on which reaction vessel material ought to be used in sorption experiments. Most studies cited in this study used plastic tubes and bottles in their experiments, e.g., polycarbonate (PC) tubes (Arnarson and Keil, 2000; Dagnelie et al., 2014; Rasamimanana

et al., 2017a,b), polypropylene (PP) bottles (Sansone et al., 1987; Joseph et al., 2011), polyethylene (PE) bottles (Ramos and Huertas, 2014), but also borosilicate glass tubes (Kang and Xing, 2007) and amber glass vials (Kubicki et al., 1999). In this study, 75-ml borosilicate centrifuge glass tubes (Rettberg GmbH, Germany) were used.

2.3.8. Experimental procedure

The experiments included one HPLC-water blank, five acetate control solutions (final concentration 50, 100, 200, 500, and 1000 µmol/l) and five oxalate control solutions of the same concentrations. Two Opalinus Clay suspensions were prepared for ICP-OES analyses. Two samples were used for HPLC analyses to obtain information on background concentrations of acetate and oxalate. The experiments were performed in duplicates. Acetate and oxalate solutions were prepared with HPLC-grade water. The experiments with acetate and oxalate were conducted in separate glass tubes to avoid potential competition among the acids for surfaces (minerals and organic matter) provided by the sample material. Based on results from pre-testing, a solid-liquid ratio of 1:10 w/w (5.0 g Opalinus Clay, 50 ml HPLC-grade water) was chosen. The suspensions were pre-equilibrated in a Heidolph Reax 20/12 overhead shaker at 15 RPM over 24 hours at room temperature (~20 °C). Following the pre-equilibration step, samples for ICP-OES and HPLC analyses were taken. The glass tubes were placed in a centrifuge operated at 3000 RPM for 30 min. A volume of 5 ml was removed from the glass tubes used in the experiments and was replaced by 5 ml of acetate or oxalate spike solution. The target concentrations of acetate and oxalate were 50, 100, 200, 500, and 1000 µmol/l, respectively. The suspensions containing either acetate or oxalate were allowed to interact with Opalinus Clay for ten minutes. Then, monitoring samples (5 ml) were taken to check the solution pH and the concentration of acetate and oxalate. The volume withdrawn from the glass tube was not renewed. After four hours, 5-ml samples were taken for HPLC measurements as well as to determine solution pH.

2.4. Analytical

2.4.1. HPLC-DAD

A modified protocol after Albert and Martens (1997) was used for the measurement of concentrations of acetate and oxalate in aqueous samples. Samples were derivatized to form colored 2-nitrophenylhydrazide compounds. A diode array detector (DAD) was used for compound detection after HPLC-separation by absorption of visible light at 550 nm. Samples were measured with a HP 1100 HPLC equipped with a Phenomenex C18 4×3.0 mm trap-column, an Agilent Eclipse XDB-C8 4.6×12.5 mm pre-column, and an Agilent Eclipse XDB-

C8 4.6×250 mm separating column. Prior to sample analyses, two blanks and four calibration standards (10, 30, 100, 300 µmol/l) were measured. Comparison of eleven calibrations showed compound and concentration specific standard deviations between 0.19 % and 1.42 %, including potential errors introduced during sample derivatization. The limit of detection was 1 µmol/l and the limit of quantification was 5 µmol/l.

2.4.2. BET

The determination of the specific surface area of the ground Opalinus Clay material was determined by N_2 adsorption using a five-point Brunauer, Emmett and Teller (BET) method (Kaufhold et al., 2010). A Micromeritics (Norcross/Georgia) Gemini III 2375 surface area analyzer was loaded with ~300 mg sample material. Prior to that, powders were degassed at 150 °C for 24 hours under vacuum.

2.4.3. ICP-OES

Dissolved cations (major, secondary, and trace elements) were analyzed by inductive coupled plasma optical emission spectrometry (ICP-OES), using a SPECTRO ARCOS device with Argon as carrier gas and CCD-chip detection. Samples were filtered (0.2 µm cellulose acetate membrane filters, VWR) and acidified with 50 µl concentrated nitric acid immediately after sampling. The limit of quantification with this method was between 0.001 mg/l and 0.1 mg/l, depending on the compound analyzed.

3. Results

Concentrations of LMWOA in the HPLC-gradient water used for the experiments were below the limit of quantification (<5 µmol/l). The samples containing only Opalinus Clay and water gave background concentrations of 17 µmol/l for acetate and 9 µmol/l for oxalate. The concentrations of acetate and oxalate in spike solutions were 65, 110, 240, 570, 1150 µmol/l and 45, 90, 170, 440, 900 µmol/l, respectively.

The concentrations of acetate and oxalate in an Opalinus Clay suspension after 0.2 and 4.0 hours are presented in Fig. 5.1 A and B. After 0.2 hours, the concentration of acetate increased compared to the concentrations of the added spike solution by 6–64 µmol/l. For samples taken after 4.0 hours the increase was 10–70 µmol/l. After 0.2 hours, the concentration of oxalate decreased in all samples to 15–35 µmol/l, compared to the added spike solutions. After 4.0 hours, an additional decrease in oxalate concentration was observed for most samples, the largest being 12 µmol/l in the 200 µmol/l sample. The concentration of major elements determined by ICP-OES measurements is presented in Table 5.1. Control samples did not show any contaminations by dissolved ions. The specific surface area of the Opalinus Clay sample material determined by BET-analysis was 27.3 m^2/g.
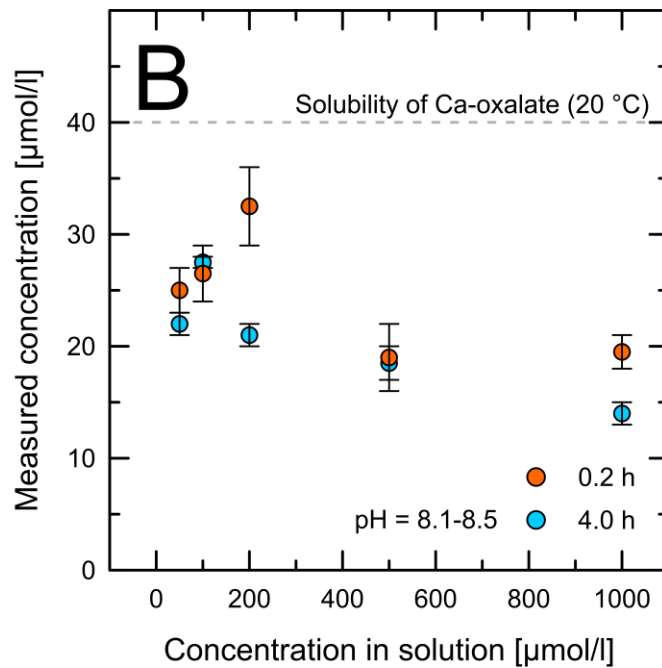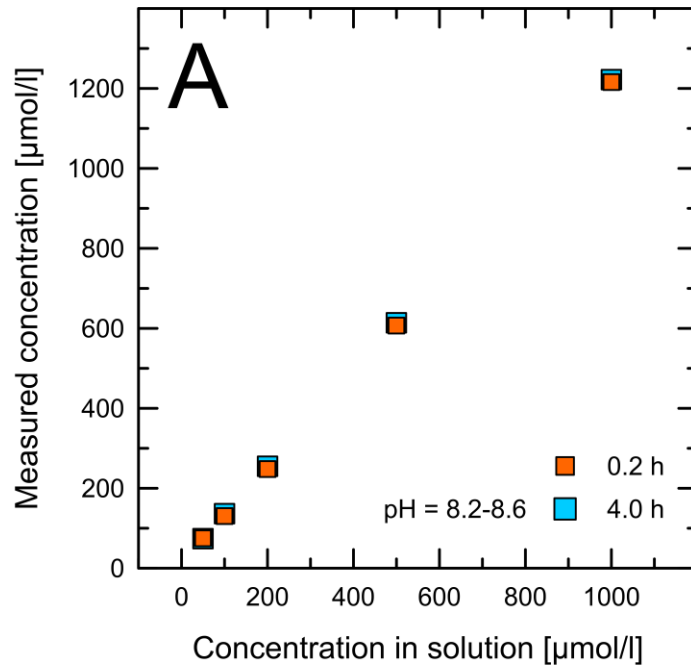
Figure 5.1: (A) Measured concentration of acetate from sorption experiments with Opalinus Clay after 0.2 hours (orange symbols) and 4.0 hours (blue symbols). Blue symbols were enlarged for better visibility. Results are presented as the mean of duplicates for each concentration. Error bars were smaller than the symbol size. (B) Measured concentration of oxalate from sorption experiments with Opalinus Clay after 0.2 hours (orange symbols) and 4.0 hours (blue symbols). Results are presented as the mean of duplicates for each concentration. Error bars indicate the range between the duplicates. The limit of quantification for acetate and oxalate were 5 µmol/l, respectively. The solubility of Ca-oxalate monohydrate [$Ca(C_2O_4) \cdot H_2O$] at 20 °C of 40 µmol/l was taken from Lide (2005).

Table 5.2: Concentration of major elements determined by ICP-OES given in [mg/l] in aqueous samples from sorption experiments with different concentrations of oxalate and Opalinus Clay (OPA). Results are presented as mean values from two samples of the same concentration.

Concentration [µmol/l]	Cl^- [mg/l]	SO_4^2 [mg/l]	Na^+ [mg/l]	K^+ [mg/l]	Ca^{2+} [mg/l]	Mg^{2+} [mg/l]	SiO_2 [mg/l]
Blank (OPA+H_2O)	36.3	235.5	103.5	18.0	21.6	6.2	1.2
50	33.0	221.0	94.4	17.7	24.0	6.7	1.3
100	33.2	223.0	95.0	18.3	26.2	7.2	1.3
200	34.5	219.0	95.7	18.2	26.3	7.3	1.4
500	33.0	215.0	94.2	18.6	28.7	8.1	1.5
1000	33.2	222.0	95.3	19.0	30.3	8.4	1.5

4. Discussion

The experiments with acetate and oxalate in an aqueous Opalinus Clay suspension with spike solutions of the respective LMWOA resulted in highly contrasting equilibrium concentrations (Fig. 5.1 A and B). The nearly constant concentrations of acetate are in good agreement with observations by Rasamimanana et al. (2017). These authors used a Callovo-Oxfordian (COx) claystone from France in their sorption experiments. Acetate showed negligible adsorption to COx claystone (Rasamimanana et al., 2017). Adsorption experiments with acetate on forest soils demonstrated that only ≤2 % of the added acetate adsorbed to the soils (van Hees et al., 2003). The duration of the sorption experiments by Rasamimanana et al. (2017) was approx. 1000 hours and facilitated microbial consumption of acetate, which was suppressed by the use of a sodium azide (NaN_3) in an additional experiment (Rasamimanana et al., 2017). The short experimental duration of 4 hours in the present study demonstrated that microbial consumption of acetate was successfully avoided. The experimental results and literature data suggest, that the adsorption of acetate to Opalinus Clay is negligible. Therefore, the generation of acetate, e.g. by thermal degradation of organic matter (Helten et al., 2022) as a result of heat emission from HLW containers might lead to increased concentrations of acetate in Opalinus Clay pore water. This bioavailable acetate can be consumed by microorganisms, which might change the chemical composition of the pore water.

Metal-ion–organic complexes are common in nature and among them carboxylates such as acetate and oxalate compounds constitute the largest group of organic minerals (Baran, 2014). According to Lide (2005) the solubility of Ca-oxalate is 0.0061 g/l (20 °C), which corresponds to ~40 µmol/l. Ibis et al. (2020) pointed out that determining the solubility of Ca-oxalate monohydrate, the most common form of this mineral, can be problematic and, historically, resulted in highly contrasting values between 46 and 2330 µmol/l. Sodium-, calcium-, and magnesium acetate, on the other hand, have a high solubility in water (Dionysiou et al., 2000; Soleymani et al., 2013), which is why they were unlikely to affect the acetate concentration in the Opalinus Clay suspension. This is in good agreement with the almost unchanged concentrations of acetate in the experiments (see also Fig. 5.1 A).

The solubility of $CaCO_3$ (calcite) is ~0.93 mol/l at 25 °C (Plummer and Busenberg, 1982). The ICP-OES data showed that between 21 and 30 mg/l Ca^{2+} were dissolved in aqueous fluid samples – which corresponds to ~910 µmol/l. When Ca^{2+} reacts with oxalate in the aqueous solution to form Ca-oxalate, the equilibrium reaction between carbonate minerals and the aqueous fluid provides new Ca^{2+} ions to balance out those that went into Ca-oxalate formation. Therefore, ICP-OES data on the concentration of Ca^{2+} in the solution is inconclusive in view of Ca-oxalate formation.

Helten et al. (2022) reported a maximum cumulative amount of substance of oxalate generated in gold bag experiments of ~4 µmol (120 °C). The raw data shows that a maximum of 50 µmol/l oxalate was measured in aqueous fluid samples from hydrous pyrolysis experiments with Opalinus Clay (see supplementary data for Helten et al., 2022). This suggests that Ca-oxalate formation might be a factor limiting the concentration of oxalate in the system minerals–water–LMWOA in the Opalinus Clay. To further evaluate this, the solubility of Ca-oxalate at ≥120 °C and the (in situ) concentration of Ca^{2+} would be needed. Consequently, there might be an increasing pool of mineral-bound oxalate present in the Opalinus Clay once heat-emitting nuclear waste initiates the generation of oxalate from the organic matter (Fig. 5.2).
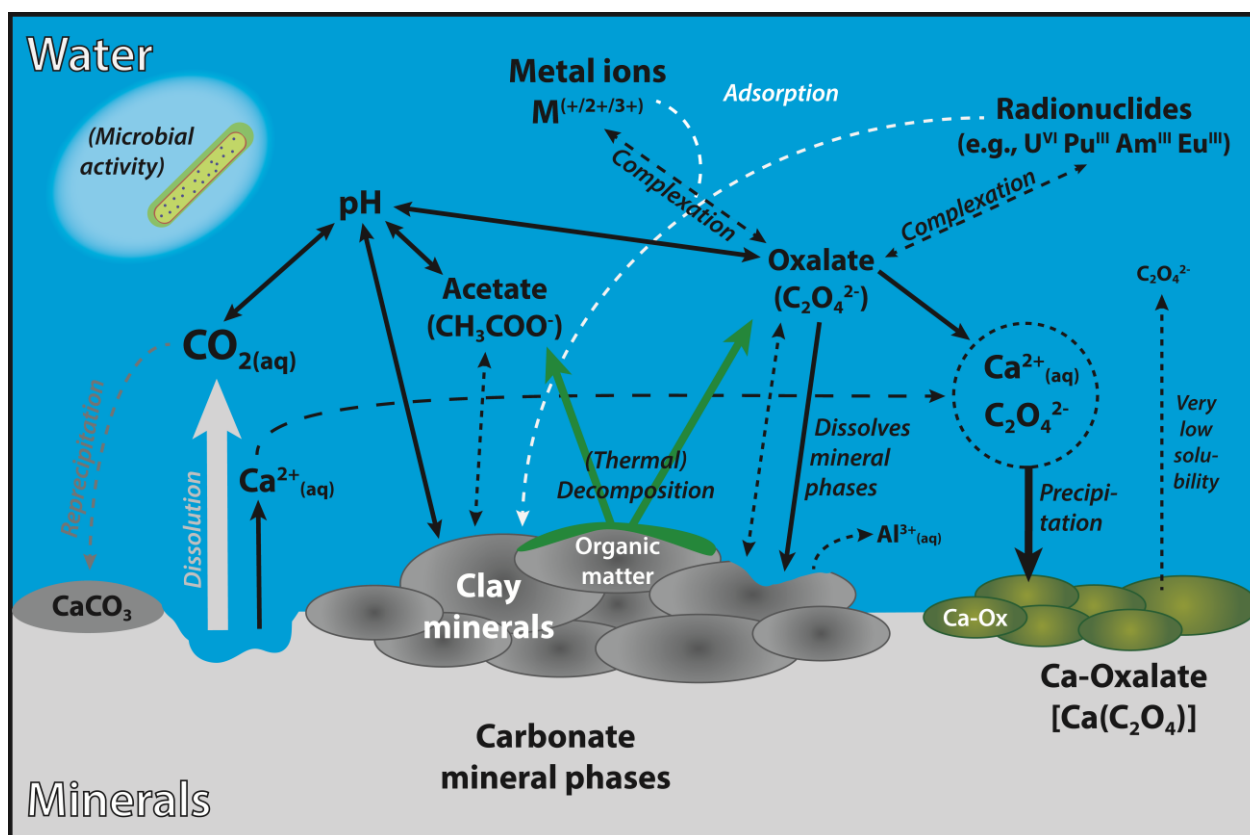
Figure 5.2: Illustration of potential reactions and interactions in the system: minerals–water–low-molecular-weight organic acids in the Opalinus Clay e.g., at elevated temperatures.

While the incorporation of oxalate in a mineral structure might have a positive effect in terms of a reduced potential for mineral dissolution (see Surdam et al., 1984), the mineral bound oxalate might become a long-term substrate reservoir for microbial communities. Microorganisms can biodegrade oxalate within days (Uren, 2018), or over longer periods if the oxalate reacts with Ca^{2+} (Ström et al., 2001). Oxalotrophy occurs among bacteria (Hervé et al., 2016) and the utilization of oxalate from Ca-oxalate minerals requires the mineral to first dissolve (Uren, 2018). Ca-oxalate dissolution is highly pH-dependent and a low pH would stabilize the activity of Ca^{2+} due to the inhibition of $CaCO_3$-precipitation (Uren, 2018).

5. Conclusion

Experiments on the interaction between low-molecular-weight organic acids (LMWOA) and Opalinus Clay mineral phases in suspension demonstrated a negligible affinity of acetate towards these solids. Oxalate was likely removed from the aqueous fluid by reactions with Ca^{2+} ions supplied by the dissolution of Opalinus Clay carbonate mineral phases. Ca-oxalate, i.e. organic minerals such as whewellite $[Ca(C_2O_4)\cdot H_2O]$ are highly insoluble and represent a sink for oxalate. Ca-oxalate might serve as a long-term reservoir of organic carbon for oxalotrophic microorganisms. The generation of LMWOA from Opalinus Clay organic matter at elevated temperature conditions expected due to heat emission from high-level radioactive waste, therefore might have no or a negligible impact on the availability of potential sorption sites on clay mineral phases in the Opalinus Clay. Consequently, the retention properties of clay mineral phases in the Opalinus Clay towards radionuclides are probably not negatively affected by competition with the investigated LMWOA. The results of this study contribute to the understanding and the evaluation of safety-relevant parameters for nuclear waste repository facilities. Our results are specific for the Opalinus Clay. Thus, the validity of the outcome has to be confirmed for other claystone formations.

Chapter VI

1. Synoptic discussion

Coupled thermo-hydro-mechanical-chemical (THMC) processes are central aspects in the performance and safety assessment for a repository for heat-emitting high-level nuclear waste (HLW) in claystone formations and other host rocks. In view of the current state of knowledge on geochemical processes in claystones, the focus in this field is primarily on the composition of pore waters and, in some cases, on the interaction between organic molecules and clay minerals, i.e. sorption processes. The transformation of claystone organic matter due to the emitted heat from HLW containers and the impact of organic matter transformation on the geochemical environment received, however, little attention. The aim of this thesis was to investigate distinct geochemical reactions in the system Opalinus Clay–water–organic matter at elevated temperatures relevant for the deep geological disposal of HLW in claystones (90–150 °C).

The thermal conductivity of claystones is rather low compared to other potential host rock types, i.e. rock salt or crystalline rocks. Heat emitted from HLW will increase the temperature in the vicinity of waste containers. This energy input will accelerate geochemical reactions such as mineral transformations (e.g., illitization) and the degradation of organic matter (e.g., generation of gaseous and/or water-soluble compounds from kerogen). Moreover, the amount and speciation of dissolved ions in pore water are affected by thermally-induced reactions in a claystone formation. All of these processes can alter the retention properties of claystones towards radionuclides. Therefore, the focus of this thesis is on the identification and quantification of distinct processes within the extensive geochemical reaction network in the Opalinus Clay. Experiments performed in the framework of this thesis used homogeneous sample material from one drill core (BHE-F1, section 2.02–2.22 m, Mont Terri underground rock laboratory, St. Ursanne, Switzerland). All observations and findings from experiments with this sample material from the clay-rich shaly facies of the Opalinus Clay will be discussed in the context of the safety criteria for a HLW repository.
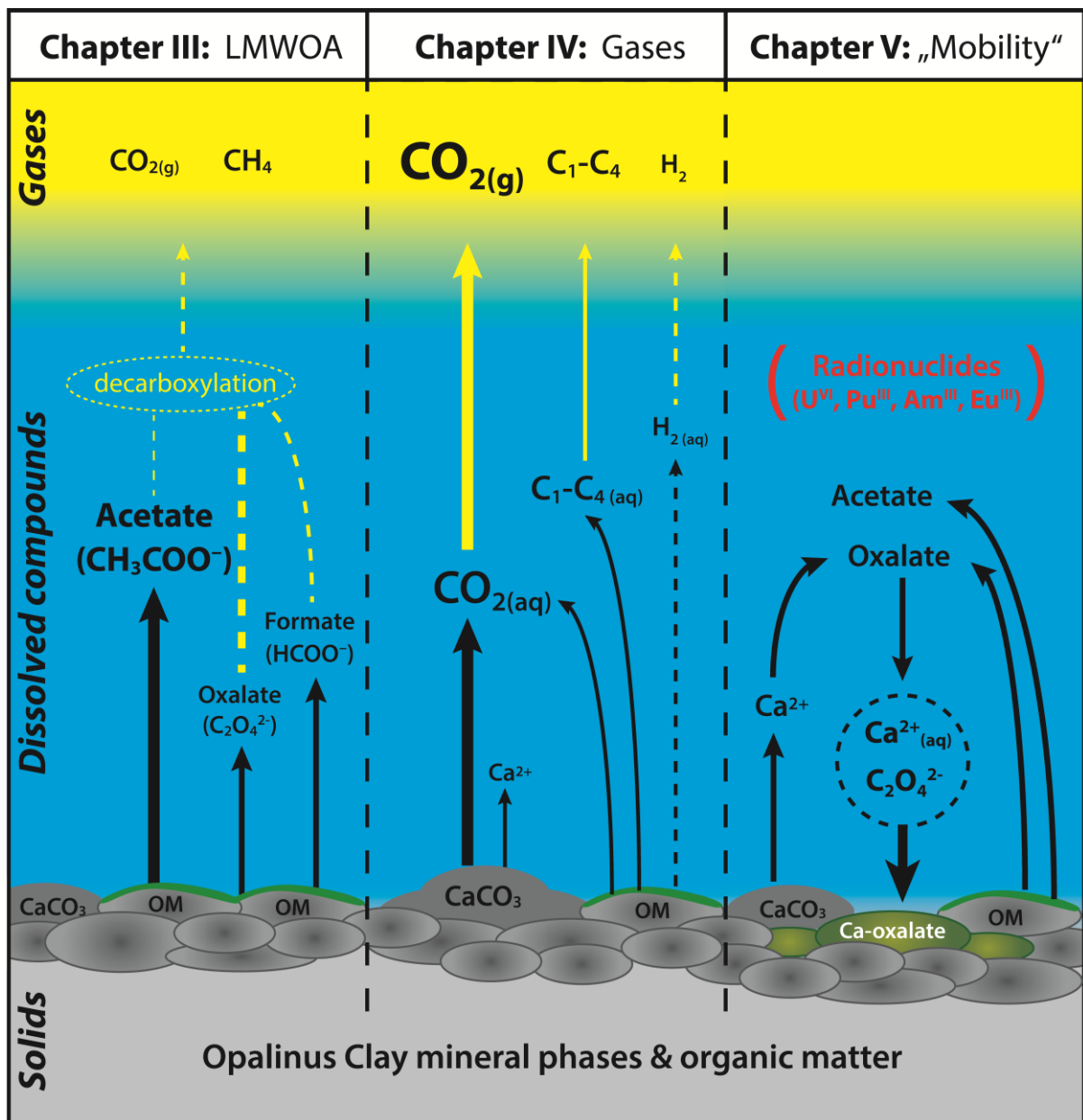
Figure 6.1: Illustration of the focus of chapters III–V. Each chapter in this thesis is thematically closely intertwined with the others – indicated by the dashed lines in this figure. OPA = Opalinus Clay; OM = organic matter; $CaCO_3$ = carbonate mineral phases; C_1–C_4 = hydrocarbon gases (methane, ethane, propane, and *n*-butane). No experiments were conducted with radioactive material, which is why radionuclides are only shown in parentheses.

1.1. Summary of Chapters III–V

While some claystone formations are investigated in the context of oil and gas exploration as either source rock or cap rock, a large portion of claystone formations is of no economic interest (Grambow, 2016). As a result, there remains a significant lack of data on some properties of claystones, which are currently of great international interest in site selection processes for HLW repositories (Delage et al., 2010; Grambow, 2016). The Opalinus Clay is the selected host rock for HLW disposal in Switzerland and a candidate as host rock for HLW disposal in Germany. The focus of this thesis was on thermal transformation reactions of Opalinus Clay organic matter to water-soluble organic compounds, i.e. low-molecular-weight organic acids (LMWOA; Chapter III) and gases (Chapter IV) under temperature conditions relevant for HLW disposal in claystone formations (90–150 °C) and beyond. Due to the potential impact of LMWOA on mineral dissolution and metal-ion (radionuclide) complexation, the interaction between LMWOA and ground Opalinus Clay in suspensions was investigated at ambient conditions (~20 °C; Chapter V).

Chapter III presents new kinetic data on the generation of LMWOA from Opalinus Clay in the experiments at elevated temperature conditions between 80 and 200 °C. The experimental approach here mimicked those used in other publications using hydrous pyrolysis equipment to quantify organic matter transformation to LMWOA. However, many studies conducted high-temperature experiments >>250 °C with short durations of ~72 hours in order to quantify the generation potential of organic matter-rich source rocks for LMWOA (see *Table 1.2 in Chapter I*). While those studies aimed to quantify the LMWOA yield, hardly any of the studies accounted for the simultaneous decomposition of newly-generated LMWOA by thermal decarboxylation reactions and the subsequent yields of gaseous by-products such as $CO_{2(g)}$ and methane ($CH_{4(g)}$). Moreover, very few of those studies included organic matter-lean sample material in their experiments (see *Table 1.2 in Chapter I*). In the context of deep geological HLW disposal, however, organic matter-lean claystones are the preferred choice as potential sources for LMWOA. The study by Helten et al. (2022) is up to now the only publication addressing the simultaneous generation and decomposition of LMWOA in a host rock for HLW disposal. Moreover, Helten et al. (2022) did this for a comparatively low temperature range of 80–200 °C and sample material with a rather low organic matter content (0.64 wt.%). The results of this study showed different yields of the LMWOA formate, acetate, and oxalate with increasing temperature. While the cumulative yield of acetate in the hydrous pyrolysis increased continuously (up to 16 µmol at 200 °C), the cumulative amount of formate stayed within a much lower range of 0.5–2.5 µmol. The cumulative yield of oxalate showed an increase with

increasing temperature up to 160 °C (~3.5 µmol), but were mostly below the limit of quantification at 200 °C. Kinetic parameters on the thermal decomposition (decarboxylation) from the literature for the three compounds demonstrated that formate and oxalate are very temperature-sensitive compared to acetate, which is reflected in the data. The potential gas yield ($CO_{2(g)}$ and $CH_{4(g)}$) from the decarboxylation of acetate was calculated as 610 µmol for a period of 100 years. Helten et al. (2022) pointed out that millimolar concentrations of acetate might be possible within the pore space of a heated Opalinus Clay and that this might serve as a feedstock for microbial life. Moreover, the impact of LMWOA on mineral dissolution, gas generation, metal-ion complexation, and sorption processes was pointed out. The lower half-lives of some LMWOA in the order of 10^{-3} years suggest that e.g., mineral dissolution processes might occur within the Opalinus Clay, affecting the permeability of the host rock. In addition, fluid-rock equilibria and the pH of the pore water need to be considered as they will likely also affect mineral dissolution processes. The reader is referred to the first column in Figure 6.1 for a schematic visualization of the content and results of Chapter III of this thesis. In addition, Figure 6.2 provides detailed information on the role of LMWOA in the system Opalinus Clay–water–organic matter.

Chapter IV presents quantitative data on the release and generation of gaseous $CO_{2(g)}$ and C_1–C_4 hydrocarbon gases in Opalinus Clay in the temperature range from 80–345 °C. Although gas release/generation from the Opalinus Clay has already been studied and quantified by in situ and lab-based experiments (Jockwer et al., 2006, 2007; Tomonaga et al., 2019), none of those studies clearly identified the sources of the gases, their respective contributions to the overall gas yield, or kinetic parameters, which are valuable information for numerical models describing long-term processes in a sealed repository. Helten et al. (in preparation) conducted hydrous pyrolysis experiments in a temperature range relevant for HLW disposal in claystones (90–150 °C) and beyond, compiling a data set that identified sources of the gases and was also used to determine kinetic parameters for gas release/generation. A safety-relevant aspect of gas generation in a sealed repository is the initiation of pore water displacement, which can involve the transport of radionuclides dissolved in pore water away from the location of HLW emplacement. The results of this study demonstrated that $CO_{2(g)}$ was the predominant gas released/generated from Opalinus Clay under the experimental conditions. Up to 180 µmol $CO_{2(g)}$ were measured in headspace vials containing ~2 ml aqueous sample, which translates to a cumulative amount of ~120 mmol/kg Opalinus Clay. Hydrocarbon gases (methane, ethane, propane, and *n*-butane) were measured in nanomolar amounts – four to five orders of magnitude less than $CO_{2(g)}$. Hydrogen sulfide ($H_2S_{(g)}$) and carbon monoxide ($CO_{(g)}$) were not detected.

Molecular hydrogen ($H_{2(g)}$) was only found in a two samples from experiments above 300 °C – out of the relevant temperature range for HLW disposal. Thermodynamic model calculations revealed that 50–100 % of dissolved $CO_{2(aq)}$ was present as dissolved inorganic carbon (DIC) in the aqueous fluid. Stable carbon isotope data ($\delta^{13}C_{CO2(g)}$) used in an isotope mass balance calculation suggested that $CO_{2(g)}$ originated from the dissolution of carbonate minerals yielding ≥80 % of the measured $CO_{2(g)}$. Accordingly, the generation of $CO_{2(g)}$ from Opalinus Clay organic matter contributed to a lesser extent to the overall gas yield. Organic matter transformation was found to be the main source of hydrocarbon gases. It was found that ~26 % of the inorganic carbon and ~6 % of the organic carbon in the Opalinus Clay sample material were transformed to $CO_{2(g)}$ (200 °C). Post-experimental analyses indicated, however, that no significant quantitative changes in the mineralogical inventory of the sample material took place, which is in line with literature data (Sauer et al., 2020). The reader is referred to the second column in Figure 6.1 for a schematic visualization of the content and results of Chapter IV of this thesis. In addition, Figure 6.2 provides detailed information on the origin and role of gases in the system Opalinus Clay–water–organic matter.

Chapter V is a data report on the interaction of the LMWOAs acetate and oxalate with Opalinus Clay minerals in a suspension at room temperature (~20 °C) and at atmospheric pressure. The interaction between organic compounds and ground claystone or intact core material has been studied in the Opalinus Clay (Chen et al., 2018a,b) or the Callovo-Oxfordian claystone (chosen host rock for HLW disposal in France; Rasamimanana et al., 2017). These experiments included percolation tests investigating the transport of organic compounds in an aqueous fluid through intact core samples and sorption experiments with ground sample material and labeled (^{13}C or ^{14}C) organic compounds. Rasamimanana et al. (2017) observed a low affinity of monocarboxylic acids like acetate for natural clay material, while the interaction between organic compounds with two or more carboxylic functional groups (–RCOOH) had been demonstrated. Helten et al. (2022) reported the generation of LMWOA from Opalinus Clay organic matter at temperatures relevant for HLW disposal in claystone formations. An unanswered question by Helten et al. (2022) was the subsequent interaction of the generated LMWOA with Opalinus Clay mineral phases in contact with an aqueous fluid, e.g., pore water. The results of the present study confirmed previous observations of almost no sorption of acetate onto clay mineral phases, which was reflected in consistent concentrations between spike solutions and measured samples. For oxalate, an abrupt decrease in the concentrations of the added spike solutions was observed. This was interpreted to be the result of the formation of Ca-oxalate complexes [$Ca(C_2O_4)$] with dissolved Ca^{2+} in the Opalinus Clay porewater.

Ca-oxalate has a very low solubility (0.0061 g/l or ~40 µmol/l at 20 °C), which might have also limited the detected concentrations of dissolved oxalate in hydrous pyrolysis experiments conducted by Helten et al. (2022) (≤50 µmol/l). The continuous supply of Ca-ions from the equilibrium reaction between carbonate minerals (e.g., $CaCO_3$) and water results in the immobilization of oxalate generated from Opalinus Clay organic matter. Consequently, the impact of oxalate on mineral dissolution and/or metal-ion (radionuclide) complexation in the Opalinus Clay is probably restricted. In general, this can be seen as a positive effect in view of safety-relevant geochemical processes for a HLW repository in Opalinus Clay. The reader is referred to the third column in Figure 6.1 for a schematic visualization of the content and results of Chapter V of this thesis. In addition, Figure 6.2 provides detailed information on the role of the interaction of LMWOA with mineral phases and dissolved ions (e.g., radionuclides) in the system Opalinus Clay–water–organic matter.
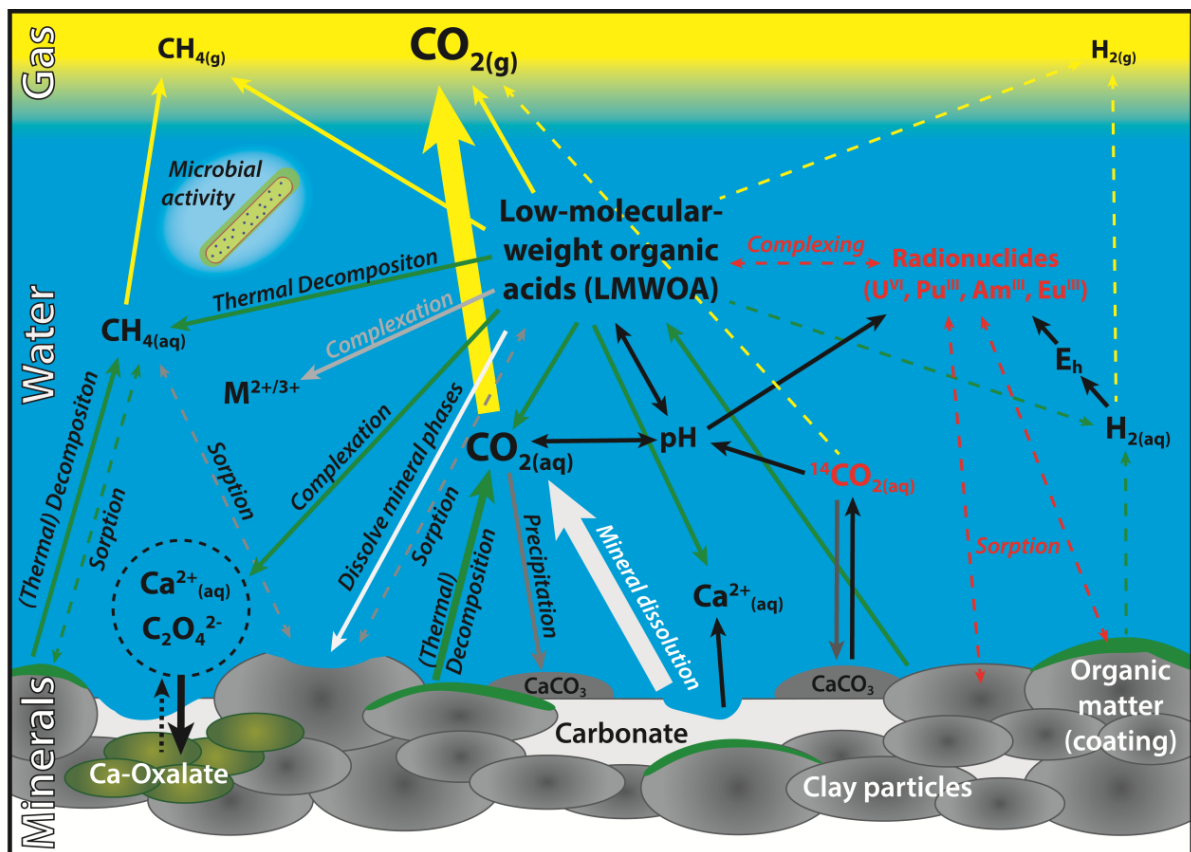
Figure 6.2: Network of co-occurring (thermo-) chemical processes and reactions in the system Opalinus Clay–water–organic matter (based on an illustration by Christian Ostertag-Henning, BGR). $CaCO_3$ = carbonate mineral phases. Microbial activity was visually accounted for as an additional co-occurring process in a HLW repository environment, but it was not investigated in the context of this thesis. No experiments were conducted with radioactive material, which is why radionuclides are only shown in parentheses.

1.2. Criteria for the safe disposal of HLW: thermal transformation of organic matter and mineral phases in the Opalinus Clay

In the context of HLW disposal in claystone formations temperature is the main parameter for the layout/geometry of the underground repository facility, i.e. the spacing between waste containers in drifts and the distances between disposal fields (Lommerzheim et al., 2019). Temperature initiates and promotes a large number of safety-relevant processes documented in feature, events, and processes (FEP) catalogues. For instance, the thermal transformation of organic matter results in the generation of gases like $CO_{2(g)}$ and hydrocarbon gases (e.g., methane) as well as water-soluble organic compounds such as low-molecular-weight organic acids, which can affect mineral transformation reactions (e.g., Surdam et al., 1984). Therefore, gas generation and mineral transformation reactions are listed as safety-relevant criteria for the assessment of the integrity of a HLW repository and can be found under the umbrella term 'processes' in FEP catalogues (Lommerzheim et al., 2019). According to Lommerzheim et al. (2019) processes are 'transformations acting within the disposal system that change the state of components'. The host rock formation (e.g., Opalinus Clay) represents a feature/component, which is further characterized by sub-components/properties, i.e. organic matter type and content as well as the mineral composition. The latter affects properties of the host rock such as thermal conductivity (quartz content), permeability (clay content), and the pore water composition (dissolved ions). Organic matter transformation results in (spatially restricted) changes in the geochemical environment within the host rock formation that affect components and their properties.

In Chapters III and IV, gas release/generation and the generation of LMWOA were addressed separately. In fact, they are simultaneous processes occurring at elevated temperatures in the system Opalinus Clay–water–organic matter. Gases and low-molecular-weight organic acids were produced at the same time from the decomposition of Opalinus Clay organic matter and by mineral dissolution. Figure 6.2 illustrates the complexity and interconnectivity in the geochemical reaction network in the Opalinus Clay – and other claystones. It needs to be pointed out that all of the processes included in the figure are directly or indirectly affected by temperature as an accelerator for geochemical reactions. In addition, it was demonstrated in this thesis that higher temperatures resulted in higher yields of gases and some LMWOA. In the following paragraphs a number of processes and events will be briefly discussed in the context of their relevance for a repository for HLW in Opalinus Clay.

1) Gas pressure: release and generation of $CO_{2(g)}$

In most scenarios for HLW disposal, the scenario of gas generation is restricted to the generation of molecular hydrogen ($H_{2(g)}$) from the anaerobic corrosion (oxidation) of steel construction material and/or waste containers in the presence of water (King, 2012). The present research by Helten et al. (in preparation) demonstrated that the generation/release of $CO_{2(g)}$ from carbonate minerals and organic matter needs to be accounted for the Opalinus Clay – and potentially other claystone formations – as well. Carbonate mineral dissolution contributed to ≥ 80 % of the measured $CO_{2(g)}$ in the hydrous pyrolysis experiments with Opalinus Clay. The dissolution of carbonates will increase the concentration of dissolved $CO_{2(aq)}$ in the pore water. The phase transition from dissolved to gaseous carbon dioxide, $CO_{2(aq)}$–$CO_{2(g)}$, depends on the partial pressure of $CO_{2(g)}$, the temperature and pressure conditions in the pore space and the presence/absence of an initial gas phase. At Mont Terri, pore pressures of ~1.5–2.5 MPa (Vinsot et al., 2017) prevail, resulting in an increased solubility of $CO_{2(g)}$ in pore water as $CO_{2(aq)}$. What might initiate a release of $CO_{2(g)}$ from the pore water within a repository is a pressure gradient between the host rock formation and the drifts/galleries. This, in turn, concerns only a limited rock volume that was disturbed during the construction phase of the repository, i.e. the excavation damage zone (EDZ; see Rübel et al., 2002). Moreover, the release of thermally generated $CO_{2(g)}$ from the host rock formation might be also limited by the extent of the pore network in the Opalinus Clay. Keller et al. (2011) and Houben et al. (2013) found that most pores in the Opalinus Clay are not interconnected and are, therefore, likely restricting the migration of ions and gases to short distances. King (2012) reported that the anaerobic oxidation of 1 mol iron/steel (~55.8 g) with water yields 1–1.33 mol $H_{2(g)}$. In comparison, in a hydrous pyrolysis experiment with 50 g ground Opalinus Clay 0.006 mol $CO_{2(g)}$ were released/generated (200 °C). This value reflects the calculated cumulative amount of $CO_{2(g)}$ based on $CO_{2(g)}$ measured in samples from the hydrous pyrolysis experiment.

Concerning the storage of HLW containers in a host rock formation, there is not one temperature to consider for the entire duration of HLW storage. Bossart et al. (2017) illustrated that the temperature in the repository environment will be at a peak shortly after waste containers are emplaced and then temperature decreases over time. Consequently, there will be a limited period in which (geo-) chemical reactions will be thermally initiated and/or accelerated – including the release/generation of gases. However, the temperature conditions within a host rock formation will be lower than those on the surface of the HLW containers, resulting in gas release/generation determined for the temperature range of 80–120 °C (≤ 0.001 mol per 50 g ground Opalinus Clay). Concerns about gas pressure build-up and

subsequent fracturing of the host rock formation of a sealed repository have been addressed e.g., by Marschall et al. (2005). These authors pointed out that the gas pressure needed to create fractures ('gasfracs') in the Opalinus Clay formation at Mont Terri is much higher than the expected evolution of the gas pressure after repository closure (Marschall et al., 2005). This thesis provided new quantitative data on the release/generation of $CO_{2(g)}$ in Opalinus Clay confirming this assumption. An investigation on the impact of $CO_{2(g)}$ on the gas pressure in a repository and the effect this might have on the displacement of pore water and the transport of dissolved radionuclides was beyond the scope of this work. Thus, processes linked to and/or initiated by the release/generation of $CO_{2(g)}$ require further research, e.g., by numerical modelling.

2) Mineral dissolution: carbonate minerals and LMWOA

This thesis demonstrated that the release/generation of gaseous CO_2 in Opalinus Clay was closely related to the dissolution of carbonate minerals and influenced the pore water pH. An isotope mass balance calculation based on the stable carbon isotope composition ($\delta^{13}C$) of $CO_{2(g)}$ suggested that up to 26 % of the inorganic carbon were dissolved at the end of the 200 °C experiment. Quantitative XRD analyses of the sample material after the experiments showed no significant change in the mineralogical composition compared to the pre-experimental measurements on non-heated Opalinus Clay. Sauer et al. (2020) reported that post-experimental analyses of Opalinus Clay from hydrous pyrolysis experiments at 200 °C did only show slight differences in XRD patterns compared to unheated sample material. Although some carbonate mineral dissolution took place during hydrous pyrolysis experiments, the post-experimental quantitative XRD analyses reported in this thesis and by Sauer et al. (2020) suggest that no significant quantitative changes in the carbonate mineral inventory of the Opalinus Clay are to be expected under elevated temperature conditions in a repository. But for a sensitive quantification of carbonate dissolution the small change in the amount of carbonates present before, during and after a heating experiment should be followed by online-analyses perhaps using an added $^{13}CO_2$ isotope label to document the dissolution/reprecipitation rates.

The impact of LMWOA on mineral dissolution processes had been shown to be primarily associated with di- and polyfunctional LMWOA (e.g., Surdam et al., 1984). Oxalate was the most prominent di-functional acid in aqueous fluid samples from the hydrous pyrolysis experiments with Opalinus Clay. At the same time, oxalate is one of the thermally least stable LMWOA (see Crossey et al., 1991; Helten et al., 2022). The relatively low half-life of oxalate for its thermal decomposition by decarboxylation in the order of 10^{-1} (80 °C) to 10^{-3} years

(200 °C) and its immobilization by complexation reactions with dissolved ions like Ca^{2+} in aqueous fluids (see next paragraph) – and therefore also in Opalinus Clay pore water – limits the potential of mineral dissolution reactions initiated by LMWOA generated from Opalinus Clay organic matter immensely. However, the complexation of Ca^{2+} by oxalate and hence its removal from the pore water might destabilize some Ca-bearing minerals resulting in their dissolution. Based on the results of this thesis, the significant dissolution of (clay) minerals initiated by LMOWA in Opalinus Clay is considered unlikely. The dissolution of carbonate minerals, however, might need careful evaluation. The overall absence of quantitative changes in the overall mineralogical inventory in unheated and heated Opalinus Clay sample material suggests that the integrity of the natural barrier properties of Opalinus Clay might not be significantly affected by geochemical reactions due to increased temperature.

3) Radionuclide mobility: sorption processes

The interaction between LMWOA and clay minerals is related to the mobility of radionuclides in claystone formations. Clay minerals such as smectite provide negatively charged surfaces that can immobilize some radionuclides by sorption. Due to the small particle size of clays (<2 µm), the resulting surface area per gram clay is high compared to other minerals. The charge of clay minerals depends on the type of clay mineral and the pore water pH (Schoonheydt and Johnston, 2006; Dohrmann et al., 2013). The ability to retain radionuclides makes claystone formations promising natural barriers for the disposal of HLW. Nevertheless, radionuclides are not the only compound class prone to sorption processes. Other metal ions as well as organic compounds dissolved in pore water interact with clay minerals and occupy sorption sites that could have otherwise been available for the retention of radionuclides. The negative surface charge of clay minerals repels anionic species such as Cl^-, I^-, and organic acid anions with deprotonated functional groups ($R–COO^-$). This anion exclusion effect (Van Loon et al., 2003) affects LMWOA once the pH of the pore water is ≥5 and the acids are deprotonated. This thesis demonstrated the generation of LMWOA over the temperature range from 80–200 °C and that the coinciding solution pH in the experiments was always >5. Moreover, experiments with LMWOA in a suspension with ground Opalinus Clay clearly indicated that the solution pH under ambient conditions was >8, which is in good agreement with data reported from the Opalinus Clay formation at Mont Terri (Switzerland; Bossart and Thury, 2008). Furthermore, the study investigating the interaction of acetate and oxalate in suspension with Opalinus Clay showed no interaction of acetate with Opalinus Clay minerals. A significant removal of oxalate was observed, which was due to complexation reactions with Ca^{2+} ions in the aqueous fluid, forming highly insoluble Ca-oxalate. Therefore, the extent of the generation of LMWOA in the

experiments has probably no negative effect on the retention properties of clay minerals in the Opalinus Clay towards radionuclides. This does not imply, however, that organic compounds in general cannot occupy sorption sites of clay minerals. A more detailed characterization of dissolved organic compounds in Opalinus Clay pore water would be beneficial.

Chapter VII

Conclusions and Outlook

This thesis demonstrated that organic matter transformation is a relevant process at temperatures expected in the context of heat-emitting high-level nuclear waste (HLW) disposal (90–150 °C) in Opalinus Clay – and potentially other claystone formations. The gases generated and released were shown to be dominated by carbon dioxide ($CO_{2(g)}$), which was released primarily from carbonate mineral ($CaCO_3$) dissolution and to a lesser extent from organic matter transformation. The cumulative amount of C_1–C_4 hydrocarbon gases was mostly in the order of nanomols [nmol] and would, therefore, only contribute in very low quantity to a gas pressure increase in a sealed repository. The cumulative amount of $CO_{2(g)}$ was in the order of low millimolar [mmol] quantities increasing with temperature. In order to quantify the impact of $CO_{2(g)}$ on the gas pressure in a sealed repository it is necessary to: (1) assess the volume of carbonate mineral bearing claystone and its organic matter content exposed to an increased temperature from HLW; (2) characterize the geochemical environment within the host rock formation and to anticipate potential changes to the pore water composition (e.g., pH); (3) quantify the volume of disturbed claystone from the excavation of galleries, which results in a pressure gradient between the pore pressure in the formation (likely several MPa) and near-ambient conditions in the galleries (~0.1 MPa) for dissolved $CO_{2(aq)}$ to undergo mass transfer into the gas phase as $CO_{2(g)}$; and (4) to account for any processes that might consume/bind $CO_{2(g)}$ in the repository environment. In order to achieve this, numerical models are needed that utilize the new quantitative geochemical data coming from hydrous pyrolysis experiments with Opalinus Clay. In addition, the new data can be added to existing estimates for pressure build-up by hydrogen gas release during the anoxic corrosion of steel in a sealed repository.

The cumulative amount of low-molecular-weight organic acids (LMWOA) from Opalinus Clay organic matter in hydrous pyrolysis experiments was in the order of several micromoles [μmol], which is in agreement with literature data on concentrations of LMWOA in Opalinus Clay pore water. The respective concentrations of the LMWOA from hydrous pyrolysis experiments are not likely to affect the dissolution of Opalinus Clay minerals, therefore, not affecting the permeability of the natural barrier properties of the host rock formation. The rapid formation

and simultaneous thermal decomposition of some LMWOA such as oxalate at temperatures between 120 and 160 °C hint at only transient presence of this otherwise reactive compound in a HLW repository in Opalinus Clay. Acetate, the main acid generated in the experiments, might accumulate in the pore water and serve as a temporary feedstock for microbial communities in the repository environment. Gas yields from the thermal decarboxylation of LMWOA were found to be approximately 1 mmol ($CO_{2(g)}$ + $CH_{4(g)}$) over the course of 100 years and per kilogram Opalinus Clay (Helten et al., 2022). While the results for the generation of LMWOA in Opalinus Clay suggest that the integrity of the natural barrier properties of this claystone are probably not negatively affected by formation or transformation of LMWOA, this finding cannot be transferred to other claystone formations, which might be characterized by completely different LMWOA yields at elevated temperatures.

The experiments on the interaction of acetate and oxalate with Opalinus Clay mineral phases in a suspension at room temperature (~20 °C) demonstrated that the concentration of acetate was not affected by the presence of potential sorption sites of Opalinus Clay minerals and organic matter and/or dissolved ions as potential complexation partners. This supports the hypothesis that acetate generated from thermal organic matter transformation could accumulate in Opalinus Clay pore water over time – if not consumed by microorganisms. Oxalate, on the other hand, was almost completely removed from the suspension within minutes. This was explained by the high affinity of oxalate to form insoluble Ca-oxalate complexes. The interpretation of relatively low concentrations of oxalate in hydrous pyrolysis experiments as the result of rapid decarboxylation was extended by the suggestion of Ca-oxalate complex formation as a limiting factor for the concentration of oxalate. The high abundance and continuous supply of Ca-ions from carbonate mineral dissolution in the Opalinus Clay limits any impact oxalate might have on the integrity of the natural barrier properties of Opalinus Clay.

This thesis highlights the importance of a thorough organic and inorganic geochemical characterization of claystone formations in the context of safety evaluation procedures for deep geological HLW disposal. Geochemical processes are often highly interdependent, temperature-related, and should not be interpreted isolated from other complementing data – when available. The transferability of the results of this thesis to other claystone formations under investigation in a HLW disposal context is probably limited and requires careful consideration. The new quantitative data on, e.g., gas production will help to refine numerical models and feature, events, and processes catalogues in the assessment of the long-term performance and safety of HLW repositories in claystone formations.

References

A

Albert, D. B., Martens, C. S. (1997) Determination of low-molecular-weight organic acid concentrations in seawater and pore-water samples via HPLC. *Marine Chemistry*, 56, 27-37. https://doi.org/10.1016/S0304-4203(96)00083-7

Andresen, B., Throndsen, T., Barth, T., Bolstad, J. (1994). Thermal generation of carbon dioxide and organic acids from different source rocks. *Organic Geochemistry*, 21, 1229-1242. https://doi.org/10.1016/0146-6380(94)90166-X

Andresen, B., Throndsen, T., Råheim, A., Bolstad, J. (1995) A comparison of pyrolysis products with models for natural gas generation. *Chemical Geology*, 126, 261-280. https://doi.org/10.1016/0009-2541(95)00122-0

Aplin, A. C., Fleet, A. J., Macquaker, J. H. (1999). Muds and mudstones: Physical and fluid-flow properties. *Geological Society, London, Special Publications*, 158, 1-8. https://doi.org/10.1144/GSL.SP.1999.158.01.01

Appelo, C. A. J., Van Loon, L. R., Wersin, P. (2010) Multicomponent diffusion of a suite of tracers (HTO, Cl, Br, I, Na, Sr, Cs) in a single sample of Opalinus Clay. *Geochimica et Cosmochimica Acta*, 74, 1201-1219. https://doi.org/10.1016/j.gca.2009.11.013

Arnarson, T. S., Keil, R. G. (2000). Mechanisms of pore water organic matter adsorption to montmorillonite. *Marine Chemistry*, 71, 309-320. https://doi.org/10.1016/S0304-4203(00)00059-1

Ashida, R., Painter, P., Larsen, J. W. (2005) Kerogen chemistry 4. Thermal decarboxylation of kerogens. *Energy & Fuels*, 19, 1954-1961. https://doi.org/10.1021/ef0501086

B

Bagnoud, A., Leupin, O., Schwyn, B., Bernier-Latmani, R. (2016a) Rates of microbial hydrogen oxidation and sulfate reduction in Opalinus Clay rock. *Applied Geochemistry*, 72, 42-50. https://doi.org/10.1016/j.apgeochem.2016.06.011

Bagnoud, A., Chourey, K., Hettich, R. L., De Bruijn, I., Andersson, A. F., Leupin, O. X., Schwyn, B., Bernier-Latmani, R. (2016) Reconstructing a hydrogen-driven microbial metabolic network in Opalinus Clay rock. *Nature Communications*, 7, 12770. https://doi.org/10.1038/ncomms12770

Barth, T. (1987) Multivariate analysis of aqueous organic acid concentrations and geological properties of North Sea reservoirs. *Chemometrics and Intelligent Laboratory Systems*, 2, 155-160. https://doi.org/10.1016/0169-7439(87)80093-X

Barth, T., Borgund, A. E., Hopland, A. U., Graue, A. (1988) Volatile organic acids produced during kerogen maturation – amounts, composition and role in migration of oil. *Organic Geochemistry*, 13, 461-465.
https://doi.org/10.1016/0146-6380(89)90020-X

Barth, T., Borgund, A. E., Hopland, A. L. (1989) Generation of organic compounds by hydrous pyrolysis of Kimmeridge oil shale—Bulk results and activation energy calculations. *Organic Geochemistry*, 14, 69-76.
https://doi.org/10.1016/0146-6380(89)90020-X

Barth, T. (1991) Organic acids and inorganic ions in waters from petroleum reservoirs, Norwegian continental shelf: a multivariate statistical analysis and comparison with American reservoir formation waters. *Applied Geochemistry*, 6, 1-15.
https://doi.org/10.1016/0883-2927(91)90059-X

Barth, T., Riis, M. (1992) Interactions between organic acids anions in formation waters and reservoir mineral phases. *Organic Geochemistry*, 19, 455-482.
https://doi.org/10.1016/0146-6380(92)90012-M

Barth, T., Bjørlykke, K. (1993) Organic acids from source rock maturation: generation potentials, transport mechanisms and relevance for mineral diagenesis. *Applied Geochemistry*, 8, 325-337.
https://doi.org/10.1016/0883-2927(93)90002-X

Barth, T., Nielsen, S. B. (1993) Estimating kinetic parameters for generation of petroleum and single compounds from hydrous pyrolysis of source rocks. *Energy & Fuels*, 7, 100-110.
https://doi.org/10.1021/ef00037a017

Becker, V., Myrttinen, A., Blum, P., Van Geldern, R., Barth, J. A. (2011) Predicting $\delta^{13}C_{DIC}$ dynamics in CCS: a scheme based on a review of inorganic carbon chemistry under elevated pressures and temperatures. *International Journal of Greenhouse Gas Control*, 5, 1250-1258.
https://doi.org/10.1016/j.ijggc.2011.05.001

Becker, V., Myrttinen, A., Nightingale, M., Shevalier, M., Rock, L., Mayer, B., Barth, J. A. (2015) Stable carbon and oxygen equilibrium isotope fractionation of supercritical and subcritical CO_2 with DIC and H_2O in saline reservoir fluids. *International Journal of Greenhouse Gas Control*, 39, 215-224.
https://doi.org/10.1016/j.ijggc.2015.05.020

Bell, J. L., Palmer, D. A., Barnes, H. L., Drummond, S. E. (1994) Thermal decomposition of acetate: III. Catalysis by mineral surfaces. *Geochimica et Cosmochimica Acta*, 58, 4155-4177.
https://doi.org/10.1016/0016-7037(94)90271-2

Bennett, P., Siegel, D. (1987) Increased solubility of quartz in water due to complexing by organic compounds. *Nature*, 326, 684-686.
https://doi.org/10.1038/326684a0

Bennett, R. H., Bryant, W. R., Keller, G. H. (1981) Clay fabric of selected submarine sediments; fundamental properties and models. *Journal of Sedimentary Research*, 51, 217-232.
https://doi.org/10.1306/212F7C52-2B24-11D7-8648000102C1865D

Berns, A., Philipp, H., Narres, H. D., Burauel, P., Vereecken, H., Tappe, W. (2008) Effect of gamma-sterilization and autoclaving on soil organic matter structure as studied by solid state NMR, UV and fluorescence spectroscopy. *European Journal of Soil Science*, 59, 540-550.
https://doi.org/10.1111/j.1365-2389.2008.01016.x

Bethke, C. (1996) Geochemical Reaction Modeling: Concepts and applications. Oxford University Press, New York, p. 414.
https://doi.org/10.1093/oso/9780195094756.001.0001

Bevan, J., Savage, D. (1989) The effect of organic acids on the dissolution of K-feldspar under conditions relevant to burial diagenesis. *Mineralogical Magazine*, 53, 415-425.
https://doi.org/10.1180/minmag.1989.053.372.02

BGE (2020) Zwischenbericht Teilgebiete gemäß § 13 StandAG. Bundesgesellschaft für Endlagerung mbH (BGE). Dokument Objekt-ID 755925: 444; Peine.
https://www.bge.de/fileadmin/user_upload/Standortsuche/Wesentliche_Unterlagen/Zwischen bericht_Teilgebiete/Zwischenbericht_Teilgebiete_barrierefrei.pdf
(last accessed: 26.11.2023)

BGE (2022a) Zeitliche Betrachtung des Standortauswahlverfahrens. Bundesgesellschaft für Endlagerung mbH (BGE). Dokument Objekt-ID 8830954: 29; Peine.
https://www.bge.de/fileadmin/user_upload/Standortsuche/Wesentliche_Unterlagen/05_-_Meilensteine/Zeitliche_Betrachtung_des_Standortauswahlverfahrens_2022/20221028_STA_Zusammenfassung_der_Rahmenterminplanung_Schritt_2_Phase_I_und_Zeitschaetzungen_Phase_II_und_III.pdf
(last accessed: 26.11.2023)

BGE (2022b) Kommunikationsstrategie zeitliche Betrachtung Standortauswahlverfahren. Bundesgesellschaft für Endlagerung mbH (BGE). Dokument Objekt-ID 8888116: 5; Peine.
https://www.bge.de/fileadmin/user_upload/Standortsuche/Wesentliche_Unterlagen/05_-_Meilensteine/Zeitliche_Betrachtung_des_Standortauswahlverfahrens_2022/20221028_STA_Anlage_3_Kommunikation_der_zeitlichen_Betrachtung_fuer_das_Standortauswahlverfahren.pdf
(last accessed: 26.11.2023)

Bjørlykke, K. (2015) Petroleum Geoscience: From Sedimentary Environments to Rock Physics. Springer: 666; Berlin Heidelberg.
https://doi.or/10.1007/978-3-642-02332-3_1

Blake, R. E., Walter, L. M. (1999) Kinetics of feldspar and quartz dissolution at 70–80°C and near-neutral pH: Effects of organic acids and NaCl. *Geochimica et Cosmochimica Acta*, 63, 2043-2059.
https://doi.org/10.1016/S0016-7037(99)00072-1

Borgund, A. E., Barth, T. (1993) Migration behaviour of petroleum-associated short-chain organic acids. *Organic Geochemistry*, 20, 1019-1025.
https://doi.org/10.1016/0146-6380(93)90110-W

Borgund, A. E., Barth, T. (1994). Generation of short-chain organic acids from crude oil by hydrous pyrolysis. *Organic Geochemistry*, 21, 943-952.
https://doi.org/10.1016/0146-6380(94)90053-1

Bossart, P., Thury, M. F. (2008) Characteristics of the Opalinus Clay at Mont Terri. Report, p. 25. https://www.researchgate.net/profile/Paul-Bossart/publication/265227432_Characteristics_of_the_Opalinus_Clay_at_Mont_Terri/links/55d3046208ae7fb244f57452/Characteristics-of-the-Opalinus-Clay-at-Mont-Terri.pdf
(last accessed: 08.11.2023)

Bossart, P., Bernier, F., Birkholzer, J., Bruggeman, C., Connolly, P., Dewonck, S., Fukaya, M., Herfort, M., Jensen, M., Matray, J.-M., Mayor, J. C., Moeri, A., Oyama, T., Schuster, C., Shigeta, N., Vietor, T., Wieczorek, K. (2017). Mont Terri rock laboratory, 20 years of research: introduction, site characteristics and overview of experiments. *Swiss Journal of Geosciences*, 110, 3-22.
https://doi.org/10.1007/978-3-319-70458-6_1

Bottinga, Y. (1968) Calculation of fractionation factors for carbon and oxygen isotopic exchange in the system calcite-carbon dioxide-water. *The Journal of Physical Chemistry*, 72, 800-808.
https://doi.org/10.1021/j100849a008

Bryan, N. D., Abrahamsen, L., Evans, N., Warwick, P., Buckau, G., Weng, L., Van Riemsdijk, W. H. (2012). The effects of humic substances on the transport of radionuclides: recent improvements in the prediction of behaviour and the understanding of mechanisms. *Applied Geochemistry*, 27, 378-389.
https://doi.org/10.1016/j.apgeochem.2011.09.008

Bu, H., Yuan, P., Liu, H., Liu, D., Liu, J., He, H., Zhou, J., Song, H., Li, Z. (2017). Effects of complexation between organic matter (OM) and clay mineral on OM pyrolysis. *Geochimica et Cosmochimica Acta*, *212*, 1-15.
https://doi.org/10.1016/j.gca.2017.04.045

Burdige, D. J., Komada, T., Magen, C., Chanton, J. P. (2016) Carbon cycling in Santa Barbara Basin sediments: A modeling study. *Journal of Marine Research*, 74, 133-159.
https://doi.org/10.1357/002224016819594818

Burnham A. K., Braun R. L., Sweeney J. J., Reynolds J. G., Vallejos C., Talukdar S. (1992) Kinetic modeling of petroleum formation in the Maracaibo basin: final report. U.S. Department of Energy Report DOE/BC/92001051, Bartlesville, Oklahoma, p. 137.
https://doi.org/10.2172/10164496

C

Carothers, W. W., Kharaka, Y. K., 1978. Aliphatic acid anions in oil-field waters—implications for origin of natural gas. *AAPG Bulletin*, 62, 2441-2453.
https://doi.org/10.1306/C1EA5521-16C9-11D7-8645000102C1865D

Chen, Y., Glaus, M., Van Loon, L., Mäder, U. (2018a) Transport behaviour of low molecular weight organic compounds in multi-mineral clay systems. A comparison between measured and predicted values. *Applied Clay Science*, 165, 247-256.
https://doi.org/10.1016/j.clay.2018.08.004

Chen, Y., Glaus, M. A., Van Loon, L. R., Mäder, U. (2018b) Transport of low molecular weight organic compounds in compacted illite and kaolinite. *Chemosphere*, 198, 226-237.
https://doi.org/10.1016/j.chemosphere.2018.01.137

Chen, C., Yuan, T., Lu, R., Fischer, C., Kolditz, O., Shao, H. (2022) The influence of sedimentary heterogeneity on the diffusion of radionuclides in the sandy facies of Opalinus Clay at the field scale. *Advances in Geosciences*, 58, 77-85.
https://doi.org/10.5194/adgeo-58-77-2022

Claret, F., Sakharov, B. A., Drits, V. A., Velde, B., Meunier, A., Griffault, L., Lanson, B. (2004) Clay minerals in the Meuse-Haute Marne underground laboratory (France): Possible influence of organic matter on clay mineral evolution. *Clays and Clay Minerals*, 52, 515-532. https://doi.org/10.1346/CCMN.2004.0520501

Clark, I., Fritz, P. (1997) Environmental Isotopes in Hydrogeology. CRS Press: 341; Boca Raton London New York. https://doi.org/10.1201/9781482242911

Colwell, F. S., D'Hondt, S. (2013) Nature and extent of the deep biosphere. *Reviews in Mineralogy and Geochemistry*, 75, 547-574. https://doi.org/10.2138/rmg.2013.75.17

Conrad, R., Claus, P., Chidthaisong, A., Lu, Y., Scavino, A. F., Liu, Y., Angel, R., Galand, P., Casper, P., Guerin, F. (2014) Stable carbon isotope biogeochemistry of propionate and acetate in methanogenic soils and lake sediments. *Organic Geochemistry*, 73, 1-7. https://doi.org/10.1016/j.orggeochem.2014.03.010

Conrad, R., Klose, M., Enrich-Prast, A. (2020) Acetate turnover and methanogenic pathways in Amazonian lake sediments. *Biogeosciences*, 17, 1063-1069. https://doi.org/10.5194/bg-17-1063-2020

Cooles, G., Mackenzie, A., Parkes, R. (1987) Non-hydrocarbons of significance in petroleum exploration: volatile fatty acids and non-hydrocarbon gases. *Mineralogical Magazine*, 51, 483-493. https://doi.org/10.1180/minmag.1987.051.362.03

Courdouan, A., Christl, I., Meylan, S., Wersin, P., Kretzschmar, R. (2007) Characterization of dissolved organic matter in anoxic rock extracts and in situ pore water of the Opalinus Clay. *Applied Geochemistry*, 22, 2926-2939. https://doi.org/10.1016/j.apgeochem.2007.09.001

Crossey, L. J. (1991) Thermal degradation of aqueous oxalate species. *Geochimica et Cosmochimica Acta*, 55, 1515-1527. https://doi.org/10.1016/0016-7037(91)90124-N

Cuadros, J. (2006) Modeling of smectite illitization in burial diagenesis environments. *Geochimica et Cosmochimica Acta*, 70, 4181-4195. https://doi.org/10.1016/j.gca.2006.06.1372

Cumberland, S. A., Douglas, G., Grice, K., Moreau, J. W. (2016) Uranium mobility in organic matter-rich sediments: A review of geological and geochemical processes. *Earth-Science Reviews*, 159, 160-185. https://doi.org/10.1016/j.earscirev.2016.05.010

Curti, L., Moore, O. W., Babakhani, P., Xiao, K.-Q., Woulds, C., Bray, A. W., Fisher, B. J., Kazemian, M., Kaulich, B., Peacock, C. L. (2021) Carboxyl-richness controls organic carbon preservation during coprecipitation with iron (oxyhydr)oxides in the natural environment. *Communications Earth & Environment*, 2, 1-13. https://doi.org/10.1038/s43247-021-00301-9

D

Dagnelie, R., Descostes, M., Pointeau, I., Klein, J., Grenut, B., Radwan, J., Lebeau, D., Georgin, D., Giffaut, E. (2014) Sorption and diffusion of organic acids through clayrock: comparison with inorganic anions. *Journal of Hydrology*, 511, 619-627.
https://doi.org/10.1016/j.jhydrol.2014.02.002

Davis, J. A. (1982). Adsorption of natural dissolved organic matter at the oxide/water interface. *Geochimica et Cosmochimica Acta*, 46, 2381-2393.
https://doi.org/10.1016/0016-7037(82)90209-5

Delage, P., Cui, Y. J., Tang, A. M. (2010) Clays in radioactive waste disposal. *Journal of Rock Mechanics and Geotechnical Engineering*, 2, 111-123.
https://doi.org/10.3724/SP.J.1235.2010.00111

Descostes, M., Tevissen, E. (2004) Definition of an equilibration protocol for batch experiments on Callovo-Oxfordian argillite. *Physics and Chemistry of the Earth*, 29, 79-90.
https://doi.org/10.1016/j.pce.2003.11.010

Dias, R. F., Freeman, K. H., Lewan, M. D., Franks, S. G. (2002) $\delta^{13}C$ of low-molecular-weight organic acids generated by the hydrous pyrolysis of oil-prone source rocks. *Geochimica et Cosmochimica Acta*, 66, 2755-2769.
https://doi.org/10.1016/S0016-7037(02)00871-2

Dickson, F., Blount, C. W., Tunell, G. (1963) Use of hydrothermal solution equipment to determine the solubility of anhydrite in water from 100 degrees C to 275 degrees C and from 1 bar to 1000 bars pressure. *American Journal of Science*, 261, 61-78.
https://doi.org/10.2475/ajs.261.1.61

Diomidis, N., Cloet, V., Leupin, O. X., Marschall, P., Poller, A., Stein, M. (2016) Production, consumption and transport of gases in deep geological repositories according to the Swiss disposal concept. National Cooperative for the Disposal of Radioactive Waste (NAGRA), Technical Report 16-03: 148; Wettingen.
https://nagra.ch/wp-content/uploads/2022/08/e_ntb16-003.pdf
(last accessed: 08.11.2023)

Dionysiou, D., Tsianou, M., Botsaris, G. (2000) Extractive Crystallization for the Production of Calcium Acetate and Magnesium Acetate from Carbonate Sources. *Industrial & Engineering Chemistry Research*, 39, 4192-4202.
https://doi.org/10.1021/ie9906823

Dohrmann, R., Kaufhold, S., Lundqvist, B. (2013) The Role of Clays for Safe Storage of Nuclear Waste. In: Bergaya, F., Lagaly, G. (Eds.), Developments in Clay Science, Volume 5, Elsevier Ltd.: 677-710; Amsterdam.
https://doi.org/10.1016/B978-0-08-098259-5.00024-X

Durce, D., Bruggeman, C., Maes, N., Van Ravestyn, L., Brabants, G. (2015) Partitioning of organic matter in Boom Clay: Leachable vs mobile organic matter. *Applied Geochemistry*, 63, 169-181.
https://doi.org/10.1016/j.apgeochem.2015.08.009

Dziadkowiec, J., Røyne, A. (2020) Nanoscale Forces between Basal Mica Surfaces in Dicarboxylic Acid Solutions: Implications for Clay Aggregation in the Presence of Soluble Organic Acids. *Langmuir*, 36, 14978-14990.
https://doi.org/10.1021/acs.langmuir.0c02290

E

Echigo, T., Kimata, M. (2010) Crystal chemistry and genesis of organic minerals: a review of oxalate and polycyclic aromatic hydrocarbon minerals. *The Canadian Mineralogist*, 48, 1329-1358.
https://doi.org/10.3749/canmin.48.5.1329

Eglinton, T. I., Curtis, C. D., Rowland, S. J. (1987) Generation of water-soluble organic acids from kerogen during hydrous pyrolysis: implications for porosity development. *Mineralogical Magazine*, 51, 495-503.
https://doi.org/10.1180/minmag.1987.051.362.04

Elie, M., Mazurek, M. (2008) Biomarker transformations as constraints for the depositional environment and for maximum temperatures during burial of Opalinus Clay and Posidonia Shale in northern Switzerland. *Applied Geochemistry*, 23, 3337-3354.
https://doi.org/10.1016/j.apgeochem.2008.05.022

Emrich, K., Ehhalt, D., Vogel, J. (1970) Carbon isotope fractionation during the precipitation of calcium carbonate. *Earth and Planetary Science Letters*, 8, 363-371.
https://doi.org/10.1016/0012-821X(70)90109-3

Engle, M. A., Doolan, C. A., Pitman, J. A., Varonka, M. S., Chenault, J., Orem, W. H., McMahon, P. B., Jubb, A. M. (2020) Origin and geochemistry of formation waters from the lower Eagle Ford Group, Gulf Coast Basin, south central Texas. *Chemical Geology*, 550, 119754.
https://doi.org/10.1016/j.chemgeo.2020.119754

Ewing, R. C., Whittleston, R. A., Yardley, B. W. (2016) Geological disposal of nuclear waste: a primer. *Elements*, 12, 233-237.
https://doi.org/10.2113/gselements.12.4.233

F

Fälber, R., Hansmann, D., Narten, M., Brandes C., Achmus, M., Winsemann, J. (2022) Eignung paläogener Tone und Tonsteine im Rahmen des Standortauswahlverfahrens zur Endlagerung radioaktiver Abfälle. Leibnitz Universität Hannover: 154; Hannover/Germany.
https://uploads-ssl.webflow.com/5f4796c78ddf417e366f04d7/63105661a6a7253830aee44a_Abschlussbericht_Eignung%20pal%C3%A4ogener%20Tone%20und%20Tonsteine%20im%20Rahmen%20des%20Standortauswahlverfahrens.pdf
(last accessed: 08.11.2023)

Fein, J. B., Hestrin, J. E. (1994) Experimental studies of oxalate complexation at 80°C: Gibbsite, amorphous silica, and quartz solubilities in oxalate-bearing fluids. *Geochimica et Cosmochimica Acta*, 58, 4817-4829.
https://doi.org/10.1016/0016-7037(94)90213-5

Fernández, A. M., Turrero, M. J., Sánchez, D. M., Yllera, A., Melón, A. M., Sánchez, M., Peña, J., Garralón, A., Rivas, P., Bossart, P., Hernán, P. (2007). On site measurements of the redox and carbonate system parameters in the low-permeability Opalinus Clay formation at the Mont Terri Rock Laboratory. *Physics and Chemistry of the Earth, Parts A/B/C*, 32, 181-195.
https://doi.org/10.1016/j.pce.2006.02.057

Fernández, A. M., Sánchez-Ledesma, D. M., Tournassat, C., Melón, A., Gaucher, E. C., Astudillo, J., Vinsot, A. (2014) Applying the squeezing technique to highly consolidated clayrocks for pore water characterisation: Lessons learned from experiments at the Mont Terri Rock Laboratory. *Applied Geochemistry*, 49, 2-21. https://doi.org/10.1016/j.apgeochem.2014.07.003

Filius, J. D., Hiemstra, T., Van Riemsdijk, W. H. (1997) Adsorption of small weak organic acids on goethite: Modeling of mechanisms. *Journal of Colloid and Interface Science*, 195, 368-380. https://doi.org/10.1006/jcis.1997.5152

Fisher, J. B. (1987) Distribution and occurrence of aliphatic acid anions in deep subsurface waters. *Geochimica et Cosmochimica Acta*, 51, 2459-2468. https://doi.org/10.1016/0016-7037(87)90297-3

Fralova, L., Lefèvre, G. G., Madé, B., Marsac, R., Thory, E., Dagnelie, R. V. (2021) Effect of organic compounds on the retention of radionuclides in clay rocks: Mechanisms and specificities of Eu (III), Th (IV), and U (VI). *Applied Geochemistry*, 127, 104859. https://doi.org/10.1016/j.apgeochem.2020.104859

Freeman, K. H., Hayes, J. M., Trendel, J. M., Albrecht, P. (1990) Evidence from carbon isotope measurements for diverse origins of sedimentary hydrocarbons. *Nature*, 343, 254-256. https://doi.org/10.1038/343254a0

Freund, H., Clouse, J. A., Otten, G. A. (1993) Effect of pressure on the kinetics of kerogen pyrolysis. *Energy & Fuels*, 7, 1088-1094. https://doi.org/10.1021/ef00042a055

Fripiat, J. J., & Cruz-Cumplido, M. I. (1974) Clays as catalysts for natural processes. *Annual Review of Earth and Planetary Sciences*, 2, 239-256. https://doi.org/10.1146/annurev.ea.02.050174.001323

G

Gadd, G. M., Bahri-Esfahani, J., Li, Q., Rhee, Y. J., Wei, Z., Fomina, M., Liang, X. (2014) Oxalate production by fungi: significance in geomycology, biodeterioration and bioremediation. *Fungal Biology Reviews*, 28, 36-55. https://doi.org/10.1016/j.fbr.2014.05.001

Gaucher, E. C., Lassin, A., Lerouge, C., Fléhoc, C., Marty, N. C., Henry, B., Tournassat, C., Altmann, S., Vinsot, A., Buschaert, S., Matray, J.-M., Leupin, O. X., De Craen, M. (2010) CO_2 partial pressure in clayrocks: a general model. In: Water-Rock Interaction WRI-13. Taylor & Francis Group (CRC Press): 855-858; Guanajuato, Mexico. https://hal-brgm.archives-ouvertes.fr/file/index/docid/664967/filename/Gaucher_WRI13_855_858.pdf (last accessed: 08.11.2023)

Galimov, E. M. (1988) Sources and mechanisms of formation of gaseous hydrocarbons in sedimentary rocks. *Chemical Geology*, 71, 77-95. https://doi.org/10.1016/0009-2541(88)90107-6

Giordano, T. H. (1993) Metal Transport in Ore Fluids by Organic Ligand Complexation. In: Lewan, M. D., Pittman, E. D. (Eds.), Organic Acids in Geological Processes. Springer-Verlag Berlin Heidelberg, 482.
https://doi.org/10.1007/978-3-642-78356-2_11

Giordano, T. H., Kharaka, Y. K. (1994) Organic ligand distribution and speciation in sedimentary basin brines, diagenetic fluids and related ore solutions. Geological Society, London, Special Publications 78, 175-202.
https://doi.org/10.1144/GSL.SP.1994.078.01.14

Glaus, M. A., Baeyens, B., Lauber, M., Van Loon, L. R., Rabung, T. (2001) Water-extractable organic matter from opalinus clay: effect on sorption and speciation of Ni (II), Eu (III) and Th (IV). Paul Scherrer Institute (PSI), Report NTB 01–07: 55; Villigen.
https://inis.iaea.org/collection/NCLCollectionStore/_Public/50/041/50041725.pdf?r=1
(last accessed: 08.11.2023)

Glombitza, C., Egger, M., Røy, H., Jørgensen, B. B. (2019) Controls on volatile fatty acid concentrations in marine sediments (Baltic Sea). *Geochimica et Cosmochimica Acta*, 258, 226-241.
https://doi.org/10.1016/j.gca.2019.05.038

Gonçalvès, J., Matray, J.-M., Yu, C. J. (2023) Assessing relevant transport processes in Opalinus Clay at the Mont Terri rock laboratory using excess-pressure, concentration and temperature profiles. *Applied Clay Science*, 242, 107016.
https://doi.org/10.1016/j.clay.2023.107016

Grambow, B. (2016) Geological disposal of radioactive waste in clay. *Elements*, 12, 239-245.
https://doi.org/10.2113/gselements.12.4.239

Greenberg, H. R., Wen, J., Buscheck, T. A. (2013) Scoping Thermal Analysis of Alternative Dual-Purpose Canister Disposal Concepts. Lawrence Livermore National Laboratory Technical Report LLNL-TR-639869, p. 54.
https://doi.org/10.2172/1090011

Grunau, H. R. (1987) A worldwide look at the cap-rock problem. *Journal of Petroleum Geology*, 10, 245-265.
https://doi.org/10.1111/j.1747-5457.1987.tb00945.x

Gu, B., Schmitt, J., Chen, Z., Liang, L., McCarthy, J. F. (1994) Adsorption and desorption of natural organic matter on iron oxide: mechanisms and models. *Environmental Science & Technology*, 28, 38-46.
https://doi.org/10.1021/es00050a007

Gu, B., Schmitt, J., Chen, Z., Liang, L., McCarthy, J. F. (1995) Adsorption and desorption of different organic matter fractions on iron oxide. *Geochimica et Cosmochimica Acta*, 59, 219-229.
https://doi.org/10.1016/0016-7037(94)00282-Q

H

Hanor, J. S., Workman, A. L. (1986) Distribution of dissolved volatile fatty acids in some Louisiana oil field brines. *Applied Geochemistry*, 1, 37-46.
https://doi.org/10.1016/0883-2927(86)90036-3

Harrington, J. F., Horseman, S. T. (1999) Gas transport properties of clays and mudrocks. *Geological Society, London, Special Publications*, 158, 107-124. https://doi.org/10.1144/GSL.SP.1999.158.01.09

Harrison, W. J., Thyne, G. D. (1992) Predictions of diagenetic reactions in the presence of organic acids. *Geochimica et Cosmochimica Acta*, 56, 565-586. https://doi.org/10.1016/0016-7037(92)90082-T

Hatton, R. S. (1982) Dissolved volatile fatty acids in subsurface hydropressured and geopressured brines: a review of published literature on occurrence, genesis, and thermochemical properties. Report: 82; Baton Rouge, Louisiana. https://publications.mygeoenergynow.org/grc/1011593.pdf (last accessed: 08.11.2023)

Hawkes, J. A., Hansen, C. T., Goldhammer, T., Bach, W., Dittmar, T. (2016) Molecular alteration of marine dissolved organic matter under experimental hydrothermal conditions. *Geochimica et Cosmochimica Acta*, 175, 68-85. https://doi.org/10.1016/j.gca.2015.11.025

Helten, O., Ostertag-Henning, C., Bach, W., Hinrichs, K.-U. (2022) Generation and decomposition of low-molecular-weight organic acids in hydrous pyrolysis experiments with Opalinus Clay rock. *Organic Geochemistry*, 172, 104481. https://doi.org/10.1016/j.orggeochem.2022.104481

Hendrix, K., Bleyen, N., Mennecart, T., Bruggeman, C., Valcke, E. (2019) Sodium azide used as microbial inhibitor caused unwanted by-products in anaerobic geochemical studies. *Applied Geochemistry*, 107, 120-130. https://doi.org/10.1016/j.apgeochem.2019.05.014

Hendry, M. J., Solomon, D. K., Person, M., Wassenaar, L. I., Gardner, W. P., Clark, I. D., Mayer, K. U., Kunimaru, T., Nakata, K., Hasegawa, T. (2015) Can argillaceous formations isolate nuclear waste? Insights from isotopic, noble gas, and geochemical profiles. *Geofluids*, 15, 381-386. https://doi.org/10.1111/gfl.12132

Hennig, T., Stockmann, M., Kühn, M. (2020) Simulation of diffusive uranium transport and sorption processes in the Opalinus Clay. *Applied Geochemistry*, 123, 104777. https://doi.org/10.1016/j.apgeochem.2020.104777

Hennig, T., Kühn, M. (2021) Surrogate model for multi-component diffusion of uranium through Opalinus Clay on the host rock scale. *Applied Sciences*, 11, 786. https://doi.org/10.3390/app11020786

Hervé, V., Junier, T., Bindschedler, S., Verrecchia, E., Junier, P. (2016) Diversity and ecology of oxalotrophic bacteria. *World Journal of Microbiology and Biotechnology*, 32, 1-7. https://doi.org/10.1007/s11274-015-1982-3

Heuer, V. B., Krüger, M., Elvert, M., Hinrichs, K.-U. (2009) Experimental studies on the stable carbon isotope biogeochemistry of acetate in lake sediments. *Organic Geochemistry*, 41, 22-30. https://doi.org/10.1016/j.orggeochem.2009.07.004

Heuer, V. B., Inagaki, F., Morono, Y., Kubo, Y., Spivack, A. J., Viehweger, B., Treude, T., Beulig, F., Schubotz, F., Tonai, S., Bowden, S., Cramm, M., Henkel, S., Hirose, T., Homola, K., Hoshino, T., Ijiri, A., Imachi, H., Kamiya, N., Kaneko, M., Lagostina, L., Manners, H., McClelland, H.-L., Metcalfe, K., Okutsu, N., Pan, D., Raudsepp, M. J., Sauvage, J., Tsang, M.-Y., Wang, D. T., Whitaker, E., Yamamoto, Y., Yang, K., Maeda, L., Adhikari, R. R., Glombitza, C., Hamada, Y., Kallmeyer, J., Wendt, J., Wörmer, L., Yamada, Y., Kinoshita, M., Hinrichs, K.-U. (2020). Temperature limits to deep subseafloor life in the Nankai Trough subduction zone. *Science*, 370, 1230-1234.
https://doi.org/10.1126/science.abd7934

Hoefs, J. (2015) Stable Isotope Geochemistry. Springer: 402; Heidelberg New York Dordrecht London.
https://doi.org/10.1007/978-3-319-19716-6

Hofmann, B. A., Bernasconi, S. M. (1998) Review of occurrences and carbon isotope geochemistry of oxalate minerals: implications for the origin and fate of oxalate in diagenetic and hydrothermal fluids. *Chemical Geology*, 149, 127-146.
https://doi.org/10.1016/S0009-2541(98)00043-6

Horsfield, B., Schenk, H., Zink, K., Ondrak, R., Dieckmann, V., Kallmeyer, J., Mangelsdorf, K., di Primio, R., Wilkes, H., Parkes, R. J. (2006) Living microbial ecosystems within the active zone of catagenesis: implications for feeding the deep biosphere. *Earth and Planetary Science Letters*, 246, 55-69.
https://doi.org/10.1016/j.epsl.2006.03.040

Hostettler, B., Reisdorf, A. G., Jaeggi, D., Deplazes, G., Bläsi, H., Morard, A., Feist-Burkhardt, S., Waltschw, A., Dietze, V., Menkveld-Gfeller, U. (2017) Litho-and biostratigraphy of the Opalinus Clay and bounding formations in the Mont Terri rock laboratory (Switzerland). Mont Terri Rock Laboratory, 20 Years: Two Decades of Research and Experimentation on Claystones for Geological Disposal of Radioactive Waste, 23-39.
https://doi.org/10.1007/978-3-319-70458-6_2

Hoth, P., Wirth, H., Reinhold, K., Bräuer, V., Krull, P., Feldrappe, H. (2007) Endlagerung radioaktiver Abfälle in tiefen geologischen Formationen Deutschlands–Untersuchung und Bewertung von Tongesteinsformationen. BGR Bundesanstalt für Geowissenschaften und Rohstoffe: 124; Hannover/Germany.
https://www.bgr.bund.de/DE/Themen/Endlagerung/Downloads/Charakterisierung_Wirtsgesteine_geotech_Barrieren/1_Tongestein/2007-04-00_BGR_Tonstudie2007.pdf?__blob=publicationFile&v=6
(last accessed: 08.11.2023)

Houben, M. E., Desbois, G., Urai, J. L. (2013) Pore morphology and distribution in the Shaly facies of Opalinus Clay (Mont Terri, Switzerland): Insights from representative 2D BIB–SEM investigations on mm to nm scale. *Applied Clay Science*, 71, 82-97.
https://doi.org/10.1016/j.clay.2012.11.006

Hummel, W., Glaus, M. A., Loon, L. V. (1999) Complexation of radionuclides with humic substance: the metal concentration effect. *Radiochimica Acta*, 84, 111-114.
https://doi.org/10.1524/ract.1999.84.2.111

Hunt, J. M. (1979) Petroleum Geochemistry and Geology, 1st Edition, Freeman: 617; San Francisco.
https://doi.org/10.1017/S0016756800032684

Hunt, J. M. (1984) Generation and migration of light hydrocarbons. *Science*, 226, 1265-1270. https://doi.org/10.1126/science.226.4680.1265

Hunt, J. M. (1996) Petroleum Geochemistry and Geology, 2nd Edition, Freeman: 743; San Francisco. https://doi.org/10.1017/S0016756800007755

I

Ibis, F., Dhand, P., Suleymanli, S., van der Heijden, A. E. D. M., Kramer, H. J. M., Eral, H. B. (2020) A Combined Experimental and Modelling Study on Solubility of Calcium Oxalate Monohydrate at Physiologically Relevant pH and Temperatures. *Crystals*, 10, 924. https://doi.org/10.3390/cryst10100924

Ijiri, A., Harada, N., Hirota, A., Tsunogai, U., Ogawa, N. O., Itaki, T., Khim, B.-K., Uchida, M. (2012) Biogeochemical processes involving acetate in sub-seafloor sediments from the Bering Sea shelf break. *Organic Geochemistry*, 48, 47-55. https://doi.org/10.1016/j.orggeochem.2012.04.004

Inagaki, F., Hinrichs, K. U., Kubo, Y., Bowles, M. W., Heuer, V. B., Hong, W. L., Hoshino, T., Ijiri, A., Imachi, H., Ito, M., Kaneko, M., Lever, M. A., Lin, Y.-S., Methé, B. A., Morita, S., Morono, Y., Tanikawa, W., Bihan, M., Bowden, S. A., Elvert, M., Glombitza, C., Gross, D., Harrington, G. J., Hori, T., Li, K., Limmer, D., Liu, C.-H., Murayama, M., Ohkouchi, N., Ono, S., Park, Y.-S., Phillips, S. C., Prieto-Mollar, X., Purkey, M., Riedinger, N., Sanada, Y., Sauvage, J., Snyder, G., Susilawati, R., Takano, Y., Tasumi, E., Terada, T., Tomaru, H., Trembath-Reichert, E., Wang, D. T., Yamada, Y. (2015) Exploring deep microbial life in coal-bearing sediment down to ~2.5 km below the ocean floor. *Science*, 349, 420-424. https://doi.org/10.1126/science.aaa6882

Inoue, A., Udata, M. (1983) Further investigations of a conversion series of dioctahedral mica/smecties in the Shinzan hydrothermal alteration area, northeast Japan. *Clays and Clay Minerals*, 31, 401-412. https://doi.org/10.1346/CCMN.1983.0310601

Inoue, A., Utada, M., Wakita, K. (1992) Smectite-to-illite conversion in natural hydrothermal systems. *Applied Clay Science*, 7, 131-145. https://doi.org/10.1016/0169-1317(92)90035-L

J

Jacops, E., Maes, N., Bruggeman, C., Grade, A. (2017) Measuring diffusion coefficients of dissolved He and Ar in three potential clay host formations: Boom Clay, Callovo-Oxfordian Clay and Opalinus Clay. *Geological Society, London, Special Publications*, 443, 349-360. https://doi.org/10.1144/SP443.1

Jenneman, G. E., McInerney, M. J., Crocker, M. E., Knapp, R. M. (1986) Effect of sterilization by dry heat or autoclaving on bacterial penetration through Berea sandstone. *Applied and Environmental Microbiology*, 51, 39-43. https://doi.org/10.1128/aem.51.1.39-43.1986

Jobmann, M., Meleshyn, A. (2015) Evaluation of temperature-induced effects on safety-relevant properties of clay host rocks with regard to HLW/SF disposal. *Mineralogical Magazine*, 79, 1389-1395.
https://doi.org/10.1180/minmag.2015.079.6.14

Jockwer, N., Wieczorek, K., Miehe, R., Fernández, A. M. (2006) Heater Test in the Opalinus Clay of the Mont Terri URL – Gas Release and Water Redistribution Contribution to Heater Experiment (HE): Rock and bentonite thermos-hydro-mechnical (THM) processes in the nearfield. Gesellschaft für Anlagen- und Reaktorsicherheit (GRS), Report GRS-223: 81; Braunschweig. https://www.grs.de/de/aktuelles/publikationen/grs-223-heater-test-opalinus-clay-mont-terri-url
(last accessed: 08.11.2023)

Jockwer, N., Wieczorek, K., Fernández, A. M. (2007) Measurements of gas generation, water content and change in the water distribution in a heater experiment in the underground laboratory Mont Terri. *Physics and Chemistry of the Earth, Parts A/B/C*, 32, 530-537.
https://doi.org/10.1016/j.pce.2006.03.015

Johnson, J. W., Oelkers, E. H., Helgeson, H. C. (1992) SUPCRT92: A software package for calculating the standard molal thermodynamic properties of minerals, gases, aqueous species, and reactions from 1 to 5000 bar and 0 to 1000 °C. *Computers & Geosciences*, 18, 899-947.
https://doi.org/10.1016/0098-3004(92)90029-Q

Johnson, L. H., Niemeyer, M., Klubertanz, G., Siegel, P., Gribi, P. (2002) Calculations of the Temperature Evolution of a Repository for Spent Fuel, Vitrified High-Level Waste and Intermediate Level Waste in Opalinus Clay. National Cooperative for the Disposal of Radioactive Waste (NAGRA), Technical Report 01-04: 184; Wettingen.
https://nagra.ch/downloads/technical-report-ntb-01-04/
(last accessed: 08.11.2023)

Johnson, L. H., Marschall, P., Zuidema, P., Gribi, P. (2004) Effects of Post-depositional Gas Generation in a Repository for Spent Fuel, High-level Waste and Long-lived Intermediate Level Waste Sited in Opalinus Clay. National Cooperative for the Disposal of Radioactive Waste (NAGRA), Technical Report 04-06: 80; Wettingen.
https://nagra.ch/wp-content/uploads/2022/08/e_ntb04-006.pdf
(last accessed: 08.11.2023)

Joseph, C., Schmeide, K., Sachs, S., Brendler, V., Geipel, G., Bernhard, G. (2011) Sorption of uranium (VI) onto Opalinus Clay in the absence and presence of humic acid in Opalinus Clay pore water. *Chemical Geology*, 284, 240-250.
https://doi.org/10.1016/j.chemgeo.2011.03.001

K

Kang, S., Xing, B. (2007) Adsorption of dicarboxylic acids by clay minerals as examined by in situ ATR-FTIR and ex situ DRIFT. *Langmuir*, 23, 7024-7031.
https://doi.org/10.1021/la700543f

Kaufhold, S., Dohrmann, R., Klinkenberg, M., Siegesmund, S., Ufer, K. (2010) N_2-BET specific surface area of bentonites. *Journal of Colloid and Interface Science*, 349, 275-282.
https://doi.org/10.1016/j.jcis.2010.05.018

Kaufhold, S., Dohrmann, R. (2013) The variable charge of dioctahedral smectites. *Journal of Colloid and Interface Science*, 390, 225-233. https://doi.org/10.1016/j.jcis.2012.09.023

Kautenburger, R., Brix, K., Hein, C. (2019) Insights into the retention behaviour of europium (III) and uranium (VI) onto Opalinus Clay influenced by pore water composition, temperature, pH and organic compounds. *Applied Geochemistry*, 109, 104404. https://doi.org/10.1016/j.apgeochem.2019.104404

Kawamura, K., Tannenbaum, E., Huizinga, B. J., Kaplan, I. R. (1986) Volatile organic acids generated from kerogen during laboratory heating. *Geochemical Journal*, 20, 51-59. https://doi.org/10.2343/geochemj.20.51

Kawamura, K., Kaplan, I. R. (1987) Dicarboxylic acids generated by thermal alteration of kerogen and humic acids. *Geochimica et Cosmochimica Acta*, 51, 3201-3207. https://doi.org/10.1016/0016-7037(87)90128-1

Kawamura, K., Nissenbaum, A. (1992) High abundance of low molecular weight organic acids in hypersaline spring water associated with a salt diapir. *Organic Geochemistry*, 18, 469-476. https://doi.org/10.1016/0146-6380(92)90109-B

Keller, L. M., Holzer, L., Wepf, R., Gasser, P. (2011) 3D geometry and topology of pore pathways in Opalinus Clay: Implications for mass transport. *Applied Clay Science*, 52, 85-95. https://doi.org/10.1016/j.clay.2011.02.003

Kharaka, Y. K., Carothers, W. W., Rosenbauer, R. J. (1983) Thermal decarboxylation of acetic acid: implications for origin of natural gas. *Geochimica et Cosmochimica Acta*, 47, 397-402. https://doi.org/10.1016/0016-7037(83)90262-4

Kharaka, Y. K., Hull, R. W., Carothers, W. W. (1985) Water-rock interactions in sedimentary basins. In: Gautier, D., Kharaka, Y. K., Surdam, R. (Eds.), Relationship of Organic Matter and Mineral Diagenesis - SEPM Short Course No. 17. SEPM Society of Economic Paleontologists and Mineralogists, Tulsa, Oklahoma. U.S.A. https://doi.org/10.2110/scn.85.03.0079

Kharaka, Y. K., Lundegard, P. D., Ambats, G., Evans, W. C., Bischoff, J. L. (1993a) Generation of aliphatic acid anions and carbon dioxide by hydrous pyrolysis of crude oils. *Applied Geochemistry*, 8, 317-324. https://doi.org/10.1016/0883-2927(93)90001-W

Kharaka, Y. K., Ambats, G., Thordsen, J. J. (1993b) Distribution and significance of dicarboxylic acid anions in oil field waters. *Chemical Geology*, 107, 499-501. https://doi.org/10.1016/0009-2541(93)90239-F

Kim, J.-S., Kwon, S.-K., Sanchez, M., Cho, G.-C. (2011) Geological storage of high level nuclear waste. *KSCE Journal of Civil Engineering*, 15, 721-737. https://doi.org/10.1007/s12205-011-0012-8

King, F. (2012) Gaseous hydrogen issues in nuclear waste disposal. In: Gangloff, R. P., Somerday, B. P. (Eds.) Gaseous Hydrogen Embrittlement of Materials in Energy Technologies. Woodhead Publishing: 126-148. https://doi.org/10.1533/9780857093899.1.126

King, F. (2017) Nuclear waste canister materials: Corrosion behavior and long-term performance in geological repository systems. In: Apted, M. J., Ahn, J. (Eds.) Geological repository systems for safe disposal of spent nuclear fuels and radioactive waste. Woodhead Publishing: 365-408.
https://doi.org/10.1016/B978-0-08-100642-9.00013-X

Knauss, K. G., Beiriger, W. J., Peifer, D. W. (1985) Hydrothermal interaction of crushed Topopah Spring tuff and J-13 water at 90, 150, and 250 °C using Dickson-type, gold-bag rocking autoclaves. Lawrence Livermore National Laboratory (LLNL) Report UCRL-53630: 28; Livermore.

Knauss, K. G., Beiriger, W. J., Peifer, D. W. (1987) Hydrothermal interaction of solid wafers of Topopah Spring Tuff with J-13 water at 90 and 150 °C using Dickson-type, gold-bag rocking autoclaves: Long-term experiments. Lawrence Livermore National Laboratory (LLNL) Report UCRL-53722: 23; Livermore.
https://doi.org/10.2172/59918

Knauss, K. G., Copenhaver, S. A., Braun, R. L., Burnham, A. K. (1997) Hydrous pyrolysis of New Albany and Phosphoria Shales: production kinetics of carboxylic acids and light hydrocarbons and interactions between the inorganic and organic chemical systems. *Organic Geochemistry*, 27, 477-496.
https://doi.org/10.1016/S0146-6380(97)00081-8

Kneuker, T., Bartels, A., Bebiolka, A., Beilecke, T., Bense, F., Beushausen, M., Frenzel, B., Jähne-Klingberg, F., Lang, J., Lippmann-Pipke, J., May, F., Mertineit, M., Noack, V., Pollok, L., Reinhold, K., Rummel, L., Schubarth-Engelschall, N., Schumacher, S., Stück, H. Weber, J. (2020) Zusammenstellung von Erkundungszielen für die übertägige Erkundung gemäß § 16 StandAG. Bundesanstalt für Geowissenschaften und Rohstoffe (BGR), 9S2019090000. Standortauswahl - Zusammenstellung und Bewertung von geowissenschaftlichen Methoden und Programmen für die übertägige Standorterkundung (GeoMePS): 79; Hannover Berlin.

Ko, L. T., Loucks, R. G., Zhang, T., Ruppel, S. C., Shao, D. (2016) Pore and pore network evolution of Upper Cretaceous Boquillas (Eagle Ford–equivalent) mudrocks: Results from gold tube pyrolysis experiments. *AAPG Bulletin*, 100, 1693-1722.
https://doi.org/10.1306/04151615092

Kotarba, M. J., Więcław, D., Jurek, K., Waliczek, M. (2022a) Variations of bitumen fraction, biomarker, stable carbon isotope and maceral compositions of dispersed organic matter in the Miocene strata (Carpathian Foredeep, Poland) during maturation simulated by hydrous pyrolysis. *Marine and Petroleum Geology*, 137, 105487.
https://doi.org/10.1016/j.marpetgeo.2021.105487

Kotarba, M. J., Bilkiewicz, E., Bajda, T., Waliczek, M., Jurek, K. (2022b) Variations of yields and molecular and isotopic compositions in gases generated from Miocene strata of the Carpathian Foredeep (Poland) as determined by hydrous pyrolysis. *International Journal of Earth Sciences*, 111, 1823-1858.
https://doi.org/10.1007/s00531-022-02206-0

Kubicki, J., Schroeter, L., Itoh, M., Nguyen, B., Apitz, S. (1999) Attenuated total reflectance Fourier-transform infrared spectroscopy of carboxylic acids adsorbed onto mineral surfaces. *Geochimica et Cosmochimica Acta*, 63, 2709-2725.
https://doi.org/10.1016/S0016-7037(99)00194-5

Kull, H., Jockwer, N., Zhang, C. L., Wileveau, Y., Pepa, S. (2007) Measurement of thermally-induced pore-water pressure increase and gas migration in the Opalinus Clay at Mont Terri. *Physics and Chemistry of the Earth, Parts A/B/C*, 32, 937-946. https://doi.org/10.1016/j.pce.2006.04.036

L

Landais, P., Monthioux, M. (1988) Closed system pyrolysis: an efficient technique for simulating natural coal maturation. *Fuel Processing Technology*, 20, 123-132. https://doi.org/10.1016/0378-3820(88)90013-6

Landolt, D., Davenport, A., Payer, J., Shoesmith, D. (2009) A Review of Materials and Corrosion Issues Regarding Canisters for Disposal of Spent Fuel and High-level Waste in Opalinus Clay. National Cooperative for the Disposal of Radioactive Waste (NAGRA), Technical Report 09-02: 73; Wettingen. https://nagra.ch/wp-content/uploads/2022/08/e_ntb09-002.pdf (last accessed: 08.11.2023)

Lang, S. Q., Butterfield, D. A., Schulte, M., Kelley, D. S., Lilley, M. D. (2010) Elevated concentrations of formate, acetate and dissolved organic carbon found at the Lost City hydrothermal field. *Geochimica et Cosmochimica Acta*, 74, 941-952. https://doi.org/10.1016/j.gca.2009.10.045

Larsen, J. W., Islas-Flores, C., Aida, M. T., Opaprakasit, P., Painter, P. (2005) Kerogen chemistry 2. Low-temperature anhydride formation in kerogens. *Energy & Fuels*, 19, 145-151. https://doi.org/10.1021/ef0498519

Lauper, B., Jaeggi, D., Deplazes, G., Foubert, A. (2018) Multi-proxy facies analysis of the Opalinus Clay and depositional implications (Mont Terri rock laboratory, Switzerland). *Swiss Journal of Geosciences*, 111, 383-398. https://doi.org/10.1007/s00015-018-0303-x

Lee, C., Hedges, J. I., Wakeham, S. G., Zhu, N. (1992) Effectiveness of various treatments in retarding microbial activity in sediment trap material and their effects on the collection of swimmers. *Limnology and Oceanography*, 37, 117-130. https://doi.org/10.4319/lo.1992.37.1.0117

Lerouge, C., Blessing, M., Flehoc, C., Gaucher, E. C., Henry, B., Lassin, A., Marty, N., Matray, J. M., Proust, E., Rufer, D., Tremosa, J., Vinsot, A. (2015). Dissolved CO_2 and alkane gas in clay formations. *Procedia Earth and Planetary Science*, 13, 88-91. https://doi.org/10.1016/j.proeps.2015.07.021

Leśniak, P. M., Zawidzki, P. (2006) Determination of carbon fractionation factor between aqueous carbonate and $CO_{2(g)}$ in two-direction isotope equilibration. *Chemical Geology*, 231, 203-213. https://doi.org/10.1016/j.chemgeo.2006.01.025

Leu, W., Gautschi, A. (2012) Das Shale Gas (Schiefergas)-Potenzial des Opalinustons in der Nordschweiz. National Cooperative for the Disposal of Radioactive Waste (NAGRA), Report NAB 11-23: 22; Wettingen. https://nagra.ch/wp-content/uploads/2022/08/d_nab11-023.pdf (last accessed: 08.11.2023)

Lewan, M. D. (1983) Effects of thermal maturation on stable organic carbon isotopes as determined by hydrous pyrolysis of Woodford Shale. *Geochimica et Cosmochimica Acta*, 47, 1471-1479.
https://doi.org/10.1016/0016-7037(83)90306-X

Lewan, M. D. (1997) Experiments on the role of water in petroleum formation. *Geochimica et Cosmochimica Acta*, 61, 3691-3723.
https://doi.org/10.1016/S0016-7037(97)00176-2

Lewan, M. D., Winters, J. C., McDonald, J. H. (1979) Generation of oil-like pyrolyzates from organic-rich shales. *Science*, 203, 897-899.
https://doi.org/10.1126/science.203.4383.897

Lewan, M. D., Buchardt, B. (1989) Irradiation of organic matter by uranium decay in the Alum Shale, Sweden. *Geochimica et Cosmochimica Acta*, 53, 1307-1322.
https://doi.org/10.1016/0016-7037(89)90065-3

Lewan, M. D., Ulmishek, G. F., Harrison, W., Schreiner, F. (1991) Gamma ^{60}Co-irradiation of organic matter in the Phosphoria Retort Shale. *Geochimica et Cosmochimica Acta*, 55, 1051-1063.
https://doi.org/10.1016/0016-7037(91)90163-Y

Lewan, M. D., Fisher, J. B. (1994) Organic acids from petroleum source rocks. In: Pittman, E. D., Lewan, M. D. (Eds.), Organic acids in geological processes. Springer: 70-114; New York.
https://doi.org/10.1007/978-3-642-78356-2_4

Lewan, M. D., Dolan, M. P., Curtis, J. B. (2014) Effects of smectite on the oil-expulsion efficiency of the Kreyenhagen Shale, San Joaquin Basin, California, based on hydrous-pyrolysis experiments. *AAPG Bulletin*, 98, 1091-1109.
https://doi.org/10.1306/10091313059

Li, Y., Zhou, S., Li, J., Ma, Y., Chen, K., Wu, Y., Zhang, Y. (2017) Experimental study of the decomposition of acetic acid under conditions relevant to deep reservoirs. *Applied Geochemistry*, 84, 306-313.
https://doi.org/10.1016/j.apgeochem.2017.07.013

Li, J., Ma, Y., Huang, K., Zhang, Y., Wang, W., Liu, J., Li, Z., Lu, S. (2018) Quantitative characterization of organic acid generation, decarboxylation, and dissolution in a shale reservoir and the corresponding applications – A case study of the Bohai Bay Basin. *Fuel*, 214, 538-545.
https://doi.org/10.1016/j.fuel.2017.11.034

Li, H., Wang, Q., Du, X., Yang, X., Zhu, H. (2021a) Residual carboxylic acids (nonpyrolytic) in mudstones and their implications and constraints on sandstone diagenesis, Bozhong Depression, offshore Bohai Bay Basin, East China. *Organic Geochemistry*, 151, 104149.
https://doi.org/10.1016/j.orggeochem.2020.104149

Li, P., Zhou, S., Ji, B., Liu, X., Li, J., Zhang, X., Huang, J., Ma, Y. (2021b) Water-soluble organic acids in sedimentary rocks: Compositions and influencing factors. *Journal of Natural Gas Geoscience*, 6, 173-181.
https://doi.org/10.1016/j.jnggs.2021.06.003

Libert, M., Bildstein, O., Esnault, L., Jullien, M., Sellier, R. (2011) Molecular hydrogen: an abundant energy source for bacterial activity in nuclear waste repositories. *Physics and Chemistry of the Earth, Parts A/B/C*, 36, 1616-1623.
https://doi.org/10.1016/j.pce.2011.10.010

Lide, D. R. (Ed.) 2005. Physical constants of inorganic compounds. CRC Handbook of Chemistry and Physics 85th Edition Internet Version, CRC Press Boca Raton, FL, p. 2712.

Lippold, H., Lippmann-Pipke, J. (2009) Effect of humic matter on metal adsorption onto clay materials: Testing the linear additive model. *Journal of Contaminant Hydrology*, 109, 40-48. https://doi.org/10.1016/j.jconhyd.2009.07.009

Littke, R., Leythaeuser, D., Rullkötter, J., Baker, D. R. (1991) Keys to the depositional history of the Posidonia Shale (Toarcian) in the Hils Syncline, northern Germany. *Geological Society, London, Special Publications*, 58, 311-333. https://doi.org/10.1144/GSL.SP.1991.058.01.20

Lommerzheim, A., Jobmann, M., Meleshyn, A., Mrugalla, S., Rübel, A., Stark, L. (2019) Safety concept, FEP catalogue and scenario development as fundamentals of a long-term safety demonstration for high-level waste repositories in German clay formations. *Geological Society, London, Special Publications*, 482, 313-329. https://doi.org/10.1144/SP482.6

Lotrario, J., Stuart, B., Lam, T., Arands, R., O'Connor, O., Kosson, D. (1995) Effects of sterilization methods on the physical characteristics of soil: implications for sorption isotherm analyses. *Bulletin of Environmental Contamination and Toxicology*, 54, 668-675. https://doi.org/10.1007/BF00206097

Lundegard, P. D., Land, L. S., Galloway, W. E. (1984) Problem of secondary porosity: Frio Formation (Oligocene), Texas Gulf Coast. *Geology*, 12, 399-402. https://doi.org/10.1130/0091-7613(1984)12%3C399:POSPFF%3E2.0.CO;2

Lundegard, P. D., Senftle, J. T. (1987) Hydrous pyrolysis: a tool for the study of organic acid synthesis. *Applied Geochemistry*, 2, 605-612. https://doi.org/10.1016/0883-2927(87)90012-6

Lundegard, P. D., Land, L. S. (1989) Carbonate equilibria and pH buffering by organic acids – response to changes in p_{CO2}. *Chemical Geology*, 74, 277-287. https://doi.org/10.1016/0009-2541(89)90038-7

M

Ma, X., Zheng, G., Sajjad, W., Xu, W., Fan, Q., Zheng, J., Xia, Y. (2018) Influence of minerals and iron on natural gases generation during pyrolysis of type-III kerogen. *Marine and Petroleum Geology*, 89, 216-224. https://doi.org/10.1016/j.marpetgeo.2017.01.012

Ma, X., Liu, B., Brazell, C., Mastalerz, M., Drobniak, A., Schimmelmann, A. (2021) Methane generation from low-maturity coals and shale source rocks at low temperatures (80–120 °C) over 14–38 months. *Organic Geochemistry*, 155, 104224. https://doi.org/10.1016/j.orggeochem.2021.104224

MacGowan, D. B., Surdam, R. C. (1988) Difunctional carboxylic acid anions in oilfield waters. *Organic Geochemistry*, 12, 245-259. https://doi.org/10.1016/0146-6380(88)90262-8

MacGowan, D. B., Surdam, R. C. (1990) Carboxylic acid anions in formation waters, San Joaquin Basin and Louisiana Gulf Coast, USA – Implications for clastic diagenesis. *Applied Geochemistry*, 5, 687-701.
https://doi.org/10.1016/0883-2927(90)90065-D

Mäder, U. K., Waber, H. N. (2017) Characterization of pore water, ion transport and water-rock interaction in claystone by advective displacement experiments. *Procedia Earth and Planetary Science*, 17, 917-920.
https://doi.org/10.1016/j.proeps.2017.01.017

Makhnenko, R. Y., Vilarrasa, V., Mylnikov, D., Laloui, L. (2017) Hydromechanical aspects of CO_2 breakthrough into clay-rich caprock. *Energy Procedia*, 114, 3219-3228.
https://doi.org/10.1016/j.egypro.2017.03.1453

Mango, F. D. (1992) Transition metal catalysis in the generation of petroleum and natural gas. *Geochimica et Cosmochimica Acta*, 56, 553-555.
https://doi.org/10.1016/0016-7037(92)90153-A

Mango, F. D. (1996) Transition metal catalysis in the generation of natural gas. *Organic Geochemistry*, 24, 977-984.
https://doi.org/10.1016/S0146-6380(96)00092-7

Mango, F. D., Hightower, J. (1997) The catalytic decomposition of petroleum into natural gas. *Geochimica et Cosmochimica Acta*, 61, 5347-5350.
https://doi.org/10.1016/S0016-7037(97)00310-4

Marschall, P., Horseman, S., Gimmi, T. (2005) Characterisation of gas transport properties of the Opalinus Clay, a potential host rock formation for radioactive waste disposal. *Oil & Gas Science and Technology*, 60, 121-139.
https://doi.org/10.2516/ogst:2005008

Martens, C. S. (1990) Generation of short chain acid anions in hydrothermally altered sediments of the Guaymas Basin, Gulf of California. *Applied Geochemistry*, 5, 71-76.
https://doi.org/10.1016/0883-2927(90)90037-6

Martini, A. M., Walter, L. M., Ku, T. C., Budai, J. M., McIntosh, J. C., Schoell, M. (2003) Microbial production and modification of gases in sedimentary basins: A geochemical case study from a Devonian shale gas play, Michigan basin. *AAPG Bulletin*, 87, 1355-1375.
https://doi.org/10.1306/031903200184

Mauclaire, L., McKenzie, J. A., Schwyn, B., Bossart, P. (2007) Detection and cultivation of indigenous microorganisms in Mesozoic claystone core samples from the Opalinus Clay Formation (Mont Terri Rock Laboratory). *Physics and Chemistry of the Earth, Parts A/B/C*, 32, 232-240.
https://doi.org/10.1016/j.pce.2005.12.010

Mazurek, M., Hurford, A. J., Leu, W. (2006) Unravelling the multi-stage burial history of the Swiss Molasse Basin: integration of apatite fission track, vitrinite reflectance and biomarker isomerisation analysis. *Basin Research*, 18, 27-50.
https://doi.org/10.1111/j.1365-2117.2006.00286.x

Mazurek, M., Alt-Epping, P., Bath, A., Gimmi, T., Waber, H. N., Buschaert, S., De Cannière, P., De Craen, M., Gautschi, A., Savoye, S., Vinsot, A., Wemaere, I., Wouters, L. (2011) Natural tracer profiles across argillaceous formations. *Applied Geochemistry*, 26, 1035-1064.
https://doi.org/10.1016/j.apgeochem.2011.03.124

Mazurek, M., Oyama, T., Wersin, P., Alt-Epping, P. (2015) Pore-water squeezing from indurated shales. *Chemical Geology*, 400, 106-121. https://doi.org/10.1016/j.chemgeo.2015.02.008

Mazurek, M., Wersin, P., Hadi, J., Grenèche, J.-M., Prinpreecha, N., Traber, D. (2023) Geochemistry and palaeo-hydrogeology of the weathered zone in the Opalinus Clay. *Applied Clay Science*, 232, 106793. https://doi.org/10.1016/j.clay.2022.106793

McCollom, T. M., Ritter, G., Simoneit, B. R. (1999) Lipid synthesis under hydrothermal conditions by Fischer-Tropsch-type reactions. *Origins of Life and Evolution of the Biosphere*, 29, 153-166. https://doi.org/10.1023/A:1006592502746

McCollom, T. M., Seewald, J. S. (2001) A reassessment of the potential for reduction of dissolved CO_2 to hydrocarbons during serpentinization of olivine. *Geochimica et Cosmochimica Acta*, 65, 3769-3778. https://doi.org/10.1016/S0016-7037(01)00655-X

McCollom, T. M., Seewald, J. S. (2003a) Experimental constraints on the hydrothermal reactivity of organic acids and acid anions: I. Formic acid and formate. *Geochimica et Cosmochimica Acta*, 67(19), 3625-3644. https://doi.org/10.1016/S0016-7037(03)00136-4

McCollom, T. M., Seewald, J. S. (2003b) Experimental study of the hydrothermal reactivity of organic acids and acid anions: II. Acetic acid, acetate, and valeric acid. *Geochimica et Cosmochimica Acta*, 67, 3645-3664. https://doi.org/10.1016/S0016-7037(03)00135-2

McCollom, T. M., Seewald, J. S. (2006) Carbon isotope composition of organic compounds produced by abiotic synthesis under hydrothermal conditions. *Earth and Planetary Science Letters*, 243, 74-84. https://doi.org/10.1016/j.epsl.2006.01.027

McCollom, T. M., Seewald, J. S. (2007) Abiotic synthesis of organic compounds in deep-sea hydrothermal environments. *Chemical Reviews*, 107, 382-401. https://doi.org/10.1021/cr0503660

McCollom, T. M., Lollar, B. S., Lacrampe-Couloume, G., Seewald, J. S. (2010) The influence of carbon source on abiotic organic synthesis and carbon isotope fractionation under hydrothermal conditions. *Geochimica et Cosmochimica Acta*, 74, 2717-2740. https://doi.org/10.1016/j.gca.2010.02.008

McCollom, T. M., Klein, F., Moskowitz, B., Berquó, T. S., Bach, W., Templeton, A. S. (2020) Hydrogen generation and iron partitioning during experimental serpentinization of an olivine–pyroxene mixture. *Geochimica et Cosmochimica Acta*, 282, 55-75. https://doi.org/10.1016/j.gca.2020.05.016

McDermott, J. M., Seewald, J. S., German, C. R., Sylva, S. P. (2015) Pathways for abiotic organic synthesis at submarine hydrothermal fields. *Proceedings of the National Academy of Sciences*, 112, 7668-7672. https://doi.org/10.1073/pnas.1506295112

Means, J. L., Hubbard, N. (1987) Short-chain aliphatic acid anions in deep subsurface brines: a review of their origin, occurrence, properties, and importance and new data on their distribution and geochemical implications in the Palo Duro Basin, Texas. *Organic Geochemistry*, 11, 177-191.
https://doi.org/10.1016/0146-6380(87)90021-0

Miller, D., Brown, C., Pearson, T., Stanley, S. (1979) Some biologically important low molecular weight organic acids in the sediments of Loch Eil. *Marine Biology*, 50, 375-383.
https://doi.org/10.1007/BF00387015

Mitzscherling, J., Genderjahn, S., Schleicher, A.M., Bartholomäus, A., Kallmeyer, J., Wagner, D. (2023) Clay-associated microbial communities and their relevance for a nuclear waste repository in the Opalinus Clay rock formation. *MicrobiologyOpen*, 12, e1370.
https://doi.org/10.1002/mbo3.1370

Morosoli, D., Anagnostou, G., Cantieni, L. (2023) Design considerations for deep caverns in Opalinus Clay. In: Anagnostou, G., Benardos, A., Marinos, V. P. (Eds.) Expanding Underground - Knowledge and Passion to Make a Positive Impact on the World, CRC Press: 2114-2121; London.
https://doi.org/10.1201/9781003348030-254

Muraleedharan, M. G., Asgar, H., Hahn, S. H., Dasgupta, N., Gadikota, G., Van Duin, A. C. (2021) Interfacial reactivity and speciation emerging from Na-montmorillonite interactions with water and formic acid at 200 °C: insights from reactive molecular dynamics simulations, infrared spectroscopy, and X-ray scattering measurements. *ACS Earth and Space Chemistry*, 5, 1006-1019.
https://doi.org/10.1021/acsearthspacechem.0c00286

Myrttinen, A., Becker, V., Barth, J. A. C. (2012) A review of methods used for equilibrium isotope fractionation investigations between dissolved inorganic carbon and CO_2. *Earth-Science Reviews*, 115, 192-199.
https://doi.org/10.1016/j.earscirev.2012.08.004

N

Nakata, E., Tomioka, Y. (2019) Inference of origin and migration process of natural gases by stable carbon isotope ratios in Mont Terri site. Central Research Institute of Electric Power Industry (CRIEPI), Report N18006: 28; Japan.
https://criepi.denken.or.jp/hokokusho/pb/reportDetail?reportNoUkCode=N18006
(last accessed: 08.11.2023)

Naumenko-Dèzes, M., Kloppmann, W., Blessing, M., Bondu, R., Gaucher, E. C., Mayer, B. (2022) Natural gas of radiolytic origin: An overlooked component of shale gas. *Proceedings of the National Academy of Sciences*, 119, e2114720119.
https://doi.org/10.1073/pnas.2114720119

Neerdael, B., Boyazis, J. P. (1997) The Belgium underground research facility: Status on the demonstration issues for radioactive waste disposal in clay. *Nuclear Engineering and Design*, 176, 89-96.
https://doi.org/10.1016/S0029-5493(96)01346-5

Nussbaum, C., Bossart, P., Amann, F., Aubourg, C. (2011) Analysis of tectonic structures and excavation induced fractures in the Opalinus Clay, Mont Terri underground rock laboratory (Switzerland). *Swiss Journal of Geosciences*, 104, 187-210. https://doi.org/10.1007/s00015-011-0070-4

O

Ong, A., Pironon, J., Robert, P., Dubessy, J., Caumon, M. C., Randi, A., Chailan, O., Girard, J. P. (2013) In situ decarboxylation of acetic and formic acids in aqueous inclusions as a possible way to produce excess CH_4. *Geofluids*, 13, 298-304. https://doi.org/10.1111/gfl.12026

Orellana, L. F., Scuderi, M. M., Collettini, C., Violay, M. (2018) Frictional properties of Opalinus Clay: Implications for nuclear waste storage. *Journal of Geophysical Research: Solid Earth*, 123, 157-175. https://doi.org/10.1002/2017JB014931

Orem, W., Tatu, C., Varonka, M., Lerch, H., Bates, A., Engle, M., Crosby, L., McIntosh, J. (2014) Organic substances in produced and formation water from unconventional natural gas extraction in coal and shale. *International Journal of Coal Geology*, 126, 20-31. https://doi.org/10.1016/j.coal.2014.01.003

Ostertag-Henning, C., Zhang, R., Helten, O., Weger, T., Schippers, A. (2019) Using flexible gold-titanium reaction cells to simulate pressure-dependent microbial activity in the context of subsurface biomining. *JoVE (Journal of Visualized Experiments)*, 152, 60140. https://doi.org/10.3791/60140

Otte, J. M., Blackwell, N., Soos, V., Rughöft, S., Maisch, M., Kappler, A., Kleindienst, S., Schmidt, C. (2018) Sterilization impacts on marine sediment – Are we able to inactivate microorganisms in environmental samples?. *FEMS Microbiology Ecology*, 94, fiy189. https://doi.org/10.1093/femsec/fiy189

P

Palmer, D. A., Drummond, S. E. (1986) Thermal decarboxylation of acetate. Part I. The kinetics and mechanism of reaction in aqueous solution. *Geochimica et Cosmochimica Acta*, 50, 813-823. https://doi.org/10.1016/0016-7037(86)90357-1

Papafotiou, A., Senger, R. (2014) Sensitivity analyses of gas release from a SF/HLW repository in the Opalinus Clay in the candidate siting regions of Northern Switzerland. National Cooperative for the Disposal of Radioactive Waste (NAGRA), Report NAB 14-10: 72; Wettingen. https://nagra.ch/wp-content/uploads/2022/08/e_nab14-010.pdf (last accessed: 08.11.2023)

Pearson, F., Arcos, D., Bath, A., Boisson, J., Fernández, A. M., Gäbler, H., Gaucher, E., Gautschi, A., Griffault, L., Hernán, P., Waber, H. (2003) Mont Terri project: Geochemistry of water in the Opalinus clay formation at the Mont Terri Rock Laboratory. Federal Office for Water and Geology, FOWG: 321; Bern, Switzerland.

Pearson, F. J., Arcos, D., Gaucher, E., Waber, H. N. (2003) Pore water chemistry and geochemical modelling, In: Pearson, F. J., Arcos, D., Bath, A., Boisson, J., Fernández, A. M., Gäbler, H., Gaucher, E., Gautschi, A., Griffault, L., Hernán, P., Waber, H. (2003) Mont Terri project: Geochemistry of water in the Opalinus Clay formation at the Mont Terri Rock Laboratory. Federal Office for Water and Geology, FOWG: 69-106; Bern.

Philipp, T., Amann-Hildenbrand, A., Laurich, B., Desbois, G., Littke, R., Urai, J. L. (2017) The effect of microstructural heterogeneity on pore size distribution and permeability in Opalinus Clay (Mont Terri, Switzerland): insights from an integrated study of laboratory fluid flow and pore morphology from BIB-SEM images. *Geological Society, London, Special Publications*, 454, 85-106.
https://doi.org/10.1144/SP454.3

Philippe, A., Schaumann, G. E. (2014) Interactions of dissolved organic matter with natural and engineered inorganic colloids: a review. *Environmental Science & Technology*, 48, 8946-8962.
https://doi.org/10.1021/es502342r

Plummer, L. N., Busenberg, E. (1982) The solubilities of calcite, aragonite and vaterite in CO_2-H_2O solutions between 0 and 90°C, and an evaluation of the aqueous model for the system $CaCO_3$-CO_2-H_2O. *Geochimica et Cosmochimica Acta*, 46, 1011-1040.
https://doi.org/10.1016/0016-7037(82)90056-4

Poulain, S., Sergeant, C., Simonoff, M., Le Marrec, C., Altmann, S. (2008) Microbial investigations in Opalinus Clay, an argillaceous formation under evaluation as a potential host rock for a radioactive waste repository. *Geomicrobiology Journal*, 25, 240-249.
https://doi.org/10.1080/01490450802153314

Pytte, A. M., Reynolds, R. C. (1989) The thermal transformation of smectite to illite. In: Naeser, N. D., McCulloh, T. H. (Eds.) Thermal history of sedimentary basins: Methods and case histories. Springer: 133-140; New York.
https://doi.org/10.1007/978-1-4612-3492-0_8

Q

Quigley, T. M., Mackenzie, A. S. (1988) The temperatures of oil and gas formation in the sub-surface. *Nature*, 333, 549-552.
https://doi.org/10.1038/333549a0

R

Rahman, H. M., Kennedy, M., Löhr, S., Dewhurst, D. N., Sherwood, N., Yang, S., Horsfield, B. (2018) The influence of shale depositional fabric on the kinetics of hydrocarbon generation through control of mineral surface contact area on clay catalysis. *Geochimica et Cosmochimica Acta*, 220, 429-448.
https://doi.org/10.1016/j.gca.2017.10.012

Ramos, M. E., Huertas, F. J. (2014) Adsorption of lactate and citrate on montmorillonite in aqueous solutions. *Applied Clay Science*, 90, 27-34.
https://doi.org/10.1016/j.clay.2014.01.007

Rasamimanana, S., Lefèvre, G., Dagnelie, R. (2017) Various causes behind the desorption hysteresis of carboxylic acids on mudstones. *Chemosphere*, 168, 559-567.
https://doi.org/10.1016/j.chemosphere.2016.11.025

Reijenga, J., Van Hoof, A., Van Loon, A., Teunissen, B. (2013) Development of methods for the determination of pK_a values. *Analytical Chemistry Insights*, 8, 53-71.
https://doi.org/10.4137/ACI.S12304

Rübel, A. P., Sonntag, C., Lippmann, J., Pearson, F. J., Gautschi, A. (2002) Solute transport in formations of very low permeability: Profiles of stable isotope and dissolved noble gas contents of pore water in the Opalinus Clay, Mont Terri, Switzerland. *Geochimica et Cosmochimica Acta*, 66, 1311-1321.
https://doi.org/10.1016/S0016-7037(01)00859-6

S

Saidy, A., Smernik, R., Baldock, J. A., Kaiser, K., Sanderman, J. (2013) The sorption of organic carbon onto differing clay minerals in the presence and absence of hydrous iron oxide. *Geoderma*, 209, 15-21.
https://doi.org/10.1016/j.geoderma.2013.05.026

Sansone, F. J., Martens, C. S. (1982) Volatile fatty acid cycling in organic-rich marine sediments. *Geochimica et Cosmochimica Acta*, 46, 1575-1589.
https://doi.org/10.1016/0016-7037(82)90315-5

Sansone, F. J., Andrews, C. C., Okamoto, M. Y. (1987) Adsorption of short-chain organic acids onto nearshore marine sediments. *Geochimica et Cosmochimica Acta*, 51, 1889-1896.
https://doi.org/10.1016/0016-7037(87)90180-3

Santschi, P. H., Roberts, K. A., Guo, L. (2002) Organic nature of colloidal actinides transported in surface water environments. *Environmental Science & Technology*, 36, 3711-3719.
https://doi.org/10.1021/es0112588

Sauer, K., Caporuscio, F., Rock, M., Cheshire, M., Jové-Colón, C. (2020) Hydrothermal interaction of Wyoming bentonite and Opalinus Clay. *Clays and Clay Minerals*, 68, 144-160.
https://doi.org/10.1007/s42860-020-00068-8

Savoye, S., Goutelard, F., Beaucaire, C., Charles, Y., Fayette, A., Herbette, M., Larabi, Y., Coelho, D. (2011) Effect of temperature on the containment properties of argillaceous rocks: The case study of Callovo–Oxfordian claystones. *Journal of Contaminant Hydrology*, 125, 102-112.
https://doi.org/10.1016/j.jconhyd.2011.05.004

Scheck, M., Bayer, U. (1999) Evolution of the Northeast German Basin – inferences from a 3D structural model and subsidence analysis. *Tectonophysics*, 313, 145-169.
https://doi.org/10.1016/S0040-1951(99)00194-8

Schegg, R., Cornford, C., Leu, W. (1999) Migration and accumulation of hydrocarbons in the Swiss Molasse Basin: implications of a 2D basin modeling study. *Marine and Petroleum Geology*, 16, 511-531.
https://doi.org/10.1016/S0264-8172(99)00018-5

Schoonheydt, R. A., Johnston, C. T. (2006) Surface and interface chemistry of clay minerals. In: Bergaya, F., Theng, B. K. G., Lagaly, G. (Eds.) Handbook of Clay Science, Volume 1, Elsevier Ltd.: 87-113; Amsterdam.
https://doi.org/10.1016/S1572-4352(05)01003-2

Schubotz, F., Lipp, J. S., Elvert, M., Hinrichs, K.-U. (2011) Stable carbon isotopic compositions of intact polar lipids reveal complex carbon flow patterns among hydrocarbon degrading microbial communities at the Chapopote asphalt volcano. *Geochimica et Cosmochimica Acta*, 75, 4399-4415.
https://doi.org/10.1016/j.gca.2011.05.018

Seewald, J. S. (1996) Mineral redox buffers and the stability of organic compounds under hydrothermal conditions. *MRS Online Proceedings Library (OPL)*, 432, 317-331.
https://doi.org/10.1557/PROC-432-317

Seewald, J. S. (2001a) Aqueous geochemistry of low molecular weight hydrocarbons at elevated temperatures and pressures: constraints from mineral buffered laboratory experiments. *Geochimica et Cosmochimica Acta*, 65, 1641-1664.
https://doi.org/10.1016/S0016-7037(01)00544-0

Seewald, J. S. (2001b) Model for the origin of carboxylic acids in basinal brines. *Geochimica et Cosmochimica Acta*, 65, 3779-3789.
https://doi.org/10.1016/S0016-7037(01)00702-5

Seewald, J. S. (2003) Organic–inorganic interactions in petroleum-producing sedimentary basins. *Nature*, 426, 327-333.
https://doi.org/10.1038/nature02132

Seewald, J. S., Seyfried Jr., W. E., Thornton, E. C. (1990) Organic-rich sediment alteration: an experimental and theoretical study at elevated temperatures and pressures. *Applied Geochemistry*, 5, 193-209.
https://doi.org/10.1016/0883-2927(90)90048-A

Seewald, J. S., Seyfried Jr., W. E. (1991) Experimental determination of portlandite solubility in H_2O and acetate solutions at 100–350 °C and 500 bars: constraints on calcium hydroxide and calcium acetate complex stability. *Geochimica et Cosmochimica Acta*, 55, 659-669.
https://doi.org/10.1016/0016-7037(91)90331-X

Seewald, J. S., Benitez-Nelson, B. C., Whelan, J. K. (1998) Laboratory and theoretical constraints on the generation and composition of natural gas. *Geochimica et Cosmochimica Acta*, 62, 1599-1617.
https://doi.org/10.1016/S0016-7037(98)00000-3

Seewald, J. S., Zolotov, M. Y., McCollom, T. (2006) Experimental investigation of single carbon compounds under hydrothermal conditions. *Geochimica et Cosmochimica Acta*, 70, 446-460.
https://doi.org/10.1016/j.gca.2005.09.002

Seltzer, A. M., Krantz, J. A., Ng, J., Danskin, W. R., Bekaert, D. V., Barry, P. H., Kimbrough, D. L., Kulongoski, J. T., Severinghaus, J. P. (2021) The triple argon isotope composition of groundwater on ten-thousand-year timescales. *Chemical Geology*, 583, 120458.
https://doi.org/10.1016/j.chemgeo.2021.120458

Senger, R., Papafotiou, A., Marschall, P. (2013) Gas related property distributions in the proposed host rock formations of the candidate siting regions in Northern Switzerland and in the Helvetic Zone. National Cooperative for the Disposal of Radioactive Waste (NAGRA), Report NAB 13-83: 125; Wettingen.
https://nagra.ch/wp-content/uploads/2022/08/e_nab13-083.pdf
(last accessed: 08.11.2023)

Seyfried Jr., W. E., Janecky, D. R., Berndt, M. E., Ulmer, G. C., Barnes, H. L. (1987) Rocking autoclaves for hydrothermal experiments II. The flexible reaction-cell system. *Hydrothermal Experimental Techniques*, 23, 216-239.
https://www.researchgate.net/publication/283440294_Rocking_autoclaves_for_hydrothermal _experiments_II_The_flexible_reaction-cell_system
(last accessed: 08.11.2023)

Shaw, D., Alperin, M., Reeburgh, W., McIntosh, D. (1984) Biogeochemistry of acetate in anoxic sediments of Skan Bay, Alaska. *Geochimica et Cosmochimica Acta*, 48, 1819-1825.
https://doi.org/10.1016/0016-7037(84)90035-8

Skipper, H. D., Westermann, D. T. (1973) Comparative effects of propylene oxide, sodium azide, and autoclaving on selected soil properties. *Soil Biology and Biochemistry*, 5, 409-414.
https://doi.org/10.1016/0038-0717(73)90067-9

Small, J. S. (1994) Fluid composition, mineralogy and morphological changes associated with the smectite-to-illite reaction: An experimental investigation of the effect of organic acid anions. *Clay Minerals*, 29, 539-554.
https://doi.org/10.1180/claymin.1994.029.4.11

Soleymani, J., Zamani-Kalajahi, M., Ghasemi, B., Kenndler, E., Jouyban, A. (2013) Solubility of Sodium Acetate in Binary Mixtures of Methanol, 1-Propanol, Acetonitrile, and Water at 298.2 K. *Journal of Chemical & Engineering Data*, 58, 3399-3404.
https://doi.org/10.1021/je400625f

Song, J., Zhang, D. (2013) Comprehensive review of caprock-sealing mechanisms for geologic carbon sequestration. *Environmental Science & Technology*, 47, 9-22.
https://doi.org/10.1021/es301610p

Song, M., Schubotz, F., Kellermann, M. Y., Hansen, C. T., Bach, W., Teske, A. P., Hinrichs, K.-U. (2021) Formation of ethane and propane via abiotic reductive conversion of acetic acid in hydrothermal sediments. *Proceedings of the National Academy of Sciences*, 118, e2005219118.
https://doi.org/10.1073/pnas.2005219118

Stalker, L., Farrimond, P., Larter, S. R. (1994) Water as an oxygen source for the production of oxygenated compounds (including CO_2 precursors) during kerogen maturation. *Organic Geochemistry*, 22, 477-486.
https://doi.org/10.1016/0146-6380(94)90120-1

StandAG (2017) Gesetz zur Suche und Auswahl eines Standortes für ein Endlager für hochradioaktive Abfälle (Standortauswahlgesetz - StandAG). Standortauswahlgesetz vom 5. Mai 2017 (BGBl. I S. 1074), das zuletzt durch Artikel 1 des Gesetzes vom 7. Dezember 2020 (BGBl. I S. 2760) geändert worden ist.
https://www.gesetze-im-internet.de/standag_2017/BJNR107410017.html
(last accessed: 26.11.2023)

Strąpoć, D., Mastalerz, M., Dawson, K., Macalady, J., Callaghan, A. V., Wawrik, B., Turich, C., Ashby, M. (2011) Biogeochemistry of microbial coal-bed methane. *Annual Review of Earth and Planetary Sciences*, 39, 617-656.
https://doi.org/10.1146/annurev-earth-040610-133343

Ström, L., Owen, A. G., Godbold, D. L., Jones, D. L. (2001) Organic acid behaviour in a calcareous soil: sorption reactions and biodegradation rates. *Soil Biology & Biochemistry*, 33, 2125-2133.
https://doi.org/10.1016/S0038-0717(01)00146-8

Stroes-Gascoyne, S., Schippers, A., Schwyn, B., Poulain, S., Sergeant, C., Simonoff, M., Le Marrec, C., Altmann, S., Nagaoka, T., Mauclaire, L., McKenzie, J., Daumas, S., Vinsot, A., Beaucaire, C., Matray, J. M. (2007) Microbial community analysis of Opalinus clay drill core samples from the Mont Terri underground research laboratory, Switzerland. *Geomicrobiology Journal*, 24, 1-17.
https://doi.org/10.1080/01490450601134275

Surdam, R. C., Boese, S. W., Crossey, L. J. (1984) The chemistry of secondary porosity: Part 2. Aspects of porosity modification, *In* McDonald, D., Surdam, R. C. (1984) AAPG Memoir 37: Clastic Diagenesis. The American Association of Petroleum Geologists (AAPG): 127-149; Tulsa.
https://doi.org/10.1306/M37435C8

T

Takai, K., Nakamura, K., Toki, T., Tsunogai, U., Miyazaki, M., Miyazaki, J., Hirayama, H., Nakagawa, S., Nunoura, T., Horikoshi, K. (2008) Cell proliferation at 122 °C and isotopically heavy CH_4 production by a hyperthermophilic methanogen under high-pressure cultivation. *Proceedings of the National Academy of Sciences*, 105, 10949-10954.
https://doi.org/10.1073/pnas.0712334105

Thornton, E. C., Seyfried Jr., W. E. (1987) Reactivity of organic-rich sediment in seawater at 350 C, 500 bars: experimental and theoretical constraints and implications for the Guaymas Basin hydrothermal system. *Geochimica et Cosmochimica Acta*, 51, 1997-2010.
https://doi.org/10.1016/0016-7037(87)90188-8

Thury, M., Bossart, P. (1999) Mont Terri Rock Laboratory. Results of the Hydrogeological, Geochemical and Geomechanical Experiments Performed in 1996 and 1997. Geological Reports of the Swiss National Hydrogeological Survey 23: 234; Bern.

Tissot, B., Welte, D. (1978) Petroleum Formation and Occurrence: A New Approach to Oil and Gas Exploration. Springer: 538; Berlin Heidelberg.

Tomonaga, Y., Giroud, N., Brennwald, M. S., Horstmann, E., Diomidis, N., Kipfer, R., Wersin, P. (2019) On-line monitoring of the gas composition in the Full-scale Emplacement experiment at Mont Terri (Switzerland). *Applied Geochemistry*, 100, 234-243.
https://doi.org/10.1016/j.apgeochem.2018.11.015

Tourchi, S., Vaunat, J., Gens, A., Bumbieler, F., Vu, M.-N., Armand, G. (2021) A full-scale in situ heating test in Callovo-Oxfordian claystone: observations, analysis and interpretation. *Computers and Geotechnics*, 133, 104045.
https://doi.org/10.1016/j.compgeo.2021.104045

Trevors, J. (1996) Sterilization and inhibition of microbial activity in soil. *Journal of Microbiological Methods*, 26, 53-59.
https://doi.org/10.1016/0167-7012(96)00843-3

Tripati, A. K., Hill, P. S., Eagle, R. A., Mosenfelder, J. L., Tang, J., Schauble, E. A., Eiler, J. M., Zeebe, R. E., Uchikawa, J., Coplen, T. B., Ries, J. B., Henry, D. (2015) Beyond temperature: Clumped isotope signatures in dissolved inorganic carbon species and the influence of solution chemistry on carbonate mineral composition. *Geochimica et Cosmochimica Acta*, 166, 344-371.
https://doi.org/10.1016/j.gca.2015.06.021

Truche, L., Berger, G., Destrigneville, C., Pages, A., Guillaume, D., Giffaut, E., Jacquot, E. (2009) Experimental reduction of aqueous sulphate by hydrogen under hydrothermal conditions: implication for the nuclear waste storage. *Geochimica et Cosmochimica Acta*, 73, 4824-4835.
https://doi.org/10.1016/j.gca.2009.05.043

Tuominen, L., Kairesalo, T., Hartikainen, H. (1996) Sterilization and inhibition of microbial activity in soil. *Journal of Microbiological Methods*, 26, 53-59.
https://doi.org/10.1016/0167-7012(96)00843-3

U

Ulrich, G., Bower, S. (2008) Active methanogenesis and acetate utilization in Powder River Basin coals, United States. *International Journal of Coal Geology*, 76, 25-33.
https://doi.org/10.1016/j.coal.2008.03.006

Uren, N.C. (2018) Calcium oxalate in soils, its origins and fate – a review. *Soil Research*, 56, 443-450.
https://doi.org/10.1071/SR17244

V

Van Loon, L. R., Soler, J. M., Bradbury, M. H. (2003) Diffusion of HTO, $^{36}Cl^-$ and $^{125}I^-$ in Opalinus Clay samples from Mont Terri: Effect of confining pressure. *Journal of Contaminant Hydrology*, 61, 73-83.
https://doi.org/10.1016/S0169-7722(02)00114-6

Van Loon, L. R., Soler, J. M., Müller, W., Bradbury, M. H. (2004a) Anisotropic diffusion in layered argillaceous rocks: a case study with Opalinus Clay. *Environmental Science & Technology*, 38, 5721-5728.
https://doi.org/10.1021/es049937g

Van Loon, L. R., Wersin, P., Soler, J. M., Eikenberg, J., Gimmi, T., Hernan, P., Dewonck, S., Savoye, S. (2004b) In-situ diffusion of HTO, $^{22}Na^+$, Cs^+ and I^- in Opalinus Clay at the Mont Terri underground rock laboratory. *Radiochimica Acta*, 92, 757-763.
https://doi.org/10.1524/ract.92.9.757.54988

Van Loon, L. R., Baeyens, B., Bradbury, M. H. (2005) Diffusion and retention of sodium and strontium in Opalinus Clay: Comparison of sorption data from diffusion and batch sorption measurements, and geochemical calculations. *Applied Geochemistry*, 20, 2351-2363. https://doi.org/10.1016/j.apgeochem.2005.08.008

Van Hees, P., Vinogradoff, S., Edwards, A., Godbold, D., Jones, D. (2003) Low molecular weight organic acid adsorption in forest soils: effects on soil solution concentrations and biodegradation rates. *Soil Biology and Biochemistry*, 35, 1015-1026. https://doi.org/10.1016/S0038-0717(03)00144-5

Vandieken, V., Pester, M., Finke, N., Hyun, J.-H., Friedrich, M. W., Loy, A., Thamdrup, B. (2012) Three manganese oxide-rich marine sediments harbor similar communities of acetate-oxidizing manganese-reducing bacteria. *The ISME Journal*, 6, 2078-2090. https://doi.org/10.1038/ismej.2012.41

Varonka, M. S., Gallegos, T. J., Bates, A. L., Doolan, C., Orem, W. H. (2020) Organic compounds in produced waters from the Bakken Formation and Three Forks Formation in the Williston Basin, North Dakota. *Heliyon*, 6, e03590. https://doi.org/10.1016/j.heliyon.2020.e03590

Vieth, A., Mangelsdorf, K., Sykes, R., Horsfield, B. (2008) Water extraction of coals–potential for estimating low molecular weight organic acids as carbon feedstock for the deep terrestrial biosphere. *Organic Geochemistry*, 39, 985-991. https://doi.org/10.1016/j.orggeochem.2008.02.012

Villar, M. V., Romero, F. J., Matín, P. L., Gutiérrez-Rodrigo, V., Barcala, J. M. (2015) Gas Transport in Opalinus Clay. Centro de Investigaciones Energéticas, Medioambientales y Tecnológicas (CIEMAT), Technical Report 1378: 62; Madrid. http://dx.doi.org/10.13140/RG.2.2.28594.91846

Vinsot, A., Appelo, C. A. J., Lundy, M., Wechner, S., Lettry, Y., Lerouge, C., Fernández, A. M., Labat, M., Tournassat, C., De Cannière, P., Schwyn, B., McKelvie, J., Dewonck, S., Bossart, P., Delay, J. (2014) In situ diffusion test of hydrogen gas in the Opalinus Clay. *Geological Society, London, Special Publications*, 400, 563-578. https://doi.org/10.1144/SP400.12

Vinsot, A., Appelo, C. A. J., Lundy, M., Wechner, S., Cailteau-Fischbach, C., De Donato, P., Pironon, J., Lettry, Y., Lerouge, C., De Cannière, P. (2017) Natural gas extraction and artificial gas injection experiments in Opalinus Clay, Mont Terri rock laboratory (Switzerland). *Swiss Journal of* Geosciences, 110, 377-392. https://doi.org/10.1007/978-3-319-70458-6_20

Vogel, J., Grootes, P., Mook, W. (1970) Isotopic fractionation between gaseous and dissolved carbon dioxide. *Zeitschrift für Physik A Hadrons and Nuclei*, 230, 225-238. https://doi.org/10.1007/BF01394688

von Oepen, B., Kördel, W., Klein, W. (1991) Sorption of nonpolar and polar compounds to soils: processes, measurements and experience with the applicability of the modified OECD-Guideline 106. *Chemosphere*, 22, 285-304. https://doi.org/10.1016/0045-6535(91)90318-8

W

Wang, X.-C., Lee, C. (1993) Adsorption and desorption of aliphatic amines, amino acids and acetate by clay minerals and marine sediments. *Marine Chemistry*, 44, 1-23.
https://doi.org/10.1016/0304-4203(93)90002-6

Wang, W., Liu, C., Liu, W., Wang, X., Guo, P., Wang, J., Wang, Z., Li, Z., Zhang, D. (2022a) Dominant products and reactions during organic matter radiolysis: Implications for hydrocarbon generation of uranium-rich shales. *Marine and Petroleum Geology*, 137, 105497.
https://doi.org/10.1016/j.marpetgeo.2021.105497

Wang, W., Ji, L., Song, D., Zhang, D., Lü, C., Su, L. (2022b) Origin of inorganic carbon dioxide associated with hydrocarbon generation: Evidence from hydrous pyrolysis experiments and natural and shale gases. *Journal of Asian Earth Sciences: X*, 7, 100079.
https://doi.org/10.1016/j.jaesx.2021.100079

Wei, L., Schimmelmann, A., Mastalerz, M., Lahann, R. W., Sauer, P. E., Drobniak, A., Strąpoć, D., Mango, F. D. (2018) Catalytic generation of methane at 60–100 °C and 0.1–300 MPa from source rocks containing kerogen Types I, II, and III. *Geochimica et Cosmochimica Acta*, 231, 88-116.
https://doi.org/10.1016/j.gca.2018.04.012

Wei, L., Gao, Z., Mastalerz, M., Schimmelmann, A., Gao, L., Wang, X., Liu, X., Wang, Y., Qiu, Z. (2019) Influence of water hydrogen on the hydrogen stable isotope ratio of methane at low versus high temperatures of methanogenesis. *Organic Geochemistry*, 128, 137-147.
https://doi.org/10.1016/j.orggeochem.2018.12.004

Welch, S. A., Ullman, W. J. (1993) The effect of organic acids on plagioclase dissolution rates and stoichiometry. *Geochimica et Cosmochimica Acta*, 57, 2725-2736.
https://doi.org/10.1016/0016-7037(93)90386-B

Wellsbury, P., Goodman, K., Barth, T., Cragg, B. A., Barnes, S. P., Parkes, R. J. (1997) Deep marine biosphere fuelled by increasing organic matter availability during burial and heating. *Nature*, 388, 573-576.
https://doi.org/10.1038/41544

Wenk, H. R., Voltolini, M., Mazurek, M., Van Loon, L. R., Vinsot, A. (2008) Preferred orientations and anisotropy in shales: Callovo-Oxfordian shale (France) and Opalinus Clay (Switzerland). *Clays and Clay Minerals*, 56, 285-306.
https://doi.org/10.1346/CCMN.2008.0560301

Wersin, P., Soler, J. M., Van Loon, L., Eikenberg, J., Baeyens, B., Grolimund, D., Gimmi, T., Dewonck, S. (2008) Diffusion of HTO, Br⁻, I⁻, Cs⁺, $^{85}Sr^{2+}$ and $^{60}Co^{2+}$ in a clay formation: Results and modelling from an in situ experiment in Opalinus Clay. *Applied Geochemistry*, 23, 678-691. https://doi.org/10.1016/j.apgeochem.2007.11.004

Wersin, P., Leupin, O. X., Mettler, S., Gaucher, E. C., Mäder, U., De Cannière, P., Vinsot, A., Gäbler, H. E., Kunimaro, T., Kiho, K., Eichinger, L. (2011) Biogeochemical processes in a clay formation in situ experiment: Part A – Overview, experimental design and water data of an experiment in the Opalinus Clay at the Mont Terri Underground Research Laboratory, Switzerland. *Applied Geochemistry*, 26, 931-953.
https://doi.org/10.1016/j.apgeochem.2011.03.004

Wersin, P., Mazurek, M., Gimmi, T. (2022) Porewater chemistry of Opalinus Clay revisited: Findings from 25 years of data collection at the Mont Terri Rock Laboratory. *Applied Geochemistry*, 138, 105234.
https://doi.org/10.1016/j.apgeochem.2022.105234

Whiticar, M. J. (1999) Carbon and hydrogen isotope systematics of bacterial formation and oxidation of methane. *Chemical Geology*, 161, 291-314.
https://doi.org/10.1016/S0009-2541(99)00092-3

Wigger, C., Van Loon, L. R. (2017) Importance of interlayer equivalent pores for anion diffusion in clay-rich sedimentary rocks. *Environmental Science & Technology*, 51, 1998-2006.
https://doi.org/10.1021/acs.est.6b03781

Wildi, W., Funk, H., Loup, B. F. R., Amato, E., Huggenberger, P. (1989) Mesozoic subsidence history of the European marginal shelves of the alpine Tethys (Helvetic realm, Swiss Plateau and Jura). *Eclogae Géologicae Helveticae*, 82, 817-840.
https://archive-ouverte.unige.ch/unige:90558
(last accessed: 08.11.2023)

Wood, S. A. (1993) The aqueous geochemistry of the rare-earth elements: Critical stability constants for complexes with simple carboxylic acids at 25 °C and 1 bar and their application to nuclear waste management. *Engineering Geology*, 34, 229-259.
https://doi.org/10.1016/0013-7952(93)90092-Q

Wu, S. J., Cai, M. J., Yang, C. J., Li, K. W. (2016) A new flexible titanium foil cell for hydrothermal experiments and fluid sampling. *Review of Scientific Instruments*, 87, 095110.
https://doi.org/10.1063/1.4963700

Y

Yang, Z., Gould, I. R., Williams, L. B., Hartnett, H. E., Shock, E. L. (2018) Effects of iron-containing minerals on hydrothermal reactions of ketones. *Geochimica et Cosmochimica Acta*, 223, 107-126.
https://doi.org/10.1016/j.gca.2017.11.020

Yu, J., Savage, P. E. (1998) Decomposition of formic acid under hydrothermal conditions. *Industrial & Engineering Chemistry Research*, 37, 2-10.
https://doi.org/10.1021/ie970182e

Yuan, G., Cao, Y., Schulz, H.-M., Hao, F., Gluyas, J., Liu, K., Yang, T., Wang, Y., Xi, K., Li, F. (2019) A review of feldspar alteration and its geological significance in sedimentary basins: From shallow aquifers to deep hydrocarbon reservoirs. *Earth-Science Reviews*, 191, 114-140.
https://doi.org/10.1016/j.earscirev.2019.02.004

Yuan, T., Fischer, C. (2022) The influence of sedimentary and diagenetic heterogeneity on the radionuclide diffusion in the sandy facies of the Opalinus Clay at the core scale. *Applied Geochemistry*, 146, 105478.
https://doi.org/10.1016/j.apgeochem.2022.105478

Z

Zhang, C. L., Conil, N., Armand, G. (2017) Thermal effects on clay rocks for deep disposal of high-level radioactive waste. *Journal of Rock Mechanics and Geotechnical Engineering*, 9, 463-478.
https://doi.org/10.1016/j.jrmge.2016.08.006

Zheng, L., Rutqvist, J., Birkholzer, J. T., Liu, H. H. (2015) On the impact of temperatures up to 200 °C in clay repositories with bentonite engineer barrier systems: A study with coupled thermal, hydrological, chemical, and mechanical modeling. *Engineering Geology*, 197, 278-295.
https://doi.org/10.1016/j.enggeo.2015.08.026

Zhu, Y., Vieth-Hillebrand, A., Wilke, F. D., Horsfield, B. (2015) Characterization of water-soluble organic compounds released from black shales and coals. *International Journal of Coal Geology*, 150, 265-275.
https://doi.org/10.1016/j.coal.2015.09.009

Zhuang, G.-C., Montgomery, A., Joye, S. B. (2019a) Heterotrophic metabolism of C_1 and C_2 low molecular weight compounds in northern Gulf of Mexico sediments: Controlling factors and implications for organic carbon degradation. *Geochimica et Cosmochimica Acta*, 247, 243-260.
https://doi.org/10.1016/j.gca.2018.10.019

Zhuang, G.C., Montgomery, A., Samarkin, V. A., Song, M., Liu, J., Schubotz, F., Teske, A., Hinrichs, K.-U., Joye, S. B. (2019b) Generation and utilization of volatile fatty acids and alcohols in hydrothermally altered sediments in the Guaymas Basin, Gulf of California. *Geophysical Research Letters*, 46, 2637-2646.
https://doi.org/10.1029/2018GL081284

Zhuang, G. C., Peña-Montenegro, T. D., Montgomery, A., Montoya, J. P., Joye, S. B. (2019c) Significance of acetate as a microbial carbon and energy source in the water column of Gulf of Mexico: implications for marine carbon cycling. *Global Biogeochemical Cycles*, 33, 223-235.
https://doi.org/10.1029/2018GB006129

Zwaan, F., Schreurs, G., Madritsch, H., Herwegh, M. (2022) Influence of rheologically weak layers on fault architecture: insights from analogue models in the context of the Northern Alpine Foreland Basin. *Swiss Journal of Geosciences*, 115, 1-33.
https://doi.org/10.1186/s00015-022-00427-8